AD_____

Award Number: DAMD17-03-1-0066

TITLE: Biochemical Markers of Brain Injury: An Integrated Proteomics-Based Approach

PRINCIPLE INVESTIGATOR: Ronald L. Hayes, Ph.D.

CONTRACTING ORGANIZATION: University of Florida
Gainesville, FL 32610

REPORT DATE: February 2006

TYPE OF REPORT: Annual

PREPARED FOR: U.S. Army Medical Research and Materiel Command
Fort Detrick, Maryland 21702-5012

REPORT DOCUMENTATION PAGE

Form Approved
OMB No. 0704-0188

1. REPORT DATE	2. REPORT TYPE	3. DATES COVERED
01-02-2006	Annual	1 Feb 2005 – 31 Jan 2006

4. TITLE AND SUBTITLE

Biochemical Markers of Brain Injury: An Integrated Proteomics-Based Approach

5a. CONTRACT NUMBER

5b. GRANT NUMBER
DAMD17-03-1-0066

5c. PROGRAM ELEMENT NUMBER

6. AUTHOR(S)

Ronald L. Hayes, Ph.D.

5d. PROJECT NUMBER

5e. TASK NUMBER

5f. WORK UNIT NUMBER

7. PERFORMING ORGANIZATION NAME(S) AND ADDRESS(ES)

University of Florida
Gainesville, FL 32610

8. PERFORMING ORGANIZATION REPORT NUMBER

9. SPONSORING / MONITORING AGENCY NAME(S) AND ADDRESS(ES)
U.S. Army Medical Research and Materiel Command
Fort Detrick, Maryland 21702-5012

10. SPONSOR/MONITOR'S ACRONYM(S)

11. SPONSOR/MONITOR'S REPORT NUMBER(S)

12. DISTRIBUTION / AVAILABILITY STATEMENT
Approved for Public Release; Distribution Unlimited

13. SUPPLEMENTARY NOTES
Original contains colored plates: ALL DTIC reproductions will be in black and white.

14. ABSTRACT
Background: Brain injury poses a major problem to military care, accounting for 25% of all combat casualties and is the leading cause of death among wounded soldiers reaching Echelon I medical treatment. Incidence of brain injury and resultant long-term disabilities caused by traumatic insults and ischemic events is significantly greater in the civilian population. No clinically useful diagnostic tests exist for traumatic or ischemic brain injury to provide physicians with quantifiable neurochemical markers to help determine the seriousness of the injury, the anatomical and cellular pathology of the injury and to guide implementation of appropriate triage and medical management. Study Design: SOW 1 employs integrated proteomics-based technologies to identify specific proteins or peptide fragments in brain released into CSF and/or blood of rats following experimental traumatic brain injury or focal cerebral ischemia. Technologies include mass spectroscopy, 2-D gel electrophoresis, phage display of single chain antibodies and antibody chips. SOW 2 employs antibody chips to determine which proteins or peptide fragments released into CSF following injury are reliably associated with different injury magnitudes and predict changes in histopathological, behavioral and electrophysiological outcome measures. SOW 3 develops ELISA-based assays capable of detecting biomarkers in blood. Relevance: Development of "objective triage" capabilities for combat medics and/or Echelon I providers would represent a major "fieldable" breakthrough in the medical management of combat related head trauma.

15. SUBJECT TERMS
Traumatic brain injury, ischemia, biomarkers, proteomics

16. SECURITY CLASSIFICATION OF:				18. NUMBER OF PAGES	19a. NAME OF RESPONSIBLE PERSON
					USAMRMC
a. REPORT	b. ABSTRACT	c. THIS PAGE			19b. TELEPHONE NUMBER *(include area code)*
U	U	U	UU	110	

Table of Contents

INTRODUCTION

Recent combat experiences in Irag have highlighted the fact that traumatic brain injury (TBI) is one of the most frequent causes of mortality and morbidity on the modern battlefield. More than half of combat casualties in Iraq suffer from TBI. Forty percent of battlefield fatalities in Viet Nam were due to head wounds. It has also been reported that of patients arriving alive at military field hospitals, 20% with severe brain wounds die before surgery is performed, and 80% receive neurosurgical treatment with a 10% surgical mortality rate. Penetrating head injury alone accounts for 25% of all war time casualties and approximately 40% of these injuries are fatal.

Thus, the current proposal focuses on development of non-invasive diagnostics (i.e., biomarkers) of TBI that ultimately will be useful in a battlefield environment. The research has been divided into 3 SOWs reviewed below. As summarized in the body of this report, we continue to make significant progress toward the goals of the original proposal.

SOW 1: To employ integrated proteomics-based technologies to identify specific proteins or peptide fragments in brain released into CSF and/or blood of rats following experimental traumatic brain injury (TBI) or focal cerebral ischemia (middle cerebral artery occlusion: MCAO).

(A) Conduct concurrent studies employing mass spectrometry (HPLC MALDI-TOF protein profiling's Isotope-coded affinity tags-ICAT), 2D-gel electrophoresis, and phage display of single chain antibodies to detect proteins or peptide fragments in brain and CSF after TBI or MCAO.
(B) Employing injury-related proteins or peptide fragments identified in SOW 1-A, construct and validate the sensitivity of an antibody chip. Validation of the chip would on focus studies in CSF but would also explore chip utility for blood analyses.

SOW 2: Employing the antibody chip developed in SOW 1-B, determine which protein or peptide fragments released into CSF following TBI or MCAO are reliably associated with different injury magnitudes and predict changes in histopathological, behavioral and electrophysiological outcome measures.

(A) CSF will be sampled at multiple time points following injury to determine the optimal sampling time(s) predictive of injury magnitudes. If feasible based on data from SOW 1-B, limited studies will be conducted employing blood samples. (Months 25-30).
(B) Using the same injury magnitudes and data on release of protein or peptide fragments derived from the antibody chips employed in SOW 2-A, identify which sampling time(s) and which protein or peptide fragments released into CSF are optimally predictive of histopathological behavioral or electrophysiological assessments of outcome following TBI or MCAO. EEG analyses of electrophysiological alterations will be conducted following TBI and ischemia. Histopathology will be assessed by hematoxylin and eosin (H&E) staining for TBI and triphenyltetrazolium chloride (TTC) staining for MCAO. Behavioral assessments will include Morris water maze and Rotorod assessments following TBI and neurological examinations and forelimb sensorimotor assessments following MCAO.

SOW 3:
(A) Develop highly sensitive, quantitative ELISA-based assays capable of detecting blood levels of protein or peptide fragments determined to be optimally predictive of injury magnitude and outcome in SOW 2.
(B) Conduct preliminary validation of the utility of ELISA based assays employing blood samples taken following brain injury.

BODY

This year we have dramatically expanded our non-targeted biomarker discovery efforts, building on last year's success in characterizing injury magnitude and progression using a select set of markers (e.g., alphaII-spectrin) in animal and clinical samples. Our contention has been that an array of TBI biomarkers will be most effective as a diagnostic assay. To this end, it was imperative that we identify as many protein markers as possible. We have explored two complimentary high-throughput proteomics approaches for biomarker discovery, (1) bioanalytical mass spectrometry and (2) high-throughput protein immunoblotting (HTPI). Both approaches are capable of detecting thousands of proteins, and are useful in identifying protein changes between control and injured tissues.

Mass spectrometry has exploded into the area of protein chemistry over the last five years. Methodology involves the separation of proteins from complex biological samples, isolating differences between control and injured proteins, and identifying the different proteins using mass spectrometry analysis. The challenge to this approach is in the numbers – there are thousands of proteins in a brain sample differing in their abundance over a 9-order magnitude range. Further, mass spectrometry requires that all proteins be broken up into smaller peptide fragments, increasing sample complexity 100-fold. Our first approach incorporated the use of differential cyanine dyes and SDS-PAGE protein separation (**Figure 1**). Protein bands that appeared different in abundance between samples stood out against an otherwise yellow background when the red and green images were superimposed. These highlighted differences could then be excised from adjacent gel lanes containing separate naïve and TBI tissue.

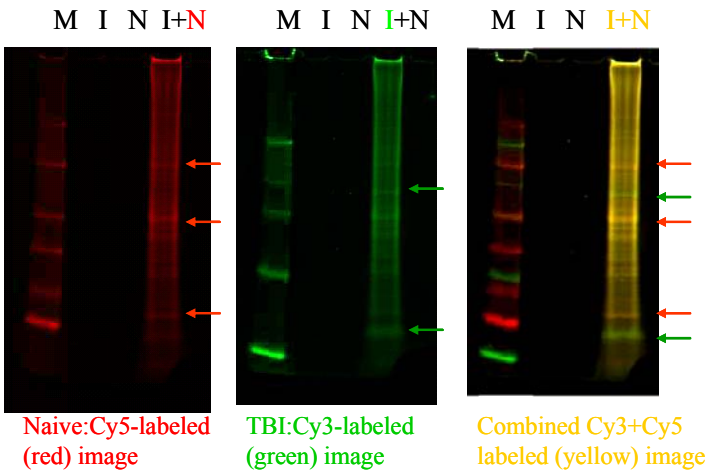

Figure 1. Differential protein analysis using cyanine dyes and SDS-PAGE. Tissue lysate from injured and naïve samples were differentially labeled with cyanine dyes and loaded onto a gel next to lanes where each sample was loaded separately. Differential proteins were identified in the dye lane as a red or green band. Adjacent gel slices were excised from the injured / naïve only lanes for mass spectrometry analysis.

Using this approach we were able to identify over 300 proteins, 57 in naïve only and 74 in injured only (**Haskins et al., J. Neurotrauma 2005, see appendix**); however, we had difficulties determining which exact protein was the differential protein we observed with the cyanine dyes. The difficulty arose when correlating the large number of proteins identified the adjacent naïve or injured gel lanes with the single differential band observed in mixed-sample cyanine dye lane. What we determined is a) that differential protein analysis must be performed using the lanes of the separate naïve and injured samples and b) that additional protein separation was required for reducing the complement of proteins identified in a single excised gel band.

Following the above study, we explored using two-dimensional gel electrophoresis (2D-PAGE), the standard for high-resolution protein separation. We immediately faced the common problem of poor gel-to-gel reproducibility, which limited our ability to perform differential protein analysis. Cyanine fluorophores have been touted as a method for avoiding reproducibility problems, but would require mixing the naïve and injured sample on the gel, reminiscent of the problems we ran into with our first mass spectrometry study. We then opted to develop a new differential analysis platform that could be

reliable for comparing two or more samples but would provide high-resolution separation like that of 2D-PAGE. Our answer is a method that involves ion-exchange chromatographic separation of each sample into multiple fractions and resolution of those fractions by 1-dimensional gel electrophoresis. The key to this approach is that fractions for each sample are paired up (i.e., fraction 1 control next to fraction 1 injured, etc.) and run side-by-side on the sample gel, thereby avoiding issues with gel-to-gel reproducibility. Likewise, we are able to maintain proteins from each sample separately, and can easily compare band density values between adjacent lanes. We were also able to false-color the separate gel lanes for a superimposed color image resembling that of the cyanine dyes for easy manual band decoding (**Figure 2**). However, in practice it was more efficient to use gel analysis software to find differential protein bands between lanes.

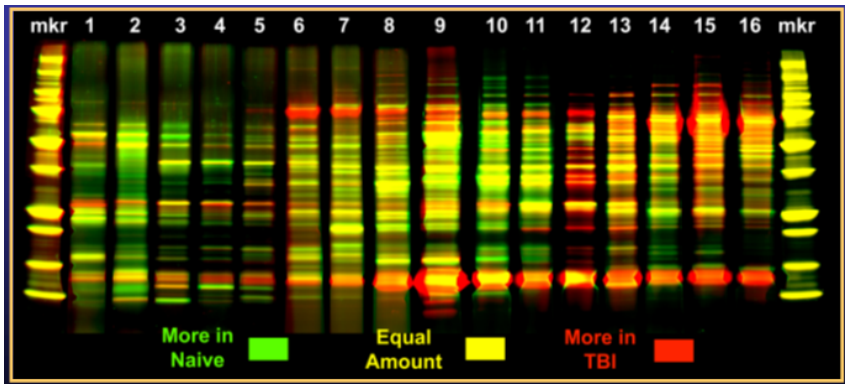

Figure 2. High-resolution protein separation of naïve and injured brain samples. Overlay of false colored naïve and injured protein fractions following novel 2D protein separations indicates proteins of varying abundance following TBI.

We have determined that this approach is comparable in protein resolving capability to that of 2D-PAGE, but provides significantly better reproducibility, with a CV value of 11%. We have also determined that this approached provides an improved mass range over 2D-PAGE, allowing the characterization of high-molecular weight cytoskeletal proteins degraded following TBI, and that more differential protein targets are identified by this approached compared with 2D-PAGE. A detailed characterization of the approach has been published (**Ottens et al., Analytical Chemistry 2005, see appendix and Wang et al., Expert Reviews in Proteomics 2005**).

We have since applied our new differential proteomics approach to biomarker discovery for TBI (**Kobeissy et al., Molecular and Cellular Proteomics 2006, see appendix**) and brain ischemia (**Ottens el al., paper in preparation 2006**). We identified 38 proteins with increased and 21 proteins with decrease abundance following TBI. Using our middle cerebral arterial occlusion (MCAo) model of ischemic stroke, we identified 24 proteins with increased and 54 proteins with decreased abundance following injury. Only 11 proteins common between the two studies showed similar trends in abundance changes, while 3 proteins appeared to react oppositely between the two injury paradigms. All of these proteins are putative biochemical markers of neurotrauma. We have selected nine proteins from the TBI study for secondary validation by Western blot analysis, and found that all demonstrated the expected abundance change and/or proteolytic degradation following injury. We are currently in the process of validating approximately 15 of the differential proteins from the MCAo study.

We have also integrated a second proteomics approach to biomarker discovery, as no single approach is capable of identifying all protein changes. In this approach, control and injured tissue lysate is applied separately to a panel of antibodies call a Power Blot® (BD Biosciences). The approach is a high-throughput immunoblotting (HTPI) technique that rapidly assesses protein changes in a similar manner to Western blot analysis, but for 1000 proteins simultaneously (**Figure 3**). With this approach we identified 9 proteins with increased and 48 proteins with decreased abundance following TBI (**Liu et al., Biochemical Journal 2006, see appendix**). In this study, we also characterized the proteolytic products (the degradome) of calpain-2 and caspase-3 following *in vitro* digestion of naïve tissue. Superimposed, the data sets indicated that 42 of the 48 decreased proteins were also degraded by calpain-2 or caspase-3.

This would suggest that a large percentage of proteomic changes following TBI are related to proteolysis, in line with our previous research findings on targeted proteins (e.g., alphaII-spectrin). The HTPI approach has also been applied to ischemic injury, to be presented in a manuscript in preparation by our WRAIR collaborators.

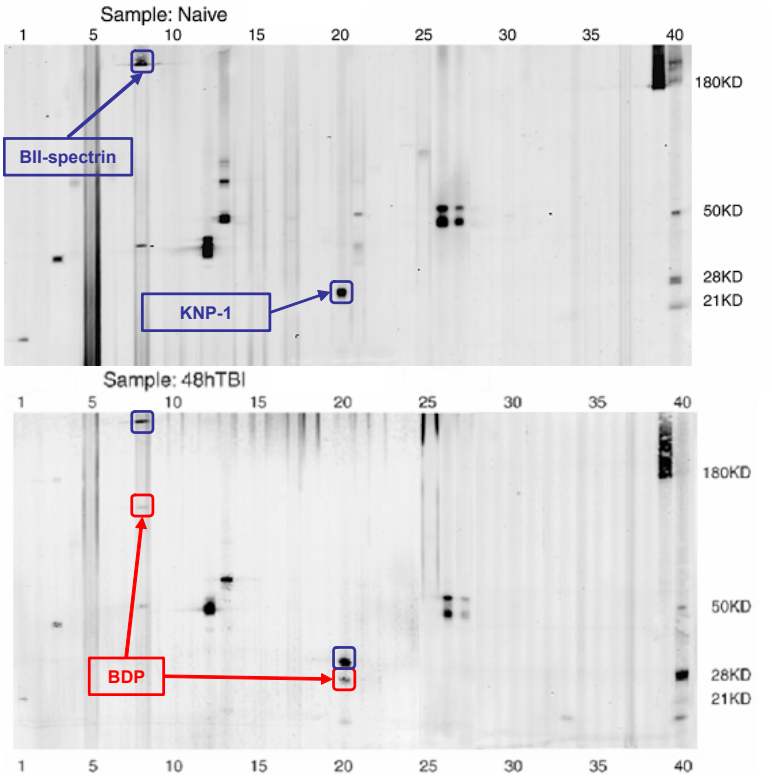

Figure 3. Post-TBI protein degradation as observed by BD PowerBlot panel. Two proteins, βII-spectrin and KNP-1, are shown degraded at 2 days following TBI. Blots were prepared with 200 µg of Naïve and 48hr TBI cortical tissue lysates. The BD Science PowerBlot is a high-throughput screening technology based on the specific nature of an antibody library. In this proposal, similar blots will be customized with antibodies specific to brain substrates of TBI-relevant protease, to observe and quantify breakdown products (BDP) at multiple post-injury time points with respect to naïve tissue.

The identification of proteolytic breakdown products has been a reoccurring theme for this project. We have been working with a number of TBI biomarkers that show degradation following injury, including map-tau, microtubual associated protein 2 (MAP2), alphaII-spectrin and myelin basic protein (MBP). We have recently published our findings on MBP (**Liu et al., J. Neurochemistry 2006, see appendix**) and have demonstrated for the first time that MBP is cleaved by calpain. We also demonstrated that this is a dominant cleavage event following TBI. We are in the processes of developing assays for MBP breakdown products in CSF. We have also expanded our scope of proteolytic processing following TBI to include caspase-7 proteolysis (**Larner et al., J. Neurochemistry 2005, see appendix**). We have demonstrated for the first time that caspase-7 is activated in the brain following TBI in rats. We continue to explore the difference in substrates between caspase-7 and the dominant caspase-3, as we anticipate that any developed therapy that might inhibit apoptosis induced capase-3 may also have to inhibit caspase-7, which may be an alternative route for protein degradation.

KEY RESEARCH ACCOMPLISHMENTS

- We have developed a novel platform for differential proteomics and have applied it to biomarker discovery in TBI (published) and MCAo (in preparation).
- We have reported the first use of high-throughput Immunoblot analysis for biomarker discovery in TBI (published) and MCAo (in preparation).
- We have validated the differential behavior of 9 TBI markers discovered with our proteomics technology and are in the process of validation upwards of 15 ischemia markers.

- We have characterized new proteolytic markers of TBI to include myelin basic protein and map-tau.
- We have expanded our efforts in studying proteolytic processing following TBI by incorporating studies of caspase-7.

REPORTABLE OUTCOMES

Publications

1. Ottens AK, Kobeissy FH, Wolper RA, Haskins WE, Hayes RL, Denslow ND, Wang KKW. A Multidimensional Differential Proteomic Platform Using Dual Phase Ion-Exchange Chromatography - Polyacrylamide Gel Electrophoresis / Reverse Phase Liquid Chromatography Tandem Mass Spectrometry. *Anal. Chem.* 2005, 77:4836-4845.
2. Haskins WE, Kobeissy FH, Wolper RA, Ottens AK, Kitlen JW, Liu MC, McClung SH, Lundberg AG, O'steen BE, Chow MM, Pineda JA, Denslow ND, Hayes RL, Wang KKW. Rapid discovery of putative protein biomarkers of traumatic brain injury by SDS-PAGE-capillary liquid chromatography-tandem mass spectrometry, *J. Neurotrauma* 2005, 22:629-644.
3. Wang KKW, Ottens AK, Liu MC, Lewis SB, Meegan C, Oli MW, Tortella FC, Hayes RL. Proteomic identification of biomarkers of traumatic brain injury. *Expert. Rev. Proteomics* 2005, 2:603-614.
4. Larner SF, McKinsey DM, Hayes RL, Wang KKW. Caspase-7: Increased expression and activation following traumatic brain injury in rats. *J. Neurochem.* 2005, 94:97-108.
5. Liu MC, Akle V, Zheng WR, Dave JR, Tortella FC, Hayes RL, Wang KKW. Comparing calpain- and caspase-3-degradation patterns in traumatic brain injury by differential proteome analysis. *Biochem. J.* 2006, 394:715-725.
6. Liu MC, Kitlen J, O'Steen B, Flint J, Dave JR, Tortella FC, Hayes, RL, Wang KKW. Extensive myelin basic protein degradation in rat brain after traumatic brain injury. *J. Neurochem*. 2006, 98:700-712.
7. Kobeissy FH, Ottens AK, Zhang Z, Liu MC, Hayes RL, Wang KKW. Novel differential neuroproteomics analysis of traumatic brain injury in rats. *Mol. Cell Proteom*. web published in 2006.

Abstracts

1. Ronald L. Hayes. An integrated platform for discovery and preclinical/clinical validation of biomarkers of brain injury. CHI Biomarker Validation meeting, San Francisco, Feb. 2005.
2. Linda Papa, Jose Pineda, Steve Lewis, Kevin Wang, Jason Demery, Shelley Heaton, Joe Tepas and Ronald Hayes. Levels of alpha-II spectrin breakdown products in human CSF and outcome after severe traumatic brain injury. Society for Academic Emergency Medicine, May, 2005.
3. Changping Yao, Anthony J Williams, X-C May Lu, Renwu Chen, Zhilin Liao, Rebeca Connors, Kevin K Wang, Ron L Hayes, Frank C Tortella, Jitendra R Dave. High throughput immunoblot

analysis of differential protein expression in rat brain tissues following penetrating or ischemic brain injuries. European Neurological Society. Abstract for poster at the 2005 meeting.

4. KW Wang, Ronald L Hayes. Identification and assessment of clinical validity of biomarkers of severe traumatic brain injury: Implications for clinical trial design. BMBD, Sept, 2005.
5. Ronald L. Hayes. Identification of novel biomarkers to assess injury severity, outcome and therapeutic efficacy following TBI. AAPMR, Oct. 2005.
6. Jose Pineda, Ronald L. Hayes, et al. Clinical validation of alphaII-spectrin breakdown products as a biomarker of severe TBI: a pilot study. NNS, 2005.

Oral Presentations

1. Invited Panelist, CHI's Translational Research conference, San Francisco CA (Feb)
2. Invited Speaker, VA Sponsored TBI Workshop, WRAMC, Silver Spring, MD
3. Invited Speaker, 3rd Pannonian Symposium on CNS Injury, Pecs, Hungary
4. Invited Lecturer, Fondazione Santa Lucia, Rome, Italy
5. Invited Speaker, National Chinese Academy Workshop on Cranial Cerebral Trauma, Shanghai, China
6. Co-Organizer and Plenary Speaker, 4th International Conference on Biochemical Markers for Brain Damage (BMBD), Boothbay Harbor, ME
7. Invited Speaker, North American Brain Injury Society Medical-Clinical Conference, Amelia Island, FL
8. Invited Speaker, National Brain Injury Research, Treatment, Training Foundation Conference, Johnstown, PA
9. Invited Speaker, American Academy of Physical Medicine & Rehabilitation, 2005 Annual Assembly, Philadelphia PA
10. Invited Speaker, Join DoD/Academic Funding Initiative Forum, University of Toronto, Canada
11. Invited Attendee and Session Discussant Leader, DoD DARPA Predicting Health & Disease Workshop, Annapolis MD

CONCLUSIONS

In summary, we continue to make significant progress in our third year of funding. We have published the development of an effective integrated proteomics-based platform to study biomarkers of acute CNS injury such as TBI and ischemia. We have significantly enhanced this discovery platform by developing novel techniques to facilitate rapid discovery of new protein biomarkers of TBI. Finally, our research has historically integrated a "degradomics" approach focusing on detecting breakdown products of calpain and caspase proteolysis. Having confirmed that this approach is successful, we are now expanding our research to examine the potential utility of developing biomarkers of other proteases such as cathepsins.

Anal. Chem. **2005,** *77,* 4836−4845

A Multidimensional Differential Proteomic Platform Using Dual-Phase Ion-Exchange Chromatography−Polyacrylamide Gel Electrophoresis/Reversed-Phase Liquid Chromatography Tandem Mass Spectrometry

Andrew K. Ottens,*,†,‡,§,∥ Firas H. Kobeissy,†,∥,⊥ Regina A. Wolper,†,§,∥ William E. Haskins,†,‡,§,∥ Ronald L. Hayes,‡,§,∥,⊥ Nancy D. Denslow,†,# and Kevin K. W. Wang†,‡,§,∥,⊥

Center for Traumatic Brain Injury Studies, Center for Neuroproteomics and Biomarker Research, Departments of Neuroscience and Psychiatry, Department of Physiological Sciences, and the Evelyn F. and William L. McKnight Brain Institute of the University of Florida, Gainesville, Florida 32610

Differential proteomic analysis has arisen as a large-scale means to discern proteome-wide changes upon treatment, injury, or disease. Tandem protein separation methods are required for large-scale differential proteomic analysis. Here, a novel multidimensional platform for resolving and differentially analyzing complex biological samples is presented. The platform, collectively termed CAX-PAGE/RPLC-MSMS, combines biphasic ion-exchange chromatography with polyacrylamide gel electrophoresis for protein separation, quantification, and differential band targeting, followed by capillary reversed-phase liquid chromatography and data-dependent tandem mass spectrometry for quantitative and qualitative peptide analysis. CAX-PAGE provides high protein resolving power with a theoretical peak capacity of 3570, extendable to 7600, a wide protein mass range verified from 16 to 273 kDa, and reproducible differential sample comparison without the added expense of fluorescent dyes and imaging equipment. Demonstrated using a neuroproteomic model, CAX-PAGE revealed an increased number of differential proteins, 137, compared with 82 found by 2D difference gel electrophoresis. When combined with RPLC-MSMS for protein identification, an additional quantification step is performed for internal validation, confirming a 2-fold or greater change in 89% of identified differential targets.

Proteomic characterization reveals protein dynamics incomprehensible at the genetic level[1−4] and essential to understanding cellular function under normal or challenged conditions.[5,6] Application to the nervous system (neuroproteomics) in health and disease has recently begun;[7] however, general difficulties persist, limiting utility. Biological complexity is the principal concern.[8] The sheer number of proteins (50 000 or more)[9] and the wide dynamic concentration range overwhelm today's technology. Many rely on two-dimensional polyacrylamide gel electrophoresis (2D-PAGE) for high-resolution protein separations.[10,11] Around since the mid 1970s, 2D-PAGE is the staple of proteomic analysis, owing to its high resolving power. However, gel-to-gel reproducibility is a problem when performing differential analysis by 2D-PAGE. 2D difference gel electrophoresis (2D-DIGE)[12−14] was introduced to alleviate this problem. Two samples are differentially labeled using matched cyanine fluorophores (Cy3 and Cy5) and combined for separation on the same gel. Differential quantification is determined by subtracting two images taken at distinct excitation and emission wavelengths for each fluorophore. Associated proteins are identified using 2D-PAGE databases or mass spectrometry, though sample mixing prevents independent mass spectrometry analysis. Another limitation is the expense of the cyanine dyes and fluorescence scanner employed. Further complications have led to the development of normalization protocols using a third cyanine dye (Cy2) for sample multiplexing,[15,16] and engineering

* To whom correspondence should be addressed. E-mail: aottens@mbi.ufl.edu.
† Center for Neuroproteomics and Biomarker Research.
‡ Center for Traumatic Brain Injury Studies.
§ Department of Neuroscience.
∥ McKnight Brain Institute of the University of Florida.
⊥ Department of Psychiatry.
Department of Physiological Sciences.

(1) Denslow, N.; Michel, M. E.; Temple, M. D.; Hsu, C. Y.; Saatman, K.; Hayes, R. L. *J. Neurotrauma* **2003**, *20*, 401−407.
(2) Freeman, W. M.; Hemby, S. E. *Neurochem. Res.* **2004**, *29*, 1065−1081.
(3) Anderson, L.; Seilhamer, J. *Electrophoresis* **1997**, *18*, 533−537.
(4) Gygi, S. P.; Rochon, Y.; Franza, B. R.; Aebersold, R. *Mol. Cell. Biol.* **1999**, *19*, 1720−1730.
(5) Hanash, S. *Nature* **2003**, *422*, 226−232.
(6) Figeys, D. *Anal. Chem.* **2003**, *75*, 2891−2905.
(7) Kim, S. I.; Voshol, J.; Oostrum, J. van; Hastings, T. G.; Cascio, M.; Glucksman, M. J. *Neurochem. Res.* **2004**, *29*, 1317−1331.
(8) Aebersold, R.; Mann, M. *Nature* **2003**, *422*, 198−207.
(9) Wells, D. A.; Weil, D. A. *LC-GC N. Am.* **2003**, *21*, 522−538.
(10) Griffin, T. J.; Aebersold, R. *J. Biol. Chem.* **2001**, *276*, 45497−45500.
(11) Peng, J.; Gygi, S. P. *J. Mass Spectrom.* **2001**, *36*, 1083−1091.
(12) Tonge, R.; Shaw, J.; Middleton, B.; Rowlinson, R.; Rayner, S.; Young, J.; Pognan, F.; Hawkins, E.; Currie, I.; Davison, M. *Proteomics* **2001**, *1*, 377−396.
(13) Patton, W. F. *J. Chromatogr., B* **2002**, *771*, 3−31.
(14) Gade, D.; Thiermann, J.; Markowsky, D.; Rabus, R. *J. Mol. Microbiol. Biotechnol.* **2003**, *5*, 240−251.
(15) Unlu, M.; Morgan, E.; Minden, J. S. *Electrophoresis* **1997**, *18*, 2071−2077.
(16) Freeman, W. M.; Hemby, S. E. *Neurochem. Res.* **2004**, *29*, 1065−1081.

10.1021/ac050478r CCC: $30.25
Published on Web 06/22/2005

of cysteine labeling saturation versions of Cy3 and Cy5 tags,[17,18] adding complexity and cost. Such limitations of 2D-PAGE technology have prompted some to explore alternative technologies.[19−23]

Of recent protein separation strategies, free-flow electrophoresis (FFE) is notable for effective sample fractionation by isoelectric point (pI) prior to either 1D-PAGE[24] or reversed-phase liquid chromatography (RPLC).[25] In the latter case, the large number of FFE fractions (80), combined with the high resolving power of RPLC, resulted in the large theoretical peak capacity of 6720, comparable to that of traditional 2D-PAGE (10^3−10^4). Other examples of mixed-mode liquid chromatography, as reviewed elsewhere,[19,26] include chromatofocusing,[27−31] liquid-phase isoelectric focusing,[30,32−34] size exclusion,[27,29] ion exchange,[35] and a combined size exclusion−strong cation-exchange medium,[36] all as first dimensions prior to RPLC. Still others have tried using capillary electrophoresis in a two-dimensional mode[37] or in combination with liquid chromatography.[38,39] All approaches provide reasonable resolving power; however, none as yet have met the needed capacity to resolve an entire proteome (>10^4).

It is apparent from these efforts that future proteomic studies will involve varying multidimensional separations.[9,10,23] Ion-exchange chromatography has often been employed in 2D separations, prior to PAGE[40,41] or orthogonal chromatographies.[11,42] One drawback to ion exchange is that a significant portion of protein from a biological sample will not bind to either a positively charged anion or a negatively charged cation exchanger due to incongruent protein surface charge. We hypothesized that more protein could be retained by combining cationic and anionic exchange media (CAX), either by placing columns in series or by mixing both media together. This principle had been previously demonstrated by El Rassi and Horvath with the separation of simple protein mixtures.[43] Remarkably, this idea received no further attention, likely because no pertinent application was then foreseen.

In translational proteomic applications, researchers are particularly interested in identifying protein expression differences or changes associated with a particular disease, injury, or treatment. This requires, in addition to proteome resolution, a means to detect and quantify differences between two or more samples (e.g., control and treated). The presented platform is designed specifically for this purpose. Combined cation−anionic exchange placed in series with polyacrylamide gel electrophoresis (CAX-PAGE) provides quantified selection of differential proteins, subsequently identified and further quantified by reversed-phase liquid chromatography tandem mass spectrometry (RPLC-MSMS). In this study, we evaluate CAX-PAGE/RPLC-MSMS by comparing the proteomes of cerebellum and cortex tissues, a model system for future application to biomarker discovery in brain injury paradigms. Retention, reproducibility, sample recovery, and resolving power are examined. Differential analysis is compared between CAX-PAGE and the current benchmark 2D-DIGE. Finally, the dual differential quantification strategy is verified using differential and nondifferential gel band pairs.

EXPERIMENTAL SECTION

Sample Preparation. Male Sprague−Dawley rats (five) purchased from Harlan (Indianapolis, IN) were acclimated for 7 days prior to sacrificing. The rats were then anesthetized with 4% isoflurane in a carrier gas of 1:1 O_2/N_2O (4 min) and were perfused with 0.9% saline transcardially prior to decapitation via guillotine. Cerebellum and cortex brain regions were dissected and transferred to microfuge tubes kept on dry ice. Sections were snap frozen in liquid nitrogen and then ground to a fine powder via mortar and pestle kept on dry ice. Powder was scraped into chilled microfuge tubes to which 0.1% SDS lysis buffer (300 μL) was added, containing 150 mM sodium chloride, 3 mM ethylenediaminetetraacetic acid (EDTA), 2 mM ethyleneglycol bis(aminoethyl ether) tetraacetic acid (EGTA), 1% ethoxylated octylphenol (all from Sigma-Aldrich, St. Louis, MO), one tablet of Complete Mini Protease Inhibitor Cocktail (Roche Diagnostics, Mannheim, Germany), and 1 mM sodium vanadate (Fisher Scientific, Fair Lawn, NJ), with the sample solution brought to neutral pH using Tris-base (Sigma-Aldrich). Cell lysis was conducted over 3 h at 4 °C with hourly vortexing. Lysates were spun down at 14 000 rpm at 4 °C for 10 min to remove DNA, lipids, and particulates. Supernatants were then filtered through 0.1-μm Millipore Ultrafree-MC filters (Bedford, MA) for further clarification. Protein concentrations were determined via Bio-Rad DC Protein Assay

(17) Alban, A.; David, S. O.; Björkesten, L.; Andersson, C.; Sloge, E.; Lewis, S.; Currie, I. *Proteomics* **2003**, *3*, 36−44.
(18) Rabilloud, T. *Anal. Chem.* **2000**, *72*, 48A−55A.
(19) Wang, H.; Hanash, S. *J. Chromatogr., B* **2002**, *787*, 11−18.
(20) Janini, G. M.; Conrads, T. P.; Veenstra, T. D.; Issaq, H. J. *J. Chromatogr., B* **2003**, 43−51.
(21) Sköld, K.; Svensson, M.; Kaplan, A.; Björkesten, L.; Åström, J.; Andren, P. E. *Proteomics* **2002**, *2*, 447−454.
(22) Bergh, G. Van den; Clerens, S.; Vandesande, F.; Arckens, L. *Electrophoresis* **2003**, *24*, 1471−1481.
(23) Steel, L. F.; Haab, B. B.; Hanash, S. M. *J. Chromatogr. B* **2005**, *815*, 275−284.
(24) Hoffmann, P.; Ji, H.; Mortiz, R. L.; Connolly, L. M.; Frecklington, D. F.; Layton, M. J.; Eddes, J. S.; Simpson, R. J. *Proteomics* **2001**, *1*, 807−818.
(25) Moritz, R. L.; Ji, H.; Schutz, F.; Connolly, L. M.; Kapp, E. A.; Speed, T. P.; Simpson, R. J. *Anal. Chem.* **2004**, *76*, 4811−4824.
(26) Issaq, H. J.; Conrads, T. P.; Janini, G. M.; Veenstra, T. D. *Electrophoresis* **2002**, *23*, 3048−3061.
(27) Opiteck, G. J.; Ramirez, S. M.; Jorgenson, J. W.; Moseley, M. A., III. *Anal. Biochem.* **1998**, *258*, 349−361.
(28) Chong, B. E.; Yan, F.; Lubman, D. M.; Miller, F. R. *Rapid Commun. Mass Spectrom.* **2001**, *15*, 291−296.
(29) Zhang, Z. L.; Smith, D. L.; Smith, J. B. *Proteomics* **2001**, *1*, 1001−1009.
(30) Lubman, D. M.; Kachman, M. T.; Wang, H.; Gong, S.; Yan, F.; Hamler, R. L.; O'Neil, K. A.; Zhu, K.; Buchanan, N. S.; Barder, T. J. *J. Chromatogr., B* **2002**, 183−196.
(31) Zhu, K.; Kachman, M. T.; Miller, F. R.; Lubman, D. M.; Zand, R. *J. Chromatogr., A* **2004**, *1053*, 133−142.
(32) Wall, D. B.; Kachman, M. T.; Gong, S. Y.; Hinderer, R.; Parus, S.; Misek, D. E.; Hanash, S. M.; Lubman, D. M. *Anal. Chem.* **2000**, *72*, 1099−1111.
(33) Hamler, R. L.; Zhu, K.; Buchanani, N. S.; Kreunin, P.; Kachman, M. T.; Miller, F. R.; Lubman, D. M. *Proteomics* **2004**, *4*, 562−577.
(34) Wang, H. X.; Kachman, M. T.; Schwartz, D. R.; Cho, K. R.; Lubman, D. M. *Proteomics* **2004**, *4*, 2476−2495.
(35) Feng, B. B.; Patel, A. H.; Keller, P. M.; Slemmon, J. R. *Rapid Commun. Mass Spectrom.* **2001**, *15*, 821−826.
(36) Hennessy, T. P.; Quaglia, M.; Kornysova, O.; Grimes, B. A.; Lubda, D.; Unger, K. K. *J. Chromatogr., B* **2005**, *817*, 127−137.
(37) Hu, S.; Michels, D. A.; Fazal, M. A.; Ratisoontorn, C.; Cunningham, M. L.; Dovichi, M. J. *Anal. Chem.* **2004**, *76*, 4044−4049.
(38) Larmann, J. P., Jr.; Lemmo, A. V.; Moore, A. W.; Jorgenson, J. W. *Electrophoreisis* **1993**, *14*, 439−447.
(39) Herr, A. E.; Molho, J. I.; Drouvalakis, K. A.; Mikkelsen, J. C.; Utz, P. J.; Santiago, J. G.; Kenny, T. W. *Anal. Chem.* **2003**, *75*, 1180−1187.
(40) Krishnan, S.; Hale, J. E.; Becker, G. W. In *Enzyme Technologies for Pharmaceutical and Biotechnological Applications*; Kirst, H. A., Yeh, W. K., Zmijewski, M. J., Jr., Eds.; Marcel Dekker: New York, 2001; pp 575−596.
(41) Krapfenbauer, K.; Fountoulakis, M.; Lubec, G. *Electrophoresis* **2003**, *24*, 1847−1870.
(42) Aebersold, R.; Goodlett, D. *Chem. Rev.* **2001**, *101*, 269−295.
(43) El Rassi, Z.; Horvath, C. *J. Chromatogr., B* **1986**, *359*, 255−264.

(Hercules, CA), after which pooled ($n = 5$) 1-mg cortex and 1-mg cerebellum samples were prepared for differential comparison.

Anion/Cation-Exchange Chromatography. A Bio-Rad Biologic DuoFlow system with QuadTec UV detector and BioFrac fraction collector was used with Uno series SAX (Q1) and SCX (S1) prepacked ion-exchange columns. For CAX chromatography, S1 and Q1 columns were placed in series. Buffers consisted of ice cold 20 mM Tris-HCl (pH 7.5 molecular biology grade, Fisher Scientific) in HPLC water (Burdick & Jackson, Muskegon, MI) (mobile phase A). A two-step elution gradient was performed with 1 M NaCl (Fisher Scientific, crystalline 99.8% certified) (mobile phase B) at a flow rate of 1 mL/min with a linear transition from 0 to 15% B in 12.5 mL, followed by 15 to 50% B in 7 mL. The composition was held at 50% B for 2 mL and then reequilibrated to 0% B in 1 mL. An optimized three-step gradient was used for differential analysis. At a flow rate of 1 mL/min, the first linear transition was from 0 to 5% B in 2.5 mL, from 5 to 15% in 9 mL, and followed by 15 to 50% in 10 mL. Again the composition was held at 50% B for 2 mL and reequilibrated to 0% B in 1 mL. UV chromatograms were collected at a wavelength of 280 nm. Twenty-five 1-mL fractions were autonomously collected via the BioFrac fraction collector into 1.5-mL screw-cap microfuge tubes (RPI, Mt. Prospect, IL) kept on ice.

1D-SDS−PAGE. Fractions collected during ion-exchange chromatography were concentrated via Millipore YM-30 centrifugal filters, which were demonstrated to retain proteins of >5 kDa. Each fraction was spun through filters prewashed with 500 μL of HPLC water as two 500-μL sequential portions at 13 500 rpm for 20 min. Laemmli sample buffer (Bio-Rad, with 5% BME) was added to the retentate and incubated for 10 min prior to collection by centrifugation at 3500 rpm for 3 min. The supernatant for each fraction was boiled at 85 °C for 2 min and then loaded onto an Invitrogen Novex 10−20% gradient, 1 mm wide, 10-well gels in a Tris-glycine buffer system (Carlsbad, CA) alongside a lane of Amersham Biosciences Rainbow Marker (Piscataway, NJ) for initial studies. Differential analysis between cerebellum and cortex tissues was performed by pairing fractions for loading side by side (i.e., cerebellum fraction 1 next to cortex fraction 1, etc.) on Bio-Rad Criterion 10−20% gradient, 1-mm 18-well gels in a Tris-glycine buffer system.

Protein Recovery and Retention of CAX. Protein recovery was evaluated with SAX, SCX, and combined-phase CAX. A constant protein amount (750 μg) in a 100-μL injection of the previously described cerebellum lysate was loaded. A 1 mL/min isocratic flow was maintained for 9 min to allow unretained proteins to flow through. The mobile-phase composition was then increased in 1 min and held for 9 min at 50% B to elute bound proteins collected in a normal gradient run. This was followed by an additional increase to 100% B in 1 min, which was held for another 9 min to check for additional protein. Throughout, UV absorbance was monitored at 280 nm, and 1-mL fractions were collected, each concentrated using Millipore YM-30 centrifugal filters and analyzed via Bio-Rad DC protein assay.

CAX-PAGE Coomassie Blue Imaging. Gels were visualized by regressive staining using concentrated Bio-Rad Coomassie Blue R250 for 20 min and destained in 40% HPLC grade ethanol (EM Science, Gibbstown, NJ)/10% acetic acid (ACS Plus grade, Fisher) for ~2 h. Images were captured with an Epson 1640 XL flatbed scanner (Long Beach, CA) and saved as eight-bit TIFF files. Differential analysis of Coomassie Blue-stained gels was performed using Phoretix 1D (Nonlinear Dynamics, Newcastle, U.K.) gel image analysis software. Band intensities were automatically calculated and manually verified for bands above a preset threshold. Intensities were output to Excel (Microsoft, Redmond, WA) for differential evaluation. Manual confirmation was aided by superimposing cerebellum lanes false colored red over adjacent cortex lanes false colored green, creating gradient color lanes for each fraction. Image contrast was improved by adjusting RGB color balance to emphasize mid-tones over shadows.

2D-DIGE. Cerebellum and cortex samples (1 mg each) were prepared from the same pooled material used for CAX-PAGE. Each was adjusted to 2% SDS, followed by TCA precipitation. The pellet was air-dried and resuspended in 150 μL of pH 8.8 urea lysis buffer. Benzonase Nuclease (Novagen, Madison, WI) and 5 mM magnesium chloride (Fisher) were added, incubating the mixture for 30 min on ice to degrade nucleic acids. The solution was clarified by centrifugation with a Beckman Coulter (Fullerton, CA) Airfuge at 100 000 g for 30 min. The supernatant was dialyzed against the urea lysis buffer overnight at room temperature. A 50-μg portion of cortex and cerebellum lysate was labeled with Cy3 and Cy5 minimal dyes (Amersham Biosciences), respectively, using the manufacturer's suggested protocol. Cyanine-labeled samples were combined with 275 μg each of unlabeled cortex and cerebellum lysates. The solution was adjusted to 0.2% IPG pH 3−10 buffer (Amersham Biosciences) and 100 mM DTT with a trace of Orange G stain (Fisher). An 18-cm nonlinear pH 3−10 IPG strip (Amersham Biosciences) was rehydrated in the mixed sample under oil overnight at room temperature. Proteins were focused on the strip at 8 kV until migration was complete (65 kV h). Proteins in the strip were reduced with 100 mM DTT in the reaction buffer, 50 mM pH 6.8 Tris-HCl, 6 M urea, 30% glycerol, and 2% SDS. Alkylation was performed with 2.5% iodoacetamide in the same reaction buffer. The strip was mounted atop a Bio-Rad precise 8−16% tris-glycine gel and run for 6 h at 25 mA and 24 °C. Separate Cy3 and Cy5 images were collected on an Amersham Typhoon 8600 fluorescence imager and processed with Phoretix 2D software (Nonlinear Dynamics).

In−Gel Digestion. Gels were thoroughly rinsed with HPLC water. Target differential bands were excised and dissected into four cubes and placed in 0.5-mL tubes. Each was washed with HPLC water and then 50% 100 mM ammonium bicarbonate (Fisher)/50% acetonitrile (Burdick-Jackson, HPLC grade). Pieces were dehydrated with 100% acetonitrile and dried by Speedvac (ISS110, Thermo Savant, Milford, MA). Cubes were rehydrated with 50 μL of 10 mM dithiothreitol (Calbiochem, San Diego, CA) in 50 mM ammonium bicarbonate and incubated for 30 min at 56 °C. Dithiothreitol was replaced by 50 μL of 55 mM iodoacetamide (Calbiochem) in 50 mM ammonium bicarbonate and reacted for 30 min in the dark at room temperature. Gel pieces were washed with 50 mM ammonium bicarbonate and dehydrated with 100% acetonitrile followed by Speedvac. Rehydration was performed with 15 μL of a 12.5 ng/μL trypsin solution (Promega Gold, Madison, WI) for 30 min at 4 °C, and then 20 μL of 50 mM ammonium bicarbonate was added and left at 37 °C overnight for digestion. The supernatant and two 50% acetonitrile/5% acetic acid extractions were placed into a new tube. The peptide extract was

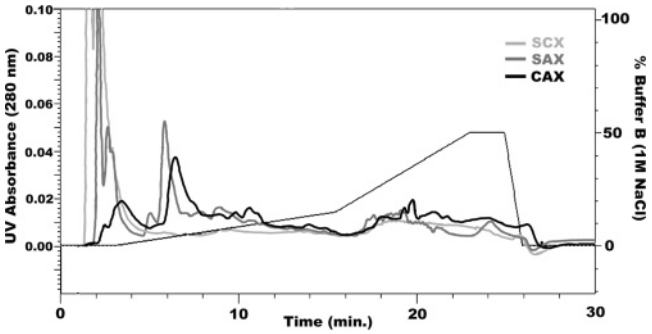

Figure 1. Tandem CAX chromatography with superior protein retention. SCX, SAX, and tandem CAX chromatograms of 1 mg of rat cerebellum lysate are shown overlaid with the same 280-nm absorbance scale. A 5-fold absorbance reduction is observed during flow-through (1−5 min) for CAX, as compared to SCX or SAX.

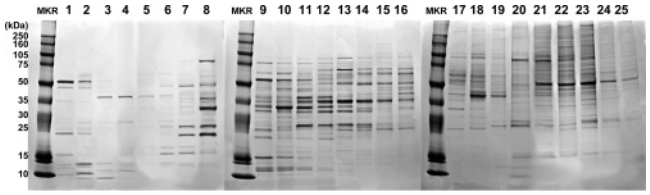

Figure 2. Rat cerebellum proteome visualized on 1D-PAGE following CAX fractionation. One milligram of rat cerebellum brain lysate was divided into 25 CAX fractions, each resolved further by 1D-polyacrylamide gel electrophoresis (10−20% acrylamide). Protein bands were then visualized by Coomassie Blue staining. MKR indicates molecular weight marker lanes.

dried by Speedvac and resuspended in 20 μL of 4% acetonitrile/0.4% acetic acid.

Capillary RPLC-MSMS. Capillary RPLC tandem ion trap mass spectrometry[44] was employed for protein identification as described previously with some modifications.[45] Nanoflow reversed-phase chromatography was performed with a 100 μm i.d. × 5 cm capillary column packed in-house with Agilent (Palo Alto, CA) 3-μm C-18 particles behind an Upchurch 0.5-μm PEEK microfilter assembly. The integrated polymerized frit was replaced with a pulled emitter made from 25-μm-i.d. capillary affixed to the other end of the microfilter assembly. Thirty-minute gradients, 4% HPLC acetonitrile/0.4% acetic acid (Fisher, Optima grade) to 60% acetonitrile/0.4% acetic acid, were used to elute tryptic peptides. Tandem mass spectra were collected on a ThermoElectron (San Jose, CA) LCQ Deca XP-Plus using data-dependent analysis.[19] Collected data were searched against the trypsin indexed complete NCBI RefSeq mammalian database filtered for rat taxonomy using ThermoElectron Bioworks Browser (version 3.1). We report protein identifications made with two or more peptides matched with strict cross-correlation values of Xc ≥ 1.8, 2.5, and 3.5 for +1, +2, and +3 charge states, respectively.[46] Data filtering was performed with DTASelect, and cerebellum versus cortex MSMS data were compared using Contrast software.[46]

RESULTS AND DISCUSSION

CAX Chromatography. The majority of proteins in biological samples, such as tissue lysates or body fluids, retain regions of significant charge on their external surfaces when at physiological pH. Though regions of external charge act independent of net charge,[47] the improvement associated with CAX chromatography can generally be explained through retention of both positively and negatively charged proteins rather than predominantly those of one net polarity. Figure 1 illustrates the difference between SCX, SAX, and CAX chromatography of a complex rat brain cortex tissue lysate. With single ion exchangers, a significant portion of the proteome is unretained, evidenced by a large peak (flow-through) at the beginning of the chromatograms and verified by SDS−PAGE. CAX binds most proteins, leaving the few with low charge density in the flow-through, which partially resolve through hydrophobic interactions[48] in the first four fractions (4-mL window). A two-stage gradient (0−15% B in 12 min, 15−50% B in 7 min) was optimized based on uniform UV absorption throughout the chromatogram, which was presumed to distribute protein for maximal resolution evenly across 25 1-mL fractions, a volume selected for compatibility with column flow rate, the fraction collector, and CAX half-height peak width (∼0.25 mL).

Coupling to 1D-PAGE. Following CAX chromatography with 1D-PAGE further resolved the brain lysate by protein mass. Microtube centrifugal filters were used to reduce the 1-mL fractions to 15 ± 5 μL to which 20 μL of 2× sample buffer was added for gel loading. Random fractions would on occasion run slowly through the filter, potentially due to membrane pore size variability, though no effect on protein retention was observed. Figure 2, visualized by Coomassie Blue stain, revealed that optimizing the CAX gradient based on uniform UV absorption resulted in high protein density toward the end of the CAX separation. The significant band overlap necessitated gradient reoptimization for more effective separation and differential analysis.

CAX-PAGE Reproducibility. The reproducibility of separations is often a limiting factor for differential analysis, particularly with 2D-PAGE.[49,50] The reproducibility of CAX-PAGE was evaluated with triplicate runs of the same rat cerebellum sample. Sequential chromatograms shown in Figure 3a overlap without significant deviation. Next, three groups of fractions spaced evenly at the beginning (1, 4, and 7), middle (10, 13, and 16), and end of the separation (18, 20, and 24) were loaded in triplicate onto 1D-PAGE (Figure 3b) and showed identical protein complements and an average intensity correlation of 94% (Phoretix 1D software). Run-to-run separation remained consistent when the experiment was repeated at a later date (data not shown); however, a nonuniform shift in retention time relative to the data in Figure 3 was observed. Peak shifting is typical of column chromatography and occurs from environmental, buffer, and column aging factors. Thus, runs must be performed sequentially when comparing samples.

CAX-PAGE Protein Recovery and Retention. Though ion exchange is known to provide high protein recovery, the pos-

(44) Haskins, W. E.; Wang, Z.; Watson, C. J.; Rostand, R. R.; Witowski, S. R.; Powell, D. H.; Kennedy, R. T. *Anal. Chem.* **2001**, *73*, 5005−5014.
(45) Haskins, W. E.; Kobeissy, F. H.; Wolper, R. A.; Ottens, A. K.; Kitlen, J. W.; Liu, M. C.; McClung, S. H.; Lundberg, A. G.; O'Steen, B. E.; Chow, M. M.; Pineda, J. A.; Denslow, N. D.; Hayes, R. L.; Wang, K. K. W. *J. Neurotrauma*. **2005**, *22*, 629−644.
(46) Tabb, D. L.; McDonald, W. H.; Yates, J. R., 3rd. *J. Proteome Res.* **2002**, *1*, 21−26.
(47) Regnier, F. E. *Science* **1987**, *238*, 319−323.
(48) Zhu, B. Y.; Mant, C. T.; Hodges, R. S. *J. Chromatogr.* **1992**, *594*, 75−86.
(49) Voss, T.; Haberl, P. *Electrophoresis* **2000**, *21*, 3345−3350.
(50) Nishihara, J. C.; Champion, K. M. *Electrophoresis* **2002**, *23*, 2203−2215.

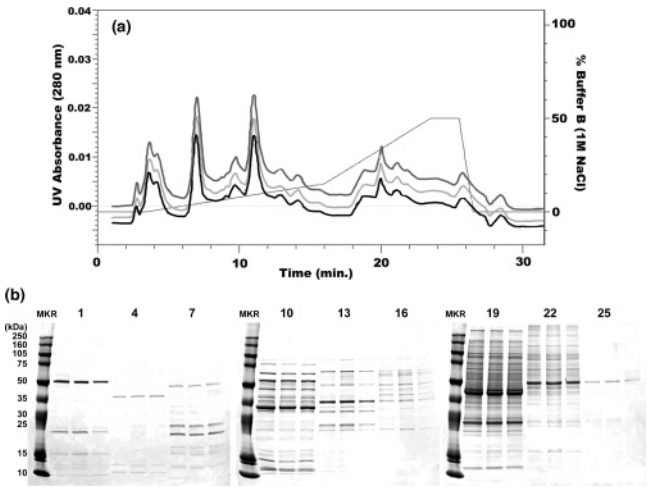

Figure 3. Reproducibility of CAX-PAGE protein separations. (a) Chromatogram of rat cerebellum brain tissue lysate (1 mg of protein) run sequentially in triplicate by CAX. (b) Selected fractions (paired as indicated) from the three replicate CAX runs resolved and visualized side by side on 1D-PAGE. Protein complement remained constant while band intensity varied on average by only 6%.

sibility of exacerbated protein loss was of concern when SAX and SCX phases were combined. A protein recovery of 88 ± 6% after CAX was determined by protein assay while accounting for the buffer change from initial lysate to CAX fractions. Unexpectedly, the sample recovery observed for SAX and SCX was lower than that of CAX, suggesting some variability between protein assay measurements. Using densitometric analysis after 1D-PAGE, microfiltration alone showed an 11 ± 5% sample reduction, the major source of protein loss for this method. In general, reported 2D separations do not discuss protein recovery, with the exception of FFE-IEF shown to have 87.6% protein recovered.[22] With 2D-PAGE, significant protein loss is known to occur, particularly for proteins above 100 kDa, with pI values outside of the 3−10 range and those too hydrophobic for solubalizition in the urea/chaps IPG buffer.[10,11,61]

CAX chromatography showed increased protein retention over SAX and SCX. In practice, 88% of recovered protein was retained by CAX for gradient elution in comparison with 66% for SAX and 47% for SCX as determined by protein assay. Peak area calculations proved similar, with CAX having had the largest retained peak area of 10 (84% of total area) compared with 5.2 (55%) for SAX

(51) Larner S. F.; McKinsey, D. M.; Hayes, R. L.; Wang, K. K. W. *J. Neurochem.* **2005**, *94*, 97−108.
(52) Pineda, J. A.; Wang, K. W. W.; Hayes, R. L. *Brain Pathol.* **2004**, *14*, 202−209.
(53) Pike, B. R.; Flint, J.; Dave, J. R.; Lu, X. C. M.; Wang, K. K. W.; Tortella, F. C.; Hayes, R. L. *J. Cer. Blood Flow Metab.* **2004**, *24*, 98−106.
(54) Shaw, J.; Rowlinson, R.; Nickson, J.; Stone, T.; Sweet, A.; Williams, K.; Tonge, R. *Proteomics* **2003**, *3*, 1181−1195.
(55) Giddings, J. C. *Unified Separation Science*; John Wiley & Sons: New York, 1991; pp 112−138.
(56) Gorg, A.; Weiss, W.; Dunn, M. J. *Proteomics* **2004**, *4*, 3665−3685.
(57) Zhang, S.; Schneider, K. A.; Barder, T. J.; Lubman, D. M. *Biotechniques* **2003**, *35*, 1202−1212.
(58) Morrison, R. S.; Kinoshita, Y.; Johnson, M. D.; Uo, T.; Ho, J. T.; McBee, J. K.; Conrads, T. P.; Veenstra, T. D. *Mol. Cell. Proteomics* **2002**, *1*, 553−560.
(59) Sanders, S. L.; Jennings, J.; Canutescu, A.; Link, A. J.; Weil, P. A. *Mol. Cell. Biol.* **2002**, *22*, 4723−4738.
(60) Peng, J.; Kim, M. J.; Cheng, D.; Duong, D. M.; Gygi, S. P. *J. Biol. Chem.* **2004**, *279*, 21003−21011.
(61) Fountoulakis, M. *Mass Spectrom. Rev.* **2004**, *23*, 231−258.

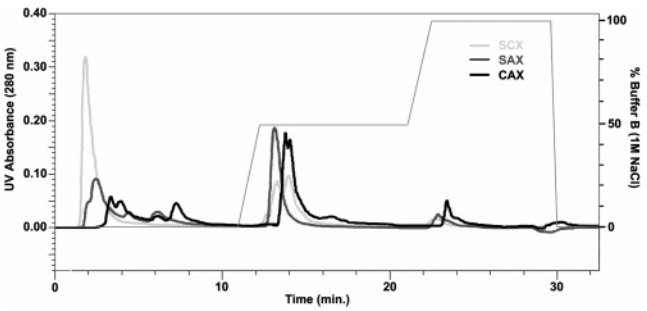

Figure 4. Recovery and retention of CAX-PAGE separation. Chromatogram of rat cerebellum tissue lysate (750 μg) performed with SCX, SAX, and CAX with two-step elution processes.

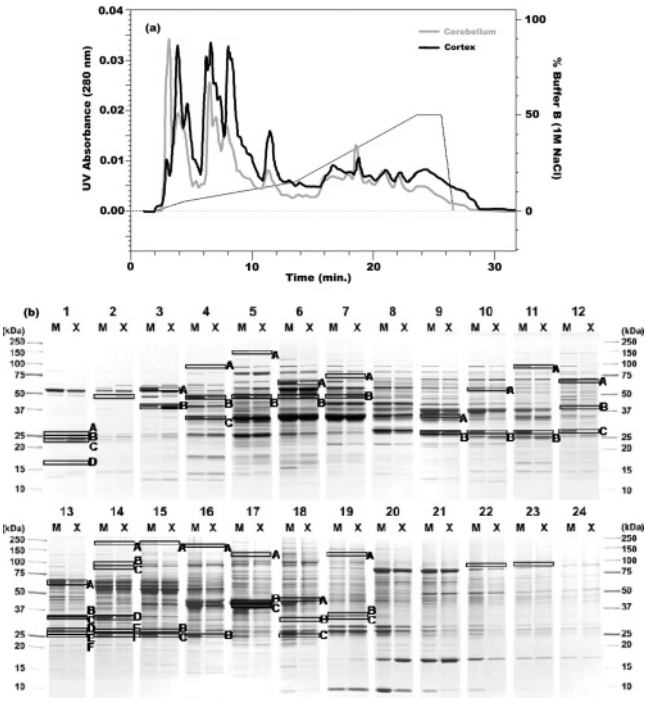

Figure 5. Comparison of rat cerebellum and cortex proteomes via sequential CAX and side-by-side 1D-PAGE. (a) Overlay of cerebellum and cortex CAX chromatograms at 280 nm. (b) Side-by-side (M, cerebellum on left; X, cortex on right) pairing of 25 fractions run on 1D-PAGE. Boxed bands were excised for protein identification; note letter labeling for correlation with Tables 1 and 2.

and 5.7 (37%) for SCX. Increased retention, the motivation for CAX, affords the ability to evenly distribute complex protein mixtures across an expandable number of fractions using gradient optimization (see Figure 4).

Differential Expression Analysis. The potential of CAX-PAGE is realized during differential expression profiling. Chromatographic differences are observed in Figure 5a between cerebellum and cortex lysates sequentially separated by CAX. For differential analysis, fractions from each run are paired and run side by side on 1D-PAGE (Figure 5b), whereby problems of gel-to-gel reproducibility are avoided through comparing matching fractions on the same gel. Side-by-side fraction pairing also allows for direct visualization of differential expression using simple, cost-efficient, visible stains (e.g., Coomassie Blue or silver).[40] Fluorescent stains such as Sypro Ruby and Deep Purple also work well, though they require a more expensive fluorescence scanner (three times the cost of the liquid chromatography system). The

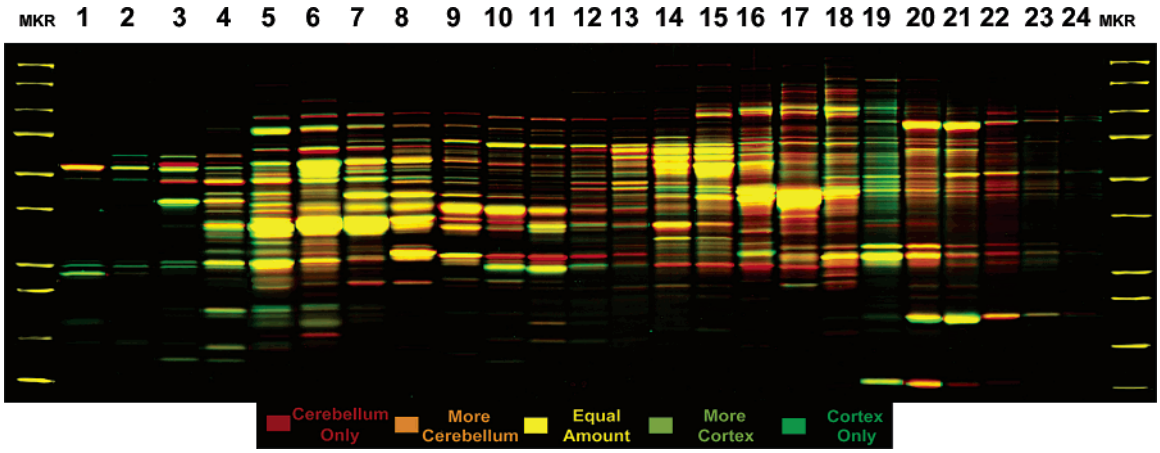

Figure 6. Colorized rat cerebellum−cortex differential proteome display after CAX-PAGE. The colorized display was performed by overlaying adjacent lanes from Figure 5b false-colored red for cerebellum and green for cortex. Color aids in manual inspection of the differential separation.

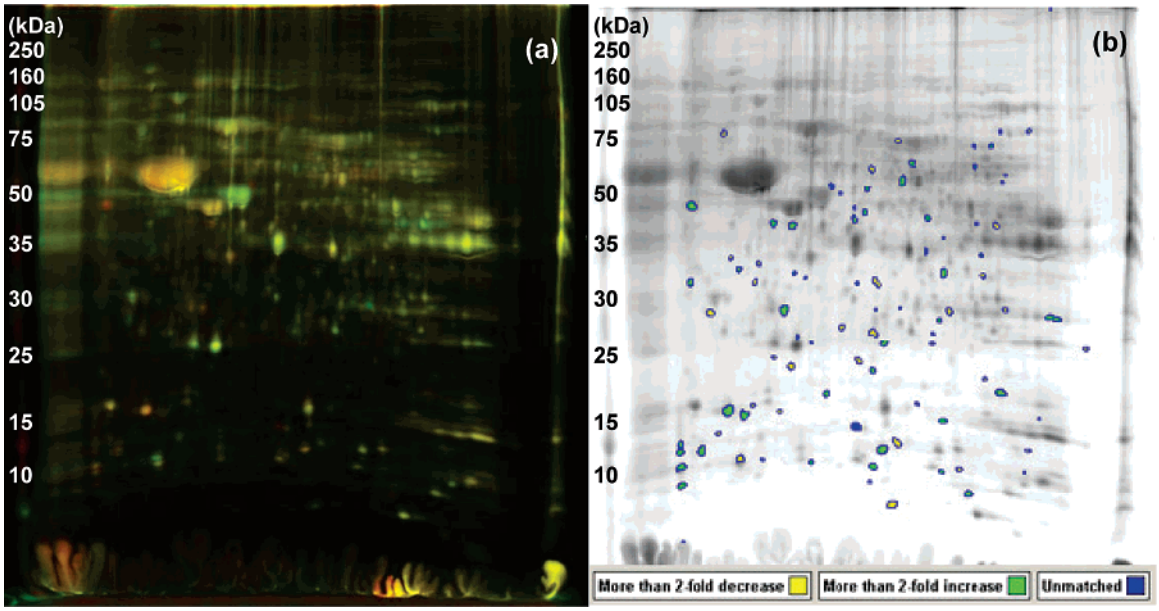

Figure 7. Rat cerebellum−cortex differential proteome display using 2D-DIGE. 2D-DIGE display of the pooled cerebellum and cortex lysates used with CAX-PAGE. (a) False-color overlay of cortex Cy3 (green) and cerebellum Cy5 (red)-labeled DIGE images. (b) Results of 2D differential software analysis comparing cortex and cerebellum tissue. Spots with a 2-fold difference between samples are indicated by yellow for greater in cortex and green for greater in cerebellum, while blue indicates spots found only in one sample.

Phoretix software was able to automatically identify gel lanes having a clear boundary along the *x*-axis; however, band height was sometimes more difficult to distinguish, requiring manual verification. A threshold of a 2-fold difference in band density between cerebellum and cortex data was used to generate a list of target bands for further analysis, whereby the mass spectrometry workload was minimized.

CAX-PAGE Differential Colorization. A false-colorization scheme can also be used to aide manual inspection of differential expression, creating images (Figure 6) similar to those produced with 2D-DIGE (Figure 7a). The colorized image was generated by converting adjacent cortex and cerebellum lanes into green and red, respectively, and superimposing the two. The human eye is adept at recognizing slight color shifts (away from yellow at equal expression) more so than recognizing slight changes in gray band intensity. The colorization map was useful for confirming Phoretix 1D output, particularly in cases of band overlap.

Comparing Differential Analysis by CAX-PAGE and 2D-DIGE. Analysis of the same cortex and cerebellum tissue lysates was performed by 2D-DIGE as a benchmark for evaluating CAX-PAGE. The Cy3 and Cy5 images shown overlaid in Figure 7a were compared using Phoretix 2D image analysis software with the result illustrated in Figure 7b. Using 2D-DIGE, 45 spots were discerned as more than twice as prominent in cerebellum and 37 spots were more than twice as prominent in cortex (Figure 7b) for a total of 82 differential protein targets. In comparison, CAX-PAGE revealed 105 band intensities more than twice as prominent in cerebellum and 41 bands more than twice as prominent in cortex for a total of 146 targets.

Proteins of high concentration pose a problem by masking less abundant proteins in both techniques. Those that show up as large spots with 2D-DIGE, separate across multiple fractions with CAX-PAGE (confirmed by RPLC-MSMS analysis), presenting an additional problem by increasing the number of apparent targets.

Nine of the 146 band pairs were redundant, reducing the number of targets to 137, still 67% more than observed by 2D-DIGE.

CAX-PAGE provided an improved mass range for differential analysis when compared with 2D-DIGE. Of the 137 differential targets, 13 were at a mass of 100 kDa or greater. In comparison, none of the differential targets uncovered by 2D-DIGE were above 100 kDa. The ability to discern differences at high mass is particularly relevant in brain injury paradigms where cytoskeletal proteins of great mass (e.g., MAPs and spectrins) are particularly prone to proteolysis associated with neuronal death after brain injury.[51−53]

In practice, we found numerous difficulties using 2D-DIGE that were absent when using CAX-PAGE. Signal intensity differed somewhat between the two cyanine dyes as noted by others,[17] giving a bias toward green or red from one gel to the next. Known problems with the stoichiometric ratio of protein to dye have been cited,[7] possibly explaining the observation. As well, more background was detected at the emission wavelength for Cy3 over Cy5, making fainter spots more difficult to discern. Rapid photobleaching made the technique difficult to use,[41] as sensitivity was quickly effected. This potentially is improved with the new saturation 2D-DIGE dyes.[54] Overall, upon comparing the two techniques, CAX-PAGE showed improved differential determination in this initial study, illustrating that CAX-PAGE can identify differential targets in a robust and cost-effective manner, and outperforms 2D-DIGE for analysis of high-mass proteins.

Resolving Power of CAX-PAGE. The most common means for comparing multidimensional separations is the use of theoretical peak capacity (n_c).[55] For 2D-PAGE, total n_c can be determined from the final spot dimensions (*x*- and *y*-axis width values) divided into the length of separation for each axis. From Figure 7, the *x*-axis n_c was 73.5 and *y*-axis n_c 74.0. This generates a theoretical total n_c of 5440 for 2D-DIGE, about the average for 2D-PAGE as cited in the literature ($10^3 - 10^4$).[22,56]

CAX-PAGE has an *x*-axis n_c equal to the fraction number, in this case 25, about one-third that of IEF, but CAX-PAGE has twice the peak capacity of 2D-PAGE along the *y*-axis at 143 due to the narrower band height achieved as a result of the larger *x*-axis width and the 1D-PAGE stacking gel region. Despite a shorter gel length, greater *y*-axis n_c of CAX-PAGE partially compensates for the small fraction number, producing a total n_c of 3570, which is 34.4% shy of that calculated for 2D-DIGE. However, calculating peak capacity based on working area, a rectangular separation space beyond which no proteins migrate, brings the values for CAX-PAGE and 2D-DIGE closer at 3120 and 4030, respectively. A recent improvement to CAX-PAGE has been shown using larger format commercial gels with an increased *y*-axis n_c of 211, and if combined with an expansion of CAX separations to 36 fractions (two gels per sample), a theoretical peak capacity of 7600 can be achieved.

CAX-PAGE resolution is comparable with other published 2D protein separation techniques,[21,22,28,30,31,57] that have first-dimension n_c values between 15 and 80 and second-dimension n_c values around 100 for combined values on the order of 10^3. In practice, all of these techniques can be viewed as complementary rather than exclusive, as they use different physical properties for separation, and none fully resolve an entire proteome. However, in the specific application of biomarker discovery, for which CAX-PAGE was developed, separation of an entire proteome is not necessary as only the most prominent proteins that demonstrate a clear expression change are of interest. CAX-PAGE in this case is advantageous as a protein separation and selection technique placed prior to RPLC-MSMS protein identification.

Differential Quantification and Protein Identification by Capillary RPLC-MSMS. A notable advantage of CAX-PAGE over 2D-DIGE[7,58] is the maintenance of spatial separation between samples, such that a second means of protein quantification can be performed. This is advantageous since 2D protein separations, having theoretical peak capacities of 10^3, are unlikely to fully resolve each protein into a single gel spot, band, or chromatographic fraction. This leaves doubt as to which identified protein is actually differentially expressed,[10,11] a common problem not generally addressed. In our platform, secondary quantification by MSMS verifies the identity of the differentially expressed protein.

To proceed, three logical assumptions were made with regard to the MSMS data. The first, (i), was that a protein producing a visible band would be identified by two or more peptides using strict Sequest cross-correlation values,[46] since the detection limit of Coomassie stain and dynamic exclusion MSMS are similar. The second assumption, (ii), was that proteins producing a 2-fold difference in band density would have similar or greater expression relative to background proteins. The last, (iii), was that only a differentially expressed protein (2-fold or greater difference) would exhibit a discernible change in peptide coverage[59,60] between the two samples.

To evaluate the protocol, two protein groups were selected for RPLC-MSMS analysis: (1) a random selection of differential band pairs, as listed in Table 1, the CAX-PAGE differential target list; and (2) a random selection of nondifferential band pairs of similar intensity as listed in Table 2. In total, 85% of MSMS runs fulfilled the first assumption i, irrespective of whether the band was differential or not. The 15% not conclusively identified were generally low-intensity bands. Enhanced mass spectrometers, such as the new linear ion traps, should improve protein identification in these cases.

Assessing assumptions ii and iii, we compared how often MSMS quantification matched, did not match, or was inconclusive (<2 peptide difference) when compared with band density data. With the differential target group (Table 1), both peptide number and band density reflected higher expression in the same tissue 89% of the time. Inconclusive MSMS quantification occurred 7% of the time, and only one case (4%) showed quantification that did not match. The matching rate of 89% demonstrated the effectiveness of dual quantification for internal verification of a differential protein's identity. In contrast, band density and MSMS quantification in the nondifferential target group (Table 2) were just as likely to match (28%) as mismatch (28%) with most showing an inconclusive determination (44%), demonstrating that the quantification correlation observed for the differential target group was not a random occurrence.

Summary of Differential Findings. The differentially identified proteins shown in Table 1 fit into three distinct protein classes known to be prominent in the brain,[58] listed here in order of prevalence: (1) metabolic enzymes such as α-enolase, pyruvate kinase 3, transketolase, GMP synthase, fatty acid synthase, etc.; (2) neuronal function proteins such as calbindins 1 and 2, translin,

Table 1. Quantification and Identification Results of Gel Band Pairs Showing Greater Than a Twofold Difference in Intensity between Cerebellum and Cortex—Differential Target List

gel data			MSMS data					data base search results		
excised band	gel band MW	% M to X diff[a]	expressed greater by MSMS[b]	no. peptides in M	M % protein covered	no. peptides in X	X % protein covered	ID'd protein MW	rat protein identified	accession no.
2	46.3	2094	X	0	0	2	5.3	47.2	α-enolase (enolase 1)	NP_036686.1
3A	53.0	−8256	M	12	22.2	0	0	57.8	pyruvate kinase 3	NP_445749.1
4A	72.5	−391	X	4	5	0	0	76.7	transferrin	NP_058751.1
5A	148.3	−365	M	6	3.5	3	2	180.1	amylo-1,6-glucosidease	XP_342332.1
6A	61.3	−101	M	10	14.5	5	8.3	71.2	transketolase	NP_072114.1
6C	15.1	−288	M	3	16.2	0	0	15.9	coactosin-like 1	XP_341701.1
7A	71.7	−178	M	3	4.4	0	0	76.7	transferrin	NP_058751.1
			M	2	3.6	0	0	70.8	GMP synthase	XP_215574.2
10A	53.8	−143	M	11	17.7	7	13.1	57.8	pyruvate kinase 3	NP_445749.1
			M	3	5.9	0	0	58	WD repeat containing protein 1	XP_341229.1
10B	27.5	−359	M	6	23.3	3	14.4	31.4	calbindin 2	NP_446440.1
11A	88.7	−168	M	3	3.5	0	0	95.3	trans elongation factor 2	NP_058914.1
11B	27.4	−443	M	9	22.5	7	29.9	31.4	calbindin 2	NP_446440.1
12A	61.5	−634	M	6	9.1	0	0	68.7	albumin	NP_599153.1
12C	27.5	−308	M	2	10.3	0	0	28.8	chloride intracellular channel 4	NP_446055.1
			M	2	8.3	0	0	25.6	platelet-activating factor acetylhydrolase	NP_446106.1
			M/X	5	16.2	5	21.4	31.4	calbindin 2	NP_446440.1
13D	28.1	−740	X	3	7.7	5	19.2	31.4	calbindin 2	NP_446440.1
13E	26.1	−1135	M	5	17.2	0	0	30	calbindin 1	NP_114190.1
13F	24.9	768	M/X	1	7.8	2	13.2	23.2	ρ-GDP dissociation inhibitor α	XP_340776.1
14A	222.5	−2170	M	6	3	0	0	273	fatty acid synthase	NP_059028.1
14B	100.0	−186	M	3	3.7	0	0	105.6	hexokinase 1	NP_036866.1
			M	2	1.8	0	0	118	insulinase (insulusin)	NP_037291.1
14C	89.2	−631	M	8	10.5	1	1.4	96.7	brain glycoprotein phosphorylase	XP_342543.1
14E	27.5	−910	M	3	12.3	0	0	30	carbonyl reductase	NP_062043.1
14F	25.8	−491	M	7	17.2	3	11.1	30	calbindin 1	NP_114190.1
15A	235.9	−208	M	5	2.1	0	0	273	fatty acid synthase	NP_059028.1
15C	26.1	−172	M	6	27.6	3	13.4	30	calbindin 1	NP_114190.1
16A	236.5	−215								
16B	25.9	−240	M	9	21.5	3	13.4	30	calbindin 1	NP_114190.1
			M	2	5.4	0	0	30	cerebellar Ca-binding protein	NP_114190.1
			M	3	16.2	0	0	26.2	translin	NP_068530.1
17A	119.3	−172	M	2	1.8	0	0	145.9	Ca-dependent activator secretion protein	NP_037351.1
18B	21.7	−586								
18C	20.1	−171	M	7		4		27	TYR 2-monooxygenase (14−3−3) ζ,η,θ	NP_062249.1
			M	2	7.3	0	0	30	calbindin 1	NP_114190.1
19A	116.4	−220	M/X	0	0	3	2.2	198.8	microtubule-associated protein 2	NP_037198.1
- -	150.0	-	M/X	3	12.6	0	0	42	brain creatin kinase	NP_036661.2
19B	22.7	227								
19C	21.6	−581	M	3	12.1	0	0	33	carbonic anhydrates 8	XP_226204.2
22	93.4	−199								
23	96.2	−297								

[a] Greater band intensity is indicated as a positive value in cortex and a negative value in cerebellum. [b] M indicates two or more peptides found for cerebellum over cortex; X indicates the opposite; M/X indicates a one- or no-peptide difference between tissues for that protein.

transferrin, etc.; and (3) cytoskeletal proteins such as chloride intracellular channel 4 and MAP2. Proteins were identified over a wide molecular mass distribution from 16 to 273 kDa. This is notably better than 2D-PAGE, which underrepresents proteins above 120 kDa due to poor diffusion into the IPG strip[7,61] and far exceeds the current mass range of top-down mass spectrometry approaches.[62] Another potential CAX-PAGE advantage is that hydrophobic membrane proteins are readily soluble in the loading buffer used, a known problem with 2D-PAGE.[61] However, this was not confirmed by this study, likely because membrane proteins are generally of low abundance and only 53 bands were analyzed by RPLC-MSMS. Future studies employing a membrane protein subproteome would be better able to address this point.

Remaining Challenges. Relative to other 2D separations, CAX-PAGE can be difficult to automate, mainly due to the sample concentration between CAX and 1D-PAGE. An envisioned solution is to use smaller i.d. ion-exchange columns to provide increased column efficiency and reduced fraction size for direct gel loading.

(62) Meng, F.; Du, Y.; Miller, L. M.; Patrie, S. M.; Robinson, D. E.; Kelleher, N. L. *Anal. Chem.* **2004**, *76*, 2852−2858.

Table 2. Quantification and Identification Results of Gel Band Pairs Showing Less Than a Twofold Difference in Intensity between Cerebellum and Cortex—Nondifferential Target List

gel data			MSMS data					data base search results		
excised band	gel band MW	% M to X diff[a]	expressed greater by MSMS[b]	no. peptides in M	M % protein covered	no. peptides in X	X % protein covered	ID'd protein MW	rat protein identified	accession no.
1A	25.9	64	M	5	20.7	3	10.6	25.9	glutathione *S*-transferase	NP_058710.1
1B	24.7	81	M/X	4	15.3	5	20.7	25.9	glutathione *S*-transferase	NP_058710.1
1C	23.2	36	M/X	2	5.6	3	10.6	25.9	glutathione *S*-transferase	NP_058710.1
1D	16.4	77	X	2	10.5	6	25.6	22.1	peroxiredoxin 5 precursor	NP_446062.1
3B	39.3	90	M/X	7	18.2	6	12.8	46.3	glutamate oxaloacetate transaminase 1	NP_036703.1
4B	45.6	−53	M	7	11.5	3	7.6	47.2	α-enolase (enolase 1)	NP_036686.1
4C	32.3	−34	M	5	21.5	3	9	34.7	pyridoxal kinase	XP_342113.1
5B	47.1	−17	M/X	5	9.7	4	7.6	47.2	α-enolase (enolase 1)	NP_036686.1
6B	46.3	28	X	3	7.6	5	7.6	47.2	α-enolase (enolase 1)	NP_036686.1
7B	47.8	70	X	3	5.3	10	14.5	47.2	α-enolase (enolase 1)	NP_036686.1
9A	34.5	−85	X	3	11	5	15.2	39.5	aldolase	NP_036629.1
9B	27.4	−32	X	2	8.3	5	24.4	28.9	phosphoglycerate mutase 1	NP_445742.1
12B	33.4	−5								
13A	60.9	−85	M/X	9	17.9	8	16.3	68.7	albumin	NP_599153.1
13B	33.6	−16	M/X	5	15.6	6	18.3	36.6	lactate dehydrogenase B	NP_036727.1
13C	32.2	51	M	5	16.9	3	9.5	35.6	malate dehydrogenase B	NP_112413.2
14D	33.6	−73	M/X	8	20.1	7	21	36.6	lactate dehydrogenase B	NP_036727.1
15B	27.8	0	M	4	14.4	1	5.9	31.4	calbindin 2	NP_446440.1
17B	35.5	−12	M/X	7	19.1	8	15.7	42	brain creatine kinase	NP_036661.2
17C	29.5	10								
18A	34.3	−67								

[a] Greater band intensity is indicated as a positive value in cortex and a negative value in cerebellum. [b] M indicates two or more peptides found for cerebellum over cortex; X indicates the opposite; M/X indicates a one- or no-peptide difference between tissues for that protein.

CAX-PAGE automation would then be similar to other 2D techniques that use fraction collection between dimensions. Protein immobilization within a gel matrix may also be viewed as a difficulty for automation; however, high-throughput staining, robotic band excision, and robotic digestion have already been developed for 2D-PAGE and would work equally well for CAX-PAGE. After robotic digestion, samples are autonimously placed into 96-well plates that interface with a capillary RPLC-MSMS autosampler.

Multiplexing large numbers of samples may prove difficult by CAX-PAGE/RPLC-MSMS. The platform works as long as the same fraction from each sample is grouped on a single gel (i.e., fraction 1 from each sample on gel 1, etc.). The maximum number of multiplexed samples is determined by the number of lanes within a single gel (up to 19 samples with large-format 20-well gels—1 lane for protein mass makers). In preliminary experiments, we have successfully multiplexed three samples.

CAX-PAGE/RPLC-MSMS in comparison with other separations strategies does not provide a direct measure of pI, which would be useful when 2D maps are employed for protein identification, as often done with 2D-PAGE. Preliminary investigation shows an apparent correlation between CAX elution and pI, though the precision was low. Foreseeably, a CAX fraction could be assigned a pI range as a means to confirm protein identity. On the other hand, CAX-PAGE provides protein mass, another good parameter to confirm protein identity that is not determined using 2D proteins separations with RPLC as the second dimension.

Dynamic range is a major complication for differential analysis, irrespective of the platform.[63] RPLC-MSMS performed in data-dependent mode has a low dynamic range due to possible signal saturation and poor ionization that can prevent triggering of MSMS scans. This negates possible CAX-PAGE improvements in protein detection using more sensitive stains. If differential analysis was performed exclusively by CAX-PAGE, then single peptide information could be used to identify proteins; however, the false positive rate would increase as the differential protein cannot clearly be distinguished from background proteins. Use of more sample, possible with the high capacity of CAX, could also help in detecting less abundant proteins up to a point. More sensitive MSMS analysis methods and instrumentation will ultimately aide identification of lower abundant proteins.

CONCLUSIONS

A novel approach was presented based on combining bipolarity ion-exchange chromatography in tandem with gel electrophoresis for protein separations, followed by capillary reversed-phase liquid chromatography online with tandem mass spectrometry for targeted peptide analysis. The platform is straightforward to perform, utilizing cost-effective traditional visualization stains and two quantification steps for internal verification of differential protein determinations. The platform was demonstrated for differential analysis comparing between cerebellum and cortex tissues, a test model for biomarker discovery in brain. Future

(63) Ahmed, N.; Rise, G. E. *J. Chromatogr., B* **2005**, *815*, 39−50.
(64) Posmantur, R. M.; Kampfl, A.; Taft, W. C.; Bhattacharjee, M.; Dixon, C. E.; Bao, J.; Hayes, R. L. *J. Neurotrauma* **1996**, *13*, 125−137.
(65) Wang, K. K. W. *Trends Neurosci. 23*, 20−26.
(66) Pike, B. R.; Flint, J.; Johnson, E.; Glenn, C. C.; Dutta, S.; Wang, K. K. W.; Hayes, R. L. *J. Neurochem.* **2001**, *78*, 1297−1306.
(67) Wang, K. K. W.; Ottens, A. K.; Haskins, W. E.; Liu, M. C.; Kobeissy, F. H.; Denslow, N. D.; Chen, S.; Hayes, R. L. In *Human Brain Proteome*; Neuhold, E. L., Ed.; Elsevier: New York, 2004; pp 215−340.
(68) McDonald, W. H.; Yates J. R. *Dis. Markers* **2002**, *18*, 99−105.
(69) Fountoulakis, M. *Amino Acids* **2001**, *21*, 363−381.

efforts are focused on improving chromatographic efficiency for direct coupling with larger format 1D-PAGE and applying the platform to biomarker discovery for clinical diagnostics of traumatic brain injury, stroke, and substance abuse.[7,36,64−69]

ACKNOWLEDGMENT

We offer our special thanks to Prof. W. W. Harrison for assistance in editing the manuscript. Our appreciation to Marjorie Chow and Timothy Chmielewski of the University of Florida Interdisciplinary Center for Biotechnology Research Protein Core Facility for performing the 2D-DIGE. This research is supported by funding from the Department of Defense, Grant DAMD17-03-1-0066.

Received for review March 21, 2005. Accepted May 22, 2005.

AC050478R

JOURNAL OF NEUROTRAUMA
Volume 22, Number 6, 2005

Pp. 629–644

Rapid Discovery of Putative Protein Biomarkers of Traumatic Brain Injury by SDS–PAGE–Capillary Liquid Chromatography–Tandem Mass Spectrometry

WILLIAM E. HASKINS,[1,2,4] FIRAS H. KOBEISSY,[1,2,3] REGINA A. WOLPER,[1,2,4] ANDREW K. OTTENS,[1,2,4] JASON W. KITLEN,[2,4] SCOTT H. McCLUNG,[5] BARBARA E. O'STEEN,[2,4] MARJORIE M. CHOW,[5] JOSE A. PINEDA,[2] NANCY D. DENSLOW,[1,5] RONALD L. HAYES,[2,3,4] and KEVIN K.W. WANG[1,2,3,4]

ABSTRACT

We report the rapid discovery of putative protein biomarkers of traumatic brain injury (TBI) by SDS–PAGE–capillary liquid chromatography–tandem mass spectrometry (SDS–PAGE–Capillary LC–MS^2). Ipsilateral hippocampus (IH) samples were collected from naive rats and rats subjected to controlled cortical impact (a rodent model of TBI). Protein database searching with 15,558 uninterpreted MS^2 spectra, collected in 3 days via data-dependent capillary LC-MS^2 of pooled cyanine dye-labeled samples separated by SDS-PAGE, identified more than 306 unique proteins. Differential proteomic analysis revealed differences in protein sequence coverage for 170 mammalian proteins (57 in naive only, 74 in injured only, and 39 of 64 in both), suggesting these are putative biomarkers of TBI. Confidence in our results was obtained by the presence of several known biomarkers of TBI (including αII-spectrin, brain creatine kinase, and neuron-specific enolase) in our data set. These results show that SDS-PAGE prior to *in vitro* proteolysis and capillary LC-MS^2 is a promising strategy for the rapid discovery of putative protein biomarkers associated with a specific physiological state (i.e., TBI) without *a priori* knowledge of the molecules involved.

Key words: controlled cortical impact (CCI); differential in-gel electrophoresis (DIGE); sodium dodecyl sulfate–polyacrylamide gel electrophoresis (SDS-PAGE); tandem mass spectometry (MS^2); traumatic brain injury (TBI)

INTRODUCTION

TRAUMATIC BRAIN INJURY (TBI), defined as brain damage due to mechanical force applied to the head, has an incidence of approximately 2 million persons annually in the United States with an annual economic cost of $25 billion. Thus, accurate diagnosis following TBI is crucial for appropriate clinical management of TBI patients and for reducing costs. Current assessment tools of TBI include computed tomography and magnetic resonance imaging. Despite the accuracy of these techniques, TBI survivors suffer long-term impairment due to late di-

[1]Center of Neuroproteomics and Biomarkers Research, [2]Center for Traumatic Brain Injury Studies, Departments of [3]Psychiatry and [4]Neuroscience, and [5]Interdisciplinary Center of Biotechnology Research University of Florida, Gainesville, Florida.

agnosis and unguided clinical management. Therefore, increased interest in the discovery of biomarkers that are indicative of injury severity and anatomical localization has been realized in recent years.

Several laboratories have examined a number of biological molecules in cerebral spinal fluid (CSF) and blood from TBI patients in an effort to discover TBI-specific molecules (Pike et al., 2002; Varma et al., 2003; Zemlan et al., 2002; Berger et al., 2002; Raabe et al., 2003). For example, our laboratory reported the discovery of nonerythroid αII-spectrin and its protease-specific degradation products as biomarkers of TBI (Pike et al., 2002). However, a major limitation of currently described biomarkers is a lack of TBI specificity and a poor understanding of the biochemical mechanisms of brain trauma. Thus, the discovery of novel protein biomarkers of TBI that serve as reliable indicators of injury severity would be highly beneficial for predicting outcome and managing patients (Denslow et al., 2003). Moreover, novel biomarkers of TBI, particularly neurodegenerative and neuroprotective proteins, provide insights on pathophysiology and may serve as therapeutic targets for various neurological diseases.

Rapid discovery of protein biomarkers in complex samples by state-of-the-art mass spectrometry methods, capable of identifying thousands of proteins in a single sample by protease-specific peptide sequences, is precluded by several limitations. "Shotgun" capillary liquid chromatography (LC)–tandem mass spectrometry (MS^2) methods (McDonald and Yates, 2002) require extended analysis times for each sample (days) and information about post-translational modifications (PTMs), particularly protein degradation, is often lost during *in vitro* proteolysis (e.g., trypsination). Liquid-phase protein separation (e.g., 2D gels and LC-LC) prior to *in vitro* proteolysis and capillary LC-MS^2, preserves more information about PTMs, but can require 10–100-fold more sample and even greater analysis times for complete characterization (weeks). Reproducible replicate analysis, required for preliminary biomarker validation, and limited resources (e.g., mass spectrometer time) further compound these problems.

Recently, the large dynamic range and high quantum yield of cyanine dye-labeled proteins were combined with 2D gels in order to improve gel-to-gel reproducibility and reduce analysis time via sample multiplexing (Gharbi et al., 2002; Leimgruber et al., 2002; Macdonald et al., 2001, Tonge et al., 2001). This technique, differential in-gel electrophoresis (DIGE), provides quantitative information complementary to isotope coded affinity tag (ICAT)–capillary LC–MS^2 approaches (Gygi et al., 1999), while preserving more information about PTMs. DIGE also provides a reduction in analysis time because only gel spots with a significant difference in the ratio of their fluorescence signals need to be targeted for protein identification by mass spectrometry (Gharbi et al., 2002; Kernec et al., 2001; Shaw et al., 2003; Tonge et al., 2001; Yan et al., 2002). However, poorly resolved proteins elude identification, while well-resolved, multiply labeled, proteins produce redundant identifications. Given our emphasis on rapid analysis, rather than more comprehensive characterization, we selected the limited resolving power of SDS-PAGE as an effective means to reduce redundant identifications and accelerate the discovery of putative protein biomarkers.

In this report, we describe the application of a novel differential analysis strategy, SDS-PAGE–capillary liquid chromatography–tandem mass spectrometry (SDS-PAGE–Capillary LC–MS^2), to the discovery of putative protein biomarkers of TBI in hippocampus tissue. Herein, protein database searching of uninterpreted MS^2 spectra, collected via data-dependent capillary LC–MS^2 of pooled cyanine dye-labeled samples separated by SDS-PAGE, was combined with differential proteomic analysis. We hypothesized that a subset of putative protein biomarkers of TBI, including some with PTMs, would be rapidly revealed by comparing the protein sequence coverage of naive and injured samples.

MATERIALS AND METHODS

Chemicals and Reagents

The chemicals and reagents used are described elsewhere (Haskins et al., 2001). Tryptic digests were purchased from Michrom Bioresources (Auburn, CA) for use as quality control standards. Cyanine dye labeling reagents were purchased from Amersham Biosciences (Piscataway, NJ).

Controlled Cortical Impact

The controlled cortical impact (CCI) device used to model TBI in male Sprague-Dawley rats was described in detail elsewhere (Pike et al., 2002). The magnitude of injury used in these studies produces significant cortical contusions and less overt injury that often extends into the region of the hippocampus (Posmantur et al., 1997; Dixon et al., 1991). Although overt hippocampal damage is not usually associated with this model, there is evidence of increased pathological calpain-mediated proteolysis in the hippocampus following cortical impact injury (Newcomb et al., 1997). Cortical impact injury is usually associated with intraparenchymal hemorrhage and dural disruption, but extensive subdural hemorrhage is not a primary feature of this model. The

adult rats were anesthetized with 4% isoflurane in a carrier gas of 1:1 O_2/N_2O (4 min) followed by maintenance anesthesia of 2.5% isoflurane in the same carrier gas. Core body temperature was monitored continuously by a rectal thermistor probe and maintained at 37 ± 1°C by placing an adjustable temperature controlled heating pad beneath the rats. Animals were mounted in a stereotactic frame in a prone position and secured by ear and incisor bars. A midline cranial incision was made, the soft tissues were reflected, and a unilateral (ipsilateral to site of impact) craniotomy (7 mm diameter) was performed adjacent to the central suture, midway between bregma and lambda. The dura mater was kept intact over the cortex. Brain trauma was produced by impacting the right cortex (ipsilateral cortex) with a 5-mm-diameter aluminum impactor tip (housed in a pneumatic cylinder) at a velocity of 3.5 m/sec with a 1.6-mm compression and 150-msec dwell time (compression duration). Velocity was controlled by adjusting the pressure (compressed N_2) supplied to the pneumatic cylinder. Velocity and dwell time were measured by a linear velocity displacement transducer (Lucas Shaevitz™ model 500 HR, Detroit, MI) that produced an analog signal that was recorded by a storage-trace oscilloscope (BK Precision, model 2522B, Placentia, CA). At 48 h post-injury, the animals were anesthetized with 4% isoflurane in a carrier gas of 1:1 O_2/N_2O (4 min) and subsequently sacrificed by decapitation. Hippocampus samples were rapidly dissected, washed with saline solution, snap-frozen in liquid nitrogen, and stored at −80°C until further processing. Naive animals underwent identical surgical procedures but did not receive an impact injury. Appropriate pre- and post-injury management was maintained to insure compliance with guidelines set forth by the University of Florida Institutional Animal Care and Use Committee and the National Institutes of Health guidelines detailed in the *Guide for the Care and Use of Laboratory Animals*.

Sample preparation. Hippocampus samples were homogenized in a glass tube with a Teflon dounce pestle in 15 volumes of ice-cold detergent-free buffer (50 mM Tris-HCl, pH 7.4, 1 mM EDTA, 2 mM EGTA, 0.33 M sucrose, 1 mM DTT) containing a broad-range protease inhibitor cocktail (Roche Molecular Biochemicals, no. 1-836-145) and sonicated. Samples were then centrifuged at 9000*g* for 5 min at 4°C. The supernatant was stored at −80°C. The protein concentration of each sample was determined by DC protein assay (Biorad, Hercules, CA) with albumin standards. Proteins were diluted to 5 $\mu g/\mu L$ in DIGE lysis buffer containing a 1% protease inhibitor cocktail (P8340, Sigma, St. Louis, MO) to prevent proteolysis during labeling.

SDS-PAGE. The Cyanine dye labeling reaction was performed with minimal labeling conditions (50 μg of protein at 5 $\mu g/\mu L$) per the manufacturer's instructions unless stated otherwise (Amersham, Piscataway, NJ). Labeled proteins from pooled and individual (naive or injured) samples were reduced with 5 mM DTT, alkylated with 55 mM iodoacetamide, and heated to 95°C for 2 min prior to separation with Tris-tricine SDS-PAGE gels (10–20% polyacrylamide, Invitrogen, Carlsbad, CA) at 4°C. Fluorescence imaging was performed with 1-sec exposure times (ProExpress, PerkinElmer, Boston, MA). Alternatively, unlabeled proteins were separated with the same gel system and stained with Coomassie blue. In both cases, image analysis (ImageJ, NIH) was performed to target specific regions of the gel; however, 1.5 mm × 4 mm gel slices spanning the entire gel lane were excised and stored at −80°C for trypsinization.

In vitro *proteolysis*. Excised gel bands were destained, reduced with 5 mM DTT, and alkylated with 55 mM iodoacetamide prior to overnight digestion with 400 ng of trypsin (Trypsin gold, Promega, Madison, WI) in 100 mM NH_4HCO_3.

Preparation of capillary LC columns with integrated electrospray emitters. The preparation of capillary LC columns with integrated electrospray emitters is described elsewhere (Haskins et al., 2001); however, 5 cm of 3-μm C18 particles (Alltima C18, Alltech, Deerfield, IL) and 50-μm-i.d. capillary LC columns were used in this work.

Automated two-pressure capillary LC-MS^2 system. The capillary LC-MS^2 system is described elsewhere (Haskins et al., 2001). The system utilizes 2 six-port valves to select the pump and flow path for preconcentration, desalting, and separation/electrospray steps. During the preconcentration and desalting steps the high-flow-rate pump was selected without splitting of the sample in order to minimize the sample loading time. During the separation/electrospray step, the low-flow-rate pump was selected with splitting of the gradient in order to maximize the separation and electrospray efficiency and to minimize the delay time of the gradient, respectively.

In this work, 4.5 μL from a 12-μL sample of tryptic peptides was transferred into a 2-μL sample loop with an autosampler and analyzed every 38 min by preconcentrating/desalting at 600 nL/min and separating/electrospraying at 60 nL/min. All measurements were made with the following capillary LC-MS^2 parameters, unless specified otherwise: preconcentration time = 3.3 min (2.0 μL), desalting time = 3.3 min (2.0 (L), separa-

tion/electrospray time = 30 min (10 min pump gradient from 5% to 45% mobile phase B; mobile phase A = 2% acetonitrile: 1% acetic acid; mobile phase B = 98% acetonitrile: 1% acetic acid), re-equilibration time = 1.4 min. The mass spectrometer was a QIT (LCQ-Deca XP+, ThermoFinnigan, San Jose, CA) with the following parameters, unless specified otherwise: automatic gain control (AGC) on, max AGC time = 300 msec, q = 0.25, isolation width = 3 *m/z*, normalized collision energy = 35%, activation time = 0.25 msec and the default number of microscans and target count values. Data-dependent MS/MS spectra (MS, 4 × MS/MS) were collected using a precursor ion window of *m/z* 400–1800 and a product ion window calculated for z = +2.

Differential proteomic analysis. Protein database searching (RefSeq 785,143 sequences (Pruitt and Maglott, 2001) with uninterpreted MS^2 spectra and differential proteomic analysis of unmodified proteins were performed with Sequest (Yates et al., 1998) and DTASelect (Tabb et al., 2002), respectively. The default precursor and product ion tolerances of 1.5 and 0.0 were selected for Sequest, while only singly, doubly, and triply charged tryptic peptide sequences with Xcorr > 1.8, 2.5, and 3.5 were considered significant for DTASelect. No molecular mass constraints were placed on protein identification by protein database searching. A TBI database containing unmodified peptide and protein sequences that were observed in naive only, injured only, or both conditions was constructed in-house (from the DTASelect files via Microsoft Access 2002) as a function of the 1D-DIGE gel position (gel slices were numbered 1–50 from high to low molecular mass). PTMs were investigated with Mascot (Perkins et al., 1999) using the same protein database as Sequest but with the recommended precursor and product ion tolerances of 2.0 and 0.8, respectively. PTMs were considered significant if the Mascot score indicated homology with greater than 95% probability.

RESULTS

SDS-PAGE-Capillary LC-MS²

Naive and injured hippocampal protein samples were processed and labeled with Cy-3 and Cy-5 dye separately. Labeled proteins from pooled and individual samples were separated side-by-side, and naive and injured samples were run on separate lanes (Fig. 1). Our results show the consistency in protein loading, cyanine dye labeling, and separation efficiency. Alternatively, unlabeled proteins were separated with the same gel system and stained with Coomassie blue (data not shown). In general, we did not find a significant advantage of cyanine-dye labeling for our purposes. Fifty 1.5 mm × 4 mm gel slices spanning each (naive or injured) gel lane were excised, trypsinized and subjected to automated capillary LC-MS^2. We collected 15,558 uninterpreted MS^2 spectra in 3 days for pooled cyanine dye-labeled samples separated by SDS-PAGE. Protein database searching identified more than 306 unique proteins. Overall, we obtained 156 ± 60 MS^2 spectra per gel slice and 1–3 tryptic peptide sequences per protein. Figure 2 shows the correlation between the database-derived molecular mass ($M_r$calc), and SDS-PAGE–predicted molecular mass ($M_r$obs). The migration of proteins in the SDS-PAGE gel inversely correlates with $M_r$calc for unmodified proteins identified by capillary LC-MS^2 and database searching (solid line), as expected. Accordingly, $M_r$obs directly correlates with $M_r$calc. In addition, protein sequence coverage shows an inverse correlation with $M_r$calc (dashed line). That is, the higher the molecular mass of the protein, the less sequence coverage is obtained. However, it is important to note that we have successfully identified (by peptide sequences rather than by peptide masses) more than 20 proteins of high molecular mass (150–300 kDa). In contrast, proteins in this molecular mass range are almost impossible to visualize and identify by 2D gels (Fountoulakis et al., 1999b).

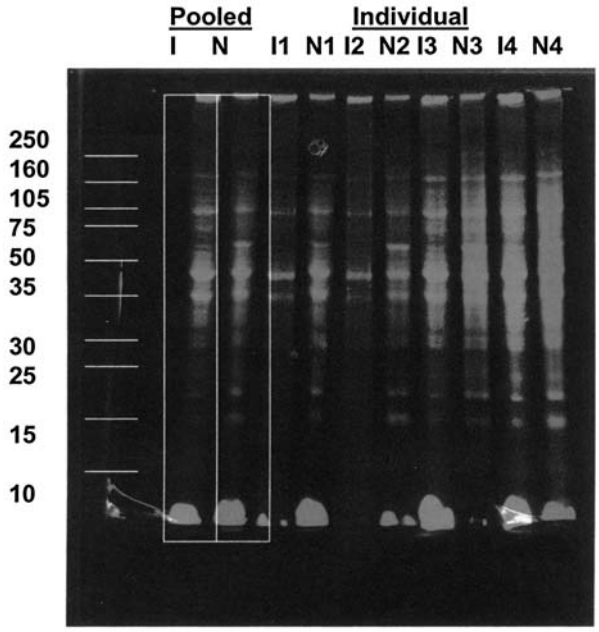

FIG. 1. Cyanine-dye labeled proteins separated by SDS-PAGE. Fluorescence image of 25 μg of Cy3– and Cy5–labeled proteins from naive (N) and injured (I) ipsilateral hippocampus (IH) samples separated on a Tris-tricine SDS-PAGE gel (10–20% polyacrylamide).

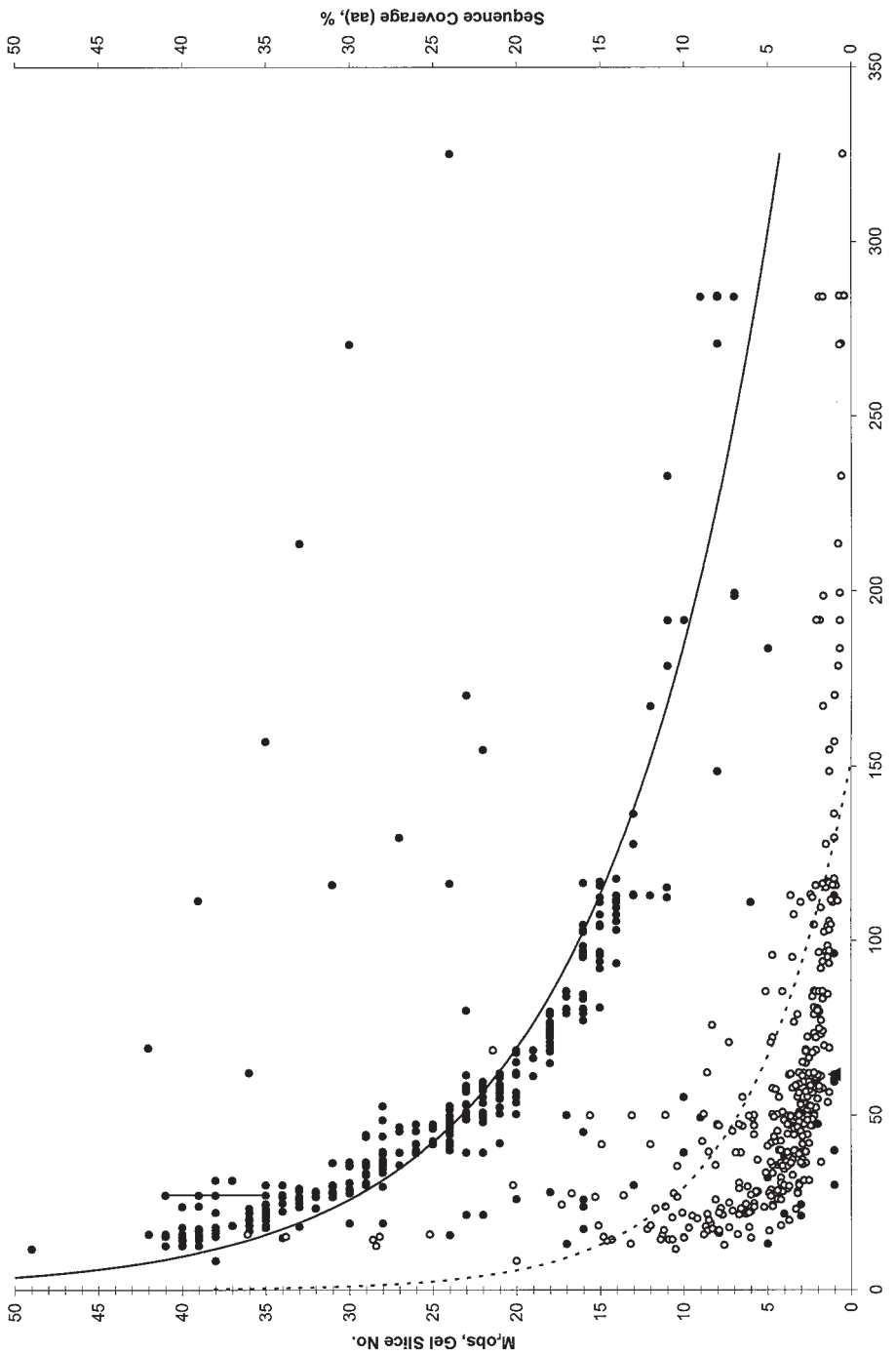

FIG. 2. Correlation between the database-derived molecular mass ($M_r$calc), and SDS-PAGE-predicted molecular mass ($M_r$obs). The migration of proteins in the SDS-PAGE gel inversely correlates with $M_r$calc for unmodified proteins identified by capillary LC-MS^2 and database searching (solid line), as expected. Accordingly, $M_r$obs directly correlates with $M_r$calc. In addition, protein sequence coverage shows an inverse correlation with $M_r$calc (dashed line).

Table 1. Differential Proteomic Analysis of Mammalian Protein

RefSeq accession number	*Protein description*	*$M_r$calc (kDa)*	*$M_r$obs (kDa)*
Protein appears in naïve animals only			
NM_022007	FXYD domain-containing ion transport regulator 7 [*Mus musculus*]	8	13–17
NM_181029	casein alpha-S1 [*Bos taurus*]	25	>250
NM_012966	heat shock 10 kDa protein 1 (chaperonin 10) [*Rattus norvegicus*]	11	10–13
NM_017236	phosphatidylethanolamine binding protein [*Rattus norvegicus*]	21	15–25
NM_018947	cytochrome c [*Homo sapiens*]	12	<10
NM_057114	peroxiredoxin 1 [*Rattus norvegicus*]	22	15–25
NM_022511	profilin [*Rattus norvegicus*]	15	10–15
NM_174294	casein kappa [*Bos taurus*]	21	>250
NM_028207	dual specificity phosphatase 3 [*Mus musculus*]	20	15–25
NM_016956	hemoglobin, beta adult minor chain; beta min; beta minor globin [*Mus musculus*]	16	10–15
NM_017169	thioredoxin peroxidase 1 [*Rattus norvegicus*]	22	15–25
NM_017055	transferrin [*Rattus norvegicus*]	76	50–75
NM_182839	RIKEN cDNA 2900041A09 [*Mus musculus*]	23	17–27
NM_010471	hippocalcin [*Mus musculus*]	22	15–25
NM_023716	tubulin, beta [*Mus musculus*]	50	35–50
NM_021316	BM88 antigen [*Mus musculus*]	15	15–25
NM_053511	neural F box protein NFB42 [*Rattus norvegicus*]	34	30–35
NM_009610	Actin, gamma 2 (smooth muscle) [*Mus musculus*]	42	40–60
NM_022922	triosephosphate isomerase 1 [*Rattus norvegicus*]	27	17–27
NM_019131	tropomyosin 1, alpha [*Rattus norvegicus*]	29	27–33
NM_012498	aldehyde reductase 1 [*Rattus norvegicus*]	36	13–17
NM_000410	hemochromatosis protein 1 [*Homo sapiens*]	10	35–50
NM_017025	lactate dehydrogenase A [*Rattus norvegicus*]	36	27–33
NM_008617	malate dehydrogenase, mitochondrial [*Mus musculus*]	35	27–33
NM_023716	RIKEN cDNA 2410129E14 gene [*Mus musculus*]	50	35–50
NM_002634	prohibitin [*Homo sapiens*]	30	17–27
NM_011553	t-complex protein 10b [*Mus musculus*]	49	>250
NM_001069	tubulin, beta polypeptide [*Homo sapiens*]	50	35–50
NM_002301	lactate dehydrogenase C [*Homo sapiens*]	36	27–33
NM_012949	enolase 3, beta; [*Rattus norvegicus*]	47	35–50
NM_014364	glyceraldehyde-3-phosphate dehydrogenase, testis-specific [*Homo sapiens*]	44	27–33
NM_013506	eukaryotic translation initiation factor 4A2 [*Mus musculus*]	46	35–50
NM_133977	transferrin; hypotransferrinemia with hemochromatosis [*Mus musculus*]	77	50–75
NM_003026	SH3-domain GRB2-like 2 [*Homo sapiens*]	40	33–40
NM_139254	tubulin, beta 3 [*Rattus norvegicus*]	50	35–50
NM_022399	calreticulin [*Rattus norvegicus*]	48	35–50
NM_031140	vimentin [*Rattus norvegicus*]	54	35–50
NM_012497	aldolase C, fructose-biphosphate [*Rattus norvegicus*]	39	33–40
NM_031034	guanine nucleotide binding protein (G protein) alpha 12 [*Rattus norvegicus*]	44	30–35
XM_236277	protein phosphatase PP2A [*Rattus norvegicus*]	65	50–75
NM_019225	solute carrier family 1, member 3 [*Rattus norvegicus*]	60	>250
NM_017009	glial fibrillary acidic protein [*Rattus norvegicus*]	50	35–50
NM_025407	ubiquinol-cytochrome c reductase core protein 1 [*Mus musculus*]	53	35–50
NM_145614	dihydrolipoamide S-acetyltransferase [*Mus musculus*]	68	50–75

Table 1. Differential Proteomic Analysis of Mammalian Protein (*Continued*)

RefSeq accession number	*Protein description*	*$M_r$calc (kDa)*	*$M_r$obs (kDa)*
NM_022229	heat shock protein 60 (chaperonin) [*Rattus norvegicus*]	61	40–60
NM_145518	NADH dehydrogenase (ubiquinone) Fe-S protein 1 [*Mus musculus*]	80	50–75
NM_175199	heat shock protein 12A [*Mus musculus*]	75	50–75
NM_008449	kinesin heavy chain 5C, neuron-specific [*Mus musculus*]	109	80–130
NM_031715	phosphofructokinase, muscle [*Rattus norvegicus*]	86	60–90
NM_145779	pregnancy-zone protein [*Rattus norvegicus*]	167	115–205
NM_013559	HSP105 [*Mus musculus*]	97	80–130
NM_031604	H^+ transporting ATPase, lysosomal (vacuolar proton pump) [*Rattus norvegicus*]	96	>250
NM_021343	spermatogenesis associated factor [*Mus musculus*]	97	75–105
NM_007804	cut-like 2 [*Mus musculus*]	155	35–50
NM_152296	ATPase, Na^+/K^+ transporting, alpha 3 polypeptide [*Homo sapiens*]	112	80–130
NM_054004	TBP-interacting protein 120A [*Rattus norvegicus*]	136	105–160
NM_019167	beta-spectrin 3 [*Rattus norvegicus*]	271	>250
Protein appears in injured animals only			
NM_003509	H2A histone family, member C [*Homo sapiens*]	14	10–15
NM_080777	synuclein, beta [*Rattus norvegicus*]	15	10–15
NM_000976	ribosomal protein L12 [*Homo sapiens*]	18	15–25
NM_025562	RIKEN cDNA 2010003O14 [*Mus musculus*]	17	13–17
NM_016068	CGI-135 protein [*Homo sapiens*]	17	13–17
NM_025313	RIKEN cDNA 0610008F14 [*Mus musculus*]	18	10–15
NM_026369	actin-related protein 2/3 complex, subunit 5 [*Mus musculus*]	16	13–17
NM_012038	visinin-like 1 [*Mus musculus*]	22	15–25
NM_009923	cyclic nucleotide phosphodiesterase 1 [*Mus musculus*]	47	35–50
NM_133796	Rho GDP dissociation inhibitor (GDI) alpha [*Mus musculus*]	23	17–27
NM_014231	VAMP-1A; synaptobrevin [*Homo sapiens*]	13	10–15
NM_017101	peptidylprolyl isomease A (cyclophilin A) [*Rattus norvegicus*]	18	10–15
NM_009001	RAB3A, member RAS oncogene family [*Mus musculus*]	25	15–25
NM_000518	beta globin [*Homo sapiens*]	16	10–15
NM_024349	adenylate kinase [*Rattus norvegicus*]	21	15–25
NM_031603	14-3-3 epsilon [*Rattus norvegicus*]	29	15–25
NM_017051	superoxide dismutase 2, mitochondrial [*Rattus norvegicus*]	25	15–25
NM_026267	RIKEN cDNA 1200016B17 [*Mus musculus*]	30	30–35
NM_008907	peptidylprolyl isomerase A; cyclophilin A [*Mus musculus*]	18	13–17
NM_053610	peroxiredoxin 5 precursor [*Rattus norvegicus*]	22	13–17
NM_016131	ras-related GTP-binding protein RAB10 [*Homo sapiens*]	23	15–25
NM_011670	ubiquitin carboxy-terminal hydrolase L1; gracile axonal dystrophy; protein gene product 9.5 [*Mus musculus*]	25	15–25
NM_019376	14-3-3 protein gamma [*Rattus norvegicus*]	28	17–27
NM_011739	14-3-3 theta [*Mus musculus*]	28	17–27
NM_010312	guanine nucleotide-binding protein, beta-2 subunit [*Mus musculus*]	37	30–35
NM_023200	protein phosphatase-1 regulatory subunit 7 [*Mus musculus*]	41	35–50
NM_019632	N-ethylmaleimide sensitive fusion protein attachment protein beta; brain protein I47 [*Mus musculus*]	34	27–33
NM_017327	GTP-binding protein alpha o; RATBPGTPC [*Rattus norvegicus*]	40	30–35
NM_026646	RIKEN cDNA 1300006L01 [*Mus musculus*]	35	30–35
NM_005165	aldolase C, fructose-bisphosphate; Aldolase C, fructose-bisphosphatase [*Homo sapiens*]	39	33–40

(*continued*)

Table 1. Differential Proteomic Analysis of Mammalian Protein (*Continued*)

RefSeq accession number	*Protein description*	*$M_r$calc (kDa)*	*$M_r$obs (kDa)*
NM_025942	RIKEN cDNA 2810409H07 [*Mus musculus*]	45	35–50
NM_019291	carbonic anhydrase 2 [*Rattus norvegicus*]	37	27–33
NM_017215	solute carrier family 1, member 2 [*Rattus norvegicus*]	62	>250
NM_005917	cytosolic malate dehydrogenase [*Homo sapiens*]	36	17–27
NM_006032	copine 6; neuronal copine; N-copine [*Homo sapiens*]	62	50–75
NM_006136	F-actin capping protein alpha-2 [*Homo sapiens*]	33	27–33
NM_002074	G protein, beta-1 subunit; transducin beta chain 1I [*Homo sapiens*]	37	30–35
NM_014203	adaptin, alpha A; [*Homo sapiens*]	108	80–130
NM_002635	phosphate carrier precursor isoform 1b; mitochondrial [*Homo sapiens*]	40	>250
NM_018754	stratifin; 14-3-3 sigm [*Mus musculus*]	28	17–27
NM_024221	pyruvate dehydrogenase (lipoamide) beta [*Mus musculus*]	39	30–35
NM_025899	ubiquinol cytochrome c reductase core protein 2 [*Mus musculus*]	48	35–50
NM_002300	lactate dehydrogenase B [*Homo sapiens*]	37	27–33
NM_012570	glutamate dehydrogenase 1; memory related gene 2 [*Rattus norvegicus*]	61	40–60
NM_138828	apolipoprotein E [*Rattus norvegicus*]	36	27–33
NM_013681	synapsin II [*Mus musculus*]	52	40–60
NM_033235	malate dehydrogenase 1[*Rattus norvegicus*]	36	27–33
NM_011861	protein kinase C and casein kinase substrate in neurons 1 [*Mus musculus*]	51	40–60
NM_004077	citrate synthase precursor; citrate synthase, mitochondrial [*Homo sapiens*]	52	35–50
NM_007505	ATP synthase, H^+ transporting, mitochondrial F1 complex, alpha subunit, isoform 1 [*Mus musculus*]	60	35–50
NM_057118	contactin 1 [*Rattus norvegicus*]	113	105–160
NM_010481	heat shock protein, A [*Mus musculus*]	74	50–75
NM_019703	phosphofructokinase [*Mus musculus*]	86	60–90
NM_012491	adducin 2, beta [*Rattus norvegicus*]	81	80–130
NM_003178	synapsin IIb [*Homo sapiens*]	52	40–60
NM_009947	copine VI; copine 6; neuronal copine [*Mus musculus*]	62	50–75
NM_011393	solute carrier family 1, member 2; glial high affinity glutamate transporter [*Mus musculus*]	61	>250
NM_153781	brain glycogen phosphorylase [*Mus musculus*]	97	75–105
NM_006644	heat shock 105 kD [*Homo sapiens*]	92	80–130
NM_031783	neurofilament, light polypeptide [*Rattus norvegicus*]	61	50–75
NM_006950	synapsin Ia [*Homo sapiens*]	74	50–75
NM_013066	microtubule-associated protein 2 [*Rattus norvegicus*]	199	>250
NM_021979	heat shock 70 kDa protein 2 [*Homo sapiens*]	70	50–75
NM_012607	neurofilament, heavy polypeptide [*Rattus norvegicus*]	115	115–205
NM_181092	synaptic Ras GTPase activating protein 1 [*Rattus norvegicus*]	128	105–160
NM_005348	heat shock 90 kDa protein 1, alpha [*Homo sapiens*]	85	75–105
NM_010438	hexokinase 1; downeast anemia [*Mus musculus*]	106	80–130
NM_000477	albumin precursor [*Homo sapiens*]	69	10–15
NM_001385	dihydropyrimidinase [*Homo sapiens*]	57	50–75
NM_001127	Seta-adaptin [*Homo sapiens*]	105	80–130
NM_003334	ubiquitin-activating enzyme E1 [*Homo sapiens*]	118	80–130
NM_001835	Clathrin, heavy chain [*Homo sapiens*]	179	115–205
NM_005657	tumor protein p53 binding protein, 1 [*Homo sapiens*]	214	15–25
NM_002374	microtubule-associated protein 2a [*Homo sapiens*]	199	>250

Table 1. Differential Proteomic Analysis of Mammalian Protein (*Continued*)

RefSeq accession number	*Protein description*	*$M_r$calc (kDa)*	*$M_r$obs (kDa)*
Higher sequence coverage in injured than naïve (protein appears in both)			
NM_005530	mitochondrial; isocitrate dehydrogenase (NAD^+) alpha [*Homo sapiens*]	40	30–35
NM_024398	mitochondrial aconitase [*Rattus norvegicus*]	85	60–90
NM_005566	lactate dehydrogenase A [*Homo sapiens*]	37	27–33
NM_057143	fertility protein SP22 [*Rattus norvegicus*]	200	15–25
NM_013083	heat shock 70 kD protein 5 [*Rattus norvegicus*]	72	50–75
NM_019169	synuclein, alpha [*Rattus norvegicus*]	15	10–15
NM_024398	mitochondrial aconitase [*Rattus norvegicus*]	85	60–90
XM_237718	tubulin alpha 6 [*Rattus norvegicus*]	50	35–50
NM_171983	alpha-spectrin 2 [*Rattus norvegicus*]	285	>250
NM_139325	enolase 2, gamma; neuronal [*Rattus norvegicus*]	50	35–50
NM_006597	heat shock 70 kDa protein 8 isoform 1 [*Homo sapiens*]	71	50–75
NM_015981	CaM kinase II alpha subunit; isoform 1 [*Homo sapiens*]	55	40–60
NM_011738	14-3-3 eta [*Mus musculus*]	28	17–27
NM_017042	protein phosphatase 3 (calcineurin) subunit A beta [*Rattus norvegicus*]	59	40–60
NM_005507	cofilin 1 (non-muscle) [*Homo sapiens*]	19	15–25
NM_146100	hypothetical protein MGC25352 [*Mus musculus*]	55	50–75
XM_217040	tubulin alpha-1 [*Rattus norvegicus*]	50	35–50
Same sequence coverage in naïve and injured			
NM_006870	destrin [*Homo sapiens*]	19	15–25
NM_173102	tubulin, beta 5 [*Rattus norvegicus*]	50	35–50
NM_006000	tubulin, alpha 1; testis-specific [*Homo sapiens*]	50	35–50
NM_001102	actinin, alpha 1 [*Homo sapiens*]	103	80–130
NM_008634	microtubule-associated protein 1b [*Mus musculus*]	270	27–33
NM_008084	glyceraldehyde-3-phosphae dehydrogenase [*Mus musculus*]	36	30–35
NM_023964	glyceraldehyde-3-phosphate dehydrogenase type 2 [*Rattus norvegicus*]	47	30–35
NM_153629	(NM_153629) heat shock 70 kDa protein 4 [*Rattus norvegicus*]	94	80–130
NM_012529	(NM_012529) creatine kinase, brain [*Rattus norvegicus*]	43	33–40
NM_012734	hexokinase 1 [*Rattus norvegicus*]	103	75–105
NM_009497	vesicle-associated membrane protein 2; synaptobrevin II [*Mus musculus*]	13	10–15
NM_016774	ATP synthase, H^+ transporting mitochondrial F1 complex, beta subunit [*Mus musculus*]	58	35–50
NM_010777	(NM_010777) myelin basic protein; myelin deficient [*Mus musculus*]	27	10–27
NM_031728	synaptosomal-associated protein (AP180) [*Rattus norvegicus*]	94	80–130
NM_000517	alpha 2 globin [*Homo sapiens*]	15	10–15
NM_002965	S100 A9; calgranulin B [*Homo sapiens*]	13	I: >250, N: 60–90
NM_030873	profilin II [*Rattus norvegicus*]	15	10–15
NM_012673	thymus cell surface antigen [*Rattus norvegicus*]	18	15–25
NM_012635	(NM_012635) pancreatic trypsin 1 [*Rattus norvegicus*]	26	75–105
NM_013177	Glutamate oxaloacetate transaminase 2 mitochondrial [*Rattus norvegicus*]	27	33–40
NM_012504	ATPase, Na^+K^+ transporting, alpha 1 [*Rattus norvegicus*]	113	105–160
NM_010324	glutamate oxaloacetate transaminase 1, cytosolic [*Mus musculus*]	26	33–40
NM_080583	adaptor-related protein complex 2, beta 1 subunit; beta adaptin [*Rattus norvegicus*]	105	75–105

(*continued*)

Table 1. Differential Proteomic Analysis of Mammalian Protein (*Continued*)

RefSeq accession number	*Protein description*	*$M_r$calc (kDa)*	*$M_r$obs (kDa)*
NM_026508	(NM_026508) RIKEN cDNA 2410002K23 [*Mus musculus*]	80	75–105
NM_006310	puromycin-sensitive aminopeptidase; metalloproteinase MP100 [*Homo sapiens*]	99	75–105
Higher sequence coverage in naïve than injured (protein appears in both)			
NM_030773	beta tubulin 1, class VI [*Homo sapiens*]	50	35–50
NM_019299	clathrin, heavy polypeptide (Hc) [*Rattus norvegicus*]	192	160–250
NM_003127	alpha-spectrin 2 (alpha-fodrin) [*Homo sapiens*]	284	>250
NM_013096	hemoglobin, alpha 1 [*Rattus norvegicus*]	15	10–15
NM_018753	14-3-3 protein beta [*Mus musculus*]	28	17–27
NM_000944	protein phosphatase 3 (calcineurin A alpha) [*Homo sapiens*]	59	40–60
NM_057213	ATPase, H^+ transporting, lysosomal beta 2 [*Rattus norvegicus*]	57	40–60
NM_138548	nucleoside diphosphate kinase (NM23A) [*Rattus norvegicus*]	17	10–15
NM_033234	Hemoglobin, beta [*Rattus norvegicus*]	16	10–15
NM_053543	neurochondrin [*Rattus norvegicus*]	79	50–75
NM_003406	14-3-3 zeta [*Homo sapiens*]	28	17–27
NM_031353	voltage-dependent anion channel 1 [*Rattus norvegicus*]	31	27–33
NM_138597	ATP synthase, H^+ transporting, mitochondrial F1 complex, O subunit [*Mus musculus*]	23	15–25
NM_053291	phosphoglycerate kinase 1 [*Rattus norvegicus*]	45	35–50
NM_000034	aldolase A; fructose-biphosphate aldolase [*Homo sapiens*]	39	33–40
NM_017245	translation elongation factor 2 [*Rattus norvegicus*]	95	75–105
NM_023119	enolase 1, alpha non-neuron [*Mus musculus*]	47	35–50
NM_005918	mitochondrial malate dehydrogenase [*Homo sapiens*]	36	27–33
NM_053297	/pyruvate kinase, muscle [*Rattus norvegicus*]	58	40–60
NM_080689	dynamin 1 [*Rattus norvegicus*]	96	75–105
NM_011123	myelin proteolipid protein [*Mus musculus*]	30	I, N: 15–30, N: 105–160
NM_134326	albumin [*Rattus norvegicus*]	69	50–75

The RefSeq (Pruitt and Maglott, 2001) accession number, protein description, database-derived molecular mass ($M_r$calc), and SDS-PAGE-predicted molecular mass ($M_r$obs) are shown for putative protein biomarkers of TBI.

Differential proteomic analysis of the gel slices (high to low $M_r$obs) revealed differences in protein sequence coverage for 170 mammalian proteins (57 in naive only, 74 in injured only, and 39 of 64 in both) as listed in Table 1. Inspection of the proteins falling into each of the three categories of protein markers shows that several well-studied proteins involved in TBI were observed in both naive and injured samples, including brain creatine kinase (CKB), αII-spectrin, neuron-specific enolase (NSE), α-synuclein (α-Syn), microtubule associated protein 2a and 2b (MAP2), neurofilament (NF), proteolipid protein (PLP), and myelin basic protein (MBP). The injured-to-naive ratio of protein sequence coverage suggests putative biomarkers that may exhibit significant differences in protein concentration between naive and injured samples. However, protein sequence coverage is only a semi-quantitative measure of protein concentration. This is particularly true for protein identifications based on single tryptic peptide sequences, and it is even more pronounced for degraded proteins. However, proteins observed only in naive samples, or proteins observed with greater sequence coverage in naive samples than in injured samples, suggest a subset of putative biomarkers that are down-regulated, released, or degraded during TBI, for example, (αII-spectrin (Pike et al., 2002), MAP2 (Huh et al., 2003), NF (Posmantur et al., 1996, 1998) and PLP (Banik et al., 1985; Domanska-Janik et al., 1992). Likewise, proteins observed only in injured samples, or proteins observed with greater sequence coverage in injured samples than in naive samples, suggest a subset of putative biomarkers that are up-regulated, accumulated, or aggregated during TBI, for example, NSE (Varma et al., 2003), amyloid precursor protein, amyloid β 1-42, tau (Franz et al., 2003), and α-Syn (Uryu et al., 2003; Bramlett and Dietrich 2003; Newell et al., 1999; Smith et al., 2003). Since the fragments of degraded proteins, for ex-

ample, breakdown products of αII-spectrin (Pike et al., 2002) may also be observed, it is important to relate $M_r$calc to $M_r$obs for putative protein biomarkers of TBI.

In order to evaluate whether any of our biomarkers were fragments of degraded proteins rather than intact proteins, we performed differential proteomic analysis as a function of $M_r$obs. Degraded protein biomarkers may not be revealed by differences in protein sequence coverage using current differential proteomic analysis tools, even when proteins are separated prior to *in vitro* proteolysis and capillary LC-MS^2, because $M_r$obs, which is encoded in SDS-PAGE–Capillary LC–MS^2 data, may not be preserved during data reduction. For example, MBP was identified by database searching ($M_r$calc = 27 kDa) in both naive and injured samples with a sequence coverage of 13.6%, incorrectly suggesting that it is not a putative biomarker of TBI. However, the vertical line in Figure 2 illustrates that MBP was observed in gel slices 35–41 ($M_r$obs ~ 27 kDa to 10 kDa, respectively) in injured (and not naive) samples, suggesting possible degradation, as confirmed by Western blot (Liu et al., unpublished observations).

Classification of Putative Protein Biomarkers of TBI

Stratification of the putative protein biomarkers discovered in this work, based on function and distribution, suggests several classes of proteins are of interest (Figs. 3 and 4). Careful examination of the fraction of proteins from each class that were observed in naive only, injured only, and both naive and injured samples highlights the most promising classes for biomarkers of TBI. For example, Figure 3 shows that 10% of the putative biomarkers observed only in injured samples were neuronal proteins including: PLP, Syn (α and β), NSE, NF (light and heavy), synapsin (I and II), vesicle associated membrane protein 1, and apolipoprotein E. Other promising classes of biomarkers observed only in injured samples include heat shock proteins (e.g., chaperonin 10) and kinases (e.g., calcium/calmodulin protein kinase II). These observations are reflected by peaks in the line plot shown in Figure 4. Thus, neuronal proteins, heat shock proteins, and kinases are a promising class of biomarkers that are up-regulated, accumulated, or aggregated during TBI. In contrast, the valley for dehydrogenases (e.g., lactate dehydrogenase) only in naive samples indicates a promising class of biomarkers that are down-regulated, released, or degraded. A complete discussion of the putative protein biomarkers discovered in this work is beyond the scope of this paper. While some ambiguity is expected, for example, glutamate dehydrogenase was observed only in injured samples while the neuronal protein glial fibrillary acidic protein (GFAP) was observed only in naive samples, the classification of putative protein biomarkers of TBI, combined with differential analysis methods such as this one, provides direction for biomarker research.

Preliminary Validation

The relative concentration of several putative protein biomarkers of TBI was investigated by targeted capillary LC-MS^2 (Haskins et al., 2001) of selected tryptic peptides (Fig. 4). Two- to ten-fold changes in tryptic peptide concentration for injured versus naive samples reflect the semi-quantitative differences in protein sequence coverage observed. For example, glutamate dehydrogenase (memory related gene 2), shown in Figure 5C, was ~10-fold higher in injured samples than in naive samples: corresponding to 2.9% protein sequence coverage in injured samples and 0.0% protein sequence coverage in naive samples (i.e., no tryptic peptides were observed in naive samples). A high yield of sequence-specific b- and y-type product ions was observed following isolation and fragmentation of selected tryptic precursor ions by collision-induced dissociation. Absolute quantification (AQUA) (Gerber et al., 2003) of these proteins can be readily achieved by incorporating an isotopically labeled tryptic peptide as an internal standard during trypsin digestion (publication in preparation). Assuming that the analytical variability exceeds the biological variability in pooled samples such as these, a false-positive rate as high as 30% is expected for data-dependent capillary LC-MS^2 of complex mixtures (unpublished work). While only a 29% overlap of proteins conserved between naive and injured samples underscores the need for higher-resolution protein separation methods, this must be balanced with the need for faster results. Indeed, preliminary validation of biomarkers is a significant bottleneck for proteomics as the speed of discovery continues to outpace the speed of validation (Bodovitz and Joos, 2004).

Comparison with Previous Work

This is the first report of SDS-PAGE–Capillary LC–MS^2 for biomarker discovery. Several of the putative protein biomarkers described herein at 48 h post-injury were suggested previously by a microarray- and RNA-based gene expression experiment (Matzilevich et al., 2002) In 10 oligonucleotide array pairs, 261 of 8800 genes were significantly affected at 24 h post-injury, including NF (light), MAP2, GFAP, and beta-tubulin.

More recently, a proteomics approach using 2D gels and database searching of 2D gel images (Fountoulakis et al., 1999a) at 24 h post-injury was presented (Jenkins et al., 2002). In that work, 50 (<95 kDa proteins) of

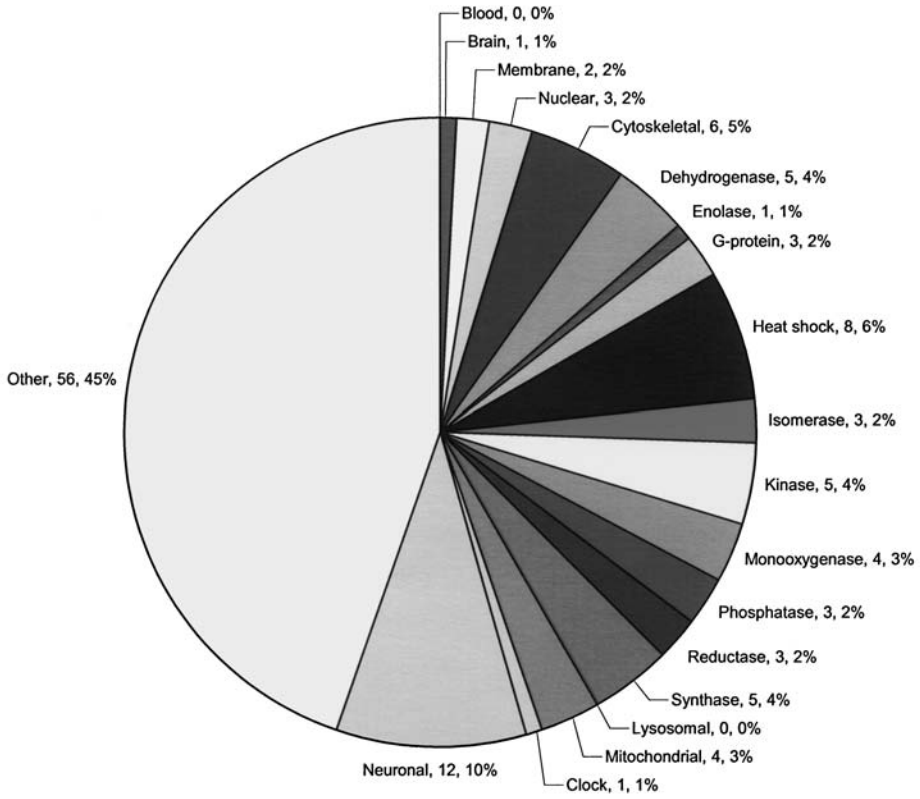

FIG. 3. Stratification of the putative protein biomarkers discovered in injured hippocampus only. Protein class, number of proteins, fraction of protein biomarkers. Proteins were sorted into classes based on function and localization with increasingly stringent specificity: blood, brain < membrane < nuclear < cytoskeletal < dehydrogenase, enolase, clock, G-protein, heat shock, isomerase, kinase, monooxygenase, phosphatase, reductase < synthase < lysosomal, mitochondrial < neuronal.

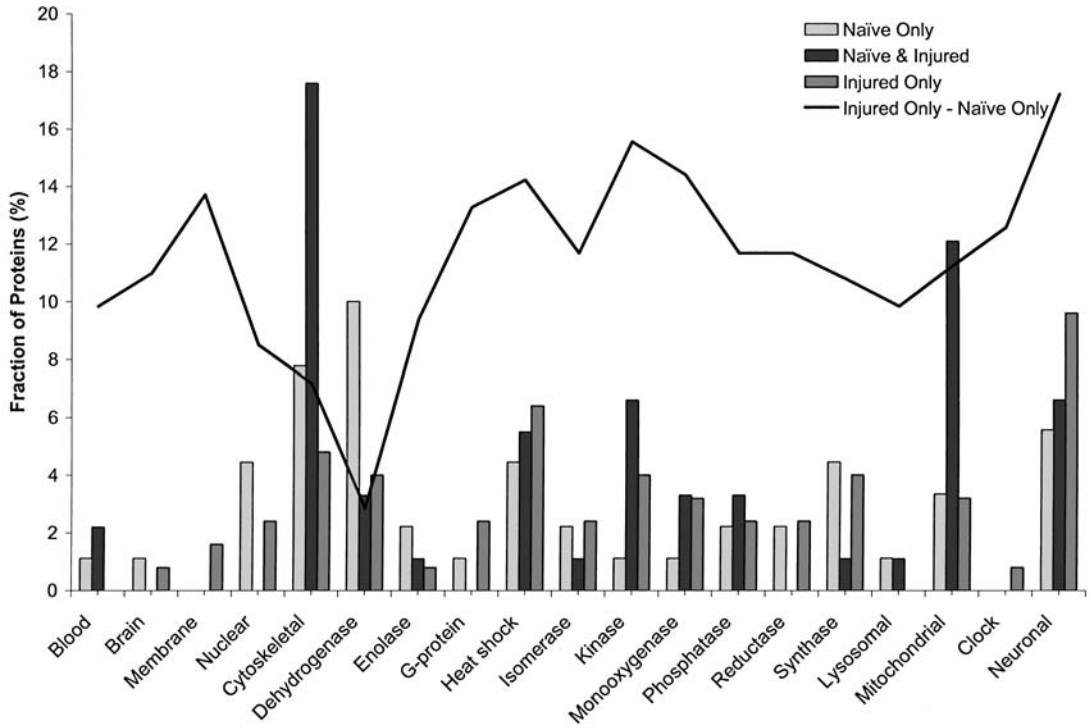

FIG. 4. Stratification of putative protein biomarkers discovered in naive only, injured only, and both naive and injured hippocampal samples. The fractions of biomarkers in "Naive Only" (light grey columns), "Injured Only" (dark grey), and both "Naive and Injured" samples (black). were plotted against each function and localization class. In addition, the difference in the fraction between the "Injured Only" group and the "Naive Only" group was plotted as a line graph on the same scale. Peaks in the line plot suggest classes of proteins that are elevated, upregulated, or aggregated (e.g., neuronal, kinase) in injured hippocampus, while valleys in the line plot are those that are down-regulated, released, or degraded (e.g., dehydrogenase) in injured hippocampus.

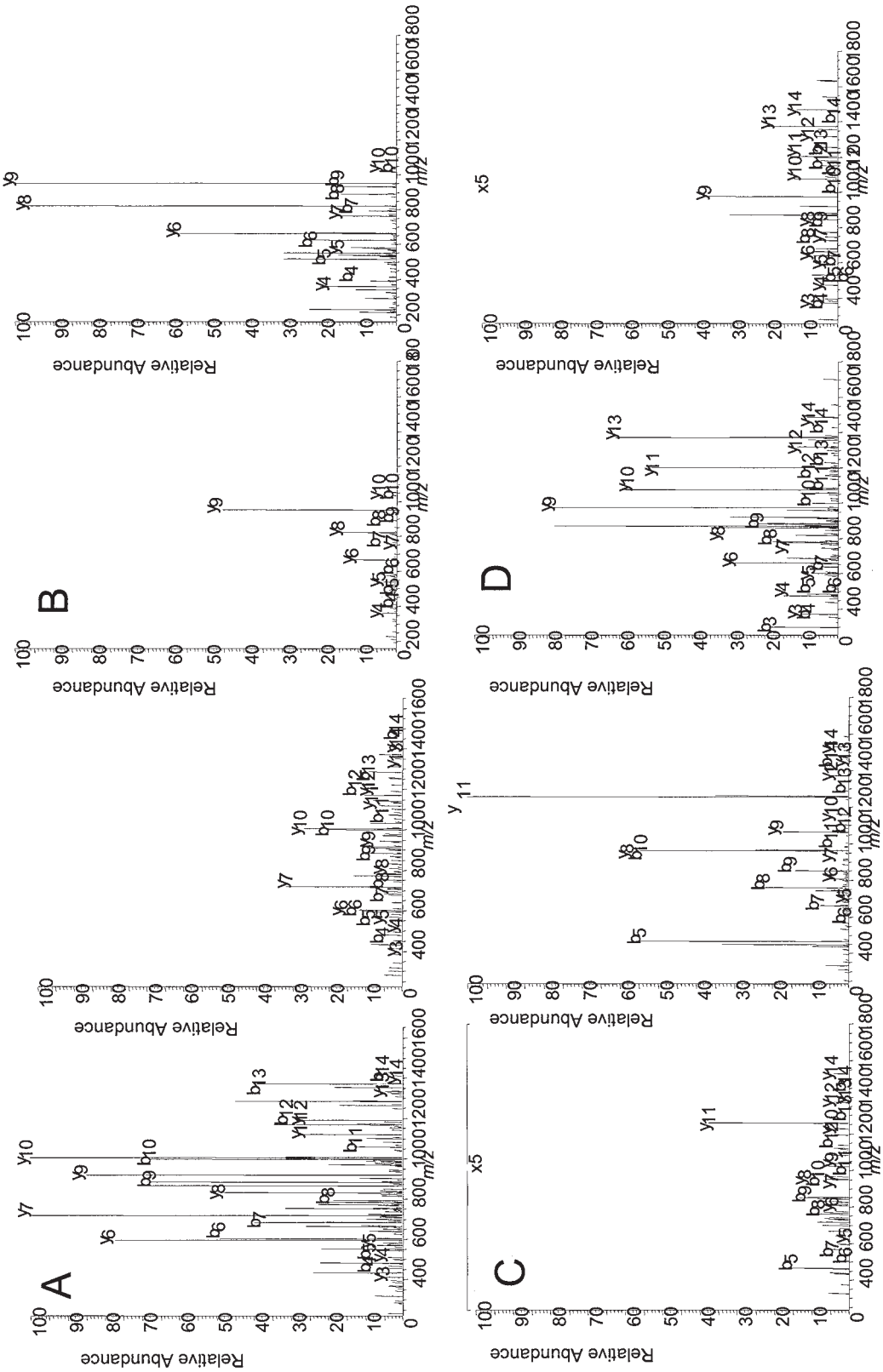

FIG. 5. Representative targeted MS^2 spectra collected in naive (left) and injured (right) hippocampus samples. (**A**) CKB-rat, (**B**) α-Syn, (**C**) Memory-related gene 2, (**D**) αII-Spectrin. The tryptic peptide sequences corresponding to these spectra are LAVEALSSLDGDLSGR (A), KEGVLYVGSK (B), HGGTIPVVPTAEFQDR (C), and DLAALGDKVNSLGETAQR (D), respectively.

~1500 protein spots were tentatively identified by matching the 2D gel-derived molecular masses and isoelectric points of the protein spots with a rat brain database of 210 proteins. However, only six putative protein biomarkers were revealed by significant changes across six of six gel pairs (individual rather than pooled samples). Interestingly, an increase in the mitochondrial protein Cu/Zn superoxide dismutase, and a decrease in the cytoskeletal proteins α- and β-tubulin, were also observed in this work.

Confidence in previously reported putative biomarkers is significantly strengthened by sequence-specific discovery of these proteins by SDS-PAGE–Capillary LC–MS^2. Protease-specific peptide sequences provide a means to unambiguously identify putative protein biomarkers and various PTMs (e.g., degradation) from large protein databases (e.g., RefSeq 785,143 sequences) (Pruitt and Maglott, 2001). In contrast, microarray experiments suffer from our incomplete understanding of the interaction between transcription and translation; that is, RNA levels do not accurately reflect protein levels, and database searching of 2D gel images suffers from a low success rate for protein identification. Despite the limitations of these techniques, the unambiguous identification of several previously reported putative biomarkers by SDS-PAGE–Capillary LC–MS^2 provides evidence for the validity of this approach to biomarker discovery.

DISCUSSION

Using differential proteomic analysis, we revealed differences in protein sequence coverage for 170 mammalian proteins (57 in naive only, 74 in injured only, and 39 of 64 in both). Our data suggest that these are putative biomarkers of TBI in hippocampus tissue, as these are expected to either accumulate in the CSF and blood, or form aggregate in the extracellular compartment of the brain. However, we must further establish if these markers can distinguish TBI from various other brain diseases, and the kinetics for their degradation and clearance from tissue to CSF and blood must be favorable in order to obtain reliable indicators of injury severity. A subset of the putative protein biomarkers of TBI described herein, particularly the neuronal proteins, are expected to meet these criteria for biomarker validation. In the meantime, these biomarkers may also find use in the laboratory setting. For example, β3-tubulin and GFAP are used to distinguish neuronal differentiation in stem cell research (Kornblum and Geschwind, 2001). Lastly, this work provides proof-of-principle for more rapid and comprehensive sequence-specific biomarker discovery strategies incorporating protein separation prior to capillary LC-MS^2.

ACKNOWLEDGMENTS

We thank Professor Steven Gygi (Harvard Medical), Dr. David Tabb (Oak Ridge National Laboratory), and Drs. Anu Waghray and Clair Ringger (University of Florida) for insightful discussion. This work was supported by DoD grants DAMD17-03-1-0066, DAMD17-01-1-0765, and DAMD17-99-1-9565; NIH grants R01 NS39091 and R01 NS40182.

REFERENCES

BANIK, N.L., McALHANEY, W.W., and HOGAN, E.L. (1985). Calcium-stimulated proteolysis in myelin: evidence for a Ca^{2+}-activated neutral proteinase associated with purified myelin of rat CNS. J Neurochem. **45,** 581–588.

BERGER, R.P., PIERCE, M.C., WISNIEWSKI, S.R., et al. (2002). Neuron-specific enolase and S100B in cerebrospinal fluid after severe traumatic brain injury in infants and children. Pediatrics **109,** E31.

BODOVITZ, S., and JOOS, T. (2004). The proteomics bottleneck: strategies for preliminary validation of potential biomarkers and drug targets. Trends Biotechnol. **22,** 4–7.

BRAMLETT, H.M. and DIETRICH, W.D. (2003). Synuclein aggregation: possible role in traumatic brain injury. Exp. Neurol. **184,** 27–30.

BUKI, A., OKONKWO, D.O., WANG, K.K.W., and POVLISHOCK, J.T. (2000). Cytochrome c release and caspase activation in traumatic axonal injury. J. Neurosci. **20,** 2825–2834.

DENSLOW, N., MICHEL, M.E., TEMPLE, M.D., HSU, C.Y., SAATMAN, K., and HAYES, R.L. (2003). Application of proteomics technology to the field of neurotrauma. J. Neurotrauma **20,** 401–407.

DIXON, C.E., CLIFTON, G.L., LIGHTHALL, J.W., YAGHAMAI, A.A., and HAYES, R.L. (1991). A controlled cortical impact model of traumatic brain injury in the rat. J. Neurosci. Methods **39,** 253–262.

DOMANSKA-JANIK, K., DE NECHAUD, B., INOMATA, M., KAWASHIMA, S., and ZALEWSKA, T. (1992). Calcium-activated neutral protease (CANP). in normal and dysmyelinating mutant paralytic tremor rabbit myelin. Mol. Chem. Neuropathol. **16,** 273–288.

FOUNTOULAKIS, M., SCHULLER, E., HARDMEIER, R., BERNDT, P., and LUBEC, G. (1999a). Rat brain proteins: two-dimensional protein database and variations in the expression level. Electrophoresis **20,** 3572–3579.

FOUNTOULAKIS, M., SCHULLER, E., HARDMEIER, R., BERNDT, P. and, LUBEC, G. (1999b). Rat brain proteins: two-dimensional protein database and variations in the expression level. Electrophoresis **20,** 3572–3579.

FRANZ, G., BEER, R., KAMPFL, A., et al. (2003). Amyloid beta 1–42, and tau in cerebrospinal fluid after severe traumatic brain injury. Neurology **60,** 1457–1461.

GERBER, S.A., RUSH, J., STEMMAN, O., KIRSCHNER, M.W., and GYGI, S.P. (2003). Absolute quantification of proteins and phosphoproteins from cell lysates by tandem MS. Proc. Natl. Acad. Sc.i USA **100,** 6940–6945.

GHARBI, S., GAFFNEY, P., YANG, A., et al. (2002). Evaluation of two-dimensional differential gel electrophoresis for proteomic expression analysis of a model breast cancer cell system. Mol. Cell. Proteomics **1,** 91–98.

GYGI, S.P., RIST, B., GERBER, S.A., TURECEK, F., GELB, M.H., and AEBERSOLD, R. (1999). Quantitative analysis of complex protein mixtures using isotope-coded affinity tags. Nat. Biotechnol. **17,** 994–999.

HASKINS, W.E., WANG, Z.Q., WATSON, C.J., et al. (2001). Capillary LC-MS^2 at the attomole level for monitoring and discovering endogenous peptides in microdialysis samples collected *in vivo*. Anal. Chem. **73,** 5005–5014.

HUH, J.W., RAGHUPATHI, R., LAURER, H.L., HELFAER, M.A., and SAATMAN, K.E. (2003). Transient loss of microtubule-associated protein 2 immunoreactivity after moderate brain injury in mice. J. Neurotrauma **20,** 975–984.

JENKINS, L.W., PETERS, G.W., DIXON, C.E., et al. (2002). Conventional and functional proteomics using large format two-dimensional gel electrophoresis 24 hours after controlled cortical impact in postnatal day 17 rats. J. Neurotrauma **19,** 715–740.

KERNEC, F., UNLU, M., LABEIKOVSKY, W., MINDEN, J.S., and KORETSKY, A.P. (2001). Changes in the mitochondrial proteome from mouse hearts deficient in creatine kinase. Physiol. Genomics **6,** 117–128.

KORNBLUM, H.I., and GESCHWIND, D.H. (2001). Molecular markers in CNS stem cell research: hitting a moving target. Nat. Rev. Neurosci. **2,** 843–846.

LEIMGRUBER, R.M., MALONE, J.P., RADABAUGH, M.R., LAPORTE, M.L., VIOLAND, B.N., and MONAHAN, J.B. (2002). Development of improved cell lysis, solubilization and imaging approaches for proteomic analyses. Proteomics **2,** 135–144.

MACDONALD, N., CHEVALIER, S., TONGE, R., et al. (2001). Quantitative proteomic analysis of mouse liver response to the peroxisome proliferator diethylhexylphthalate (DEHP). Arch. Toxicol. **75,** 415–424.

MATZILEVICH, D.A., RALL, J.M., MOORE, A.N., GRILL, R.J., and DASH, P.K. (2002). High-density microarray analysis of hippocampal gene expression following experimental brain injury. J. Neurosci. Res. **67,** 646–663.

MCDONALD, W.H., and YATES, J.R. (2002). Shotgun proteomics and biomarker discovery. Dis. Markers **18,** 99–105.

NEWCOMB, J.K., KAMPFL, A., POSMANTUR, R.M., et al. (1997). Immunohistochemical study of calpain-mediated breakdown products to a-spectrin following controlled cortical impact injury in the rat. J. Neurotrauma **14,** 369–383.

NEWELL, K.L., BOYER, P., GOMEZ-TORTOSA, E., et al. (1999). Alpha-synuclein immunoreactivity is present in axonal swellings in neuroaxonal dystrophy and acute traumatic brain injury. J. Neuropathol. Exp. Neurol. **58,** 1263–1268.

PERKINS, D.N., PAPPIN, D.J., CREASY, D.M., and COTTRELL, J.S. (1999). Probability-based protein identification by searching sequence databases using mass spectrometry data. Electrophoresis **20,** 3551–3567.

PIKE, B.R., FLINT, J., DUTTA, S., WANG, D.S., WANG, K.K.W., and HAYES, R.L. (2002). Accumulation of spectrin and calpain-cleaved spectrin breakdown products in CSF after traumatic brain injury. J. Neurochem. **81,** 73.

POSMANTUR, R.M., KAMPFL, A., LIU, S.J., et al. (1996). Cytoskeletal derangements of cortical neuronal processes three hours after traumatic brain injury in rats: an immunofluorescence study. J. Neuropathol. Exp. Neurol. **55,** 68–80.

POSMANTUR, R., KAMPFL, A., SIMAN, R., et al. (1997). A calpain inhibitor attenuates cortical cytoskeletal protein loss after experimental traumatic brain injury in the rat. Neuroscience **77,** 875–888.

POSMANTUR, R.M., ZHAO, X., KAMPFL, A., CLIFTON, G.L., and HAYES, R.L. (1998). Immunoblot analyses of the relative contributions of cysteine and aspartic proteases to neurofilament breakdown products following experimental brain injury in rats. Neurochem. Res. **10,** 1265–1276.

PRUITT, K.D., and MAGLOTT, D.R. (2001). RefSeq and LocusLink: NCBI gene-centered resources. Nucleic Acids Res. **29,** 137–140.

RAABE, A., KOPETSCH, O., WOSZCZYK, A., et al. (2003). Serum S-100B protein as a molecular marker in severe traumatic brain injury. Restor. Neurol. Neurosci. **21,** 159–169.

SHAW, J., ROWLINSON, R., NICKSON, J., et al. (2003). Evaluation of saturation labeling two-dimensional difference gel electrophoresis fluorescent dyes. Proteomics **3,** 1181–1195.

SMITH, D.H., URYU, K., SAATMAN, K.E., TROJANOWSKI, J.Q., and MCINTOSH, T.K. (2003). Protein accumulation in traumatic brain injury. Neuromol. Med. **4,** 59–72.

TABB, D.L., MCDONALD, W.H., and YATES, J.R. (2002). DTASelect and contrast: tools for assembling and comparing protein identifications from shotgun proteomics. J. Proteome Res. **1,** 21–26.

TONGE, R., SHAW, J., MIDDLETON, B., et al. (2001). Validation and development of fluorescence two-dimensional differential gel electrophoresis proteomics technology. Proteomics **1,** 377–396.

URYU, K., GIASSON, B.I., LONGHI, L., et al. (2003). Age-dependent synuclein pathology following traumatic brain injury in mice. Exp. Neurol. **184,** 214–224.

VARMA, S., JANESKO, K.L., WISNIEWSKI, S.R., et al. (2003). F-2–isoprostane and neuron-specific enolase in cerebrospinal fluid after severe traumatic brain injury in infants and children. J. Neurotrauma **20,** 781–786.

YAN, J.X., DEVENISH, A.T., WAIT, R., STONE, T., LEWIS, S., and FOWLER, S. (2002). Fluorescence two-dimensional difference gel electrophoresis and mass spectrometry based proteomic analysis of *Escherichia coli*. Proteomics **2,** 1682–1698.

YATES, J.R., MORGAN, S.F., GATLIN, C.L., GRIFFIN, P.R., and ENG, J.K. (1998). Method to compare collision-induced dissociation spectra of peptides: potential for library searching and subtractive analysis. Anal. Chem. **70,** 3557–3565.

ZELMAN, F.P., JAUCH, E.C., MULCHAHEY, J.J., et al. (2002). C-tau biomarker of neuronal damage in severe brain-injured patients: association with elevated intracranial pressure and clinical outcome. Brain Res. **947,** 131–139.

Address reprint requests to:
Kevin K.W. Wang, Ph.D.
McKnight Brain Institute, L4-100F
University of Florida (P.O. Box 100256)
100 S. Newell Dr.
Gainesville, FL 32610

E-mail: kwang@psychiatry.ufl.edu

Journal of Neurochemistry, 2005, **94**, 97–108 doi:10.1111/j.1471-4159.2005.03172.x

Caspase 7: increased expression and activation after traumatic brain injury in rats

Stephen F. Larner,* Deborah M. McKinsey,* Ronald L. Hayes*,† and Kevin K. W. Wang*,†

**Center for Traumatic Brain Injury Studies, Department of Neuroscience and*

†Center for Neuroproteomics and Biomarkers Research, Department of Psychiatry, McKnight Brain Institute of the University of Florida, Gainesville, Florida, USA

Abstract

Caspases, a cysteine proteinase family, are required for the initiation and execution phases of apoptosis. It has been suggested that caspase 7, an apoptosis executioner implicated in cell death proteolysis, is redundant to the main executioner caspase 3 and it is generally believed that it is not present in the brain or present in only minute amounts with highly restricted activity. Here we report evidence that caspase 7 is up-regulated and activated after traumatic brain injury (TBI) in rats. TBI disrupts homeostasis resulting in pathological apoptotic activation. After controlled cortical impact TBI of adult male rats we observed, by semiquantitative real-time PCR, increased mRNA levels within the traumatized cortex and hippocampus peaking in the former about 5 days post-injury and in the latter within 6–24 h of trauma. The activation of caspase 7 protein after TBI, demonstrated by immunoblot by the increase of the active form of caspase 7 peaking 5 days post-injury in the cortex and hippocampus, was found to be up-regulated in both neurons and astrocytes by immunohistochemistry. These findings, the first to document the up-regulation of caspase 7 in the brain after acute brain injury in rats, suggest that caspase 7 activation could contribute to neuronal cell death on a scale not previously recognized.

Keywords: apoptosis, caspase, caspase 7, cell death, traumatic brain injury.

J. Neurochem. (2005) **94,** 97–108.

Traumatic brain injury (TBI), a serious health issue in the USA according to the Centers for Disease Control and Prevention, afflicts about 1.5 million new patients annually. TBI is frequently referred to as the silent epidemic because the resulting pathologies tend to be emotional and cognitive (e.g. impaired memory, change in character traits and difficulty in concentrating) rather than physical (Gerberding 2003). Despite about 2% of the US population suffering from some form of TBI-related disability, no known pharmacological treatment is currently available. TBI causes progressive neuronal degeneration resulting from acute and delayed cell death mediated in part by calpains (Kampfl *et al*. 1996) and in part by apoptotic-inducing caspases (Rink *et al*. 1995; Colicos *et al*. 1996; Yakovlev *et al*. 1997; Conti *et al*. 1998; Newcomb *et al*. 1999; Clark *et al*. 2000).

Apoptosis, programmed cell death (type I), a conserved active molecular process, often requires transcription and translation of proteins for initiation (Rink *et al*. 1995). Characterized by proteolysis of cellular components, apoptosis is critical to the pruning of the CNS during development (Oppenheim 1991; Raff *et al*. 1993; Vaux and Korsmeyer 1999) and for tissue homeostasis requiring the elimination of aged and abnormal cells (Johnson *et al*. 1999). Although apoptosis is under strict control under normal conditions, alterations in the apoptotic pathways have been implicated in many diseases, such as cancer and neurodegenerative disorders (Thompson 1995; Yuan and Yankner 2000), and play a role in the pathology that occurs after TBI.

Apoptosis is often associated with the sequential-activating cascade of a family of cysteine-dependent aspartate-

Received December 10, 2004; revised manuscript received February 15, 2005; accepted February 18, 2005.

Address correspondence and reprint requests to Stephen F. Larner, PhD, Center for Traumatic Brain Injury Studies, Department of Neuroscience, 100 S. Newell Drive, Box 100244, McKnight Brain Institute of the University of Florida, Gainesville, FL 32610, USA.
E-mail: sflarner@ufl.edu

Abbreviations used: DAPI, 4′,6′-diamino-2-phenylindolehydrocloride; DEPC, Diethyl pyrocarbonate; ER, endoplasmic reticulum; GAPDH, Glyceraldehyde-3-phosphatedehydrogenase; PARP, Poly (ADP-Ribose); SDS, sodium dodecyl sulfate; TAE, Tris Acetate Electrophoresis; TBI, traumatic brain injury.

specific proteinases known as caspases. Caspases, translated as zymogens, are proteolytically processed to become mature active enzymes (Cohen 1997). Divided into two broad groups, caspases include the initiator caspases (2, 8, 9, 10 and 12) activated via upstream events which, in turn, activate the downstream effector or executioner caspases (3, 6 and 7). The three executioners cleave a subset of intracellular proteins promoting the characteristic apoptotic morphology.

Caspase 7, like caspases 3 and 6, contains a short prodomain and, upon apoptotic induction, the 35-kDa proform is converted into a 32-kDa intermediate or pre-active form which is further processed into two active subunits consisting of the p20 or large (18-kDa) subunit and the p10 or small (11-kDa) subunit (Duan *et al*. 1996; Wolf and Green 1999). Active caspase 7 has been shown to cleave a number of substrates including the nuclear substrate Poly (ADP-Ribose) (PARP) (Germain *et al*. 1999). Caspase 7 is structurally and functionally most similar to caspase 3 although the two only share 53% sequence identity (67% similarity) (Fernandes-Alnemri *et al*. 1995; Juan *et al*. 1997; Wei *et al*. 2000; Riedl *et al*. 2001). The crystallized primary procaspase 7 isoform of 303 amino acids (Riedl *et al*. 2001) showed that the enzymatic site of caspase 7 differs from caspase 3 in the S4 pocket near the P4 aspartic acid where it has a negative electrostatic potential while caspase 3 is neutral in this region. This may allow caspase 7 to act on substrates that may differ from caspase 3. Three such caspase 7 specifically-targeted proteins have been reported which include kinectin (Machleidt *et al*. 1998), which is found on the cytoplasmic face of endoplasmic reticulum (ER) membranes (Toyoshima *et al*. 1992) and has been shown to interact with the cargo-binding site of conventional kinesin, a protein found to be most abundant in the brain (Hollenbeck 1989), caspase 12 (Rao *et al*. 2001) and tumor necrosis factor receptor I (Ethell *et al*. 2001).

The caspase 7 contribution to neuronal apoptosis remains controversial. The current paradigm is that caspase 7 mRNA and protein are either not present in the brain (Juan *et al*. 1997; Ray and Cardone 2002) or, if present, have little impact (Zhang *et al*. 2000; Slee *et al*. 2001; Henshall *et al*. 2002; Le *et al*. 2002). This view is held even though an early study reported caspase 7 (Mch3) mRNA in brain samples albeit in very low quantities (Fernandes-Alnemri *et al*. 1995). This belief was predicated on a number of studies, including one on caspase 3-deficient mice that showed no evidence of compensatory activation of caspase 7 in the nervous system after *in vivo* cerebral ischemia or *in vitro* oxygen glucose deprivation (Le *et al*. 2002) unlike that found in the liver. However, recent studies clearly imply that caspase 7 has an important, non-redundant role in normal physiology and apoptosis. For example, while CASPASE 3–/– post-natal mice exhibit neurodegenerative disorders (Kuida *et al*. 1996), CASPASE 7–/– mice have an early embryonic lethal phenotype (Slee *et al*. 2001) and a human solid cancer study showed that inactivating mutations in the CASPASE 7 gene led to the loss of the apoptotic function contributing to their pathogenesis (Soung *et al*. 2003). In a similar study where the human neuroblastoma cell line SH-SY5Y was exposed to the anticancer apoptotic-inducing drug paclitaxel, the addition of the natural antioxidant *trans*-resveratrol was able to inhibit the activation of caspase 7 thereby modulating the apoptotic signals (Nicolini *et al*. 2001). This suggests that caspase 7 and caspase 3 have complementary but not completely overlapping roles. It is our hypothesis that caspase 7 is present in the brain and is up-regulated and activated after traumatic injury.

Materials and methods

Rat PC12 pheochromocytoma cell culture, collection and preparation

PC12 cells were grown on polystyrene tissue culture dishes (Falcon, Becton Dickinson, Franklin Lakes, NJ, USA) in Dulbecco's modified Eagle's medium (Gibco, Invitrogen Corp., Grand Island, NY, USA) supplemented with 10% fetal calf serum (Gibco), 5% horse serum (Gibco), 1% Fungizone (Gibco), 100 units/mL penicillin and 100 μg/mL streptomycin (Gibco) and kept at 37°C in a humidified 5% CO_2 incubator for 12–24 h before treatment. When required, cell cultures were pre-treated for 1 h before thapsigargin (Research Biochemical International, Natick, MA, USA) challenge (1 μM) with the pan-caspase (100 μM) inhibitor carbobenzoxy-Asp-$CH_2OC(O)$-2,6-diclorobenzena (Bachem, Torrance, CA, USA) (Nath *et al*. 1996). Cells were challenged with thapsigargin for 6, 12, 24 and 48 h (data for 48 h not shown).

The cell cultures were suspended in ice-cold detergent-free buffer (50 mM Tris-HCl, pH 7.4, 1 mM EDTA, 2 mM EGTA, 0.33 M sucrose, 1 mM dithiothreitol) containing a broad-range protease inhibitor cocktail (Roche Molecular Biochemicals, Indianapolis, IN, USA) and then passed three to five times through a 27½-gauge needle. The samples were fractionated by centrifuge: 600 *g* for 10 min at 4°C to isolate the nuclei and 10 000 *g* at 4°C for 10 min to remove the mitochondria. The nuclei pellet was resuspended in a lysis buffer [20 mM HEPES, 1 mM EDTA, 2 mM EGTA, 150 mM NaCl, 0.1% sodium dodecyl sulfate (SDS), 1% Igepal and 0.5% deoxycholic acid, pH 7.5] containing a broad-range protease inhibitor cocktail (Roche Molecular Biochemicals) and sonicated in preparation for immunoblot analysis (nuclear fraction). The subcellular supernatant fluid, containing the microsomal/ER and cytosolic proteins, was also collected (ER/cytosol fraction).

Surgical preparation and controlled cortical impact traumatic brain injury

A previously described cortical impact injury device was used to produce TBI in adult rats (Dixon *et al*. 1991; Pike *et al*. 1998). Cortical impact TBI results in cortical deformation within the vicinity of the impactor tip associated with contusion and neuronal and axonal damage largely confined to the hemisphere ipsilateral to the site of injury. Adult male (280–300 g) Sprague-Dawley rats (Harlan, Indianapolis, IN, USA) were anesthetized with 4% isoflurane (Halocarbon Laboratories, River Edge, NJ, USA) in a carrier gas of 1 : 1 O_2 : N_2O (4 min) followed by maintenance

anesthesia of 2.5% isoflurane in the same carrier gas. Core body temperature was monitored continuously by a rectal thermistor probe and maintained at 37 ± 1°C by placing an adjustable temperature-controlled heating pad beneath the rats. Animals were mounted in a stereotactic frame in a prone position and secured by ear and incisor bars. A midline cranial incision was made, the soft tissues reflected and a unilateral (ipsilateral to site of impact) craniotomy (7 mm diameter) was performed adjacent to the central suture, midway between bregma and lambda. The dura mater was kept intact over the cortex. Brain trauma was produced by impacting the right cortex (ipsilateral cortex) with a 5-mm diameter aluminum impactor tip (housed in a pneumatic cylinder) at a velocity of 3.5 m/s with a 1.0, 1.2 or 1.6 mm compression and 150 ms dwell time (compression duration). Velocity, controlled by adjusting the pressure (compressed N_2) supplied to the pneumatic cylinder, and dwell time were measured by a linear velocity displacement transducer (model 500 HR; Lucas Shaevitz™, Detroit, MI, USA) that produces an analog signal recorded by a storage-trace oscilloscope (model 2522B; BK Precision, Placentia, CA, USA). Sham-injured (craniotomy-injured) animals underwent identical surgical procedures but did not receive the impact injury. Naive animals received no surgery or injury. Appropriate pre- and post-injury management guidelines were maintained and these measures complied with all guidelines set forth by the University of Florida Institutional Animal Care and Use Committee and the National Institutes of Health guidelines detailed in the *Guide for the Care and Use of Laboratory Animals*.

Tissue lysis and protein purification

Cortical and hippocampal tissues were collected from naive animals or at 6 h to 14 days after craniotomy injury or TBI. At appropriate post-injury time-points, the animals were anesthetized with 4% isoflurane in a carrier gas of 1 : 1 O_2 : N_2O (4 min) and then killed by decapitation. For immunoblot studies, ipsilateral and contralateral (to the impact site) cortices and hippocampi were rapidly dissected and snap-frozen in liquid nitrogen. Tissue samples were stored at −20°C. The ipsilateral samples were homogenized in a glass tube with a Teflon dounce pestle in 15 volumes of ice-cold detergent-free buffer (described above) and then passed three to five times through a 27½-gauge needle. Samples were fractionated as described above. No further work was performed on the contralateral tissue after it was determined by immunohistochemical analysis that caspase 7 was virtually undetectable in this brain region. This corresponds with our previous findings of the lack of spectrin proteolysis in contralateral tissue (Pike *et al*. 2001).

Semiquantitative RT-PCR

RNA purification

Total RNA was isolated from control and injured samples of cortical or hippocampal tissue using TRIzol reagent (Gibco BRL, Gaithersburg, MD, USA). Isopropanol precipitation and ethanol washes were performed according to the manufacturer's instructions. Samples were resuspended in 50–100 μL Diethylpyrocarbonate (DEPC)-treated water.

Reverse Transcription (RT)

Total RNA (3 μg) was incubated with 1 μL oligo(dT) (0.5 mg/mL; Gibco BRL), the RNA-oligo(dT) sample was added to an RT reaction containing 20 mM Tris-HCl, pH 8.4, 50 mM KCl, 5 mM $MgCl_2$, 500 μM dNTPs, 10 mM dithiothreitol, 50 units SuperScript II reverse transcriptase (Gibco BRL) and 40 units RNaseOUT recombinant ribonuclease inhibitor (Gibco BRL) and incubated according to the manufacturer's instructions.

Primer selection

Caspase 7-specific 5′ (TGAGCCACGGAGAAGAGAAT, bp 427–446) and 3′ (TTTGCTTACTCCACGGTTCC, bp 663–682) primers (GeneBank locus AF072124 *Rattus norvegicus*) and Glyceraldehyde-3-phosphate dehydrogenase (GAPDH)-specific 5′ (GGCTGCCTTCTCTTGTGAC, bp 903–921) and 3′ (GGCCGCCTGCTTCACCAC, bp 1624–1641) primers (GeneBank locus AF106860) were obtained from Integrated DNA Technologies (Coralville, IA, USA). Primer sets were identified using the Primer3 software (Rozen and Skaletsky 1998).

Standard PCR

PCR reaction buffer was added to the RT product to give a final volume containing 20 mM Tris-HCl, pH 8.4, 50 mM KCl, 2.5 mM $MgCl_2$, 200 μM dNTPs, 0.5% dimethylsulfoxide and 1.25 units Taq DNA polymerase (Gibco BRL). After PCR, reaction aliquots of PCR products were run on 1.5% agarose gels and separated by electrophoresis in Tris Acetate Electrophoresis (TAE) buffer (40 mM Tris-acetate, 1 mM EDTA, pH 7.5) containing 5 μg/mL ethidium bromide. To assay for genomic DNA contamination, RNA samples underwent PCR amplification without prior RT. Samples showing genomic contamination underwent repurification and repeat assay for genomic contamination before PCR analysis for transcript expression.

Semiquantitative/LightCycler RT-PCR

Real-time semiquantitative RT-PCR was performed using a LightCycler rapid thermal cycler system (Roche Diagnostics, Indianapolis, IN, USA) according to the manufacturer's instructions. Reactions were performed in a 10-μL volume with 0.5 μM primers and 2.5 mM $MgCl_2$. Other reagents, including nucleotides, FastStart Taq DNA polymerase and buffer, were used as provided in the LightCycler-FastStart DNA Master SYBR Green I reaction mix (Roche Diagnostics). Specificity of the amplification product from each primer pair was confirmed by melting curve analysis of the PCR product and subsequent gel electrophoresis. Quantification was performed by online monitoring for identification of the exact time-point at which the logarithmic linear phase can be distinguished from the background (crossing point). The crossing point was expressed as a cycle number.

Standard curve preparation and semiquantitative RT-PCR analysis

Total RNA from ipsilateral cortex and hippocampus was collected 6 h and 1 day after injury, respectively, reversed transcribed into cDNA and serially diluted to generate a standard curve of relative amounts of RNA. Aliquots underwent analysis for each cDNA dilution sample (100, 33.3, 11.1 and 3.7%) using the LightCycler quantitative RT-PCR for each primer pair (caspase 7 or GAPDH specific). Quantitative RT-PCR analysis yielded a crossing point cycle number for each dilution for each transcript-specific primer set at which the PCR amplification entered the log-linear region. After the standard curves were generated, by plotting the log concentration of total RNA vs. the crossing point cycle number, a linear

regression analysis was performed. Using the standard curve for each primer set, the amount of caspase 7 or GAPDH mRNA was determined. The calculated mRNA levels are the percent increase of the injured samples for each time-point over the pooled craniotomy samples for each time-point.

Immunoblot analysis

Protein concentrations of the subcellular cell lysate homogenate fractions were determined by the Detergent Compatible Assay for Protein (Bio-Rad Laboratories, Hercules, CA, USA) with albumin standards. Aliquots (100–200 μg) of each sample were prepared for SDS–polyacrylamide gel electrophoresis by addition of 8× loading buffer (1× contains 125 mM Tris-HCl, pH 6.8, 100 mM 2-mercaptoethanol, 4% SDS, 0.01% bromophenol blue and 10% glycerol). Samples were heated for 2 min at 96°C, centrifuged for 1 min at 10 000 *g* and then resolved by SDS–polyacrylamide gel electrophoresis on 4–20% Tris/glycine gels (Invitrogen Life Technologies, Carlsbad, CA, USA) at 175 V for 70 min at room temperature (~22.7°C). After electrophoresis, the proteins were transferred to Immobilon-P polyvinylidene fluoride membrane (Bio-Rad Laboratories) by the semidry method in a transfer buffer containing 39 mM glycine, 48 mM Tris and 5% methanol at 20 V for 2 h at room temperature. Blots were blocked for 1 h at room temperature in 5% non-fat dry milk in Tris-buffered saline with Tween-20 (20 mM Tris-HCl, 150 mM NaCl and 0.003% Tween-20, pH 7.5). Immunoblots were probed with either anti-β-actin monoclonal antibody (Sigma-Aldrich Co., St Louis, MO, USA) to confirm equal amounts of protein loading or anti-caspase 7 antibody (no. 551239; BD Biosciences Pharmingen, San Diego, CA, USA) which recognizes the 35-kDa proform, 32-kDa pre-active form and 18-kDa p20 active form of the protein. After overnight incubation at 4°C (1 : 1000 for primary antibodies) in 5% blocking solution (non-fat dry milk/Tris-buffered saline with Tween-20) and three washes in Tris-buffered saline with Tween-20, the blots were incubated for 1 h at room temperature in 5% blocking solution containing a biotinylated-conjugated goat anti-mouse IgG (1 : 1000; Amersham Life Science, Inc., Arlington Heights, IL, USA). Blots were then incubated for 30 min at room temperature in blocking solution containing a streptavidin alkaline phosphatase conjugate (1 : 3000; Amersham Life Science, Inc.). Bound antibodies were visualized at room temperature by color development with 5-bromo-4-chloro-3-indolylphosphate/nitroblue tetrazolium (BCIP/NBT) Phosphatase Substrate (Kirkegaard & Perry Laboratories, Gaithersburg, MD, USA). Positive control was camptothecin-treated Jurkat cell lysates (20 μL; BD Biosciences Pharmingen).

Test for anti-caspase 7 antibody specificity

Aliquots of 1, 10, 25 and 50 ng of caspase 7 and caspase 3 human recombinant protein (designed to autoactivate) (Chemicon, Temecula, CA, USA) were prepared and resolved by SDS–polyacrylamide gel electrophoresis on 4–20% Tris/glycine gels (Invitrogen Life Technologies) before being transferred to Immobilon-P polyvinylidene fluoride (Bio-Rad Laboratories) blots. The blots were probed by anti-caspase 7 antibody (1 : 1000; no. 551239; BD Biosciences Pharmingen), which recognizes the pre-active and p20 active form of the protein, and anti-caspase 3 antibody (1 : 1000; no. 9661; Cell Signaling, Beverly, MA, USA), which recognizes the active forms of the protein. For further details, see Immunoblot analysis above.

Immunohistochemistry

Immunohistochemistry preparation

Brain tissues were collected from naive animals or 5 days after craniotomy or TBI. At the appropriate time-points, the animals were anesthetized using 4% isoflurane in a carrier gas of 1 : 1 O_2 : N_2O (4 min), transcardially perfused with 200 mL 2% heparin (Elkins-Sinn, Inc., Cherry Hill, NJ, USA) in 0.9% saline (pH 7.4) followed by 400 mL 4% paraformaldehyde in 0.1 M phosphate buffer (pH 7.4) and then killed by decapitation and the brains removed. A total of 2 h in fixative was followed by storage in either phosphate-buffered saline or cryoprotection buffer. Vibratome (Ted Pella, Inc., Redding, CA, USA) cut 40-μm sections were fluorescently immunolabeled with cell type-specific monoclonal antibody, the cleaved anti-caspase 7 antibody and the nuclear counterstain 4′,6′-diamidino-2-phenylindolehydrochloride (DAPI).

Analysis

Briefly, tissue sections were rinsed in phosphate-buffered saline, incubated for 1 h at room temperature in 10% goat serum/0.2% Triton-X 100 in Tris-buffered saline (block) to decrease non-specific labelling and then incubated with the primary cleaved anti-caspase 7 antibody (1 : 500; Cell Signaling) and either the mouse anti-neuron-specific nuclear protein antibody (neuronal nuclei) (1 : 1000; Chemicon) or the mouse astrocyte-specific anti-glial fibrillary acidic protein antibody (1 : 1000; Roche Molecular Biochemicals) for 4 days in block at 4°C. After being rinsed in phosphate-buffered saline, the tissue sections were incubated with species-specific Alexa Fluor (1 : 3000; Molecular Probes, Inc., Eugene, OR, USA) secondary antibodies in block for 1 h at room temperature. The sections were then washed in phosphate-buffered saline, coverslipped in Vectashield with DAPI (Vector Laboratories, Burlingame, CA, USA), viewed and digitally captured with an Axioplan 2 microscope (Zeiss, Thornwood, NY, USA) equipped with a Spot Real Time Slider high resolution color CCD digital camera (Diagnostic Instruments, Inc., Sterling Heights, MI, USA). Tissue sections without primary antibodies were similarly processed to control for binding of the secondary antibodies. Appropriate control sections were performed and no specific immunoreactivity was detected.

Statistical analyses

For the immunoblots, semiquantitative analysis was performed by computer-assisted densitometric scanning (ImageJ, version 1.29x; NIH, Bethesda, MD, USA). Data were acquired as integrated densitometric values and transformed to percentages of the densitometric levels obtained from naive animals visualized on the same blot. One-way ANOVA with Dunnett's multiple comparison tests was performed on the data using Prism Version 3.03 for Windows (GraphPad Software, San Diego, CA, USA). The 1- and 7-day densitometric values for craniotomy-injured animals were pooled after analysis by one-way ANOVA with Dunnett's multiple comparison tests, for each specific time-point, revealed no statistical differences. The calculated protein levels are the percent increase of the injured samples for each time-point over the pooled craniotomy samples. All values are given as mean ± SEM. Differences were considered significant if $p < 0.05$.

It had been verified in a previous paper from our laboratory that the semiquantitative RT-PCR method yielded results similar to

northern blot analysis (Tolentino *et al*. 2002). In summary, the northern blot analysis demonstrated a temporal profile of transcript induction in response to cortical injury. A linear regression analysis was performed comparing mRNA expression determined by PCR and northern blot and the results from northern blot and PCR analyses fit a linear correlation with a slope of 1.01 ($r^2 = 0.95$). One-way ANOVA with Dunnett's multiple comparison tests was performed on the semiquantitative RT-PCR data using Prism Version 3.03 for Windows (GraphPad Software). The data were normalized using logarithmic transformation. All values are given as mean ± SEM. Differences were considered significant if $p < 0.05$.

Results

Presence and activation of caspase 7 protein in PC12 cells after thapsigargin treatment

Caspase 7 has frequently been characterized as redundant to the more studied primary executioner caspase 3, perhaps playing only a minor role in the rat brain. We attempted to detect caspase 7 in the rat neuronal pheochromocytoma cell line PC12. Before this, to confirm that anti-caspase 7 antibody selectively binds to caspase 7 and not to caspase 3 as a prelude to immunoblot analysis, anti-caspase 7 and anti-caspase 3 antibodies were tested against human caspase 7 and caspase 3 recombinant proteins which were bioengineered to allow them to autoactivate. As Fig. 1 illustrates, the anti-caspase 7 antibody (BD Biosciences Pharmingen) detects only caspase 7 and not caspase 3 and conversely anti-caspase 3 antibody detects only caspase 3 and not caspase 7. This suggests that the antibody for caspase 7 selectively distinguishes caspase 7 from caspase 3.

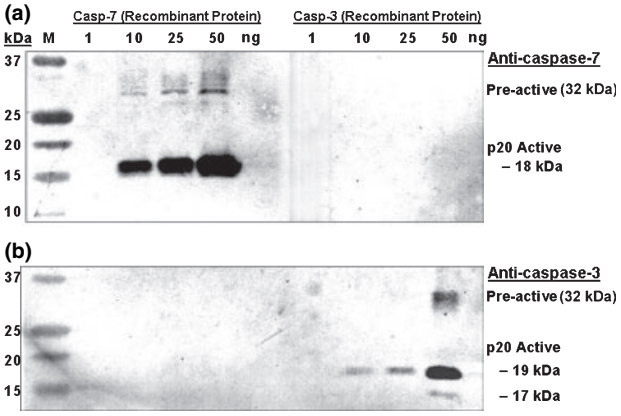

Fig. 1 Confirmation of anti-caspase 7 antibody specificity. Antibodies to caspase 7 (no. 551239; BD Biosciences Pharmingen) and caspase 3 (no. 9661; Cell Signaling) were tested against autoactivating caspase 7 and caspase 3 human recombinant proteins. (a) Anti-caspase 7 reacts solely with the pre-active form and the active form of the caspase 7 protein and not with caspase 3. (b) Anti-caspase 3 reacts solely with the caspase 3 protein as represented by the pre-active form and the two activated forms at 19 and 17 kDa and not with caspase 7. The increasing intensity of the bands correlates with the increasing amounts (in ng) of recombinant protein loaded for both caspases.

Previous studies have established that PC12 cells are a convenient cell model of sympathetic neurons and have proven useful in apoptotic signaling pathway studies (Haviv *et al*. 1998; Edsall *et al*. 2001). After challenge with thapsigargin (1 μM), an ER-associated Ca^{2+}-ATPase inhibitor, fractionated PC12 cell lysates were examined 6, 12 and 24 h post-treatment for caspase 7 activation. The ER/cytosolic (ER/cytosol) fraction and the nuclear fraction both demonstrated increasing levels and activation of the large p20 subunit (18 kDa) of caspase 7 peaking at 24 h (Figs 2a and b) at 456 ± 236 and 451 ± 92%, respectively (data for 48 h are not shown). To determine whether the 18-kDa active form accurately represented active caspase 7, the cells were pre-treated for 1 h with carbobenzoxy-Asp-CH_2OC(O)-2,6-diclorobenzena (100 μM), a pan-caspase inhibitor, before thapsigargin treatment. The inhibitor provided significant protection from active caspase 7, reducing activation of the large subunit to near control levels (Figs 2c and d).

Semiquantitative real-time PCR analysis of caspase 7 mRNA up-regulation after traumatic brain injury

To test the hypothesis that caspase 7 is present, up-regulated and activated in the brain, we first examined caspase 7 mRNA transcription levels in uninjured, craniotomy-injured and injured tissue in our rat model of TBI.

Standard curves were prepared to determine the relative amounts of caspase 7 or GAPDH mRNA present in brain tissue after injury or craniotomy, as well as from uninjured tissues. After the standard curves were generated (see Materials and methods) by plotting the log concentration of total RNA versus the crossing point cycle number, a linear regression analysis was performed. The r^2 ranged from 0.9570 to 0.9992. Figure 3 shows the linear regression analysis of each primer set's crossing point cycle number for each brain region versus the logarithm of the dilution factor. For each primer set, the range of crossing point cycle numbers required to cover the serially diluted standard curve varied: 14–21 cycles for cortical GAPDH, 24–28 cycles for caspase 7 (hippocampus) and 24–29 cycles for caspase 7 (cortex). These differences primarily reflect the abundance of the transcripts. GAPDH mRNA was the most abundant transcript requiring the fewest cycles, whereas caspase 7 cortical mRNA was the least abundant transcript and therefore required the most cycles.

Using the standard curves generated as described, the crossing point cycle numbers of the experimental samples were converted to relative amounts of mRNA. These relative amounts for the injured tissue were then expressed as percentage of craniotomy control (Fig. 4). In order to evaluate the magnitude of injury on mRNA expression, three levels of injury severity, mild, moderate and moderate–

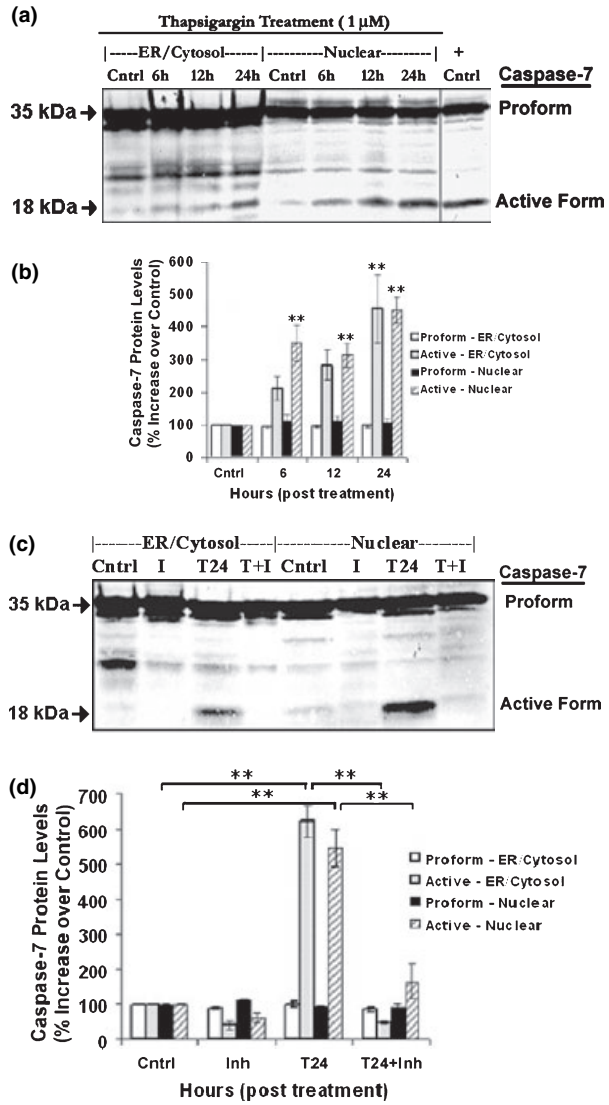

Fig. 2 Thapsigargin-mediated caspase 7 activation in PC12 cells. (a) Representative immunoblot showing caspase 7 levels for fractionated (see Materials and methods) thapsigargin (T)-treated (1 μM) PC12 cells after 6, 12 and 24 h. The positive control (+ Cntrl) was camptothecin-treated Jurket cell lysate. (b) Quantification by densitometry of immunoblots showed that caspase 7 levels were significantly elevated in fractionated thapsigargin-treated PC12 cells compared with control (Cntrl) cells. The values are the mean ± SEM; statistical analysis was performed by one-way ANOVA with Dunnet's multiple comparison test. $n = 5$; $^{**}p < 0.01$. (c) With the pan-caspase inhibitor (I) carbobenzoxy-Asp-$CH_2OC(O)$-2,6-diclorobenzena (Z-D-DCB) (100 μM), fractionated thapsigargin (T)-treated PC12 cells showed inhibition of caspase 7 activation by 24 h. (d) Quantification by densitometry of immunoblots showed that caspase 7 levels were statistically elevated in fractionated thapsigargin (T24)-treated PC12 cells compared with PC12 cells pre-treated with the Z-D-DCB pan-caspase inhibitor (Inh) before thapsigargin treatment or with control cells. The values are the mean and ± SEM; statistical analysis was performed by one-way ANOVA with Dunnet's multiple comparison test. $n = 4$; $^{**}p < 0.01$. ER, endoplasmic reticulum.

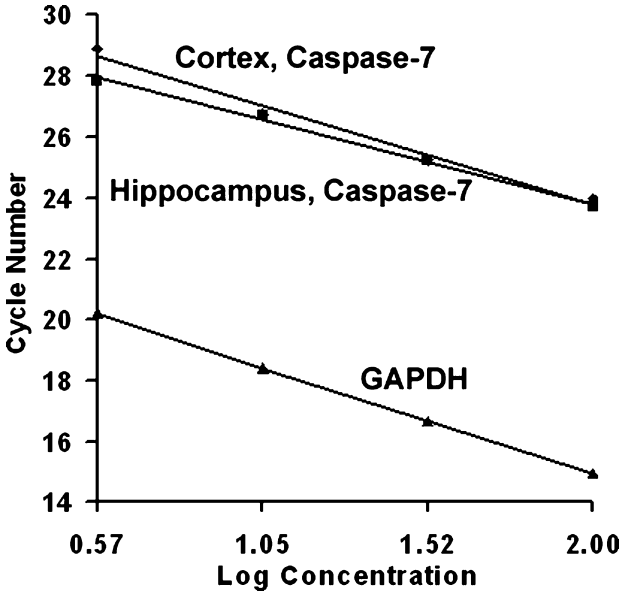

Fig. 3 Standard curve generation for caspase 7 and GAPDH mRNA-specific semiquantitative real-time PCR. Total RNA was extracted from rat ipsilateral hippocampal (6 h post-injury) and cortical (1 day post-injury) tissue for caspase 7 expression and from ipsilateral cortical tissue (3 days post-injury) for GAPDH expression. RNA samples were reverse transcribed and cDNAs were serially diluted. Aliquots of the cDNA dilution curve underwent real-time PCR using primer pairs for caspase 7 mRNA or GAPDH mRNA. For each dilution and each primer set, the cycle number at which the PCR amplification entered the log-linear region was identified (crossing point cycle number). Standard curves were generated by plotting the log concentration of total mRNA vs. the crossing point cycle number. A linear regression analysis was performed and the r^2 ranged from 0.9570 to 0.9992. For quantitation, mRNA samples from naive, craniotomy-injured and injured rats underwent real-time PCR, generating a crossing point cycle number for each primer set. Using the standard curves, the cycle number was converted to a relative amount of mRNA.

severe (1.0, 1.2 and 1.6 mm of compression, respectively), were performed and the ipsilateral cortex and ipsilateral hippocampus were examined after controlled cortical impact injury. The data convey the similarities in the up-regulation of mRNA levels after injury and illustrate the effect of injury severity on caspase 7 mRNA expression. In the ipsilateral cortex, maximal and statistically significant caspase 7 mRNA expression was observed for all three magnitudes 5 days after injury (392 ± 65, 358 ± 65 and 515 ± 90%, respectively) the latest time-point examined (Fig. 4a). All three magnitudes showed an upward trend earlier with the 1.2- and 1.6-mm injury magnitudes producing significant increases in mRNA expression on day 3 (332 ± 26 and 348 ± 44%, respectively). In the hippocampus, however, maximal and significant caspase 7 mRNA levels were observed for the 1.0- and 1.2-mm injury magnitudes as early as 6 h post-trauma (491 ± 167 and 626 ± 23%, respectively) before declining and returning to near naive levels by day 5

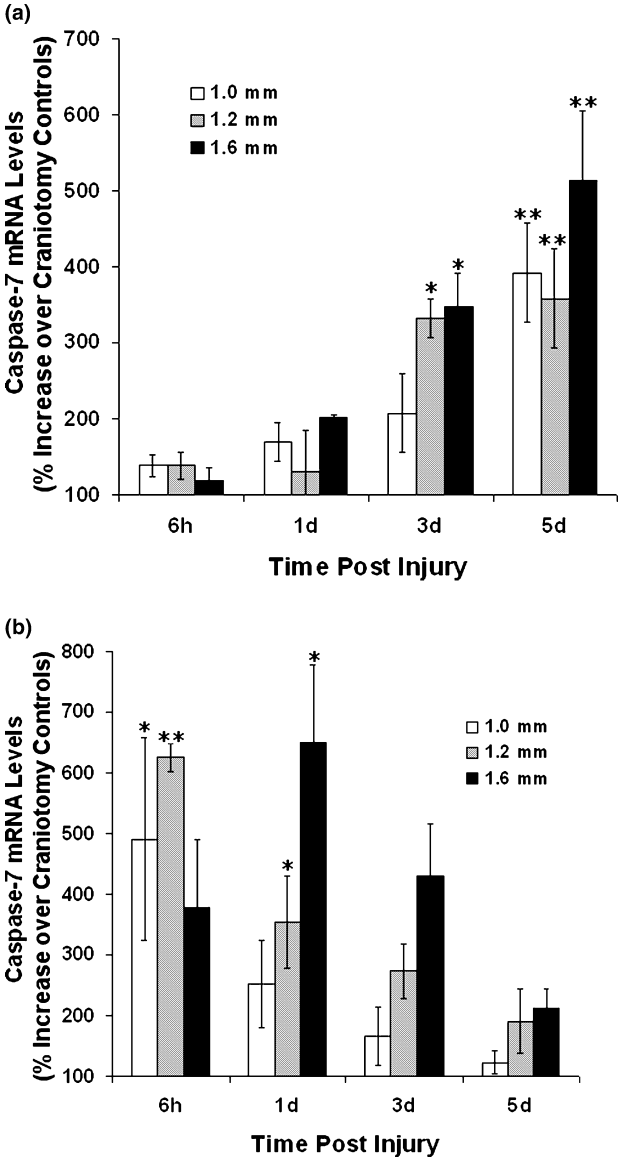

Fig. 4 Semiquantitative real-time PCR analysis of caspase 7 mRNA expression. cDNA samples for the ipsilateral cortex (a) and the ipsilateral hippocampus (b) from naive, craniotomy-injured and injured rats underwent real-time PCR generating a crossing point cycle number for each primer set. Using the standard curves, the cycle number was converted to a relative amount of mRNA. The transcript amounts for the injured rats are expressed as a percentage of craniotomy controls. Values are the mean ± SEM and one-way ANOVA with Dunnet's multiple comparison test was performed to evaluate statistical significance. $n = 3$; $^{*}p < 0.05$, $^{**}p < 0.01$.

(Fig. 4b). The 1.6-mm injury magnitude peaked later at day 1 post-injury (650 ± 129%) and then declined to near naive levels by day 5. The difference in pattern of expression between the cortex and hippocampus can be understood when the type of injury (necrosis vs. apoptosis), cell sensitivity to perturbation and the levels of damage which each brain region sustains after impact are taken into consideration, especially the distance from the injury site.

Immunoblot analysis of caspase 7 expression and activation after traumatic brain injury *in vivo*

To test the hypothesis that caspase 7 protein is present and could be up-regulated and activated in the brain, we examined caspase 7 activation after injury in our rat model of TBI. As caspase 7 has been characterized as a protein known to associate with the ER (Chandler *et al*. 1998; Meller *et al*. 2002), the ER/cytosolic fraction (see Materials and methods) was prepared from the ipsilateral cortex and hippocampus to test the results of the 1.6-mm injury level examined in the mRNA expression experiments (Fig. 4). For the 1.6-mm compression, representing a moderate–severe level of injury, caspase 7 expression was examined using an antibody that recognizes the proform, pre-active form and large, or p20, active subunit of caspase 7 (BD Biosciences Pharmingen). The densitometric analyses for the injured and craniotomy tissues were quantified as a fold increase over naive control levels. The results are expressed as the percentage increase of injured over the pooled craniotomy controls (Figs 5b and d). Figures 5(a and c) are representative immunoblots for caspase 7 expression in ipsilateral cortex and hippocampus, respectively, for naive rats, craniotomy-injured control rats at 1 and 7 days post-injury and animals subjected to TBI 6 h and 1, 3, 5, 7 and 14 days post-injury. Immunoblots were also run with equivalent amounts of protein and probed with the anti-β-actin antibody serving as an internal protein loading and transfer control. Loading and transfer were essentially equivalent in all wells, as shown by the 42-kDa signal intensities.

Ipsilateral cortex tissue samples were taken from the penumbra and lesion site where the brain damage was extensive. Tissue samples from the craniotomy-injured animals, while not displaying the hallmarks of TBI, did show a modest decrease in caspase 7 proform expression on day 1 after the craniotomy that was not statistically significant and returned to naive levels by day 7 (Fig. 5b). There was no statistically significant change in the active form in the craniotomy-injured control animals. A statistically significant induction of the caspase 7 proform (35 kDa), pre-active form (32 kDa) and active form (18 kDa) was observed within 3 days of cortical injury when compared with the pooled craniotomy controls (Fig. 5b). The proform peaked at 3 days post-injury (197 ± 28%) while the active form peaked on day 5 (611 ± 93%), remaining significantly elevated to 7 days post-TBI, and the pre-active form peaked at day 7 (557 ± 123%). All three returned to near naive levels by day 14.

Tissue samples from the ipsilateral hippocampus for the craniotomy-injured control animals showed no statistically significant increase in procaspase 7 expression (Fig. 5d) and,

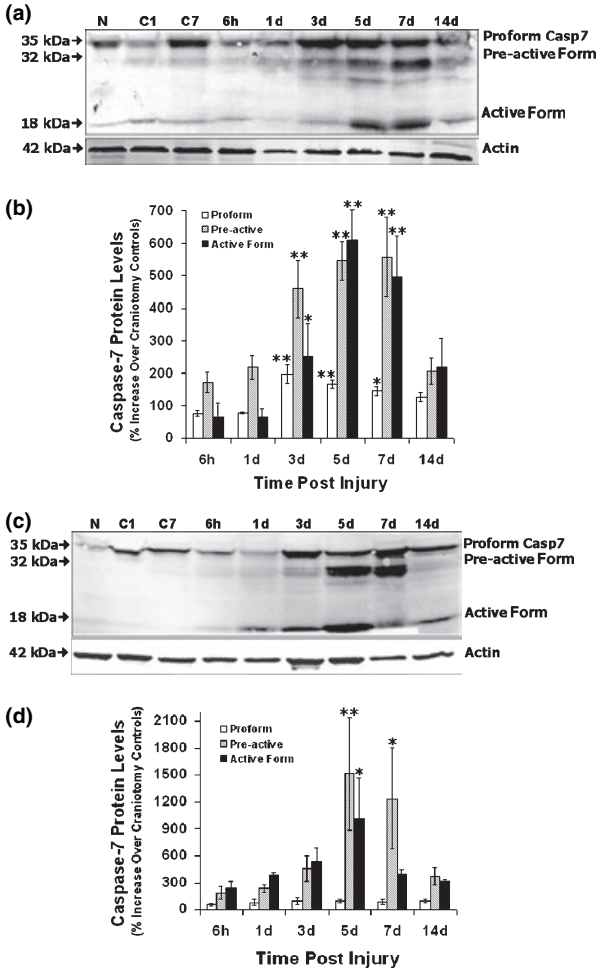

Fig. 5 Traumatic brain injury (TBI)-mediated caspase 7 protein activation. Representative immunoblot of the proform (35 kDa), pre-active (32 kDa) and active (18 kDa) form of caspase 7 protein in ipsilateral cortical (a) ($n = 6$) and ipsilateral hippocampal (c) ($n = 4$) samples after controlled cortical impact model of TBI (1.6-mm compression) in rats 6 h and 1, 3, 5, 7 and 14 days post-injury. β-actin was directly assessed as a protein-loading method control. As β-actin may itself be cleaved by caspases, blots were examined for cleaved fragments; no fragments were detected. Immunoblot analyses using the anti-caspase 7 antibody were quantified by densitometry and the levels of caspase 7 (proform, pre-active and active form) expression in the ipsilateral cortex (b) and ipsilateral hippocampus (d) of injured animals were calculated as a percentage of pooled craniotomy (C1 and C7) controls. Values are the mean ± SEM and one-way ANOVA with Dunnett's multiple comparison test was performed to evaluate statistical significance (*$p < 0.05$, **$p < 0.01$). N, naive animals.

likewise, there was no detectable change in the active form. A statistically significant induction of the caspase 7 pre-active and active forms, when compared with pooled craniotomy controls, peaked around day 5 post-injury (1519 ± 627 and 1022 ± 442%, respectively) before returning to near naive levels (Fig. 5d) statistically by day 14 post-injury.

Immunohistochemical analysis of cleaved caspase 7 activation after traumatic brain injury

To determine in which cell type TBI-mediated activation of caspase 7 occurs, brain sections 5 days post-injury, as well as naive and 5 day craniotomy-injured brain sections, were examined for cleaved caspase 7. High magnification photomicrographs of the Alexa Fluor stains of uninjured (naive) and craniotomy-injured animals revealed healthy cell bodies and little detectable cleaved caspase 7 expression (Figs 6c and d). In contrast, cleaved caspase 7 expression was readily observed in tissue samples in both the ipsilateral cortex and hippocampus 5 days post-injury (Figs 6a and b and 7a and b), with a considerable degree of staining in the cortex in the immediate vicinity of the impact site.

The ipsilateral cortex revealed an increase in cleaved caspase 7 expression with decreasing levels distal to the impact site. The morphology of the injury site where elevated levels of cleaved caspase 7 activation was located had a decidedly disorganized, almost chaotic, appearance when compared with the contralateral naive or craniotomy-injured tissue. Due to this disorganized and chaotic condition, quantification of the percentage of cells or cell types in which caspase 7 was activated, although considered, was not undertaken as it was believed that the results would be misleading. In the ipsilateral cortex, cleaved caspase 7 colocalized with immunopositive neurons as marked by anti-neuronal nuclei NeuN, a neuronal cell-specific antibody (Fig. 6a), and appeared to include those cells with evidence of morphopathology. The ipsilateral hippocampus also revealed that activated cleaved caspase 7 colocalized with the neuronal cell-specific marker NeuN, (Fig. 6b) but the hippocampal tissue did not display the same disorganized appearance as viewed in the cortex. Cleaved caspase 7 was also found to colocalize with immunopositive astrocytes as marked by anti-glial fibrillary acidic protein, GFAP, an astrocytic cell-specific antibody, in the ipsilateral cortex (Fig. 7a) and the ipsilateral hippocampus (Fig. 7b) and also appeared to include those cells with apoptotic bodies.

Discussion

Caspase 7 is emerging as an important apoptotic protease in its own right, suggesting that it is more than a redundant clone of caspase 3. Our findings firmly establish the presence of caspase 7 in the rat brain, suggesting that it may play a role in the apoptotic cell death response after TBI. To our knowledge, this study is the first to demonstrate that caspase 7 is present, induced at the mRNA (Fig. 4) and up-regulated and activated at the protein (Fig. 5) levels in both the hippocampus and cortex. Such an elevated and activated level for caspase 7 after TBI is sustained 3–7 days post-injury (Fig. 5). We also demonstrated that the cleaved caspase 7 protein is activated in both neurons and astrocytes in the ipsilateral

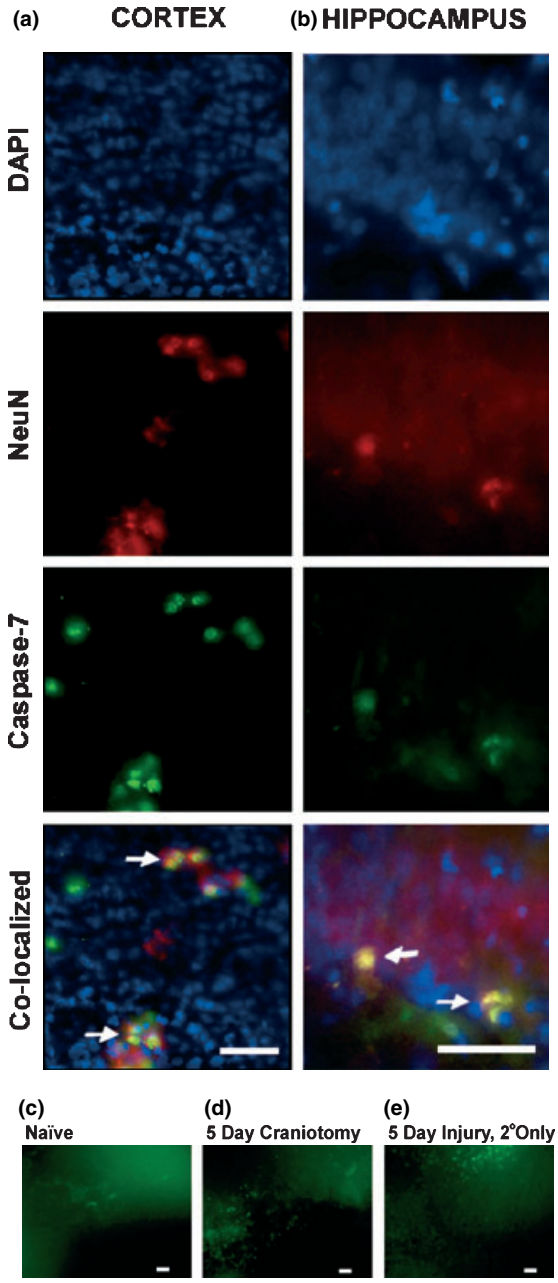

Fig. 6 Traumatic brain injury (TBI) activation of caspase 7 in neurons in the cortex and hippocampus. Caspase 7 expression induced in cortical (a) and hippocampal (b) neurons after TBI was examined using immunohistochemical techniques on 40-μm brain tissue sections. Chromatin was visualized with DAPI, neurons with the neuron-specific antibody anti-neuronal nuclei (NeuN) (red) and caspase 7 with a cleaved anti-caspase 7 antibody (green) with colocalization resulting in yellow and orange (arrows). Photomicrographs are at 400x; scale bars, 20 μm. Controls for caspase 7 expression were examined on 40-μm brain tissue sections of naive (c), 5-day craniotomy (d) and 5-day injured tissue (secondary antibody only) (e). No caspase 7 expression was evident and only typical background manifestations were observed. Photomicrographs are at 200x; scale bars, 20 μm.

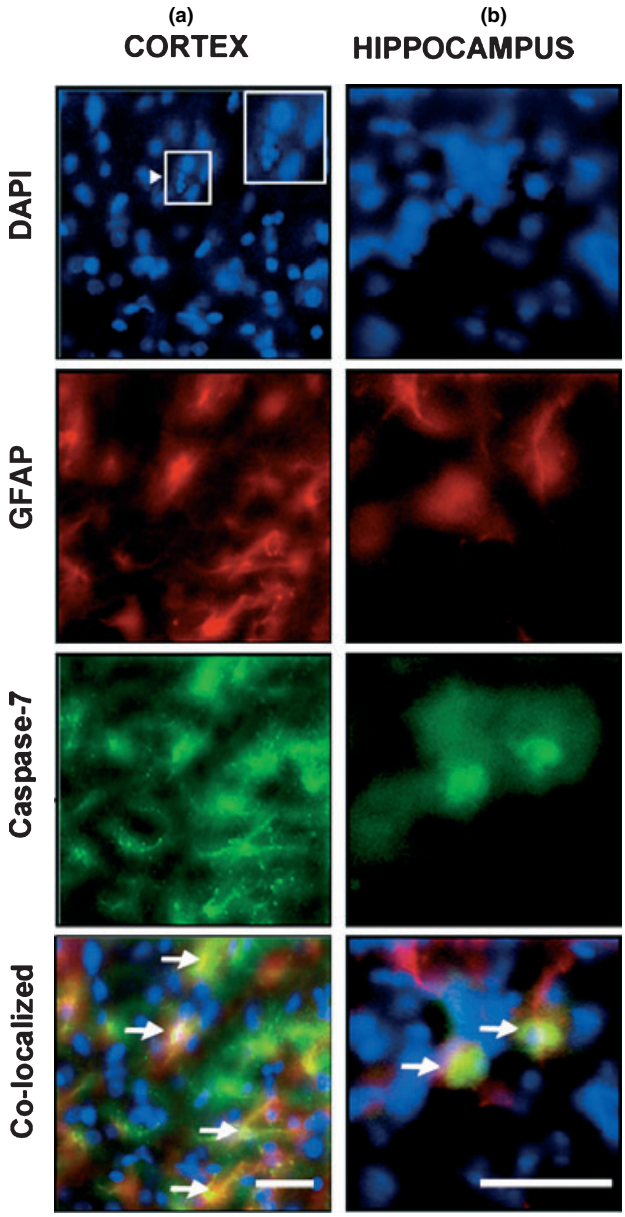

Fig. 7 Traumatic brain injury (TBI) activation of caspase 7 in astrocytes in the cortex and hippocampus. Caspase 7 expression induced in cortical (a) and hippocampal (b) astrocytes after TBI was examined using immunohistochemical techniques on 40-μm brain tissue sections. Chromatin was visualized with DAPI, astrocytes with the astrocytic-specific antibody anti-glial fibrillary acidic protein (GFAP) (red) and caspase 7 with a cleaved anti-caspase 7 antibody (green) with colocalization resulting in yellow and orange (arrows) including in cells showing apoptotic bodies (insert and arrowhead). Photomicrographs are at 400x; scale bars, 20 μm.

cortex and hippocampus with the most robust levels in and immediately adjacent to the lesion site. The more distal regions, including the hippocampus, had fewer cells expressing activated caspase 7 (Figs 6 and 7).

Of the three apoptotic pathways that may activate caspase 7, the intrinsic pathway, mediated through the mitochondria by caspase 9, and the extrinsic pathway, mediated through the plasma membrane by caspase 8 and caspase 10, have been the most studied. The third pathway, initiated under ER stress, is mediated through the ER membrane and appears to involve caspase 12 and caspase 7. It has been reported that the ER chaperone GRP78 (BiP) constitutively associates with procaspase 7 (Reddy *et al*. 2003) forming a complex with caspase 7 and caspase 12 (Rao *et al*. 2002). Under ER stress, BiP is released and caspase 7 cleaves caspase 12 (Rao *et al*. 2001) activating the caspase apoptotic cascade thereby coupling ER stress to the cell death program. Our PC12 cell culture data verify that caspase 7 is activated by ER stress when initiated by thapsigargin treatment (Fig. 2). A differential subcellular distribution study of specific caspases *in vivo* demonstrated that active caspase 3 was primarily cytosolic, whereas active caspase 7 associated almost exclusively with the mitochondrial and microsomal (ER) fractions and, in the latter, the ER-associated caspase 7 was blocked by a pan-caspase inhibitor (Chandler *et al*. 1998).

The ER-associated protein caspase 12, a caspase 7 target (Nakagawa *et al*. 2000), is also processed after TBI (Larner *et al*. 2004). Caspase 12 activation peaked at 1 day post-TBI (Larner *et al*. 2004) while this study demonstrated that caspase 7 peaks about day 5 post-injury (Fig. 3). These data suggest that calpain, which also activates caspase 12 (Nakagawa and Yuan 2000), may be an early activator of caspase 12 while caspase 7 plays a more prominent role later in addition to engaging in its normal executioner role (Rao *et al*. 2001). It is also possible that caspase 7 was activated very early after TBI at statistically undetectable levels yet still cleaved caspase 12, akin to the previous report of Korfali *et al*. (2004). It may then become engaged in a feedback loop that may be responsible, in part, for the continual loss of neurons that has been noted to occur over an extended period of time after TBI (Colicos *et al*. 1996; Smith *et al*. 1997; Conti *et al*. 1998; Sato *et al*. 2001; Shiozaki *et al*. 2001). This low level feedback loop is suggested by findings that, while caspase 7 may become activated early in the apoptotic pathway, it peaks after caspase 12 and that it may be activated by active caspase 12 via caspase 9 (Rao *et al*. 2001, 2002).

Consistent with our studies several recent *in vivo* studies found caspase 7 mRNA or protein in brain tissue. At the mRNA level, a caspase 7 increase of 1.5–2+-fold within 24 h was detected in the ipsilateral cortex in the focal ischemia rat middle cerebral artery occlusion model (Harrison *et al*. 2001). Caspase 7 mRNA also appeared elevated in the entorhinal cortex and was closely associated with neurofibrillary tangles and, to a lesser extent, neuritic plaque density in Alzheimer's disease patients (Pompl *et al*. 2003). At the protein level, besides this study, only one other report found elevated active caspase 7 in a nerve system injury paradigm and its expression was highly localized (Repici *et al*. 2003).

It is worth noting that, in this study, the cortex caspase 7 mRNA levels were statistically elevated within 3–5 days after TBI. This is consistent with the significant elevated levels of activated caspase 7 protein occurring 3–7 days post-injury. In the hippocampus the activated proteins did not peak until day 5 while caspase 7 mRNA levels for the 1.6-mm compression injury were elevated much earlier (peaking at 1 day post-injury). One possible explanation for this inconsistency is that mRNA translation may be delayed due to the early unfolded protein response which initiates general global inhibition of protein synthesis as the cells attempt to regain control over their cellular metabolism, yet it appears to leave mRNA transcription unaffected (Larner *et al*. 2004). Another possibility is that caspase 7 translation product is being lost due to ubiquination or ER-associated degradation, also a part of the unfolded protein response, suggesting that this brain region is being sheltered from apoptotic stimuli more effectively due to its distance from the lesion site. Given our current knowledge of unfolded protein response and other molecular mechanisms after TBI, which is still in the early stages of elucidation, there is insufficient information to precisely point to a complete explanation at this time.

In summary, this study demonstrates that caspase 7 is significantly induced, up-regulated and activated in both neurons and astrocytes after TBI in rats and may play a role in the cell death in TBI patients. Further studies are underway to confirm and further elucidate the relative contribution of caspase 7 versus caspase 3 in TBI pathology.

Acknowledgements

This study was supported by grants from the Department of Defense (DAMD 17-99-1-9565 and 17-03-1-0066) and the National Institutes of Health (NIH R01-NS39091 and R01-NS40182).

References

Chandler J. M., Cohen G. M. and MacFarlane M. (1998) Different subcellular distribution of caspase-3 and caspase-7 following Fas-induced apoptosis in mouse liver. *J. Biol. Chem.* **273**, 10 815–10 818.

Clark R. S., Kochanek P. M., Watkins S. C. *et al.* (2000) Caspase-3 mediated neuronal death after traumatic brain injury in rats. *J. Neurochem.* **74**, 740–753.

Cohen G. M. (1997) Caspases: the executioners of apoptosis. *Biochem. J.* **326**, 1–16.

Colicos M. A., Dixon C. E. and Dash P. K. (1996) Delayed, selective neuronal death following experimental cortical impact injury in rats: possible role in memory deficits. *Brain Res.* **739**, 111–119.

Conti A. C., Raghupathi R., Trojanowski J. Q. and McIntosh T. K. (1998) Experimental brain injury induces regionally distinct apoptosis during the acute and delayed post-traumatic period. *J. Neurosci.* **18**, 5663–5672.

Dixon C. E., Clifton G. L., Lighthall J. W., Yaghmai A. A. and Hayes R. L. (1991) A controlled cortical impact model of traumatic brain injury in the rat. *J. Neurosci. Meth.* **39**, 253–262.

Duan H., Chinnaiyan A. M., Hudson P. L., Wing J. P., He W. W. and Dixit V. M. (1996) ICE-LAP3, a novel mammalian homologue of the Caenorhabditis elegans cell death protein Ced-3 is activated during Fas- and tumor necrosis factor-induced apoptosis. *J. Biol. Chem.* **271**, 1621–1625.

Edsall L. C., Cuvillier O., Twitty S., Spiegel S. and Milstien S. (2001) Sphingosine kinase expression regulates apoptosis and caspase activation in PC12 cells. *J. Neurochem.* **76**, 1573–1584.

Ethell D. W., Bossy-Wetzel E. and Bredesen D. E. (2001) Caspase 7 can cleave tumor necrosis factor receptor-I (p60) at a non-consensus motif, in vitro. *Biochim. Biophys. Acta* **1541**, 231–238.

Fernandes-Alnemri T., Takahashi A., Armstrong R. *et al.* (1995) Mch3, a novel human apoptotic cysteine protease highly related to CPP32. *Cancer Res.* **55**, 6045–6052.

Gerberding J. L. (2003) *Report to Congress on Mild Traumatic Brain Injury in the United States: Steps to Prevent a Serious Public Health Problem.* Centers for Disease Control and Prevention, National Center for Injury Prevention and Control, Atlanta, GA, USA.

Germain M., Affar E. B., D'Amours D., Dixit V. M., Salvesen G. S. and Poirier G. G. (1999) Cleavage of automodified poly (ADP-ribose) polymerase during apoptosis. Evidence for involvement of caspase-7. *J. Biol. Chem.* **274**, 28 379–28 384.

Harrison D. C., Davis R. P., Bond B. C., Campbell C. A., James M. F., Parsons A. A. and Philpott K. L. (2001) Caspase mRNA expression in a rat model of focal cerebral ischemia. *Brain Res. Mol. Brain Res.* **89**, 133–146.

Haviv R., Lindenboim L., Yuan J. and Stein R. (1998) Need for caspase-2 in apoptosis of growth-factor-deprived PC12 cells. *J. Neurosci. Res.* **52**, 491–497.

Henshall D. C., Skradski S. L., Meller R., Araki T., Minami M., Schindler C. K., Lan J. Q., Bonislawski D. P. and Simon R. P. (2002) Expression and differential processing of caspases 6 and 7 in relation to specific epileptiform EEG patterns following limbic seizures. *Neurobiol. Dis.* **10**, 71–87.

Hollenbeck P. J. (1989) The distribution, abundance and subcellular localization of kinesin. *J. Cell Biol.* **108**, 2335–2342.

Johnson F. B., Sinclair D. A. and Guarente L. (1999) Molecular biology of aging. *Cell* **96**, 291–302.

Juan T. S., McNiece I. K., Argento J. M., Jenkins N. A., Gilbert D. J., Copeland N. G. and Fletcher F. A. (1997) Identification and mapping of Casp7, a cysteine protease resembling CPP32 beta, interleukin-1 beta converting enzyme, and CED-3. *Genomics* **40**, 86–93.

Kampfl A., Posmantur R., Nixon R., Grynspan F., Zhao X., Liu S. J., Newcomb J. K., Clifton G. L. and Hayes R. L. (1996) mu-calpain activation and calpain-mediated cytoskeletal proteolysis following traumatic brain injury. *J. Neurochem.* **67**, 1575–1583.

Korfali N., Ruchaud S., Loegering D., Bernard D., Dingwall C., Kaufmann S. H. and Earnshaw W. C. (2004) Caspase-7 gene disruption reveals an involvement of the enzyme during the early stages of apoptosis. *J. Biol. Chem.* **279**, 1030–1039.

Kuida K., Zheng T. S., Na S., Kuan C., Yang D., Karasuyama H., Rakic P. and Flavell R. A. (1996) Decreased apoptosis in the brain and premature lethality in CPP32-deficient mice. *Nature* **384**, 368–372.

Larner S. F., Hayes R. L., McKinsey D. M., Pike B. R. and Wang K. K. (2004) Increased expression and processing of caspase-12 after traumatic brain injury in rats. *J. Neurochem.* **88**, 78–90.

Le D. A., Wu Y., Huang Z. *et al.* (2002) Caspase activation and neuroprotection in caspase-3-deficient mice after *in vivo* cerebral ischemia and in vitro oxygen glucose deprivation. *Proc. Natl Acad. Sci. USA* **99**, 15 188–15 193.

Machleidt T., Geller P., Schwandner R., Scherer G. and Kronke M. (1998) Caspase 7-induced cleavage of kinectin in apoptotic cells. *FEBS Lett.* **436**, 51–54.

Meller R., Skradski S. L., Simon R. P. and Henshall D. C. (2002) Expression, proteolysis and activation of caspases 6 and 7 during rat C6 glioma cell apoptosis. *Neurosci. Lett.* **324**, 33–36.

Nakagawa T. and Yuan J. (2000) Cross-talk between two cysteine protease families. Activation of caspase-12 by calpain in apoptosis. *J. Cell Biol.* **150**, 887–894.

Nakagawa T., Zhu H., Morishima N., Li E., Xu J., Yankner B. A. and Yuan J. (2000) Caspase-12 mediates endoplasmic-reticulum-specific apoptosis and cytotoxicity by amyloid-beta. *Nature* **403**, 98–103.

Nath R., Raser K. J., Stafford D., Hajimohammadreza J., Posner A., Allen H., Talanian R. V., Yuen P., Gilbertsen R. B. and Wang K. K. W. (1996) Non-erythroid alpha-spectrum breakdown by calpain and interleukin1 beta-converting-enzyme-like protease(s) in apoptotic cells: contributory roles of both protease families in neuronal apoptosis. *Biochem. J.* **319**, 683–690.

Newcomb J. K., Zhao X., Pike B. R. and Hayes R. L. (1999) Temporal profile of apoptotic-like changes in neurons and astrocytes following controlled cortical impact injury in the rat. *Exp. Neurol.* **158**, 76–88.

Nicolini G., Rigolio R., Miloso M., Bertelli A. A. and Tredici G. (2001) Anti-apoptotic effect of trans-resveratrol on paclitaxel-induced apoptosis in the human neuroblastoma SH-SY5Y cell line. *Neurosci. Lett.* **302**, 41–44.

Oppenheim R. W. (1991) Cell death during development of the nervous system. *Annu. Rev. Neurosci.* **14**, 453–501.

Pike B. R., Zhao X., Newcomb J. K., Posmantur R. M., Wang K. K. and Hayes R. L. (1998) Regional calpain and caspase-3 proteolysis of alpha-spectrin after traumatic brain injury. *Neuroreport* **9**, 2437–2442.

Pike B. R., Flint J., Dutta S., Johnson E., Wang K. K. W. and Hayes R. L. (2001) Accumulation of non-erythroid αII-spectrin and calpain-cleaved αII-spectrin breakdown products in cerebrospinal fluid after traumatic brain injury in rats. *J. Neurochem.* **78**, 1297–1306.

Pompl P. N., Yemul S., Xiang Z., Ho L., Haroutunian V., Purohit D., Mohs R. and Pasinetti G. M. (2003) Caspase gene expression in the brain as a function of the clinical progression of Alzheimer disease. *Arch. Neurol.* **60**, 369–376.

Raff M. C., Barres B. A., Burne J. F., Coles H. S., Ishizaki Y. and Jacobson M. D. (1993) Programmed cell death and the control of cell survival: lessons from the nervous system. *Science* **262**, 695–700.

Rao R. V., Hermel E., Castro-Obregon S., del Rio G., Ellerby L. M., Ellerby H. M. and Bredesen D. E. (2001) Coupling endoplasmic reticulum stress to the cell death program. Mechanism of caspase activation. *J. Biol. Chem.* **276**, 33 869–33 874.

Rao R. V., Peel A., Logvinova A., del Rio G., Hermel E., Yokota T., Goldsmith P. C., Ellerby L. M., Ellerby H. M. and Bredesen D. E. (2002) Coupling endoplasmic reticulum stress to the cell death program: role of the ER chaperone GRP78. *FEBS Lett.* **514**, 122–128.

Ray N. and Cardone M. H. (2002) The caspases: from here to eternity, in *Apoptosis: the Molecular Biology of Programmed Cell Death* (Jacobson M. D. and McCarthy N., eds), p. 117. Oxford University Press, New York, NY, USA.

Reddy R. K., Mao C., Baumeister P., Austin R. C., Kaufman R. J. and Lee A. S. (2003) Endoplasmic reticulum chaperone protein GRP78 protects cells from apoptosis induced by topoisomerase inhibitors: role of ATP binding site in suppression of caspase-7 activation. *J. Biol. Chem.* **278**, 20 915–20 924.

Repici M., Atzori C., Migheli A. and Vercelli A. (2003) Molecular mechanisms of neuronal death in the dorsal lateral geniculate nucleus following visual cortical lesions. *Neuroscience* **117**, 859–867.

Riedl S. J., Fuentes-Prior P., Renatus M., Kairies N., Krapp S., Huber R., Salvesen G. S. and Bode W. (2001) Structural basis for the activation of human procaspase-7. *Proc. Natl Acad. Sci. USA* **98**, 14 790–14 795.

Rink A., Fung K. M., Trojanowski J. Q., Lee V. M., Neugebauer E. and McIntosh T. K. (1995) Evidence of apoptotic cell death after experimental traumatic brain injury in the rat. *Am. J. Pathol.* **147**, 1575–1583.

Rozen S. and Skaletsky H. J. (1998) *Primer3 (v. 0.9).* Whitehead Institute for Biomedical Research. Code available at http://www–genome.wi.mit.edu/genome_software/other/primer3.html. Last access: May 6, 2004.

Sato M., Chang E., Igarashi T. and Noble L. J. (2001) Neuronal injury and loss after traumatic brain injury: time course and regional variability. *Brain Res.* **917**, 45–54.

Shiozaki T., Akai H., Taneda M., Hayakata T., Aoki M., Oda J., Tanaka H., Hiraide A., Shimazu T. and Sugimoto H. (2001) Delayed hemispheric neuronal loss in severely head-injured patients. *J. Neurotrauma* **18**, 665–674.

Slee E. A., Adrain C. and Martin S. J. (2001) Executioner caspase-3, -6, and -7 perform distinct, non-redundant roles during the demolition phase of apoptosis. *J. Biol. Chem.* **276**, 7320–7326.

Smith D. H., Chen X. H., Pierce J. E., Wolf J. A., Trojanowski J. Q., Graham D. I. and McIntosh T. K. (1997) Progressive atrophy and neuron death for one year following brain trauma in the rat. *J. Neurotrauma* **14**, 715–727.

Soung Y. H., Lee J. W., Kim H. S. *et al.* (2003) Inactivating mutations of CASPASE-7 gene in human cancers. *Oncogene* **22**, 8048–8052.

Thompson C. B. (1995) Apoptosis in the pathogenesis and treatment of disease. *Science* **267**, 1456–1462.

Tolentino P. J., DeFord S. M., Notterpek L., Glenn C. C., Pike B. R., Wang K. K. and Hayes R. L. (2002) Up-regulation of tissue-type transglutaminase after traumatic brain injury. *J. Neurochem.* **80**, 579–588.

Toyoshima I., Yu H., Steuer E. R. and Sheetz M. P. (1992) Kinectin, a major kinesin-binding protein on ER. *J. Cell Biol.* **118**, 1121–1131.

Vaux D. L. and Korsmeyer S. J. (1999) Cell death in development. *Cell* **96**, 245–254.

Wei Y., Fox T., Chambers S. P., Sintchak J., Coll J. T., Golec J. M., Swenson L., Wilson K. P. and Charifson P. S. (2000) The structures of caspases-1, -3, -7 and -8 reveal the basis for substrate and inhibitor selectivity. *Chem. Biol.* **7**, 423–432.

Wolf B. B. and Green D. R. (1999) Suicidal tendencies: apoptotic cell death by caspase family proteinases. *J. Biol. Chem.* **274**, 20 049–20 052.

Yakovlev A. G., Knoblach S. M., Fan L., Fox G. B., Goodnight R. and Faden A. I. (1997) Activation of CPP32-like caspases contributes to neuronal apoptosis and neurological dysfunction after traumatic brain injury. *J. Neurosci.* **17**, 7415–7424.

Yuan J. and Yankner B. A. (2000) Apoptosis in the nervous system. *Nature* **407**, 802–809.

Zhang Y., Goodyer C. and LeBlanc A. (2000) Selective and protracted apoptosis in human primary neurons microinjected with active caspase-3, -6, -7, and – 8. *J. Neurosci.* **20**, 8384–8389.

online data

Comparing calpain- and caspase-3-mediated degradation patterns in traumatic brain injury by differential proteome analysis

Ming Cheng LIU*†, Veronica AKLE*†, Wenrong ZHENG*†, Jitendra R. DAVE‡, Frank C. TORTELLA‡, Ronald L. HAYES*†§ and Kevin K. W. WANG*†§[1]

*Center for Neuroproteomics and Biomarkers Research, Department of Psychiatry, McKnight Brain Institute, University of Florida, P.O. Box 100256, Gainesville, FL 32610, U.S.A., †Center for Traumatic Brain Injury Studies, Department of Neuroscience, McKnight Brain Institute, University of Florida, P.O. Box 100256, Gainesville, FL 32610, U.S.A., ‡Department of Neuropharmacology and Molecular Biology, Division of Neurosciences, Walter Reed Army Institute of Research, Silver Spring, MD, U.S.A., and §Banyan Biomarkers, Inc. 12085 Research Drive, Suite 180, Alachua, FL 32615, U.S.A.

A major theme of TBI (traumatic brain injury) pathology is the over-activation of multiple proteases. We have previously shown that calpain-1 and -2, and caspase-3 simultaneously produced αII-spectrin BDPs (breakdown products) following TBI. In the present study, we attempted to identify a comprehensive set of protease substrates (degradome) for calpains and caspase-3. We further hypothesized that the TBI differential proteome is likely to overlap significantly with the calpain- and caspase-3-degradomes. Using a novel HTPI (high throughput immunoblotting) approach and 1000 monoclonal antibodies (PowerBlot™), we compared rat hippocampal lysates from 4 treatment groups: (i) naïve, (ii) TBI (48 h after controlled cortical impact), (iii) *in vitro* calpain-2 digestion and (iv) *in vitro* caspase-3 digestion. In total, we identified 54 and 38 proteins that were vulnerable to calpain-2 and caspase-3 proteolysis respectively. In addition, the expression of 48 proteins was down-regulated following TBI, whereas that of only 9 was up-regulated. Among the proteins down-regulated in TBI, 42 of them overlapped with the calpain-2 and/or caspase-3 degradomes, suggesting that they might be proteolytic targets after TBI. We further confirmed several novel TBI-linked proteolytic substrates, including βII-spectrin, striatin, synaptotagmin-1, synaptojanin-1 and NSF (*N*-ethylmaleimide-sensitive fusion protein) by traditional immunoblotting. In summary, we demonstrated that HTPI is a novel and powerful method for studying proteolytic pathways *in vivo* and *in vitro*.

Key words: calpain, caspase, degradome, high throughput immunoblotting (HTPI), proteomics, traumatic brain injury (TBI).

INTRODUCTION

TBI (traumatic brain injury) represents a major central nervous system disorder without any clinically proven therapy. However, significant progress has been made in understanding the biochemical mechanisms of injury. Indeed, protease over-activation is a major theme in traumatic and ischaemic brain injury. These cysteine proteases include calpain-1 and -2, caspase-3, cathepsin-B and -L [1], and metalloproteases e.g. MMP (matrix metallprotease)-2 and -9 [2–3], and the proteasome [4]. Of particular interest are calpains and caspase-3 [5]. Calpain is activated during both oncotic (necrotic) and apoptotic cell-death in neurons, whereas caspase-3 is strictly activated only in neuronal apoptosis. Evidence demonstrates that both necrotic and apoptotic cell death are present in traumatic or ischaemic brain injury. Our research has shown that calpain-produced and caspase-3-produced SBDPs (αII-spectrin breakdown products) are present following both traumatic and ischaemic brain injury. We have also shown that the same SBDPs can be found in cerebrospinal fluid following TBI in rats [6]. In addition, many other brain proteins have been independently identified as vulnerable to proteolytic attack after toxic neural insults, or to calpain and/or caspase-3 actions. These include CaMPK (calcium/calmodulin-dependent protein kinase)-IV and CaMPK-II [5,7,8].

Novel HTPI (high throughput immunoblotting) technology (PowerBlot™, BD Biosciences) [9–16] has recently been developed. This proteomic method employs a panel of 1000 monoclonal antibodies targeting human or rat and mouse proteins. A total of 5 large SDS/PAGE blots were produced. Subsquently each of these blots was separated into 40 lanes using a manifold system. Each lane was then probed with multiple monoclonal antibodies that target protein antigens with good separation data [MM (molecular mass) difference], thus achieving a high throughput analysis. Since HTPI is still a Western blot in principle, it is an excellent method for separating intact proteins and their potential BDPs. We argue that it is an excellent system with which to study proteolysis. We further hypothesize that HTPI can assist us in identifying the complete set of brain protein substrates (degradome) that undergo proteolytic degradation during and after TBI. We term this the 'TBI degradome', fashioned after the term 'degradome' coined by Lopez-Otin and Overall [17,22]. It is likely that following TBI, some proteins will be up- or down-regulated, rather than just being proteolytically modified. Thus to further identify those that are degradomic, we contrasted the TBI differential proteome in parallel with calpain-2- and caspase-3-mediated degradation patterns, as generated by *in vitro* digestion of a naïve hippocampal lysate with these two proteases. To our knowledge, this is the first report using an HTPI approach to explore proteolytic systems in both an *in vitro* and *in vivo* system. Our method might also prove useful in identifying protein substrates for novel proteases of unknown function.

Abbreviations used: BDP, breakdown product; CaMPK, calcium/calmodulin-dependent protein kinase; CASK, calcium/calmodulin-dependent serine protein kinase; CCI, controlled cortical impact; Cdc, cell division cycle; DTT, dithiothreitol; GST, glutathione S-transferase; HTPI, high throughput immunoblotting; MM, molecular mass; NSF, *N*-ethylmaleimide sensitive fusion protein; Psme3, proteasome activator subunit 3; SBDP, αII-spectrin BDP; SNARE, soluble NSF attachment protein receptor; SNAP, synaptosome-associated protein (numerical values 23 and 25 are kDa); TBI, traumatic brain injury; where the annotation A3 etc is given, A is template A etc, 3 is lane 3 etc, on HTPI gels.

[1] To whom correspondence should be addressed (email kwang1@ufl.edu).

EXPERIMENTAL

In vivo model of TBI

A CCI (controlled cortical impact) device was used to model TBI in rats as described [28]. Briefly, adult male (280–300 g) Sprague–Dawley rats (Harlan, Indianapolis, U.S.A.) were anaesthetized with 4 % isofluorane in a carrier gas of O_2/N_2O, 1:1 (4 min duration) followed by maintenance anaesthesia with 2.5 % isofluorane in the same carrier gas. Core body-temperature was monitored continuously by a rectal thermistor probe and maintained at 37 ± 1 °C by placing an adjustable temperature controlled heating pad beneath the rats. Animals were supported in a stereotactic frame in a prone position and secured by ear and incisor bars. A midline cranial incision was made, the soft tissues revealed, and a unilateral (ipsilateral to the site of impact) craniotomy (7 mm diameter) was performed adjacent to the central suture, midway between bregma and lambda. The dura mater was kept intact over the cortex. Brain trauma was produced by impacting the right cortex (ipsilateral cortex) with a 5 mm diameter aluminum impactor tip (housed in a pneumatic cylinder) at a velocity of 3.5 m/s with a 1.6 mm (severe) compression and 150 ms dwell-time (compression duration). These injuries were associated with local cortical contusion and diffuse axonal damage. Velocity was controlled by adjusting the pressure (compressed N_2) supplied to the pneumatic cylinder. Velocity and dwell-time were measured by a linear velocity displacement transducer (Lucas Shaevitz™ model 500 HR, Detroit, MI, U.S.A.) that produced an analogue signal which was recorded by a storage-trace oscilloscope (BK Precision, model 2522B, Placentia, CA, U.S.A.). Sham-injured control animals underwent identical surgical procedures but did not receive an impact injury. Pre- and post-injury management were in compliance with guidelines set forth by the University of Florida Institutional Animal Care and Use Committee and the NIH (National Institutes of Health) guidelines detailed in the Guide for the Care and Use of Laboratory Animals.

Hippocampal tissue collection and protein extraction

After CCI (48 h), animals were anaesthetized and immediately killed by decapitation. Brains were immediately removed, rinsed with ice-cold PBS and halved. For the injured hemispheres, the hippocampus was rapidly dissected out, rinsed in ice-cold PBS, snap-frozen in liquid nitrogen, and frozen at −80 °C until further use. For Western blot analysis, the brain samples were pulverized to a fine powder with a small mortar/pestle set over solid CO_2. The pulverized hippocampal tissue powder was then lysed for 90 min at 4 °C with 50 mM Tris (pH 7.4), 5 mM EDTA, 1 % (v/v) Triton X-100 and 1 mM DTT (dithiothreitol). Owing to the need for *in vitro* protease-mediated digestion, protease inhibitor cocktail was not used. Instead, extreme care was taken to keep samples as cold as possible and to work rapidly to reduce formation of post-mortem artefacts. The brain lysate was then centrifuged at 8000 ***g*** for 5 min at 4 °C, to clear and remove insoluble debris, snap-frozen and stored at −85 °C until further use.

Calpain-2 and caspase-3 digestion of naïve brain lysate and purified proteins

Hippocampal lysates were prepared as described above. For purified protein digestion, βII-spectrin and synaptotagmin were used. βII-Spectrin (as a subunit of the αII/βII-spectrin heterotetramer) was purified from rat brain as described previously [27]. Recombinant synaptotagmin-1 [as an N-terminal GST (glutathione S-transferase) fusion protein, approx. 90 kDa] was obtained from Abnova Corp (Taiwan).

In vitro protease digestion of the naïve rat hippocampal lysate (5 mg) or purified protein with purified proteases, human calpain-2 (Calbiochem; 1 μg/μl) and recombinant human caspase-3 (Chemicon; 1 unit/μl) (at a protein/protease ratio of 1:200 and 1:50 respectively), was performed in a buffer containing 100 mM Tris/HCl (pH 7.4) and 20 mM DTT. For calpain-2, 10 mM $CaCl_2$ was also added, and the solution then incubated at room temperature for 30 min. For caspase-3, 2 mM EDTA was added instead of $CaCl_2$ and was incubated at 37 °C for 4 h. The protease reaction was stopped by the addition of SDS/PAGE sample buffer containing 1 % (w/v) SDS.

HTPI

Four sets of pooled samples ($n = 6$; naïve rat hippocampus, TBI hippocampus, calpain-digested hippocampus, and caspase-3-digested hippocampus) were prepared and subjected to 5 sets of gel/blots (templates A–E). The electrophoresis and blots were performed at the BD Bioscience facility (Bringamham, KY, U.S.A.). Briefly, the gels were 13 cm × 10 cm, SDS/4–15 % gradient polyacrylamide and 0.5 mm thick (Bio-Rad Criterion IPG well comb). A gradient system was used so that a large size-range of proteins could be detected on one gel. The protein extract (200 μg) was loaded onto one large well spanning the entire width of the gel. This translates into approx. 10 μg of protein extract per lane on a standard 10-well mini-gel. The gel was run for 1.5 h at 150 V. Proteins separated in the gel were transferred to an Immobilon-P membrane (0.2 μm, Millipore) over 2 h at 200 mA. We used a wet electrophoretic transfer apparatus TE Series from Hoefer. After transfer, the membrane was dried and re-wet in methanol. The membrane was blocked for 1 h with blocking buffer (LI-COR Biosciences). Next, the membrane was clamped with a Western blotting manifold that isolates 40 channels across the membrane. In each channel, a complex antibody cocktail (4–6 antibodies) was added and allowed to hybridize for 1 h at 37 °C. Each blot has 39 usable lanes and one lane on the far right probed with antibodies against MM markers; 1 lane (number 40) in templates A, B, C and D was loaded with a cocktail composed of MM standards: p190 (190 kDa), adaptin β (106 kDa), STAT-3 (signal transducer and activator of transcription-3) (92 kDa), PTP1D (non-transmembrane protein-tyrosine phosphatase) (72 kDa), MEK-2 [MAPK (mitogen-activated protein kinase)/ERK (extracellular-signal-regulated kinase) kinase] (46 kDa), RACK-1 (receptor for activated C-kinase) (36 kDa), GRB-2 (growth factor receptor-bound protein-2) (24 kDa) and Rap2 (21 kDa). Lanes 20 and 40 of template E blots were loaded with 2 standardization cocktails (1, 112, 83, 62, 55, 42, 28 and 15 kDa; 2, 190, 120, 101, 60, 50, 27 and 21 kDa). The blot was removed from the manifold, washed and hybridized for 30 min at 37 °C with secondary goat anti-mouse antibodies conjugated to an Alexa Fluor® 680 fluorchrome (Molecular Probes). The membrane was washed, dried and scanned at 700 nm for monoclonal antibody target detection using the Odyssey Infrared Imaging System (LI-COR Biosciences). Samples were run in triplicate and analysed using a 3 × 3 matrix comparison method.

Traditional immunoblotting

Tissue samples (20 μg) were subjected to electrophoresis, equal volumes of samples for SDS/PAGE were prepared in a 2-fold loading buffer [0.25 M Tris (pH 6.8), 0.2 M DTT, 8 % SDS, 0.02 % Bromophenol Blue and 20 % glycerol in distilled H_2O], and gels were run at 120 V for 2 h in a mini-gel unit (Invitrogen). Protein bands were transferred to PVDF membrane on a semi-dry Transblot unit (Bio-Rad) at 20 V for 2 h. After electrotransfer, blotting membranes were blocked for 1 h at ambient temperature in 5 %

non-fat milk in TBST [20 mM Tris/HCl (pH 7.4), 150 mM NaCl and 0.05 % (w/v) Tween-20), then incubated with the primary monoclonal antibody in TBST/5 % milk. Primary antibodies used were anti-αII-spectrin from Affiniti, anti-βII-spectrin, anti-CaMPK-II, anti-CaMPK-IV, anti-striatin, anti-synaptojanin-1, anti-synaptotagmin and anti-NSF (*N*-ethylmaleimide-sensitive fusion protein) (all from BD Bioscience). The blot was then washed 3 times for 15 min with TBST and exposed to biotinylated secondary antibodies (Amersham) followed by a 30 min incubation with streptavidin-conjugated alkaline phosphatase (colorimetric method). Colorimetric development was performed with a one-step 5-bromo-4-chloro-3-indolyl phosphate-reagent (Sigma). The MMs of intact proteins and their potential BDPs were assessed by running along-side rainbow coloured MM standards (Amersham). Semi-quantitative evaluation of protein and BDP levels was performed via computer-assisted densitometric scanning (Epson XL3500 high resolution flatbed scanner) and image analysis using Image-J 1.5 software (NIH).

RESULTS

αII-Spectrin immunoblot – a positive control before HTPI

Our experimental design called for 4 treatment groups: naïve hippocampal lysate (naïve), TBI (CCI with 1.6 mm deformation distance) hippocampal lysate, and *in vitro* calpain-2 and caspase-3 digestion of naïve hippocampal lysates. We initially considered using unpooled individual samples for HTPI analysis, but running $n = 6$ samples for the 4 conditions (naïve, calpain, caspase and TBI) would mean a total of 24 samples. The cost of running such expansive analyses would be formidable and extremely time consuming. We have, therefore, decided on an alternative strategy of pooling 6 samples from each group to enhance signal-to-noise ratio and to identify 'putative' hits. Subsequently, our strategy was to rely on follow-up 'hit'-confirmation using individual brain lysate sample analysis with traditional immunoblots. The naïve hippocampal lysate was separately prepared from 6 individual rats and 1 mg of protein from each sample was pooled. Similarly, TBI samples were prepared from 6 individual injured rats and 1 mg of protein from each sample was pooled. As for calpain-2 and caspase-3 digestion, 3 mg of protein from pooled naïve samples was digested separately with calpain-2 or caspase-3 at protease/substrate protein ratios of 1:200 and 1:50 respectively. This process was repeated twice to obtain up to 6 mg of protein digest.

To ensure that the quality of the pooled samples was sound before subjecting them to the rigorous HTPI process, we subjected these pooled samples to traditional immunoblotting for αII-spectrin, a well established target of both calpains and caspases [5]. Naïve brains present only intact αII-spectrin of MM 280 kDa. Calpain-2 digestion decreased the levels of intact αII-spectrin and produced BDPs of 150 and 145 kDa (SBDP150 and SBDP145), whereas caspase-3 digestion also decreased the levels of intact αII-spectrin and yielded BDPs of 149 (SBDP149; also known as SBDP150i) and 120 kDa (SBDP120), as expected, based on our previous experience [5,18] (Figure 1). In the pooled TBI hippocampal samples, the decrease in αII-spectrin levels was not as notable, but a mixture of SBDP150/149, SBDP145 and SBDP120 was observed (Figure 1), as previously identified [19]. This confirmed that the 4 samples we prepared for this proteomic study have preserved the expected characteristic features.

Each pooled sample was run in triplicate on each of the 5 HTPI templates (A–E). Of the 1000 antibodies probed, 550 of them gave a recognized and quantifiable signal after development. In addition, triplicate naïve samples developed in template A blots showed relatively high-reproducibility in overall banding-profiles (see Supplementary Figure 1 at http://www.BiochemJ.org/bj/394/bj3940715add.htm). However, some variation in the intensity of selected protein bands was observed, as expected with this type of analysis. Thus it is important that samples are always run and compared in triplicate. Other templates (B–D) also showed similar levels of same-sample-consistency (results not shown).

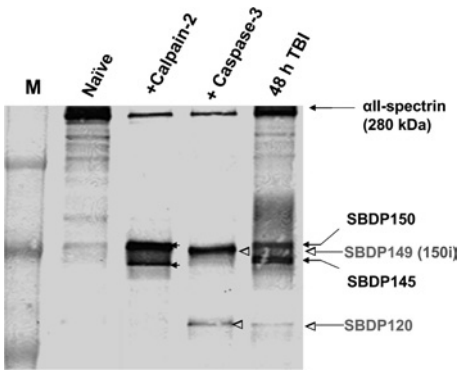

Figure 1 αII-Spectrin immunoblot, a positive control before HTPI

Pooled naïve rat hippocampal lysate, lysates digested with calpain-2 or caspase-3 *in vitro*, and rat TBI hippocampal lysate. Separate naïve and TBI hippocampi from 6 individual animals respectively were pooled. To confirm that the extent of proteolysis in the last 3 samples was comparable, we analysed 20 μg of protein from each of these samples by traditional SDS/6 % PAGE, immunoblotting and probing with monoclonal anti-αII-spectrin antibody (Affiniti anti-fodrin). Intact protein (280 kDa) was observed under all conditions. Calpain-2 digestion produced major fragments SBDP150 (150 kDa) and SBDP145 (145 kDa) (solid arrows), whereas caspase-3 digestion produced SBP149 (SBDP150i, 149 kDa) and SBDP120 (120 kDa) (open arrow heads) [5]. In TBI samples, a mixture of SBDP150, SBDP149, SBDP145 and SBDP120 was observed. M, molecular mass marker.

Calpain-2 and caspase-3 degradomes and the TBI differential proteome identified by HTPI

Since samples were run in triplicate, for each pairwise comparison (e.g. calpain-2 versus naïve), a 3×3 matrix comparison was made to cover all 9 combinations. Based on vigorous densitometric-computer-assisted and manual comparisons, we focused on parent protein-bands with significantly decreased intensity while also looking for the appearance of potential BDP bands after calpain-2/caspase-3 digestion (Figures 2 and 3) or after TBI (Figure 4). For example, representative template A blots for naïve and calpain-2 digestion are contrasted in Figure 3. We noted that 23 parent proteins had an average intensity that was reduced more than 2-fold after calpain digestion whereas 9 potential BDP bands (lanes 2, 10, 11, 13 and 36) were observed after calpain-2 digestion (Figure 2, lower panel). Similarly, 12 parent proteins in template A were significantly reduced in intensity after caspase-3 digestion as a result of proteolysis, with at least three identifiable BDPs observed in lanes 8 and 13 (Figure 3). Again, when template A for naïve hippocampus was compared with that of the TBI counterpart, 16 parent proteins were reduced in intensity, and therefore were either expression-down-regulated proteins or were potential proteolytic substrates (Figure 4). In addition, 2 potential BDPs can be readily observed (lanes 13, 18 and 29). In parallel, 2 proteins were found at up-regulated levels after TBI [CASK (calcium/calmodulin-dependent serine protein kinase), template A, lane 3, and Psme3 (proteasome activator subunit 3), A29] (Figure 4).

Template B comparisons also identified 13 to 12 potential proteolytic targets for calpain-2 and caspase-3 respectively and

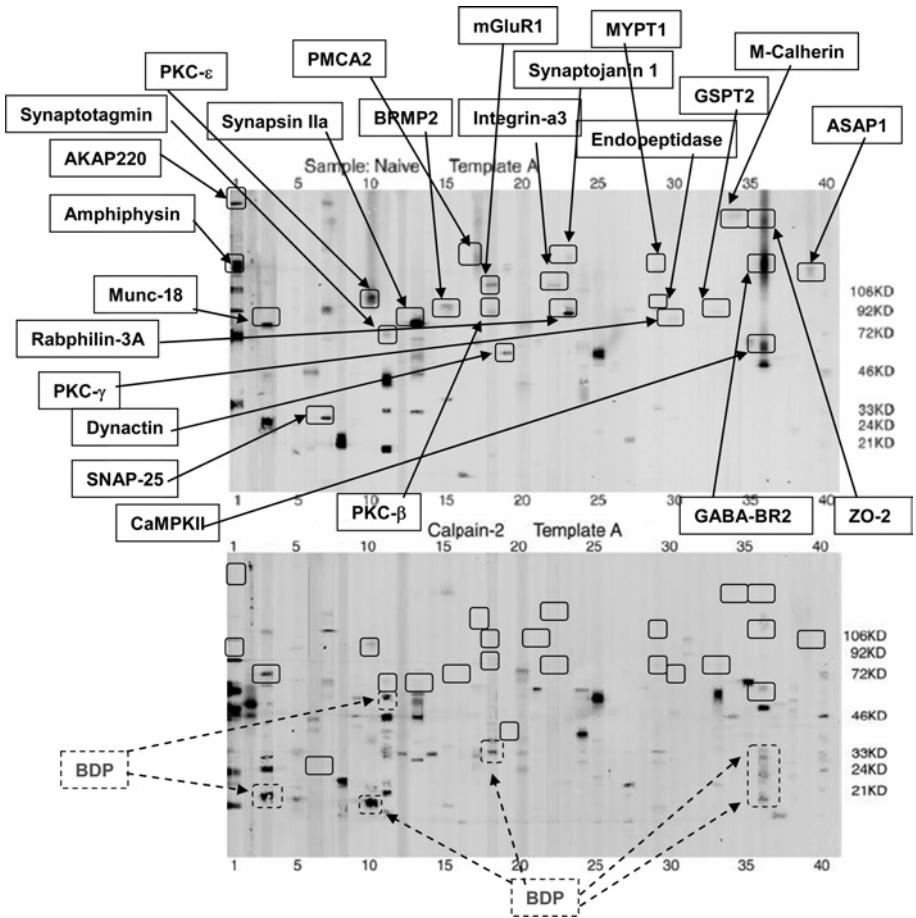

Figure 2 Example of the calpain-2 degradome (Template A)

A-templates from naïve hippocampus (upper panel) and calpain-2-digested hippocampal lysate (lower panel) were compared in triplicate (9 comparisons in total). One set of representative blots is shown. MM markers (lane 40) are indicated on the right. Protein bands with sufficient intensity were subsequently decoded and quantified using computer software as described in the Experimental section. We noted that for a number of proteins (solid box; upper panel), their average intensity decreased more than 2-fold after calpain digestion and several BDPs were also observed (BDP, dotted box; lower panel). ZO, zona occludin; for further definitions see Table 1, legend.

14 differentially regulated proteins in TBI (see Supplementary Figure 2 at http://www.BiochemJ.org/bj/394/bj3940715add.htm). In addition, templates C–E showed very similar proteomic patterns (results not shown). Table 1 summarizes the number of hits from each template when naïve hippocampal lysate was compared with calpain-2, caspase-3 and TBI treated samples respectively. In all, 54 and 38 proteins were putatively sensitive to calpain-2 and caspase-3 proteolysis respectively, whereas 48 proteins appeared to be down-regulated or degraded following TBI, and only 9 proteins were up-regulated [CASK, Psme3, α-actinin, ceruloplasmin, cdk2 (cyclin-dependent kinase2), NES1 (serine protease inhibitor kallikrein), TBP (TATA box-binding polypeptide), GS27 (Golgi SNARE 27) and Smg] (Figure 5A). Parent-protein signal reduction ranged from 2-fold to more than 10-fold. Based on 1000 antibodies used, the 'hit' rate for calpain digestion versus naïve lysate, and caspase-3 digestion versus naïve lysate, and TBI versus naïve lysate were 5.4 %, 3.8 % and 5.7 % respectively. Furthermore, 40 of these proteins were common to the calpain-2 degradome and the TBI differential proteome, whereas 31 proteins were common to the caspase-3 degradome and the TBI differential proteome, as illustrated by the Venn diagram (Figure 5B). There were also significant overlaps (34 proteins) between the calpain-2 and caspase-3 degradomes. Lastly, 29 proteins were identified as putative degradomic targets under all three treatment conditions. However, it is important to note that the TBI differential proteome is not necessarily entirely degradative, but, in part, a result of changes in protein expression. Besides the 42 proteins in TBI samples that overlapped with the calpain/caspase-3 degradomes, we also found 6 additional proteins with decreased signal but with no calpain/caspase degradation counterparts [RIP2/RICK (receptor-interacting protein kinase2/Rip-like interacting caspase-like apoptosis-regulatory protein kinase), C26; syntaxin-6, C7; RONa, D27; PEX19 (peroxisome assembly factor 19), D29; SCAMP1 (secretory carrier-associated membrane protein1), D38 and SLK (Ste20-like kinase), E13] (Figure 5A, Table 1). Table 1 further details the identity of putative calpain-2 and caspase-3 substrates and TBI differential target proteins. As expected, some previously known calpain substrates were identified by HTPI, including CaMPK-II, (A36) [7], dynamin (B26) [19], PKC (protein kinase C)-α (B25) -β (A18) and -γ (A30) [5,18]. SNAP25 (synaptosome-associated protein 25)-(A7) was described as a calpain substrate, although it was not well studied [20]. Previously reported dual calpain/caspase-3 substrates identified by HTPI included the PMCA2 (plasma membrane calcium pump isoform2) (A17) [20,21], βII-spectrin (E8) [18] and CaMPK-IV (C12) [8] (Table 1). Of 48 TBI-down-regulated proteins, (Table 1), 9 proteins are associated with synaptic vesicle docking and trafficking: synaptojanin-1 (a synaptic

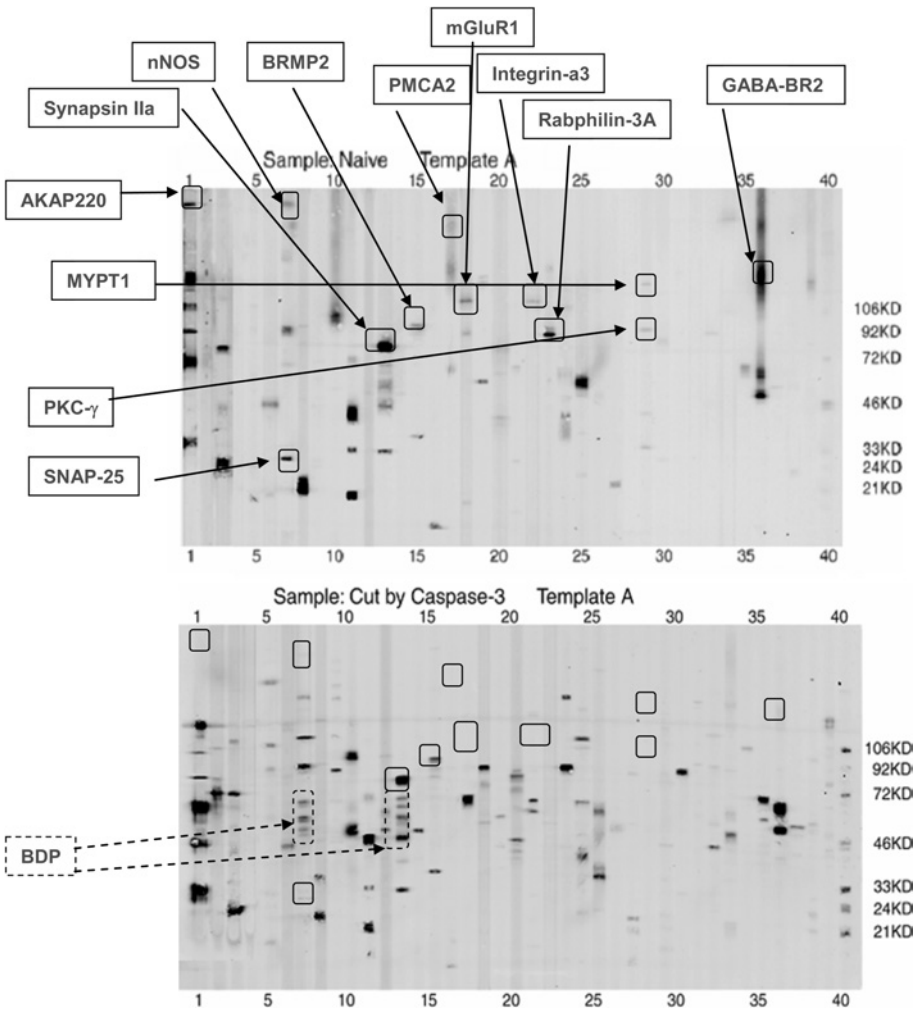

Figure 3 Example of the caspase-3 degradome (Template A)

A-templates from naïve hippocampus (upper panel) and caspase-3-digested hippocampal lysate (lower panel) were compared in triplicate. Only 1 set of representative blots is shown. MM markers (lane 40) are indicated on the right. Similarly to Figure 3, the expression of 9 parent proteins in template A (solid box, upper panel) was significantly decreased after caspase-3 digestion as a result of proteolysis, and several BDPs were observed (dotted box; lower panel). For definitions see Table 1, legend.

inositol 1,4,5-trisphosphate-kinase), synaptotagmin-1 (a synaptic vesicle-exocytosis calcium sensor) and NSF, and synapsin-Ia and -II, SNAP-25, Munc-18 (non-neuronal syntaxin binding protein), α/β-SNAP, amphiphysin and rabphilin-3A. These data suggest that proteolysis might play a significant role in synaptic dysfunctions following TBI.

Cytoskeleton-associated proteins dynamin and dynactin, as well as the actin-binding protein, profilin, were also identified as TBI-proteolytic substrates. Adhesion molecules (M-calherin and integrin-α3) and adaptor proteins β-catenin and adaptin were also identified. Again, proteolysis of these proteins can lead to cytoskeletal degradation and compromise cell shape. Two neurotransmitter receptors, mGluR1 (metabotropic glutamate receptor 1) and GABA-B-R2 (γ-aminobutyric acid-B receptor 2), also appeared to be sensitive to proteolysis (Table 1).

Two cell cycle proteins [Ki-67 and p55-Cdc (cell division cycle)] were also identified in the TBI differential proteome. The TBI differential proteome also includes two apoptosis-associated proteins that have not previously been identified as sensitive to proteases, Bad protein (B36) that translocates to mitochondria, as well as the mitochondria-released Smac/Diablo (B6) that binds inhibitor of apoptosis proteins 1 and 2, thus facilitating the induction of apoptosis. How proteolysis influences the functions of some of these proteins remains to be elucidated.

Degradome and TBI differential proteome target validation

In order to assess the confidence of the degradomic target assignment based on HTPI, we first asked how the HTPI results compared with traditional immunoblotting for a specific protein. From E8, we observed that out of all triplicate runs, the βII-spectrin (240 kDa) level consistently diminished upon protease treatments, whereas putative BDPs of 110 kDa were identified upon calpain digestion, and BDPs of 108 kDa and 85 kDa were observed upon caspase-3 digestion. TBI also produced loss of intact βII-spectrin and fainter BDP bands of 110/108 and 85 kDa (see Figure 8A). In parallel to HTPI, we applied the pooled naïve hippocampal lysate and those subjected to calpain-2 and capase-3 digestion to traditional SDS/PAGE followed by immunoblotting with a monoclonal anti-βII-spectrin antibody (BD Biosciences) that was identical to that used in the HTPI. As illustrated in Figure 6(B), although naïve brains contained no BDPs, calpain-2 and capase-3 digestion produced BDPs of 110 kDa and of 108 and 85 kDa respectively, virtually identical to the patterns generated by HTPI

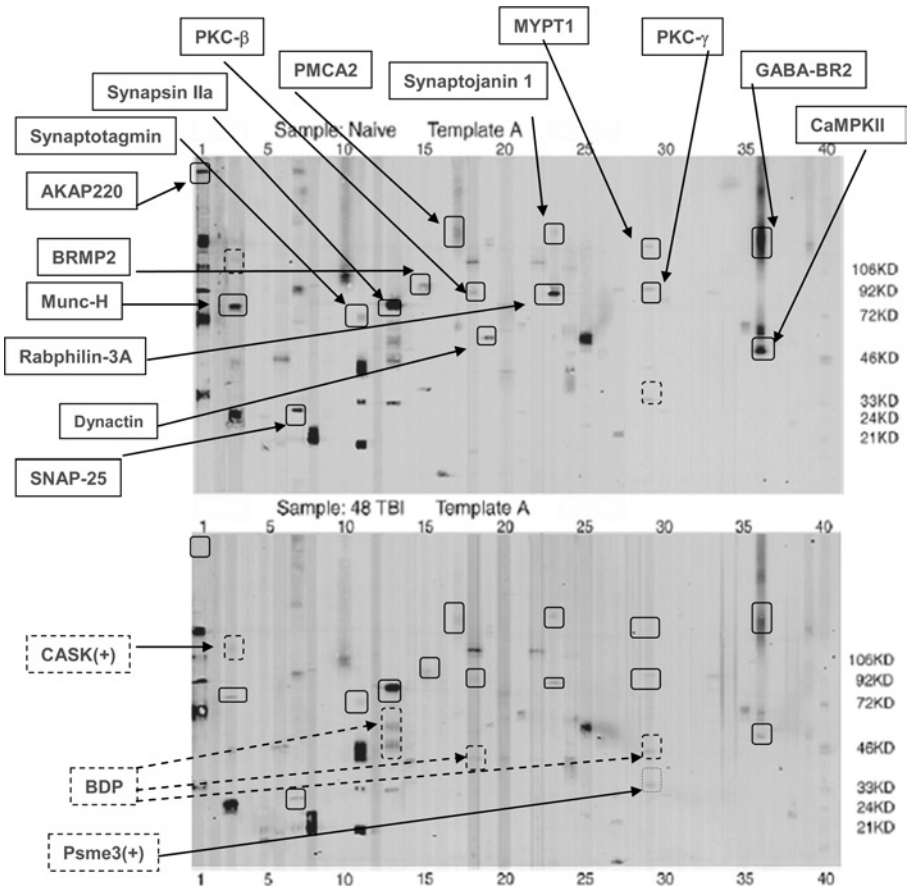

Figure 4 Example of the TBI differential proteome (Template A)

Template A for naïve hippocampus (upper panel) was compared with that for the TBI (1.6 mm deformation distance, 48 h) counterpart (lower panel). Comparisons were made in triplicate. A set of representative blots is shown. MM markers (lane 40) are indicated on the right. A total of 13 proteins in Template A were decreased in average intensity (down-regulated) after TBI (solid box; upper panel). In addition, several BDPs were readily observed (dotted box; lower panel). The only 2 proteins found to be up-regulated after TBI were CASK (A3) and Psme3 (A29) (dotted boxes). For definitions please see Table 1, legend.

(Figure 8A). In addition, we also assessed the integrity of βII-spectrin in 4 individual naïve and 4 individual TBI hippocampal samples. Consistent with the HTPI data shown in Figure 7(A), we again observed, in traditional immunoblots, the presence of BDPs of 110, 108 and 85 kDa in all 3 TBI hippocampal samples, but not in the naïve samples (Figure 8B).

In this study, we identified over 30 novel protease substrates (see Table 1). To ascertain that these are truly proteolytic substrates, traditional immunoblots were again performed for 4 selected 'novel' degradomic targets: striatin (C22) and NSF (E13) as a calpain-2/caspase-3/TBI triple target; and synaptojanin-1 (A23) and synaptotagmin-1 (A11) as calpain/TBI double targets (see Table 1). Traditional immunoblotting results showed that striatin (110 kDa) was indeed sensitive to calpain-2 digestion, producing BDPs of 40 kDa and 35 kDa as predicted from HTPI. Caspase-3 digestion also produced a high MM fragment of 100 kDa (Figure 7A), which was not readily observed in HTPI. TBI samples also showed both a caspase-produced BDP of 100 kDa and calpain-produced BDPs of 40 and 35 kDa. Next, we confirmed that synaptojanin-1 (140 kDa) was highly sensitive to calpain digestion, producing a BDP of 70 kDa. Caspase-3 digestion also partially degraded synaptojanin-1 to a faint 70 kDa fragment, which was not observed in HTPI, probably due to sensitivity differences. Importantly, following TBI, intact synaptojanin-1 protein was almost completely degraded to the 70 kDa BDP (Figure 7B). Synaptotagmin-1 (65 kDa, A11) was degraded by calpain-2 to a BDP of 33 kDa but not by caspase-3 (Figure 7C). The BDP-33 kDa was also readily observed in all 4 TBI hippocampal samples (Figure 7C). Lastly, NSF was degraded by calpain and caspase-3 (to a lesser extent) to BDPs of 30 and 25 kDa (Figure 7D). We also established that both of these BDPs were readily observed in TBI samples but not in naïve samples (Figure 7D).

Finally, to directly prove that purified HTPI-identified target proteins are indeed vulnerable to calpain and/or caspase-3 digestion, we tested two proteins. We obtained purified βII-spectrin (as a subunit of the rat brain αII/βII-spectrin heterotetramer) and recombinant GST–synaptotagmin-1, and subjected them to calpain/caspase-3 digestion. Coomassie Blue staining of an SDS gel revealed that both αII- and βII-spectrin subunits (280 and 260 kDa respectively) were degraded by calpain and caspase-3, producing multiple fragments (Figure 8A). To ascertain that βII-spectrin was indeed a substrate for calpain and caspase-3, immunoblotting of the same samples probed with anti-βII-spectrin antibody was performed. βII-Spectrin breakdown patterns (BDP-110 kDa for calpain, BDP-108 kDa and -85 kDa for caspase-3) (Figure 8A) was virtually identical to those observed after HTPI of the hippocampal lysate digest (Figure 6). Similarly, recombinant GST–synaptotagmin-1 was vulnerable to calpain-2 proteolysis, producing 3 major fragments (65, 33 and 21 kDa)

Table 1 Identity of the degradomic protein targets for calpain-2 and capase-3, and differentially regulated proteins after TBI

Protein names or abbreviations are listed in the far left column. Their template and lane location are listed on the second column. Swiss Pro ID and predicted MMs are also listed. Where a protein is altered in levels in one of the three conditions (calpain-2, capase-3 or TBI), the fold-change of the parent protein is indicated in the 3 columns on the far right. Since the majority of proteins showed decreased levels in the treatment group versus control (naive), the fold-change always indicates decrease as the default. When a protein level is increased (for some proteins in TBI), the fold-change increase is indicated with a (+) sign and the fold-change is given inside brackets. Also, we have used high stringency inclusion criteria. Only proteins with a band decrease or increase of at least 1.5-fold in all 9 possible comparisons between 3 treatment replicas and 3 control replicas are shown. *, Fold changes for each treatment group are given against controls (naïve). AKAP220, A-kinase anchoring protein; Arp, actin-related protein; ASAP1, Arf GTPase-activating protein; BRMP2, amphiphysin; c-Cbl, casitas B-lineage lymphoma; CtBP1, C-terminal-binding protein 1; cdk2, cyclin-dependent kinase2; DRBP76, double-stranded RNA-binding nuclear protein76; GABA-B-R2, γ-aminobutyric acid-B-receptor2; GS27, Golgi SNARE 27; GSTP, GTP-binding protein appearing to be essential for the G1 to S phase transition of the cell cycle; hPRP17, human homologue of yeast Prp17; MEF2D, myocyte-enhancer-binding factor 2D; mGluR1, metabotropic glutamate receptor1; MEK, MAPK/ERK kinase; Munc-18, non-neuronal syntaxin binding protein; MYPT1, myosin phosphatase target protein1; Nck, Nck adaptor protein 1; Nek2, NIMA (never in mitosis A)-related kinase; NES1, serine protease inhibitor kallikrein; nNOS, neuronal nitric oxide synthase; NSP1, non-structural protein 1; PEX19, peroxisome assembly factor 19; PKC, protein kinase C; PMCA2, plasma membrane calcium pump isoform2; RIP2/RICK (receptor-interacting protein kinase2/Rip-like interacting caspase-like apoptosis-regulatory protein kinase; SCAMP1, secretory carrier-associated membrane protein1; SCAR-1, suppressor of cAMP receptor-1; SLK, Ste20-like kinase; Smg/GDS, stimulatory GDP/GTP exchange protein; TBP, TATA box-binding polypeptide; TFIIS, transcription factor IIS; TNIK, Traf2 and Nck-interacting kinase.

Protein	Lane	Swiss Pro ID	MM (kDa)	Calpain-2* (fold-decrease)	Caspase-3* (fold-decrease)	TBI* [fold-decrease/(increase)]
Template A						
AKAP220	1	Q62924	220	> 10	> 10	> 10
Amphiphysin	1	Q95163	125	> 10		
ASAP1	39	Q9QWY8	130	> 10		
BRMP2	15	O08539	96/89	> 10	7.31	
CaMPK-II	36	P11275	52	5.23		5.67
CASK	3	Q62915	120			(+5.8)
Dynactin	19	Q13561	50	> 10	> 10	> 10
Endopeptidase	29	P42676	80	> 10		
GABA-BR2	36	O088871	130	> 10	> 10	> 10
GSTP2	33	O88180	88	4.77		
Integrin-α3	22	Q62470	135	> 10	> 10	> 10
M-calherin	34	P10287	130	> 10		
mGluR1	19	P23385	133	> 10		
Munc-18	3	Q99PV2	68	> 10		> 10
MYPT1	29	Q9DBR7	130	3.38	3.93	5.00
nNOS	7	P29475	155		> 10	
PKC-β	18	P05771	80	> 10		7.31
PKC-ε	10	Q02156	90	6.50		
PKC-γ	30	P05129	80	> 10	3.30	> 10
PMCA2	17	P11506	133	> 10	> 10	> 10
Psme3	29	Q12920	36			(+4.7)
Rabphilin-3A	23	P47709	75	> 10		> 10
SNAP-25	7	P13795	25	> 10	> 10	> 10
Synapsin-IIa	13	Q63537	74	> 10	1.70	10.10
Synapsin-1	23	Q62910	140	> 10		> 10
Synaptotagmin	11	P21579	65	2.91		1.50
Template B						
α-Actinin	9	AAA51582	104			(+8.41)
Adaptin	29	P17426	112	> 10		6.12
Bad	30	Q61337	23	10.80	3.23	3.00
β-Catenin	5	Q02248	92	> 10	> 10	> 10
Cathepsin L	22	P07711	43	7.18	> 10	7.71
Ceruloplasmin	37	Q61147	150			(>+ 10)
Dynamin	26	P21575	> 100	10.69	> 10	4.41
Ki-67	8	P46013	395		> 10	> 10
MEF2D	3	Q63943	70	> 10	> 10	
Nck	2	P16333	47		> 10	
NSP1	24	Q9Y2X4	72	> 10	> 10	> 10
p150Glued	26	P28023	150	> 10	> 10	> 10
p190	3	Q13017	190	> 10	> 10	> 10
PKC-α	25	P17252	82	3.67		> 10
SII/TFIIS	32	P23193	38	> 10	> 10	> 10
Smac/Diablo	6	Q9NR28	22	> 10	> 10	> 10
DRBP76	7	Q13906	90	> 10		
Template C						
Arp-3	18	P32391	50		> 10	> 10
CaMPK-IV	12	Q16566	60	3.11	2.63	4.26
c-Cbl	9	P22681	120	> 100		
cdk2	9	P24941				(>+ 10)
hPRP-17	15	O60508	66		3.33	2.36
MEK2	5	P51955	46	> 10		
NES1	38	O43520	30			(>+ 10)
p55-Cdc	8	Q9BW56	55	> 10		
Profilin	28	P07737	15	> 10	> 10	
RIP2/RICK	26	AAH04553	61			2.59
α/β-SNAP	21	P54920	35/36	> 10		13.79

Table 1 (contd.)

Protein	Lane	Swiss Pro ID	MM (kDa)	Calpain-2* (fold-decrease)	Caspase-3* (fold-decrease)	TBI* [fold-decrease/(increase)]
Syntaxin 6	7	Q63635	31			3.81
Striatin	22	P70483	110	9.31	3.01	6.51
TBP	26	P20226	37			(+7.31)
TNIK	38	Q9UKE5	150		2.59	
Template D						
Catenin/p120	32	P30999	120	>10	>10	>10
GS27	10	O14653	27			(>+10)
p190-B	28	Q13017	195	>10	>10	>10
PEX19	29	P40855	38			6.31
RONa	27	Q04912	40			>10
SCAMP1	38	O15126	36			7.40
Synapsin-Ia	38	P09951	80	>10		9.90
ATP synthase	21	P15999	55	>10	5.84	>10
βII-Spectrin	8	Q01082	240	>10	>10	6.30
β-Raf	25	P15056	95/72	>10	>10	2.71
Clathirin heavy chain	39	P11442	120	>10	>10	7.43
CtBP1	26	Q91W16	48	>10	>10	
NSF	13	P46459	82	>10	3.30	2.59
SCAR-1	4	Q92588	80	>10	7.50	3.23
SLK	13	NP_055535	125			4.00
Smg/GDS	13	CAA45067	57			(>+10)

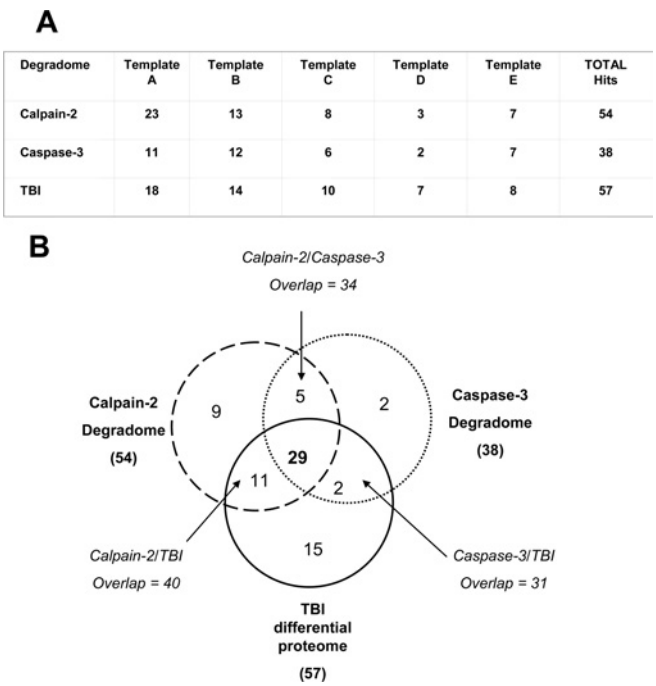

Figure 5 Summary of the calpain-2 and caspase-3 degradomes and differential TBI proteome results from HTPI

(**A**) The number of putative degradomic hits for each template based on calpain-2 versus naïve, caspase-3 versus naïve, and TBI versus naïve comparisons were tabulated. The total number of degradome hits is listed on the far right. (**B**) Venn diagram showing overlap of protein targets in the 3 degradomes (calpain, dashed line; caspase-3, dotted line; TBI, solid line). The total number of protein targets is in brackets. Overlaps and triple overlap numbers are indicated.

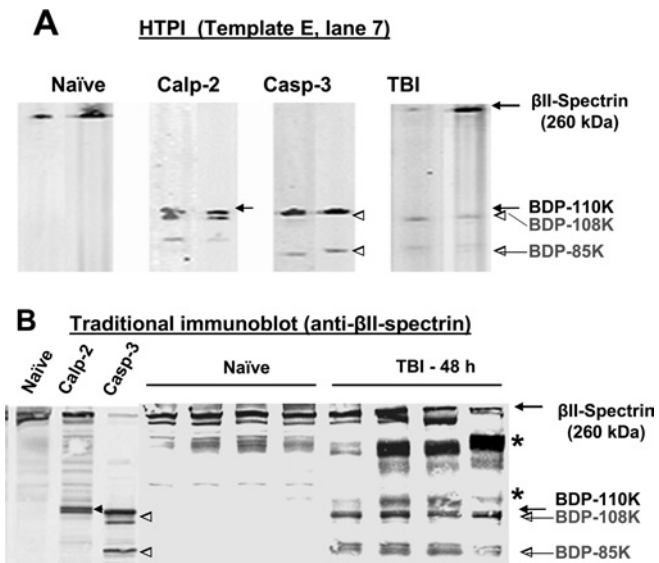

Figure 6 An HTPI approach allows rapid target confirmation

(**A**) Extracted lanes (E7) from template E of the HTPI gel: intact βII-spectrin (240 kDa) expression level was shown to be significantly decreased by calpain-2 digestion, caspase-3 digestion and after TBI. A calpain-mediated BDP of 110 kDa (black label) and 2 caspase-mediated BDPs of 108 and 85 kDa respectively (grey labels) were tentatively identified. These 3 BDPs were also tentatively identified in the TBI samples. (**B**) Traditional SDS/PAGE and Western blotting were also performed using identical monoclonal anti-βII-spectrin antibodies. Samples analysed were naïve (pooled) versus calpain-2 and capase-3 digestion (left 3 lanes), as well as 4 separate naïve and TBI samples. Again, BDPs of 110 kDa (solid arrow) and of 108 and 85 kDa (open arrow heads) were observed. * Indicates rat heavy-chain IgG and fragments from contaminating blood that cross-react with the secondary anti-(mouse IgG) antibody detection system used.

(Figure 8B). Again, to ensure that the fragments were derived from the intact synaptotagmin portion of the fusion protein, we performed immunoblotting with anti-synaptotagmin antibody and identified 2 immunoreactive polypeptides (65 and 33 kDa) (Figure 8B). Although the 65 kDa fragment represents the full-length synaptotagmin truncated from the GST portion (appearing as a 21 kDa fragment) at the artificial linker region, the 33 kDa synaptotagmin BDP was identical in size to that produced when the hippocampal lysate was digested with calpain (Figure 7).

DISCUSSION

In the present study, we combined two powerful and emerging areas in proteomics: degradomics [22] and high-throughput

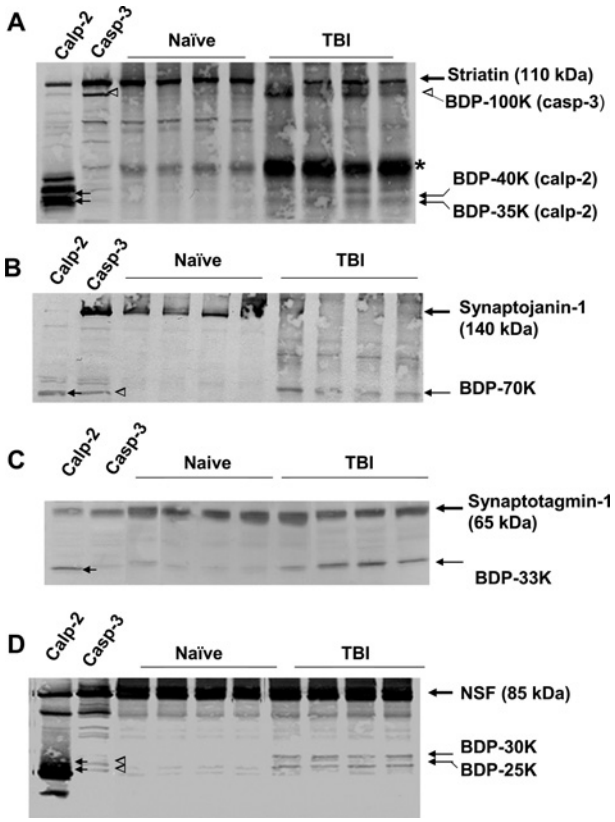

Figure 7 Examples of 4 proteins identified by HTPI as novel proteolytic targets

A total of 4 proteins were identified as proteolytic targets for either calpain-2, capase-3 and/or in TBI: striatin (**A**), synaptojanin-1 (**B**), synaptotagmin-1 (**C**) and NSF (**D**). Traditional SDS/PAGE and Western blotting were also performed using monoclonal antibodies against striatin, synaptojanin-1, synaptotagmin (isoform I) and NSF. Samples analysed were calpain-2 and capase-3 digestions (2 left-hand lanes), as well as 4 separate naïve and TBI samples. In (**A**–**D**), intact proteins are shown with bold arrows (with MM in brackets). Calpain-2-mediated BDPs are shown with solid arrows. Caspase-3-mediated BDPs are shown with open arrow heads. MMs are as indicated. * In (**A**) indicates rat light-chain IgG from contaminating blood that cross-reacts with the secondary anti-(mouse IgG) antibody detection system used.

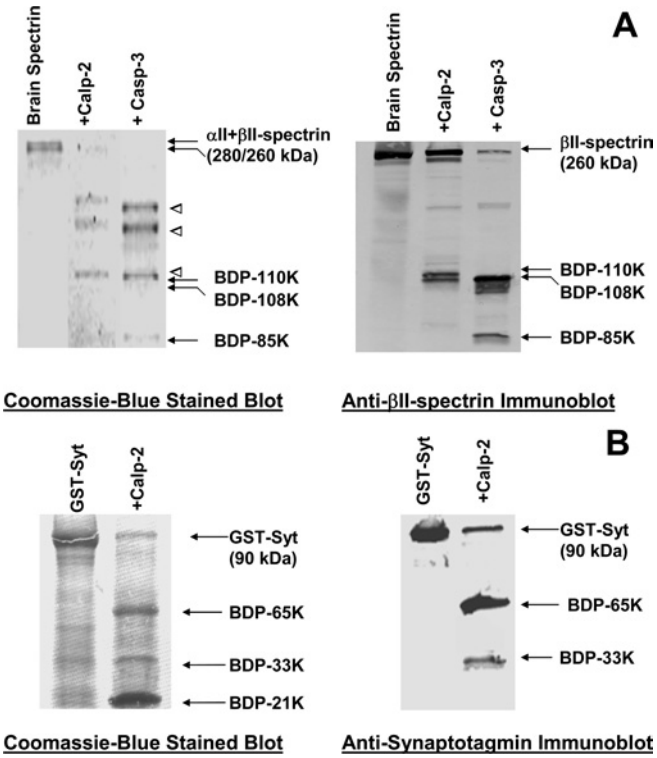

Figure 8 Examples of 2 purified proteins confirmed as proteolytic targets for calpain/caspase-3: βII-spectrin and synaptotagmin-1

Purified βII-spectrin (as a subunit of rat brain αII/βII-spectrin) (**A**) and recombinant GST–synaptotagmin-1 (**B**) were subjected to calpain-2/caspase-3 digestion, and calpain-2 only digestion respectively. Both Coomassie Blue stained blotting-membrane (left panels) and immunoblotting analysis with anti-βII-spectrin and anti-synaptotagmin-1 antibodies (right panels) were performed. Intact proteins and major BDPs are labelled with arrows. Several major αII-spectrin BDPs were also identified (open triangles).

monoclonal antibody panel-based immunoblotting (HTPI) for protein identification [9,11]. Based on others' and our previous evidence showing dual attacks on neural proteins by calpains and caspase-3 under neural injury situations [5], we hypothesized that there would be significant overlap between the neuronal proteins vulnerable to proteolysis by direct calpain and caspase-3 digestion, and following TBI (i.e. calpain, caspase-3, and TBI-degradomes).

For our specific study, we compared and contrasted naïve with traumatically injured hippocampal lysates. Control craniotomies (sham operated) were performed, but not included in this study as this procedure also produced a mild form of brain trauma. As for the classical and ubiquitously distributed calpain-1 and -2, our evidence and others' has concluded that they share identical substrate sets [23]. Thus for simplicity, only calpain-2 was used for the *in vitro* digestion of hippocampal lysate. Similarly, various caspases are activated in brain-injury induced neuronal apoptosis (caspase-3, -8, -9 and -12) [23–26]. Among the execution caspases, the most relevant and well studied is caspase-3. Therefore it was selected for the present comparative degradomic study. The calpain-2 and caspase-3 degradomic data generated were then compared with TBI degradomic data (Table 1, Figure 5).

Using HTPI, we identified 43 proteins in the rat hippocampal proteome that were putatively degraded after TBI, whereas 54 and 38 proteins respectively were vulnerable to calpain-2 and caspase-3 proteolysis (Table 1). We further identified significant overlaps among the calpain-2 and caspase-3 degradomes, and TBI differential proteome, with 29 of these proteins common to the three degradomes (Figure 5). Within the calpain-2 and caspase-3 degradomes previously identified are calpain and capsase-3 substrates such as βII-spectrin, CaMPK-II and CaMPK-IV (Table 1). We identified and confirmed a number of previously unknown protease-sensitive target proteins in TBI, such as striatin, synaptotagmin-1, synaptojanin-1 and NSF, using traditional immunoblotting analysis of treated and untreated hippocampal lysates (Figure 7). We further confirmed that purified βII-spectrin and synaptotagmin-1 were *in vitro* substrates of calpain and/or caspase-3 (Figure 8).

Based on the significant overlaps among the calpain degradome, caspase-3 degradome and TBI differential proteome, it appears that these two proteases are operating in concert in TBI by attacking a subset of cellular proteins that are important to neuronal functions. For example, many novel TBI proteolytic targets are synaptic vesicle proteins (Table 1; Figure 7). It is tempting to suggest that proteolysis plays a significant role in the synaptic dysfunction following TBI. Many cytoskeleton proteins (dynamin, dynactin, and profilin and βII-spectrin) and cell adhesion proteins (adaptin and β-catenin) also appear to be at risk from proteolysis following TBI (Table 1). It should be noted that there are differences between the TBI differential proteome and the

combined calpain/caspase-3 degradomes: although 42 TBI-down regulated proteins overlapped in calpain/caspase-3 degradomes, 6 other TBI-down-regulated proteins have no calpain/caspase counterparts. In addition, there are also 9 prominently up-regulated proteins in TBI lysates that could not be accounted for in calpain/capase-3 degradomes (Table 1, Figure 7).

To date, there are only a handful of published studies using HTPI/PowerBlot™ to address a biological problem [9–14]. Interestingly, only one previous paper used HTPI, in order to study post-translational modification protein conjugation to ISG15 (interferon stimulated gene15), a ubiquitin-like protein [12]. Thus to our knowledge, the present paper is the first report to use HTPI to study protein proteolysis. Although there are now several emerging proteomic technologies, including tryptic peptide analysis by tandem MS antibody microarray [29], the HTPI is the most ideally suited proteomic method to rapidly identify potential targets for a protease system. Most proteomic methods (MS/MS, antibody microarray) cannot readily distinguish intact proteins from their fragmented forms. However, HTPI, by contrast, is built on traditional immunoblotting technology. Thus intact proteins and their potential fragments were first resolved by one-dimensional SDS/PAGE before progression to electrotransfer and antibody probing. This method has been proven to be extremely powerful in identifying the occurrence of proteolysis, as well as distinct protein fragments (Figure 5B). We determined this to also be the case for HTPI (Figure 5A). Another powerful aspect of HTPI is the relative ease of protein identification and 'hits' confirmation. Since all the protein bands in the 5 templates are already annotated based on the applied monoclonal antibodies, putative protein identification is very rapid. Furthermore, since the exact antibodies used in the HTPI analysis are individually available, hit confirmation is rapid and robust (Figures 7 and 8). One potential drawback of using an antibody array approach is that antibody recognition of antigens might be species-specific. However, the 1000 antibody sets we employed were tested for species cross-reactivity (human/rat/mouse) and over 90 % cross-react with protein antigen in human, rat and mouse. Of the 74 total hits in Table 1, all but 3 have confirmed rat-reactivity (95 % cross-reactivity). The 3 exceptions are DRBP76 (double-stranded RNA-binding nuclear protein76), cathepsin L and p55-Cdc.

One of the potential limitations of the HTPI method is that it is not exhaustive. Currently the expansion of HTPI is limited by the availability of antibodies to specific protein antigens. However, in only a few years, the HTPI panel has already grown from 700 [9] to over 1000 monoclonal antibodies (present study). Another concern in using HTPI to identify proteolytic substrates *in vivo* is that this method will also detect proteins with significantly reduced expression levels rather than those that are degraded. However, we have compared the *in vivo* TBI differential proteome with *in vitro* protease degradomes (Figures 2–4), followed by traditional immunoblots which confirms the detection of BDPs (Figure 6). Therefore our approach adds another level of confidence to our interpretation of the degradomic data. Finally, any degradomic targets identified by HTPI (Figures 2–4) should be confirmed independently in follow-up studies, including cell-based studies where proteases of interest can be activated.

In summary, we have demonstrated that HTPI is a powerful and novel method for studying proteolytic pathways. In the present study, we have used the hippocampal proteome as an example to demonstrate the feasibility of using HTPI to study proteolytic targets *in vivo* and *in vitro*. This platform technology is applicable to the identification of potential targets for novel proteases with unknown functions. In addition, it is possible to identify specific protein hydrolysis/processing in a unique organ or cell system under physiological or pathological conditions.

The authors would like to acknowledge support from Department of Defense grants DAMD17-03-1-0066 and DAMD17-01-1-0765, and NIH grant R01 NS049175-01 A1. This paper has been reviewed by the Walter Reed Army Institute of Research and there is no objection to its presentation and/or publication. The opinions or assertions contained herein are the private views of the authors, and are not to be construed as official, or as reflecting true views of the Department of the Army or the Department of Defense. K. K. W. W. and R. L. H. hold equity in Banyan Biomarkers, Inc.

REFERENCES

1 Yamashima, T. (2000) Implication of cysteine proteases calpain, cathepsin and caspase in ischemic neuronal death of primates. Prog. Neurobiol. **62**, 273–295
2 Asah, M., Asahi, K., Jung, J. C., del Zoppo, G. J., Fini, M. E. and Lo, E. H. (2000) Role for matrix metalloproteinase 9 after focal cerebral ischemia, effects of gene knockout and enzyme inhibition with BB-94. J. Cereb. Blood Flow Metab. **20**, 1681–1689
3 Clark, A. W., Krekoski, C. A., Bou, S. S., Chapman, K. R. and Edwards, D. R. (1997) Increased gelatinase A (MMP-2) and gelatinase B (MMP-9) activities in human brain after focal ischemia. Neurosci. Lett. **238**, 53–56
4 Phillips, J. B., Williams, A. J., Adams, J., Elliott, P. J. and Tortella, F. C. (2000) Proteasome inhibitor PS519 reduces infarction and attenuates leukocyte infiltration in a rat model of focal cerebral ischemia. Stroke **31**, 1686–1693
5 Wang, K. K. W. (2000) Calpain and caspase, can you tell the difference. Trends Neurosci. **23**, 20–26
6 Pike, B. R., Flint, J., Johnson, E., Glenn, C. C., Dutta, S., Wang, K. K. W. and Hayes, R. L. (2001) Accumulation of calpain-cleaved non-erythroid βII-spectrin in cerebrospinal fluid after traumatic brain injury in rats. J. Neurochem. **78**, 1297–1306
7 Hajimohammadreza, I., Nath, R., Raser, K. J., Nadimpalli, R. and Wang, K. K. W. (1997) Neuronal nitric oxide synthase and calmodulin-dependent protein kinase IIα undergo neurotoxin-induced proteolysis. J. Neurochem. **69**, 1006–1013
8 McGinnis, K. M., Whitton, M., Gnegy, M. E. and Wang, K. K. W. (1998) Calmodulin-dependent protein kinase IV differentially cleaved by caspase-3 and calpain in SH-SY5Y human neuroblastoma cells. J. Biol. Chem. **273**, 1999–2000
9 Pasinetti, G. M. and Ho, L. (2001) From cDNA microarrays to high-throughput proteomics. Implications in the search for preventive initiatives to slow the clinical progression of Alzheimer's disease dementia. Restor. Neurol. Neurosci. **18**, 137–142
10 Castedo, M., Ferri, K. F., Blanco, J., Roumier, T., Larochette, N., Barretina, J., Amendola, A., Nardacci, R., Metivier, D., Este, J. A., Piacentini, M. and Kroemer, G. (2001) Human immunodeficiency virus 1 envelope glycoprotein complex-induced apoptosis involves mammalian target of rapamycin/FKBP12-rapamycin-associated protein-mediated p53 phosphorylation. J. Exp. Med. **194**, 1097–1110
11 Melnick, M., Chen, H., Min-Zhou, Y. and Jaskoll, T. (2001) The functional genomic response of developing embryonic submandibular glands to NF-κB inhibition. BMC Dev. Biol. **1**, 15
12 Malakhov, M. P., Kim, K. I., Malakhova, O. A., Jacobs, B. S., Borden, E. C. and Zhang, D. E. (2002) High-throughput immunoblotting. Ubiquitiin-like protein ISG15 modifies key regulators of signal transduction. J. Biol. Chem. **278**, 16608–16613
13 Yoo, G. H., Piechocki, M. P., Ensley, J. F., Nguyen, T., Oliver, J., Meng, H., Kewson, D., Shibuya, T. Y., Lonardo, F. and Tainsky, M. A. (2002) Docetaxel induced gene expression patterns in head and neck squamous cell carcinoma using cDNA microarray and PowerBlot. Clin. Cancer Res. **8**, 3910–3921
14 Gifford, S. M., Cale, J. M., Tsoi, S., Magness, R. R. and Bird, I. M. (2003) Pregnancy-specific changes in uterine artery endothelial cell signaling *in vivo* are both programmed and retained in primary culture. Endocrinology **144**, 3639–3650
15 Lorenz, P., Ruschpler, P., Koczan, D., Stiehl, P. and Thiesen, H. J. (2003) From transcriptome to proteome, differentially expressed proteins identified in synovial tissue of patients suffering from rheumatoid arthritis and osteoarthritis by an initial screen with a panel of 791 antibodies. Proteomics **3**, 991–1002
16 Cicala, C., Arthos, J., Selig, S. M., Dennis, Jr, G., Hosack, D. A., Van Ryk, D., Spangler, M. L., Steenbeke, T. D., Khazanie, P., Gupta, N. et al. (2002) HIV envelope induces a cascade of cell signals in non-proliferating target cells that favors virus replication. Proc. Natl. Acad. Sci. U.S.A. **99**, 9380–9385
17 Overall, C. M., McQuibban, G. A. and Clark-Lewis, I. (2002) Discovery of chemokine substrates for matrix metalloproteinases by exosite scanning, a new tool for degradomics. Biol. Chem. **383**, 1059–1066
18 Wang, K. K. W., Posmantur, R., Nath, R., McGinnis, K., Whitton, M., Talanian, R. V., Glantz, S. and Morrow, J. (1998) Simultaneous degradation of αII- and βII-spectrin by caspase 3 (CPP32) in apoptotic cells. J. Biol. Chem. **273**, 22490–22497
19 Santella, L., Kyozuka, K., Hoving, S., Munchbach, M., Quadroni, M., Dainese, P., Zamparelli, C., James, P. and Carafoli, E. (2000) Breakdown of cytoskeletal proteins during meiosis of starfish oocytes and proteolysis induced by calpain. Exp. Cell Res. **259**, 117–126

20 Wang, K. K. W., Villalobo, A. and Roufogalis, B. D. (1989) Calmodulin-binding proteins as calpain substrates. Biochem. J. **262**, 693–706
21 Schwab, B. L., Guerini, D., Didszun, C., Bano, D., Ferrando-May, E., Fava, E., Tam, J., Xu, D., Xanthoudakis, S., Nicholson, D. W., Carafoli, E. and Nicotera, P. (2002) Cleavage of plasma membrane calcium pumps by caspases, a link between apoptosis and necrosis. Cell Death Differ. **9**, 818–831
22 Lopez-Otin, C. and Overall, C. M.. (2002) Protease degradomics, a new challenge for proteomics. Nat. Rev. Mol. Cell Biol. **3**, 509–519
23 Wang, K. K. W. and Yuen, P. W. (1994) Calpain inhibition: an overview of its therapeutic potentials. Trends Pharmacol. Sci. **15**, 412–419
24 Posmantur, R., McGinnis, K., Nadimpalli, R., Gilbertsen, R. and Wang, K.K.W. (1997) Characterization of CPP32-like protease activity following apoptotic challenge in SH-SY5Y neuroblastoma cells. J. Neurochem. **68**, 2328–2337
25 Larner, S. F., McKinsey, D. M., Torres, M., Pike, M., Hayes, R. L. and Wang, K. K. W. (2004) Upregulation of caspase-12 after traumatic brain injury in rats. J. Neurochem. **88**, 78–90
26 Beer, R., Franz, G., Krajewski, S., Pike, B. R., Hayes, R. L., Reed, J. C., Wang, K. K., Klimmer, C., Schmutzhard, E., Poewe, W. and Kampfl, A. (2001) Temporal and spatial profile of caspase 8 expression and proteolysis after experimental traumatic brain injury. J. Neurochem. **78**, 862–873
27 Levilliers, N., Peron-Renner, M., Coffe, G. and Pudies, J. (1986) Gelation and fodrin purification from rat brain extracts. Biochim. Biophys. Acta **882**, 113–126
28 Pike, B. R., Zhao, X., Newcomb, J. K., Posmantur, R. M., Wang, K. K. W. and Hayes, R. L. (1998) Regional calpain and caspase-3 proteolysis of α-spectrin after traumatic brain injury. NeuroReport **9**, 2437–2442
29 Wang, K. K. W., Ottens, A., Haskins, W. E., Liu, M. C., Denslow, N., Chen, S. S. and Hayes, R. L. (2004) Neuroproteomic studies of traumatic brain injury. Int. Rev. Neurobiol. **61**, 215–240

Received 6 June 2005/13 December 2005; accepted 14 December 2005
Published as BJ Immediate Publication 14 December 2005, doi:10.1042/BJ20050905

Journal of Neurochemistry, 2006, **98**, 700–712 doi:10.1111/j.1471-4159.2006.03882.x

Extensive degradation of myelin basic protein isoforms by calpain following traumatic brain injury

Ming Cheng Liu,*,† Veronica Akle,† Wenrong Zheng,† Jason Kitlen,† Barbara O'Steen,† Stephen F. Larner† Jitendra R. Dave,‡ Frank C. Tortella,‡ Ronald L. Hayes*,† and Kevin K. W. Wang*,†

*Department of Psychiatry, Center for Neuroproteomics and Biomarkers Research and †Department of Neuroscience, Center for Traumatic Brain Injury studies, McKnight Brain Institute, University of Florida, Gainesville, Florida, USA

‡Department of Neuropharmacology and Molecular Biology, Division of Neurosciences, Walter Reed Army Institute of Research, Silver Spring, Maryland, USA

Abstract

Axonal injury is one of the key features of traumatic brain injury (TBI), yet little is known about the integrity of the myelin sheath. We report that the 21.5 and 18.5-kDa myelin basic protein (MBP) isoforms degrade into N-terminal fragments (of 10 and 8 kDa) in the ipsilateral hippocampus and cortex between 2 h and 3 days after controlled cortical impact (in a rat model of TBI), but exhibit no degradation contralaterally. Using N-terminal microsequencing and mass spectrometry, we identified a novel *in vivo* MBP cleavage site between Phe114 and Lys115. A MBP C-terminal fragment-specific antibody was then raised and shown to specifically detect MBP fragments in affected brain regions following TBI. *In vitro* naive brain lysate and purified MBP digestion showed that MBP is sensitive to calpain, producing the characteristic MBP fragments observed in TBI. We hypothesize that TBI-mediated axonal injury causes secondary structural damage to the adjacent myelin membrane, instigating MBP degradation. This could initiate myelin sheath instability and demyelination, which might further promote axonal vulnerability.

Keywords: brain injury, cell death, demyelination, protease, proteolysis, proteomic.

J. Neurochem. (2006) **98**, 700–712.

Traumatic brain injury (TBI) represents a major CNS disorder without any clinically proven therapy (Choi and Bullock 2001). Evidence of axonal damage following TBI has been documented extensively (Pettus *et al*. 1994; Medana and Esiri 2003), and prolonged traumatic axonal injury (TAI) is a universal and critical event following TBI and a key predictor of clinical outcome (Medana and Esiri 2003). However, the integrity of myelin sheaths, which surround axons, is poorly studied. To our knowledge, only two previous studies reported increased demyelination after TBI in humans (Ng *et al*. 1994; Gale *et al*. 1995) and one in a rat model (Bramlett and Dietrich 2002), yet the underlying biochemical mechanisms were not investigated.

In the CNS, myelin sheaths are formed by oligodendrocytes. The CNS myelin sheath is comprised mainly of several structural proteins: myelin basic protein (MBP), proteolipid protein (PLP), myelin/oligodendrocyte-specific protein (MOSP) and myelin-associated glycoprotein (MAG) (Richter-Landsberg 2000). MBP is one of the most abundant (30%) myelin proteins and contains clusters of positively charged amino acid residues that facilitate myelin sheath compaction (Richter-Landsberg 2000). The loss of integrity of the myelin sheath and the degradation of myelin proteins have been extensively studied in demyelinating diseases such

Received December 9, 2005; revised manuscript received February 23, 2006; accepted February 24, 2006.

Address correspondence and reprint requests to either Dr Ming Cheng Liu or Dr Kevin K. W. Wang, McKnight Brain Institute, L4–100F, PO Box 100256, University of Florida, Gainesville, FL 32610, USA. E-mail: liumc@mbi.ufl.edu or kwang@psychiatry.ufl.edu

Abbreviations used: APP, amyloid precursor protein; BDP, breakdown product; CCI, controlled cortical impact; DTT, dithiothreitol; EAE, experimental allergic encephalomyelitis; KLH, keyhole limpet hemocyanin; MBP, myelin basic protein; MMP, matrix metalloproteases; MS, multiple sclerosis; PBS, phosphate-buffered saline; PVDF, polyvinylidene fluoride; SBDP, αII-spectrin breakdown product; SDS–PAGE, sodium dodecyl sulfate–polyacrylamide gel electrophoresis; TBI, traumatic brain injury; TBS, Tris-buffered saline; TBST, TBS with 0.05% Tween-2.

as multiple sclerosis (MS) and experimental allergic encephalomyelitis (EAE), which is an animal model of MS (Waxman 1998; Schaecher *et al*. 2001).

Proteolysis of structural proteins in the axons (such as neurofilament proteins, amyloid precursor protein, APP, and αII-spectrin) by calpains and/or caspase-3 is a signature event following TBI in both experimental animal models of TBI and in humans that have sustained head injuries (Stone *et al*. 2002; Posmantur *et al*. 1994, 1997; Saatman *et al*. 1996; Newcomb *et al*. 1997; Pike *et al*. 1998; Buki *et al*. 1999, 2000; McCracken *et al*. 1999). We therefore hypothesize that the structural myelin proteins in the myelin sheath such as MBP might be equally vulnerable to proteolysis following TBI. In this study, we use an established rat-controlled cortical impact model of TBI and both immunological and proteomic methods to examine the integrity of MBP. Here we report that the 21.5 and 18.5-kDa isoforms of MBP were extensively degraded into smaller fragments in the ipsilateral hippocampus and cortex. We also observed that the 17 and 14-kDa MBP isoforms were similarly degraded. Using proteomic-based N-terminal sequencing and tryptic digestion/mass spectrometry analysis, we have, for the first time, identified the exact *in vivo* cleavage sites on MBP after TBI.

Materials and methods

In vivo model of the TBI injury model

A controlled cortical impact (CCI) device was used to model TBI in rats as previously described (Pike *et al*. 1998). It will generate damaged brain tissue including tissue in the hippocampus and the cortex. Adult male (280–300 g) Sprague–Dawley rats (Harlan, Indianapolis, IN, USA) were anesthetized with 4% isoflurane in a carrier gas of 1 : 1 O_2/N_2O (for 4 min) followed by maintenance anesthesia of 2.5% isoflurane in the same carrier gas. The core body temperature was monitored continuously by a rectal thermistor probe and maintained at 37 ± 1°C by placing an adjustable temperature-controlled heating pad beneath the rats. Animals were mounted in a stereotactic frame in a prone position and secured by ear and incisor bars. A midline cranial incision was made, the soft tissues reflected and a unilateral (ipsilateral to site of impact) craniotomy (7 mm in diameter) was performed adjacent to the central suture, midway between bregma and lambda. The dura mater was kept intact over the cortex. Brain trauma was produced by impacting the right cortex (ipsilateral cortex) with a 5-mm diameter aluminum impactor tip (housed in a pneumatic cylinder) at a velocity of 3.5 m s^{-1} with a 1.6-mm compression and 150-ms dwell time (compression duration). These injuries were associated with different magnitudes of local cortical contusion and more diffuse axonal damage. The velocity of the impactor tip was controlled by adjusting the pressure (compressed N_2) supplied to the pneumatic cylinder. The velocity and dwell time were measured by a linear velocity displacement transducer (model 500 HR; Lucas Shaevit, Detroit, MI, USA) that produced an analog signal that was recorded by a storage-trace oscilloscope (model 2522B; BK Precision, Placentia, CA, USA). Sham-injured control animals underwent identical surgical procedures but did not receive an impact injury. Appropriate pre- and post-injury management was maintained to insure compliance with guidelines set by the University of Florida Institutional Animal Care and Use Committee and the National Institutes of Health guidelines detailed in the *Guide for the Care and Use of Laboratory Animals*. In addition, research was conducted in compliance with the Animal Welfare Act and other federal statutes and regulations relating to animals and experiments involving animals, and adheres to the principles stated in the *Guide for the Care and Use of Laboratory Animals*.

Brain tissue collection and preparation

At the appropriate time-points (2, 6 and 24 h; 2, 3, 5, 7 and 14 days) after administration, animals were anesthetized and immediately killed by decapitation. Brains were immediately removed, rinsed with ice-cold phosphate-buffered saline (PBS) and halved. Two different brain regions in the right hemispheres (cerebrocortex around the impact area and the hippocampus) were rapidly dissected, rinsed in ice-cold PBS, snap-frozen in liquid nitrogen and frozen at −85°C until used. For immunohistochemistry, brains were quick frozen in dry-ice slurry, then sectioned via a cryostat (20 μm) onto SuperFrost Plus Gold® slides (Fisher Scientific, Pittsburgh, PA, USA) and frozen at −85°C until used. For the left hemispheres, the same tissue as the right-hand side was collected. For western blot analysis, the brain samples were pulverized with a small mortar and pestle set over dry ice to a fine powder. The pulverized brain tissue powder was then lysed for 90 min at 4°C with 50 mM Tris (pH 7.4), 5 mM EDTA, 1% (v/v) Triton X-100, 1 mM dithiothreitol (DTT), 1 × protease inhibitor cocktail (Roche Molecular Biochemicals, Indianapolis, IN, USA). The brain lysates were then centrifuged at 15 000 g for 5 min at 4°C to clear and remove insoluble debris, snap-frozen and stored at − 85°C until used.

Sodium dodecyl sulfate–polyacrylamide gel electrophoresis (SDS–PAGE) and electrotransfer

The protein concentration of tissue lysates was determined by DC Protein Assay (Bio-Rad Laboratories, Hercules, CA, USA) with albumin standards. Protein-balanced samples were prepared for SDS–PAGE with two-fold loading buffer containing 0.25 M Tris (pH 6.8), 0.2 M DTT, 8% SDS, 0.02% bromophenol blue and 20% glycerol in distilled H_2O. Twenty micrograms (20 ìg) of protein per lane were routinely resolved by SDS–PAGE on 10–20% Tris/glycine gels (Cat. No. EC61352; Invitrogen, Carlsbad, CA, USA) at 130 V for 2 h. Following electrophoresis, separated proteins were laterally transferred to polyvinylidene fluoride (PVDF) membranes in a transfer buffer containing 39 mM glycine and 48 mM Tris-HCl (pH 8.3) 5% methanol at a constant voltage of 20 V for 2 h at ambient temperature in a semi-dry transfer unit (Bio-Rad).

1-D gel band analysis by mass spectrometry

After SDS–PAGE, the gel was stained by Coomassie blue staining (80% methanol, 5% acetic acid and 0.05% Coomassie Brilliant Blue R-250; Sigma, St. Louis, MO, USA) for 15 min, and we then looked for the difference between naive and TBI samples. Gel bands with differential levels (TBI vs. naive) were cut out for tryptic digestion and for submission to the Protein Core of the University of Florida to perform Matrix Assisted Laser Desorption/Ionisation Time-of-Flight (MALDI-TOF) mass spectrometry protein identification.

Immunoblotting analysis

After electrotransfer, blotting membranes were blocked for 1 h at ambient temperature in 5% non-fat milk in Tris-buffered saline (TBS) and 0.05% Tween-2 (TBST), then incubated in primary monoclonal MBP antibody (Cat. No. MAB381; Chemicon, Temecula, CA, USA) in TBST with 5% milk at 1/50 dilution, as recommended by the manufacturer, at 4°C overnight, followed by three washes with TBST and a 2-h incubation at ambient temperature with a secondary antibody linked to biotinylated secondary antibody (Cat. No. RPN1177v1; Amersham Pharmacia Biotech, Piscataway, NJ, USA) followed by a 30-min incubation with strepavidin-conjugated alkaline phosphatase (colorimetric method). Colorimetric development was performed with a one-step BCIP/NBT reagent (Cat. No. 50-81-08; KPL, Gaithersburg, MD, USA). Molecular weights of intact MBP proteins and their potential breakdown products (BDPs) were assessed by running alongside rainbow-colored molecular weight standards (Cat. No. RPN800V; Amersham Pharmacia Biotech). Semi-quantitative evaluation of intact MBP proteins and BDP levels was performed via computer-assisted densitometric scanning (Epson XL3500 high-resolution flatbed scanner; Epson, Long Beach, CA, USA) and image analysis was carried out with IMAGE J software (NIH http://rsb.info.nih.gov/nih-image/download.html). Uneven loading of samples onto different lanes might occur despite careful protein concentration determination and careful sample handling and gel loading (20 mg per land). To overcome this source of variability, β-actin (polyclonal #A5441; Sigma, St Louis, MO, USA) blots were performed routinely as protein loading evenness control. MBP isoforms-specific antibodies as well as MBP-fragment-specific antibodies were raised in rabbit, based on unique peptide sequences for the MBP 21.5- and 18.5-kDa isoforms, the MBP 17- and 14-kDa isoforms (Akiyama *et al*. 2002) and the *in vivo* MBP fragment (KNIVITPRTPP; based on our novel cleavage site). Synthetic peptides identical to these sequences were made and coupled to the carrier protein keyhole limpet hemocyanin (KLH) before injecting into the rabbit for polyclonal antibody production.

Identification of MBP cleavage site by N-terminal microsequencing

The proteins were separated by SDS–PAGE and electrotransferred to PVDF membranes. The PVDF membrane protein bands were visualized by Coomassie blue staining (80% methanol, 5% acetic acid and 0.05% Coomassie Brilliant Blue R-250) for 1 min. The BDP band (based on western blot results) was cut out and subjected to N-terminal microsequencing in order to identify its new N-terminal sequence. By matching the sequence generated from BDP band analysis with the full-length protein sequences in the rat proteome database with bioinformatic tools such as MASCOT, the cleavage site of the protein substrate can be identified. Using this method, we have already successfully identified the MBP BDP cleavage sites *in vivo* after TBI.

In vitro protease digestion of MBP in brain lysate

For this study, brain tissue collection and preparation was essentially the same, but without the use of the protease inhibitor cocktail (see above). *In vitro* protease digestion of naive rat hippocampus lysate (5 mg) with purified proteases at different substrate to protease ratios: human calpain-2 (Cat. No. 208715, 1 μg/μL; Calbiochem, San Diego, CA, USA), recombinant human caspase-3 (Cat. No. cc119, caspase-3, 1 U/μL; Chemicon), human cathepsin B (P6458c; Biomol, Plymouth Meeting, PA, USA), cathepsin D (L1129a; Biomol), matrix metalloprotease-2 (MMP-2, MAB3308; Chemicon), and MMP-9 (TP221; Torrey Pines Bio-Labs, Houston, TX, USA) was performed in a buffer containing 100 mM Tris-HCl (pH 7.4) and 20 mM dithiothreitol (except with MMPs). For calpain-2, 10 mM $CaCl_2$ was also added, and then incubated at room temperature (22°C–24°C) for 30 min. For caspase-3 digestion, 2 mM EDTA was added instead of $CaCl_2$, and was incubated at 37°C for 2 h. For cathepsin D, MMP-2 and -9, neither EDTA nor DTT was added; incubation was for 60 min at 37°C. The protease reaction was stopped by the addition of SDS–sample buffer.

Immunohistochemistry

Brain tissues were collected from either naive animals or from animals following either craniotomy or TBI. At the appropriate time point, the animals were anesthetized using 4% isoflurane in a carrier gas of 1 : 1 O_2/N_2O (for 4 min), transcardially perfused with 200 mL 2% heparin (Elkins-Sinn Inc., Saint Davids, PA, USA) in 0.9% saline (pH 7.4) followed by 400 mL 4% paraformaldehyde in 0.1 M phosphate buffer (pH 7.4), and then subsequently killed by decapitation and the brains were removed. A total of 2 h in fixative was followed by storage in either PBS or cryoprotection buffer. A vibratome cut 40-μm sections. Briefly, tissue sections were rinsed in PBS, incubated for 1 h at room temperature in 10% goat serum/0.2% Triton X-100 in TBS (block) to decrease non-specific labeling, then incubated with the primary antibody: the anti-MBP-fragment (1 : 250) and the mouse anti-CNPase antibody (Chemicon), 1 : 1000 for 4 days in block at 4°C. After being rinsed in TBST, the tissue sections were incubated with species-specific Alexa Fluor secondary antibodies (1 : 3000; Molecular Probes, Eugene, OR, USA), and the nuclear counterstain 4′,6-diamidino-2-phenylindole (DAPI) in blocking buffer for 1 h at room temperature. The sections were then washed in PBS, cover slipped in Vectashield with DAPI (Vector Laboratories), viewed and digitally captured with a Zeiss Axioplan 2 microscope (Thornwood, NY, USA) equipped with a Spot Real Time (RT) Slider high-resolution color CCD digital camera (Diagnostic Instruments Inc., Livingston, Scotland, UK). Tissue sections without primary antibodies were similarly processed to control for binding of the secondary antibodies. Appropriate control sections were performed and no specific immunoreactivity was detected.

Statistical analyses

A semi-quantitative evaluation of protein levels on immunoblots was performed via computer-assisted 1-D densitometric scanning (Epson expression 8836XL high-resolution flatbed scanner and NIH IMAGE J densitometry software). Data were acquired in arbitrary densitometric units. Changes in any outcome parameter will be compared with the appropriate control group. Consequently, the magnitude of change from control in one model system was directly compared with those from any other model system. In this study, six replicate data were evaluated by analysis of variance (ANOVA) and *post-hoc* Tukey tests. A value of $p < 0.05$ was taken as significant.

Results

Examination of MBP integrity using proteomic technologies

Using the rat CCI paradigm as a model of TBI, rat cortical samples (around the impact zone) and hippocampal samples were prepared at 48 h after injury. This time point was chosen based on our previous experience of the time course of αII-spectrin proteolysis in the same model. As MBP represents one of the major low-molecular-weight proteins in the brain, we first attempted to identify intact MBP based on its mobility in 1-D SDS–PAGE. Figure 1(a) showed that a major band (A) of about 18 kDa was noticeably weaker in all TBI samples vs. their naive counterparts. Also, a major hemoglobin (Hgb) band of about 13 kDa was observed, indicative of the hemorrhage as a result of CCI. Upon closer inspection, we also noticed a fainter band (B) that was present in TBI samples but not present in naive samples (Fig. 1a). Bands A and B were subsequently cut out and subjected to tryptic digestion and MALDI-TOF mass spectrometry protein identification. Based on molecular mass matching, three peptides from band A were found to derive from internal sequences in the 18.5-kDa isoforms of rat MBP (accession # CAA10806, 169 residues), suggesting that intact MBP (band A) was significantly reduced following TBI (Fig. 1a, right-hand and lower panels). In contrast, the 10-kDa band found only in TBI samples also yielded three tryptic peptides that again matched with MBP sequences (Fig. 1a, right-hand and lower panels). These data suggest that MBP might degrade to smaller fragments following TBI.

In order to confirm the above MS identification, we re-ran the naive and TBI cortical samples on 10–20% Tricine gel, which provides better resolution in the low-molecular-weight region, and the total protein was transferred to PVDF membrane. After being stained by 0.25% Coomassie Brilliant Blue (Bio-Rad 161–0400), the major intact MBP was readily identified based on its molecular mass and abundance in naive samples (band F; Fig. 1b). We also found two

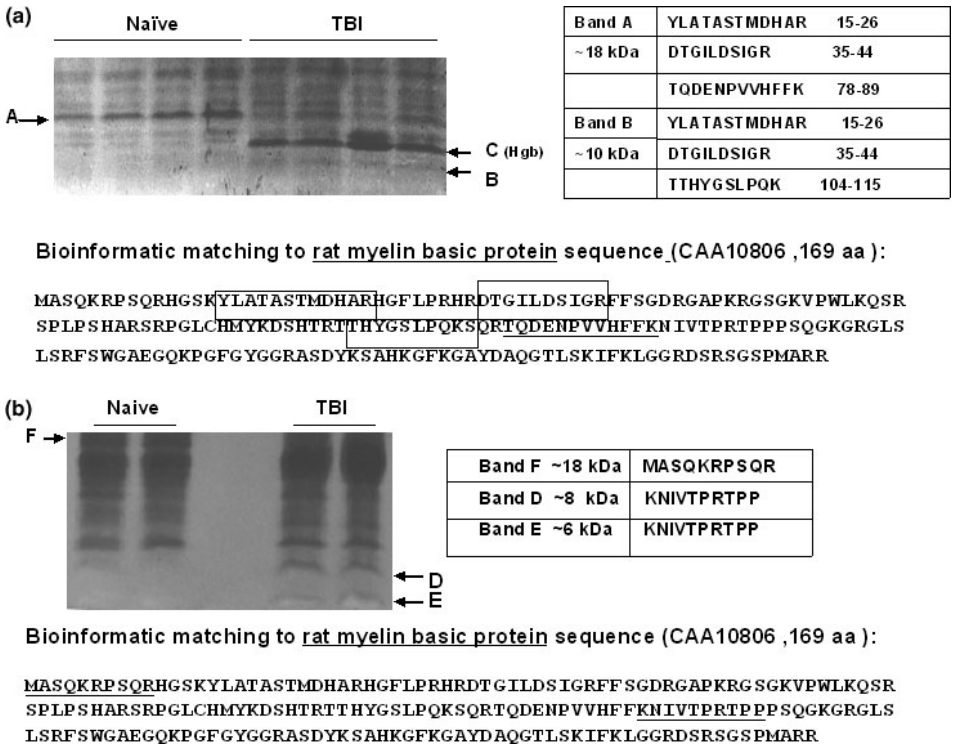

Fig. 1 Identification of myelin basic protein (MBP) proteolysis by MALDI-TOF mass spectrometry and N-terminal microsequencing. (a) Naive and traumatic brain injury (TBI) (four each) ipsilateral cortex samples were subjected to 1-D SDS–PAGE and stained with Coomassie blue. Band A (18 kDa) was consistently reduced in TBI samples whereas bands B (10 kDa) and C (13 kDa) were elevated in TBI samples. Based on tryptic peptide analysis by MALDI, band A was identified as a rat 18.5-kDa MBP isoform (protein accession # CAA10806) based on three matching tryptic peptides (underlined) and band B was also derived from myelin basic protein (MBP), based on three matching tryptic peptides (boxed). In addition, band C contains hemoglobin (α and β chains). (b) Similar naive and TBI samples were subjected to 10–20% Tricine gel and blotting to polyvinylidene fluoride (PVDF) membranes, the protein bands were then visualized by Coomassie blue-staining. Band F levels were reduced in TBI whereas the intensity of bands D (8 kDa) and E (6 kDa) was elevated in TBI samples. Using N-terminal microsequencing, band F matches with the native N-terminal (MASQKRPSQR) of rat MBP (protein accession # CAA10806) whereas bands D and E match with an internal region beginning with KNIVTPRTPP.

low-molecular-weight bands D and E that were much stronger in TBI samples than in naive samples. Bands F, D and E on the PVDF membrane were subjected to N-terminal microsequencing. The sequencing results showed that band F indeed matched with the intact N-terminus of MBP (MASQKRPSQR). It further showed that both bands D and E showed the same N-terminal sequence KNIVITPRTPP, which matches with an internal region of rat 18-kDa MBP (accession # CAA10806; Fig. 1b, right-hand and lower panels). These data, taken together, established the major *in vivo* cleavage site in MBP to be between Phe114 and Lys115 following TBI.

Characterization of MBP proteolysis following TBI

To confirm our proteomic results, we employed immunoblotting analysis using monoclonal MBP antibody that detects the N-terminal half of both the 21.5- and 18.5-kDa MBP isoforms. Our western blot results (Fig. 2a) showed that, when compared with the naive group, the 21.5- and 18.5-kDa MBP were extensively degraded into smaller fragments (of 10 and 8 kDa) in the ipsilateral cortex in the 48 h after CCI. In addition, in the contralateral counterparts, MBP was not degraded (Fig. 2c). Also, no degradation of MBP was observed in the naive and sham groups. Ipsilateral and contralateral hippocampus samples (48 h after TBI) were also analyzed and they showed very similar patterns of proteolysis (Figs 2b and d) to those observed in cortex.

We next examined the integrity of MBP in a post-TBI time course. The results showed that in the ipsilateral cortex, the 21.5- and 18.5-kDa MBP isoforms were significantly diminished as early as 2 h after TBI, and reached the lowest level at 48 h after TBI; their levels then significantly recovered by 7 days after TBI (Figs 3a and b). Also, we observed that N-terminal MBP BDPs of 10 and 8 kDa accumulated in the rat cortex beginning at 2 h after TBI, reaching a peak at 1–2 days after TBI before approaching basal levels again in 6–7 days after TBI (Figs 3a and c). In the ipsilateral hippocampus, the levels of 21.5- and 18.5-kDa MBP isoforms also diminished between 2 h and 3 days after TBI(Fig. 4a). However, unlike its cortex counterpart, intact MBP isoforms, although significantly diminished in levels, were still readily observed at all time points except at 2 days after TBI (Fig. 4b). Consistent with that, MBP BDP accumulation in rat hippocampus was much less intense than in the cortex, with the levels of 8-kDa BDP elevated only at 2 days after TBI (Fig. 4c). β-Actin blots were also performed routinely as protein loading evenness controls, thus ruling out technical artifacts (Figs 3 and 4).

We also examined the integrity of MBP in cortex and hippocampus in the sham (craniotomy) group. Interestingly, significant evidence of MBP proteolysis was also observed in the cortex around the craniotomy zero (Fig. 3d), although the BDP accumulation pattern appears to have a more transient nature (Fig. 3e, as compared with Fig. 3c). This is likely to reflect myelin injury as a result of the sham-craniotomy operation. In contrast, more distal to the craniotomy, the sham hippocampus (ipsilateral) showed no evidence of MBP proteolysis at all (Fig. 4d).

Proteolysis of all four isoforms of MBP following TBI

As the monoclonal antibody we used only appears to detect the 21.5- and 18.5-kDa isoforms of MBP (Figs 3 and 4), we sought to determine whether all four major isoforms of MBP are equally vulnerable to TBI-induced proteolysis. To address this, we examined the MBP-isoforms integrity using MBP-21.5/18.5-kDa and MBP-17/14-kDa isoforms-specific

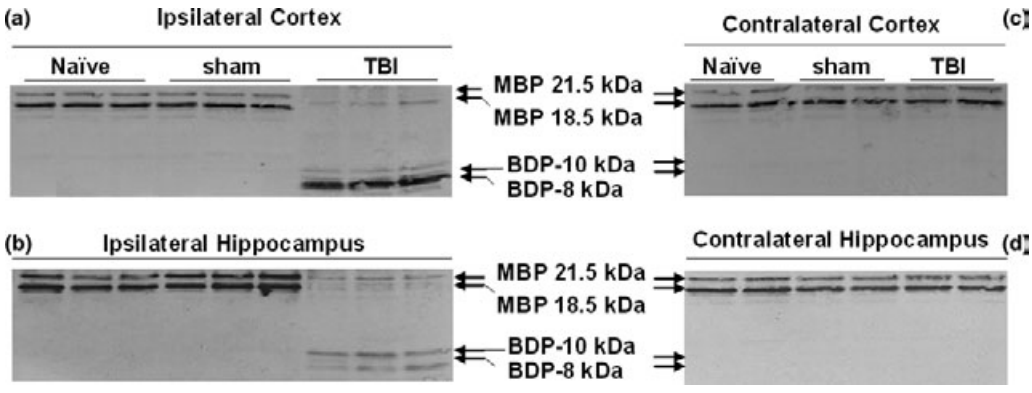

Fig. 2 Myelin basic protein (MBP) isoforms in rat cortex and hippocampus are highly vulnerable to proteolysis following traumatic brain injury (TBI). Ipsilateral cortex (a) and hippocampus (b) lysate (20 ìg) from naive sham and injured rats (at 48 h after TBI) were subjected to SDS–PAGE and western blot analysis probed with antibodies against MBP. The 21.5- and 18.5-kDa MBP isoforms were readily identified with the N-terminal-directed antibody. Major N-terminal breakdown products (BDPs) with their relative molecular weights (10 and 8 kDa) are indicated. BDPs in contralateral cortex (c) and hippocampus (d) counterparts were analyzed by western blot. No observable degradation was readily observed at 48 h after TBI.

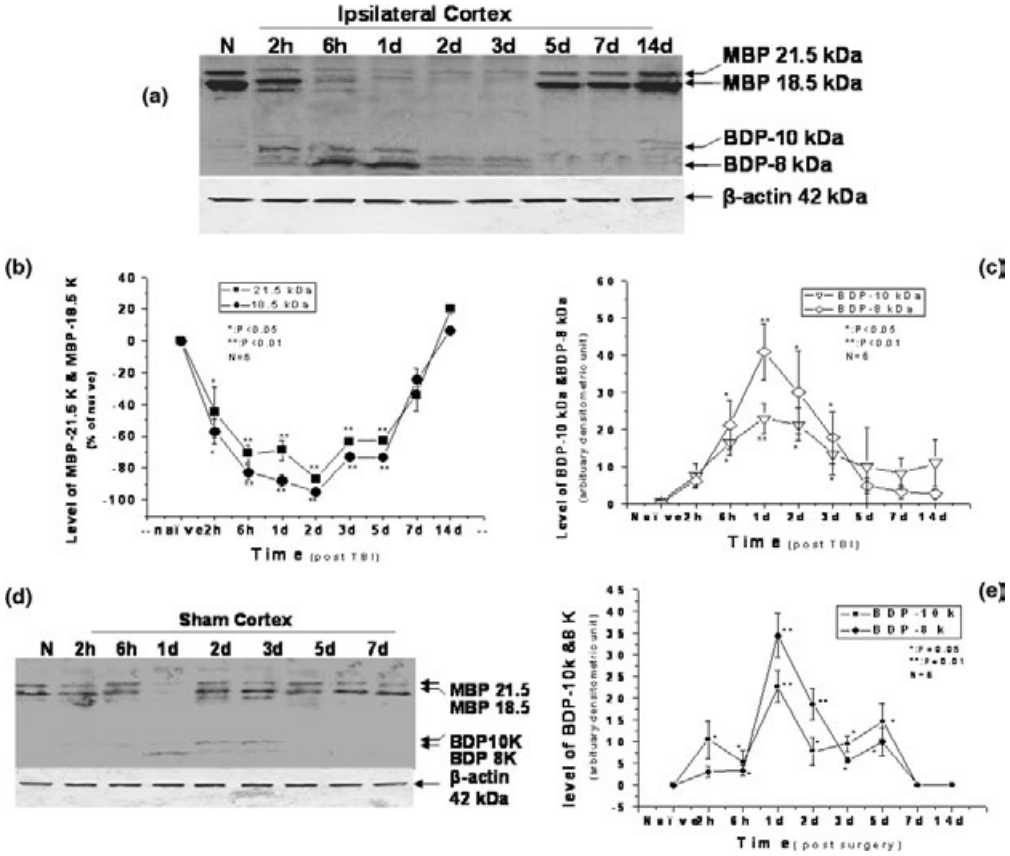

Fig. 3 Time course of traumatic brain injury (TBI)-associated myelin basic protein (MBP) proteolysis in rat cortex. (a) Western blotting analysis of MBP in rat cortex at the indicated time points after TBI compared with naive control (N). β-Actin blots were also performed as protein loading controls. (b) The density of intact MBP 21.5- (■) and 18.5-kDa (●) isoforms in naive and ipsilateral TBI cortex was plotted against various time points. The results revealed that the level of MBP 21.5 and 18.5-kDa isoforms decreased significantly (*$p < 0.05$, **$p < 0.01$; $n = 6$) after TBI. (c) The levels of two major breakdown products (BDPs) of 10 (▽) and 8 kDa (◇) were plotted against various time points (*$p < 0.05$, **$p < 0.01$; $n = 6$). (d) Western blotting analysis of MBP in rat cortex at the indicated time points after sham operation (craniotomy) compared with naive control (N). (e) The levels of two major BDPs of 10 (■) and 8 kDa (●) were plotted against various time points (*$p < 0.05$, **$p < 0.01$; $n = 6$).

antibodies (Akiyama *et al*. 2002). With MBP-21.5/18.5-kDa-specific antibody, we indeed confirmed that two major MBP isoforms were degraded to 10- and 8-kDa fragments (Fig. 5a). Importantly, when MBP-17/14-kDa-specific antibody was used, we also observed that these two smaller MBP isoforms were also subjected to extensive proteolysis at 48 h after TBI (Fig. 5b).

Development and characterization of novel MBP-fragment-specific antibodies

Based on our and others' previous success of raising spectrin breakdown product-specific antibodies (Saido *et al*. 1993; Roberts-Lewis *et al*. 1994; Bahr *et al*. 1995; Wang *et al*. 1998; Nath *et al*. 2000; Dutta *et al*. 2002), we designed a seven-residue peptide (NH_2-KNVITPR) based on the new N-terminal of the two major C-terminal fragments of MBP observed in TBI (Fig. 1). The peptide was conjugated to carrier protein KLH and injected into both rabbits and mice. Animal sera were antigen affinity purified using the same peptide-coupled resin. These purified antibodies were tested against naive and TBI cortical samples. We indeed observed that both rabbit and mouse antibodies strongly detected the C-terminal MBP fragment of 8 kDa, 6 kDa and other minor fragments. Yet, unlike the total MBP-antibody, these fragment-specific antibodies did not detect intact MBP bands at all (Fig. 6a). It is also worth noting that the total MBP-antibody that is directed to the N-terminal half of MBP, detects two N-terminal fragments of higher molecular mass (10 and 8 kDa) than the C-terminal BDPs (8 and 6 kDa) detected by the fragment-specific antibodies (Fig. 6a, see middle and right-hand panels as compared with the left-hand panel). We are now in the process of generating mouse monoclonal anti-MBP-fragment antibodies to optimize specificity.

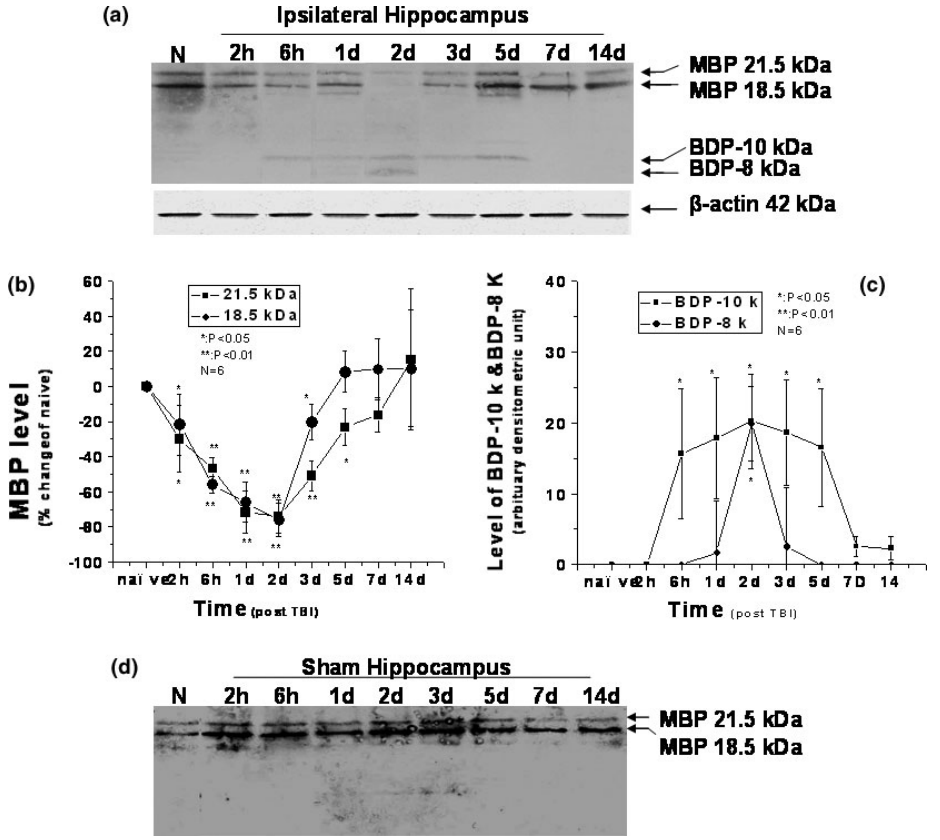

Fig. 4 Time course of traumatic brain injury (TBI)-associated myelin basic protein (MBP) proteolysis in rat hippocampus. (a) Western blotting analysis of MBP in rat cortex at the indicated time points after TBI compared with naive control (N). β-Actin blots were also performed as protein evenness controls. (b) The density of intact MBP 21.5- (■) and 18.5-kDa (●) isoforms in naive and ipsilateral TBI hippocampus was plotted against various time points. The results revealed that the levels of MBP 21.5 and 18.5 kDa decreased significantly (*$p < 0.05$, **$p < 0.01$; $n = 6$) after TBI. (c) The levels of two major BDPs of 10 (■) and 8 kDa (●) were plotted against various time points. (d) Western blotting analysis of MBP in rat hippocampus at the indicated time points after sham operation (craniotomy) compared with naive control (N). No significant MBP proteolysis was observed.

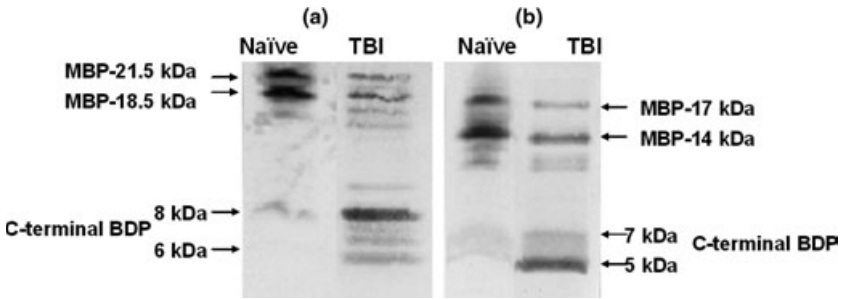

Fig. 5 Traumatic brain injury (TBI)-associated vulnerability of all myelin basic protein (MBP) isoforms to proteolysis. Naive and TBI hippocampus samples (at 48 h after TBI) were analyzed with MBP 21.5-kDa isoform-specific (a) and MBP 17–14-kDa isoform-specific (b) antibodies. (a) MBP 21.5- and 18.5-kDa isoforms were both observed in the naive sample, whereas the TBI sample showed C-terminal breakdown products (BDPs) of 8 and 6 kDa. (b) MBP 17- and 14-kDa isoforms were both observed in the naive sample, whereas the TBI sample showed C-terminal BDPs of 7 and 5 kDa.

We also submit that these novel fragment-specific antibodies should selectively stain degenerating myelin sheath in affected brain regions following TBI. Coronal sections of naive, sham-operated and TBI (24 h) rat brains were subjected to immunohistochemical staining with anti-MBP-fragment-antibody. Representative photomicrographs are

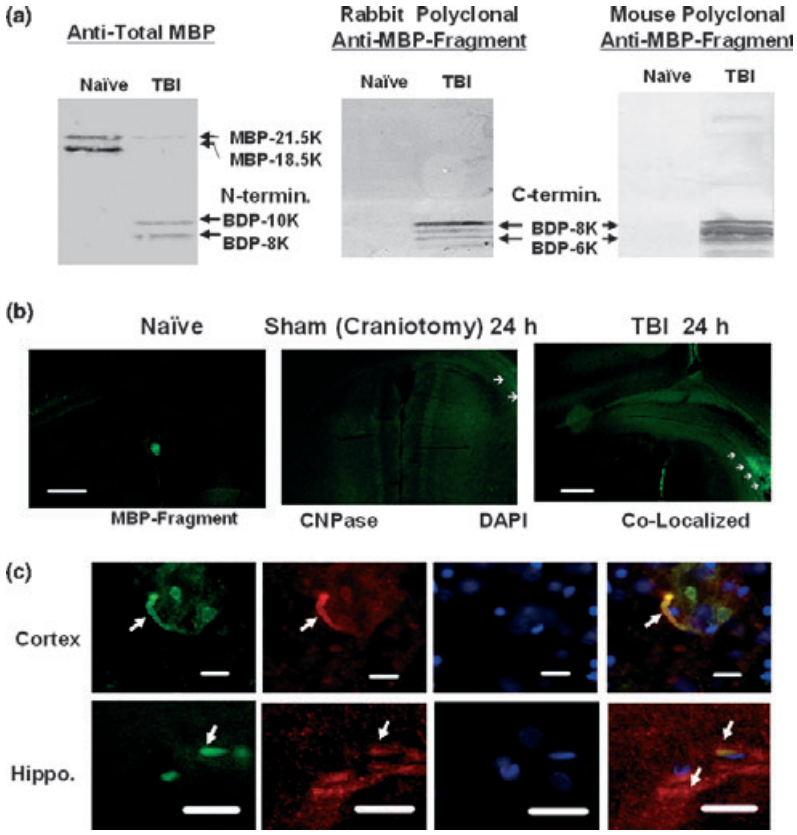

Fig. 6 Myelin basic protein (MBP) fragment-specific antibodies and their characterisations. (a) Naive and traumatic brain injury (TBI) (48 h after injury) cortex samples were analyzed by immunoblots probed with anti-total MBP antibody (left-hand panel), MBP fragment-specific rabbit (middle panel) or mouse (right-hand panel) polyclonal antibodies. Although anti-total MBP detected both intact MBP isoforms (21.5 and 18.5 kDa) as well as two N-terminal breakdown products (BDP 10 and 8 kDa), anti-MBP-fragment-specific antibodies only detected C-terminal BDPs (8 and 6 kDa). No intact MBPs were detected with these antibodies, demonstrating their selectivity for the *in vivo*-generated MBP fragments. (b) The polyclonal rabbit anti-MBP-fragment antibody was used in the immunohistochemical staining of coronal sections of naive, sham and injured rat brains. Little staining was observed in naive samples; moderate and intense staining was observed in subcortical white matter of the ipsilateral hemisphere of sham and TBI rats, respectively. Scale bar = 200 μm. (c) Immunohistochemical colocalization MBP-fragment (green) and myelin marker (CNPase, red) with DAPI nuclear DNA staining as reference (blue) in both injured cortex (upper panels) and hippocampus (lower panels) was used in the staining of coronal sections of naive, sham and injured rat brains. Scale bar = 0.5 μm.

shown in Fig. 6. Naive brains showed either little or no background Alexa Fluor-staining through the brain section (Fig. 6b, left-hand panel). In TBI sections, intense staining was detected on the ipsilateral side, concentrated in the subcortical white matter area, in the immediate vicinity of the impact site (right-hand side) (Fig. 6b, right-hand panel). Other deeper brain regions such as hippocampus and corpus callosum were also stained, but less intensely (not shown). We noted that even in the sham-brain sections, some increase in MBP-fragment staining was observed in the subcortical white matter region underneath the craniotomy site (Fig. 6b, middle panel). We further examined the cell type that expressed the MBP-fragment signal on higher photomicrograph magnification. Using CNPase as an oligodendrocyte marker, we confirmed that MBP-fragment staining indeed colocalizes with immunopositive oligodendrocytes staining in injured cortex as well as injured hippocampus (Fig. 6c). In addition, MBP-fragment-positive structures are consistent with the morphology of myelin sheaths.

Identification of protease involved in MBP fragmentation

In an attempt to identify which protease is responsible for the *in vivo* MBP cleavages we observed following TBI in rat brain, we subjected naive cortical lysate (containing intact MBPs) to various protease treatments *in vitro*. As calpain is a strong candidate MBP-degrading protease in other demyelinating diseases such as MS (Tsubata and Takahashi 1989; Shields *et al.* 1999; Schaecher *et al.* 2001; Sloane *et al.* 2003), we subjected the brain lysate to various quantities of calpain-2 (different substrate : protease ratios). The treated

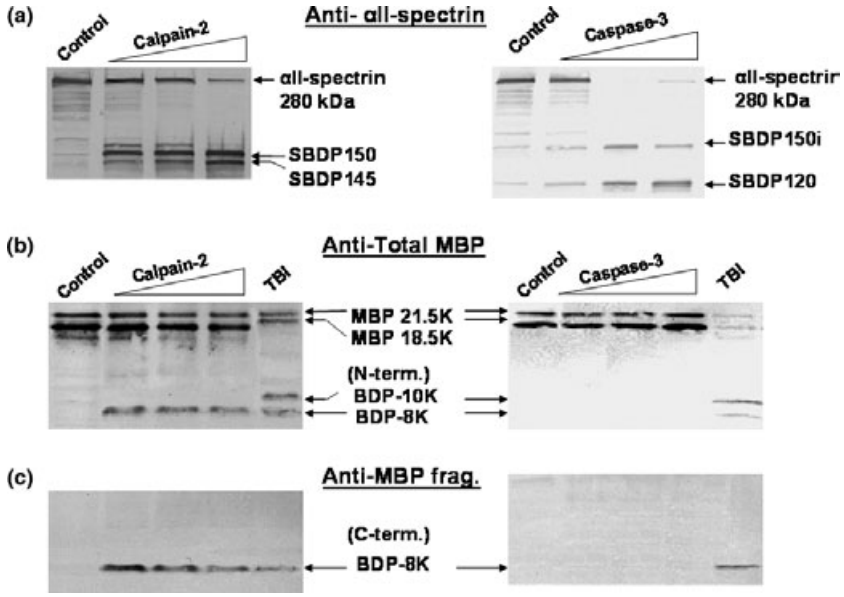

Fig. 7 *In vitro* proteolysis of myelin basic protein (MBP) with various protease treatments. Lysate of naive rat hippocampus (prepared without protease inhibitor cocktail) was digested with calpain-2 and caspase-3 *in vitro* for comparison with the fragmentation pattern observed *in vivo* at 48 h after traumatic brain injury (TBI). In the left-hand panels of (a), (b) and (c), lysate was treated with either no protease (control) or with 0.25%, 0.5% and 1% calpain-2. In the right-hand panels of (a), (b) and (c), lysate was treated with either no protease (control) or with 0.3%, 1.2% and 2.4% caspase-3. The samples were then analyzed by immunoblots probed with anti-αII-spectrin (a), anti-total MBP (b) or MBP-fragment-specific monoclonal antibody (c).

lysate samples were then analyzed by western blots probed with anti-αII-spectrin and anti-total MBP, respectively. The αII-spectrin blot revealed a dose-dependent reduction of intact protein and the formation of the characteristic BDP of 150 and 145 kDa (SBDP150 and SBDP145; Pike *et al*. 1998; Wang 2000) (Fig. 7a, left-hand panel). The MBP-blot also showed a calpain-concentration-dependent reduction of intact 21.5- and 18.5-kDa MBP. Importantly, calpain treatment also produced an 8-kDa BDP identical to the 8-kDa MBP fragment produced following TBI (Fig. 7b, left-hand panel). Digestion with calpain-1 showed identical results (data not shown). To ascertain that the calpain-produced MBP-fragment contains the novel N-terminal (KNI-VITPRTPP) observed *in vivo*, we applied the fragment-specific antibody to these samples and indeed confirmed that it cross reacts with the calpain-produced MBP-fragment (Fig. 7c, left-hand panel). Interestingly, a lower calpain : brain lysate ratio actually produced more 8-kDa BDP, suggesting that 8-kDa BDP might be further degraded by calpain.

As caspase-3 is activated in apoptosis after neuronal injury, including apoptotic oligodendrocytes (McDonald *et al*. 1998), we tested the sensitivity of MBP to caspase-3 digestion. Figure 7 (right-hand panels) shows that although αII-spectrin was degraded to the characteristic αII-spectrin breakdown products (SBDPs) SBDP150i and SBDP120 (Pike *et al*. 1998; Wang 2000), MBP was resistant to caspase-3 in the same samples, using total MBP- and MBP-fragment-specific antibodies (Figs 7b and c, right-hand panels). As MBP has also been alternately suggested to be degraded by MMPs and cathepsins in other demyelinating diseases (Marks *et al*. 1980; Berlet and Ilzenhofer 1985; Williams *et al*. 1986; Wang *et al*. 2000), we further analyzed the sensitivity of MBP (21.5 and 18.5 kDa) to various

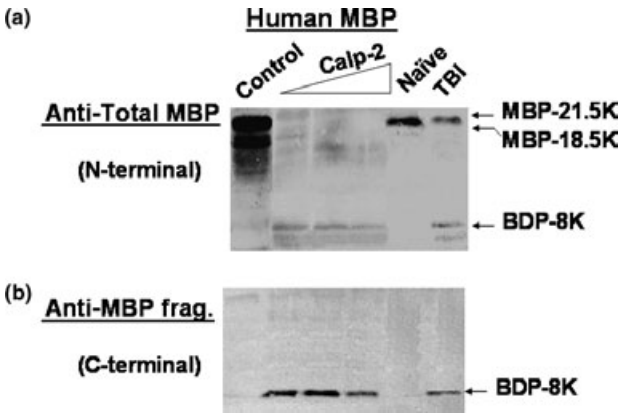

Fig. 8 *In vitro* proteolysis of purified human myelin basic protein (MBP) with calpain. Purified human MBP (18.5 kDa) was digested with calpain-2 *in vitro* under conditions similar to those described in Fig. 7. MBP (10 ng) was treated with either no protease (control) or with 0.25%, 0.5% and 1% calpain-2 for comparison with the fragmentation pattern observed *in vivo* at 48 h after TBI and with naive control (20 μg brain lysate each). The samples were then analyzed by immunoblots probed with either anti-total MBP (N-terminal) (a) or MBP-fragment-specific monoclonal antibody (b).

quantities of cathepsin B, cathepsin D, MMP-2 and MMP-9. Overall, we observed that these enzymes did not produce any TBI-associated characteristic C-terminal MBP- fragments (results not shown).

Lastly, we also subjected purified human MBP (18.5 kDa) to different levels of calpain digestion. Again, calpain digestion of purified MBP produced a characteristic N-terminal MBP-fragment of 8 kDa and a C-terminal BDP also about 8 kDa, as detected by the anti-total MBP (N-terminal) antibody and MBP-fragment-specific antibody, respectively (Figs 8a and b).

Discussion

Proteolysis of axonal proteins (such as neurofilament proteins, APP and αII-spectrin) following TBI has been extensively documented and studied as a signature event following TBI (Stone *et al*. 2002; Posmantur *et al*. 1994, 1997; Saatman *et al*. 1996; Newcomb *et al*. 1997; Pike *et al*. 1998; Wang *et al*. 1998; Buki *et al*. 1999, 2000; McCracken *et al*. 1999). Yet the integrity of myelin structural proteins has not been investigated. To our knowledge, this is the first report on the extensive degradation of MBP following TBI. Using a rat model of TBI and immunoblotting methods, we demonstrated that all four major isoforms of MBP (21.5, 18.5, 17 and 14 kDa) were all degraded within hours after TBI and the level of intact proteins did not return to basal levels for up to 3–5 days after injury (Figs 2–4). Using proteomic-based N-terminal sequencing and tryptic digestion/mass spectrometry analysis, we have further identified a novel *in vivo* cleavage site on MBP after TBI (Fig. 1). Based on the novel cleavage site, we also created a MBP-fragment-specific antibody that showed specific staining in the immunoblotting and immunohistochemical studies (Fig. 6).

The identified *in vivo* cleavage site was between F114 and K115 in the following region QDENPVVHFF* KNIVTPRTPP (based on the 21.5-kDa from of MBP). F114–K115 and the general cleavage region were present in all isoforms of human and rat MBP (Akiyama *et al*. 2002). We consistently detected at least two N-terminal fragments of MBP (of 10 and 8 kDa) (Figs 2, 3 and 4) and at least two C-terminal fragments (of 8 and 6 kDa) that contain the same new N-terminal (KNIVTP) (Fig. 5). These data suggest either that the two C-terminal fragments represent similar fragments from two different MBP isoforms or that the smaller fragment (6 kDa) might have been derived from further C-terminal truncation of the larger 8-kDa fragment.

It is of interest to note that although MBP proteolysis was extensive and sustained for several days in the ipsilateral cortex of TBI animals (Figs 2 and 3), the sham-operated animals also expressed transient but significant increases of MBP proteolysis in the cortex (Fig. 3d). The craniotomy procedure itself is not non-invasive and usually causes some degree of brain injury at the site of operation. In this model of TBI, the site of impact is the cortex. Damage to deeper brain structures such as the hippocampus is in fact caused by a compression-induced contusion force. Thus, one would expect that MBP proteolysis might occur in a more delayed manner. Our data in fact showed that this was the case, as MBP-BDP levels in the cortex appeared to peak at 24 h after TBI, whereas their hippocampal counterparts did not peak until 48 h after TBI (Figs 3 and 4). Our previous work on axonal cytoskeletal protein αII-spectrin breakdown also reflects the same trend (Ringger *et al*. 2004). In addition, caution is needed in terms of comparing what may be severely damaged cortex with more morphologically preserved tissue in hippocampus. It is interesting to observe that MBP profiles seem to 'recover' in cortical and hippocampal homogenates by day 5 after TBI. We speculate that it is partially a result of sampling conditions because by that time point, necrotic tissue is likely to have been removed by microglia and infiltrating macrophages, etc., thus leaving behind the more intact tissue for sampling. As expected, no significant MBP proteolysis was detected in the hippocampus of sham-operated animals as it is more distal to the operation site.

The loss of integrity of the myelin sheath and the degradation of myelin proteins have been extensively studied in demyelinating diseases such as MS and EAE, an animal model of MS (Waxman 1998). Moreover, oligodendrocytes are sensitive to excitotoxicity (McDonald *et al*. 1998; Karadottir *et al*. 2005; Micu *et al*. 2006; Salter and Fern 2005) and can undergo apoptosis following experimental TBI (Hutchison *et al*. 2001), spinal cord injury (Crowe *et al*. 1997) and in EAE (Hisahara *et al*. 2003). These events have also been documented in animal models of stroke (Irving *et al*. 2001), spinal cord injury and Wallerian degeneration in the spinal cord (Bartholdi and Schwab 1998; Buss and Schwab 2003). It was therefore surprising to find very few studies that address myelin protein integrity in TBI. The few studies performed with TBI have reported prolonged and sustained loss of white matter (Gale *et al*. 1995; Bramlett and Dietrich 2002) and increased demyelination (Gale *et al*. 1995; Ng *et al*. 1994). None of these studies directly examined the integrity of MBP.

In an *in vivo* model of oxidative stress, oligodendrocyte-like cells within the subcortical white matter were immunopositive for calpain-mediated spectrin BDPs (McCracken *et al*. 1999). Other studies suggest that calpain is present in myelin and is potentially involved in myelin protein turnover (Banik *et al*. 1985; Yanagisawa *et al*. 1988). MBP has been shown to be an *in vitro* substrate of brain damage (Yamashima *et al*. 1998). Consistent with these findings, our results showed that *in vitro* calpain digestion of MBP indeed directly yield the *in vivo* MBP cleavage products, as observed in TBI (Fig. 7). Interestingly, the *in vivo* MBP cleavage site between Phe114 and Lys115 is rather unobvious: this site will put the Phe-Phe, in the P2′-P1′ residue (N-terminal to the cleavage site) whereas calpain generally prefers either Leu-X or Val-X in these positions (Wang and Yuen 1997). In fact, previous work has showed that both human and bovine MBPs are excellent *in vitro* calpain substrates, producing cleavage at Val-Thr and Leu-Gly (Tsubata and Takahashi 1989; Banik *et al*. 1994). Caspase-3 is also a possible MBP-protease because it is activated in apoptosis (Pike *et al*. 1998; Wang 2000). To address this issue, we also compared *in vitro* MBP proteolysis patterns with capase-3 with the *in vivo* MBP cleavage pattern (Fig. 7). We concluded that caspase-3 was not involved in cleaving MBP.

MMPs and lysosomal proteases have been alternately suggested to be candidate MBP protease(s) (Marks *et al*. 1980; Williams *et al*. 1986; Wang *et al*. 2000). Wang *et al*. (2002) also reported the secretion of MMP-2 and MMP-9 after mechanical brain injury in rat cortical cultures. In addition, knock-out mice deficient in MMP-9 gene expression exhibited and decreased infarct volume and decreased MBP loss in both rat TBI and middle cerebral artery occlusion (MCAO) models (Wang *et al*. 2000; Asahi *et al*. 2001). Interestingly, MBP is sensitive to *in vitro* proteolysis by both cathepsin B and D (Marks *et al*. 1980; Berlet and Ilzenhofer 1985; Williams *et al*. 1986). Seyfried *et al*. (1997) showed increased cathepsin B enzyme activity in ischemic brain.

We thus tested the vulnerability of MBP to cathepsin B/D, and MMP-2/9. We found that none of them produced the characteristic MBP-fragments that are observed *in vivo* following TBI (results not shown). Consistent with these findings, the cathepsin D-mediated cleavage site of MBP at Phe113–Phe114 residues reported previously (Brostoff *et al*. 1974; Benuck *et al*. 1975) is one residue off from the Phe114 and Lys115 that we observed.

In summary, we report here extensive and sustained proteolysis of an important myelin structural protein, MBP, after TBI in a well-established animal model. We further identified the major cleavage site of MBP *in vivo*, which enabled us to produce novel MBP-fragment-specific antibodies. With this powerful MBP-fragment antibody and the αII-spectrin BDP and APP-fragment-specific antibodies (Buki *et al*. 1999, 2000; Stone *et al*. 2002), one can now begin to simultaneously detect the proteolytic changes in both axons and myelin. In addition, we also unequivocally demonstrated that calpain was one of the major proteases involved in MBP degradation in TBI. We speculate that TBI-mediated axonal damage leads to either structural damage to the adjacent myelin membrane or to secondary glutamate release that triggers the NMDA-receptor mediated excitotoxic response in oligodendrocytes (McDonald *et al*. 1998; Karadottir *et al*. 2005; Micu *et al*. 2006; Salter and Fern 2005), resulting in calpain-mediated MBP degradation. It is worth noting that it is plausible that calpain might have leaked from damaged axons and become externalized, gaining access to the MBP in the myelin sheath. In any case, the resultant MBP breakdown might lead to the instability of the myelin sheath and the initiation of demyelination, which might further increase the vulnerability of exposed axons (Stys 1998). It is therefore important to further examine whether MBP proteolysis is also observed in human TBI and if so, which therapeutic strategy can be applied to limit such myelin proteolysis. In addition, we are also in the process of examining whether the same MBP-breakdown products are present in either tissue or CSF samples from patients with MS.

Acknowledgements and disclaimers

The authors would like to acknowledge the support of Department of Defense grants DAMD17-03-1-0066 and DAMD17-01-1-0765; NIH grants R01 NS049175-01 A1. This paper has been reviewed by the Walter Reed Army Institute of Research. There is no objection to its presentation and/or publication. The opinions or assertions contained herein are the private views of the author, and are not to be construed as official, or as reflecting true views of the Department of the Army or the Department of Defense. Research was conducted in compliance with the Animal Welfare Act and other federal statutes and regulations relating to animals and experiments involving animals and adheres to principles stated in the *Guide for the Care and Use of Laboratory Animals*, NRC Publication, 1996 edition. KKW and RLH hold equity in Banyan Biomarkers Inc., a company commercializing technology of detecting brain-injury biomarkers. We would also like to acknowledge the editorial assistance of Colleen Meegan.

References

Akiyama K., Ichinose S., Omori A., Sakurai Y. and Asou H. (2002) Study of expression of myelin basic proteins (MBPs) in developing rat brain using a novel antibody reacting with four major isoforms of MBP. *J. Neurosci. Res.* **68**, 19–28.

Asahi M., Wang X., Mori T., Sumii T., Jung J. C., Moskowitz M. A., Fini M. E. and Lo E. H. (2001) Effects of matrix metalloproteinase-9 gene knock-out on the proteolysis of blood–brain barrier and white matter components after cerebral ischemia. *J. Neurosci.* **21**, 7724–7732.

Bahr B. A., Tiriveedhi S., Park G. Y. and Lynch G. (1995) Induction of calpain-mediated spectrin fragments by pathogenic treatments in long-term hippocampal slices. *J. Pharmacol. Exp. Ther.* **273**, 902–908.

Banik N. L., McAlhaney W. W. and Hogan E. L. (1985) Calcium-stimulated proteolysis in myelin: evidence for a Ca2+-activated neutral proteinase associated with purified myelin of rat CNS. *J. Neurochem.* **45**, 581–588.

Banik N. L., Chou C. H., Deibler G. E., Krutzch H. C. and Hogan E. L. (1994) Peptide bond specificity of calpain: proteolysis of human myelin basic protein. *J. Neurosci. Res.* **37**, 489–496.

Bartholdi D. and Schwab M. E. (1998) Oligodendroglial reaction following spinal cord injury in rat: transient upregulation of MBP mRNA. *Glia* **23**, 278–284.

Benuck M., Marks N. and Hashim G. A. (1975) Metabolic instability of myelin proteins. Breakdown of basic protein induced by brain cathepsin D. *Eur. J. Biochem.* **52**, 615–621.

Berlet H. H. and Ilzenhofer H. (1985) Elucidation of cathepsin B-like activity associated with extracts of human myelin basic protein. *FEBS Lett.* **7**, 299–302.

Bramlett H. M. and Dietrich W. D. (2002) Quantitative structural changes in white and gray matter 1 year following traumatic brain injury in rats. *Acta Neuropathol. (Berl.)* **103**, 607–614.

Brostoff S. W., Reuter W., Hichens M. and Eylar E. H. (1974) Specific cleavage of the A1 protein from myelin with cathepsin D. *J. Biol. Chem.* **249**, 559–567.

Buki A., Siman R., Trojanowski J. Q. and Povlishock J. T. (1999) The role of calpain-mediated spectrin proteolysis in traumatically induced axonal injury. *J. Neuropathol. Exp. Neurol.* **58**, 365–375.

Buki A., Okonkwo D. O., Wang K. K. and Povlishock J. T. (2000) Cytochrome c release and caspase activation in traumatic axonal injury. *J. Neurosci.* **20**, 2825–2834.

Buss A. and Schwab M. E. (2003) Sequential loss of myelin proteins during Wallerian degeneration in the rat spinal cord. *Glia* **42**, 424–432.

Choi S. C. and Bullock R. (2001) Design and statistical issues in multicenter trials of severe head injury. *Neurol. Res.* **23**, 190–192.

Crowe M. J., Bresnahan J. C., Shuman S. L., Masters J. N. and Beattie M. S. (1997) Apoptosis and delayed degeneration after spinal cord injury in rats and monkeys. *Nat. Med.* **3**, 73–76.

Dutta S., Chiu Y. C., Probert A. W. and Wang K. K. (2002) Selective release of calpain produced alphaII-spectrin (alpha-fodrin) breakdown products by acute neuronal cell death. *Biol. Chem.* **383**, 785–791.

Gale S. D., Johnson S. C., Bigler E. D. and Blatter D. D. (1995) Nonspecific white matter degeneration following traumatic brain injury. *J. Int. Neuropsychol. Soc.* **1**, 17–28.

Hisahara S., Okano H. and Miura M. (2003) Caspase-mediated oligodendrocyte cell death in the pathogenesis of autoimmune demyelination. *Neurosci. Res.* **46**, 387–397.

Hutchison J. S., Derrane R. E., Johnston D. L. *et al.* (2001) Neuronal apoptosis inhibitory protein expression after traumatic brain injury in the mouse. *J. Neurotrauma* **18**, 1333–1347.

Irving E. A., Bentley D. L. and Parsons A. A. (2001) Assessment of white matter injury following prolonged focal cerebral ischaemia in the rat. *Acta Neuropathol. (Berl.)* **102**, 627–635.

Karadottir R., Cavelier P., Bergersen L. H. and Attwell D. (2005) NMDA receptors are expressed in oligodendrocytes and activated in ischaemia. *Nature* **22**, 1162–1166.

Marks N., Benuck M. and Hashim G. (1980) Specificity of brain cathepsin D: cleavage of model peptides containing the susceptible Phe-Phe regions of myelin basic protein. *J. Neurosci. Res.* **5**, 217–223.

McCracken E., Hunter A. J., Patel S., Graham D. I. and Dewar D. (1999) Calpain activation and cytoskeletal protein breakdown in the corpus callosum of head-injured patients. *J. Neurotrauma* **16**, 749–761.

McDonald J. W., Althomsons S. P., Hyrc K. L., Choi D. W. and Goldberg M. P. (1998) Oligodendrocytes from forebrain are highly vulnerable to AMPA/kainate receptor-mediated excitotoxicity. *Nat. Med.* **4**, 291–297.

Medana I. M. and Esiri M. M. (2003) Axonal damage: a key predictor of outcome in human CNS diseases. *Brain* **126**, 515–530.

Micu I., Jiang Q., Coderre E. *et al.* (2006) NMDA receptors mediate calcium accumulation in myelin during chemical ischaemia. *Nature* **439**, 988–992.

Nath R., Huggins M., McGinnis K., Nadimpalli D. and Wang K. K. W. (2000) Development and characterization of antibodies specific to caspase-3-produced alpha II-spectrin 120 kDa breakdown product: Marker for neuronal apoptosis. *Neurochem. Int.* **36**, 351–361.

Newcomb J. K., Kampfl A., Posmantur R. M., Zhao X., Pike B. R., Liu S. J., Clifton G. L. and Hayes R. L. (1997) Immunohistochemical study of calpain-mediated breakdown products to alpha-spectrin following controlled cortical impact injury in the rat. *J. Neurotrauma* **14**, 369–383.

Ng H. K., Mahaliyana R. D. and Poon W. S. (1994) The pathological spectrum of diffuse axonal injury in blunt head trauma: assessment with axon and myelin strains. *Clin. Neurol. Neurosurg.* **96**, 24–31.

Pettus E. H., Christman C. W., Giebel M. L. and Povlishock J. T. (1994) Traumatically induced altered membrane permeability: its relationship to traumatically induced reactive axonal change. *J. Neurotrauma* **11**, 507–522.

Pike B. R., Zhao X., Newcomb J. K., Posmantur R. M., Wang K. K. W. and Hayes R. L. (1998) Regional calpain and caspase-3 proteolysis of alpha-spectrin after traumatic brain injury. *Neuroreport* **9**, 2437–2442.

Posmantur R., Hayes R. L., Dixon C. E. and Taft W. C. (1994) Neurofilament 68 and neurofilament 200 protein levels decrease after traumatic brain injury. *J. Neurotrauma* **11**, 533–545.

Posmantur R., Kampfl A., Siman R., Liu J., Zhao X., Clifton G. L. and Hayes R. L. (1997) A calpain inhibitor attenuates cortical cytoskeletal protein loss after experimental traumatic brain injury in the rat. *Neuroscience* **77**, 875–888.

Richter-Landsberg C. (2000) The oligodendroglia cytoskeleton in health and disease. *J. Neurosci. Res.* **59**, 11–18.

Ringger N. C., Tolentino P. J., McKinsey D. M., Pike B. R., Wang K. K. W. and Hayes R. L. (2004) Effects of injury severity on regional and temporal mRNA expression levels of calpains and caspases after TBI. *J. Neurotrauma* **21**, 829–841.

Roberts-Lewis J. M., Savage M. J., Marcy V. R., Pinsker L. R. and Siman R. (1994) Immunolocalization of calpain I-mediated spectrin degradation to vulnerable neurons in the ischemic gerbil brain. *J. Neurosci.* **14**, 3934–3944.

Saatman K. E., Bozyczko-Coyne D., Marcy V., Siman R. and McIntosh T. K. (1996) Prolonged calpain-mediated spectrin breakdown occurs regionally following experimental brain injury in the rat. *J. Neuropathol. Exp. Neurol.* **55**, 850–860.

Saido T. C., Suzuki H., Yamazaki H., Tanoue K. and Suzuki K. (1993) In situ capture of mu-calpain activation in platelets. *J. Biol. Chem.* **268**, 7422–7426.

Salter M. G. and Fern R. (2005) NMDA receptors are expressed in developing oligodendrocyte processes and mediate injury. *Nature* **22**, 1167–1171.

Schaecher K. E., Shields D. C. and Banik N. L. (2001) Mechanism of myelin breakdown in experimental demyelination: a putative role for calpain. *Neurochem. Res.* **26**, 731–737.

Seyfried D., Han Y., Zheng Z., Day N., Moin K., Rempel S., Sloane B. and Chopp M. (1997) Cathepsin B and middle cerebral artery occlusion in the rat. *J. Neurosurg.* **87**, 716–723.

Shields D. C., Schaecher K. E., Saido T. C. and Banik N. L. (1999) A putative mechanism of demyelination in multiple sclerosis by a proteolytic enzyme, calpain. *Proc. Natl Acad. Sci. USA* **96**, 11486–11491.

Sloane J. A., Hinman J. D., Lubonia M., Hollander W. and Abraham C. R. (2003) Age-dependent myelin degeneration and proteolysis of oligodendrocyte proteins is associated with the activation of calpain-1 in the rhesus monkey. *J. Neurochem.* **84**, 157–168.

Stone J. R., Okonkwo D. O., Singleton R. H., Mutlu L. K., Helm G. A. and Povlishock J. T. (2002) Caspase-3-mediated cleavage of amyloid precursor protein and formation of amyloid beta peptide in traumatic axonal injury. *J. Neurotrauma* **19**, 601–614.

Stys P. K. (1998) Anoxic and ischemic injury of myelinated axons in CNS white matter: from mechanistic concepts to therapeutics. *J. Cereb. Blood Flow Metab.* **18**, 2–25.

Tsubata T. and Takahashi K. (1989) Limited proteolysis of bovine myelin basic protein by calcium-dependent proteinase from bovine spinal cord. *J. Biochem. (Tokyo).* **105**, 23–28.

Wang K. K. W. (2000) Calpain and caspase: can you tell the difference? *Trends Neurosci.* **23**, 20–26.

Wang K. K. W. and Yuen P.-W. (1997) Development and Therapeutic Potential of Calpain Inhibitors. *Adv. Pharmacol.* **37**, 117–152.

Wang K. K., Posmantur R., Nath R., McGinnis K., Whitton M., Talanian R. V., Glantz S. B. and Morrow J. S. (1998) Simultaneous degradation of alphaII- and beta II-spectrin by caspase 3 (CPP32) in apoptotic cells. *J. Biol. Chem.* **273**, 22490–22497.

Wang X., Jung J., Asahi M., Chwang W., Russo L., Moskowitz M. A., Dixon C. E., Fini M. E. and Lo E. H. (2000) Effects of matrix metalloproteinase-9 gene knock-out on morphological and motor outcomes after traumatic brain injury. *J. Neurosci.* **20**, 7037–7042.

Wang X., Mori T., Jung J. C., Fini M. E. and Lo E. H. (2002) Secretion of matrix metalloproteinase-2 and – 9 after mechanical trauma injury in rat cortical cultures and involvement of MAP kinase. *J. Neurotrauma* **19**, 615–625.

Waxman S. G. (1998) Demyelinating diseases – new pathological insights, new therapeutic targets. *New Engl. J. Med.* **338**, 323–325.

Williams K. R., Williams N. D., Konigsberg W. and YuR. K. (1986) Acidic lipids enhance cathepsin D cleavage of the myelin basic protein. *J. Neurosci. Res.* **15**, 137–145.

Yamashima T., Kohda Y., Tsuchiya K., Ueno T., Yamashita J., Yoshioka T. and Kominami E. (1998) Inhibition of ischaemic hippocampal neuronal death in primates with cathepsin B inhibitor CA-074: a novel strategy for neuroprotection based on 'calpain-cathepsin hypothesis'. *Eur. J. Neurosci.* **10**, 1723–1733.

Yanagisawa K., Sato S., O'Shannessy D. J., Quarles R. H., Suzuki K. and Miyatake T. (1988) Myelin-associated calpain II. *J. Neurochem.* **51**, 803–807.

MCP Papers in Press. Published on June 26, 2006 as Manuscript M600157-MCP200

Novel Differential Neuroproteomics Analysis of Traumatic Brain Injury in Rats

Firas H. Kobeissy[1]†, Andrew K. Ottens[2]†, Zhiqun Zhang[1], Ming Cheng Liu[2], Nancy D. Denslow[3], Jitendra R. Dave[4], Frank C. Tortella[4], Ronald L. Hayes[1,2], Kevin K.W. Wang[1,2]╢

Center for Neuroproteomics and Biomarkers Research, Department of Psychiatry[1]
Center for Traumatic Brain Injury Studies, Department of Neuroscience[2]
Departments of Physiological Sciences and Biochemistry and Molecular Biology[3]
Department of Neuropharmacology and Molecular Biology, Division of Neurosciences, Walter Reed Army Institute of Research, Silver Spring, MD[4]
McKnight Brain Institute of the University of Florida, Gainesville, FL 32610, USA

Running Title: Neuroproteomic Analysis of Rat TBI

╢Corresponding author: All correspondence should be addressed to: Dr. Kevin K.W. Wang, Department of Psychiatry, University of Florida, P.O. Box 100256, Gainesville, FL 32610-0256, Office Tel: (352) 392-3681 Fax: (352) 392-2579

Email: kwang@psychiatry.ufl.edu

†Equal contribution to this work

Key words: Traumatic brain injury, neurotrauma, proteomics, neuroproteomics, proteolysis, breakdown products, biomarkers.

Abbreviations:

TBI: traumatic brain injury

CAX-PAGE: cationic/anionic-exchange chromatography – polyacrylamide gel electrophoresis

RPLC-MSMS: reversed-phase liquid chromatography – tandem mass spectrometry

DIGE: difference gel electrophoresis

C-RP: C-reactive protein

GAPDH: glyceraldehyde-3-phosphate dehydrogenase

CRMP-2: collapsin response mediator protein-2

MAP: microtubule associated protein

BBB: blood brain barrier

BDP: breakdown product

SBDP: spectrin breakdown product

Summary

Approximately 2 million traumatic brain injury (TBI) incidents occur annually in the United States, yet there are no specific therapeutic treatments. The absence of brain injury diagnostic endpoints was identified as a significant roadblock to TBI therapeutic development. To this end, our laboratory has studied mechanisms of cellular injury for biomarker discovery and possible therapeutic strategies. In this study, pooled naïve and injured cortical samples (48 hours post-injury; rat controlled cortical impact model) were processed and analyzed using a differential neuroproteomics platform. Protein separation was performed using combined cationic/anionic-exchange chromatography – polyacrylamide gel electrophoresis (CAX-PAGE). Differential proteins were then trypsinized and analyzed with reversed-phase liquid chromatography tandem mass spectrometry (RPLC-MSMS) for protein identification and quantitative confirmation. The results included 59 differential protein components of which 21 decreased and 38 increased in abundance after TBI. Proteins with decreased abundance included collapsin response mediator protein-2 (CRMP-2), glyceraldehyde-3-phosphate dehydrogenase, microtubule associated proteins MAP-2A/2B, and hexokinase. Conversely, C-reactive protein, transferrin and breakdown products of CRMP-2, synaptotagmin and αII-spectrin were found elevated after TBI. Differential changes in the above-mentioned proteins were confirmed by quantitative immunoblotting. Results from this work provide insight into mechanisms of traumatic brain injury, and yield putative biochemical markers to potentially facilitate patient management by monitoring the severity, progression and treatment of injury.

Introduction

Traumatic brain injury (TBI), defined as brain damage due to mechanical force applied to the head, has an annual economic cost of $65 billion in the United States (1). There are over 2 million TBI incidents, with approximately 500,000 hospitalizations and 100,000 deaths annually (2-5) TBI is particularly prevalent among the young, considered the leading cause of death and disability among children and young adults. Despite these facts, there are no specific therapeutic treatments for TBI.

TBI is difficult to assess by current clinical techniques such as magnetic resonance imaging and computer tomography. Surrogate markers such as brain temperature, oxygen level and pressure lack sensitivity, specificity and availability (5-7). There is thus a need for a sensitive and specific biochemical marker(s) of TBI, with the diagnostic ability to evaluate post-concussion intracranial pathology to improve patient management and facilitate therapeutic evaluation (6). In particular altered neurodegenerative or protective proteins could be of great value if they could provide insight into injury severity and outcome (8). A small number of TBI protein markers have been reported including lactate dehydrogenase, glial fibrillary acid protein, enolase, and S-100B; however, all either lack the necessary sensitivity, TBI specificity, or both to be exclusively effective (5, 7, 9, 10). Further, the biochemical mechanism that produces post-TBI changes in these proteins are not understood, leaving them as potential surrogate markers rather than true biochemical markers of known injury pathways. To this end, breakdown products of proteolyzed proteins are of particular interest in neurotrauma as they provide a direct assessment of a known neurodegenerative mechanisms with the potential for therapeutic intervention.

Following TBI there is a shift in the balance between pro- and anti-apoptotic protein machinery promoting either cell survival or death (11-13). Studies reported from our and other laboratories provided substantial evidence for the involvement of over-activated cysteine proteases as major intracellular effectors of neuronal cell death via both necrotic and apoptotic pathways (5, 14). The primary mechanical injury produces a robust pattern of necrotic cell death in close proximity to the impact site, which is mediated by calpains – calcium activated cysteine proteases implicated in oncosis (14). Czogalla *et al.* in a recent review stressed with high emphasis on trauma related pathology this pivotal role of calpain in neurodegenerative disease (14). However, secondary insults often involve apoptotic cell death in regions caudal to the impact site. Apoptosis involves complex cascading pathways resulting in the activation of executioner proteases such as caspase-3 by intrinsic and extrinsic mechanisms involving caspases-8 and -9 (11, 15). Caspase-3 then acts on a number of cytosolic and cytoskeletal neuronal substrates, for example the cytoskeletal protein αII-spectrin, which upon proteolysis yield signature breakdown products (BDPs) that are indicative of neuronal cell death dynamics (4-6, 14, 16-18).

Recently, proteomics has been identified as a potential means for biomarker discovery, with the ability to identify proteome dynamics in response to experimental stimuli (3, 8, 19-23). Gel electrophoresis with or without cyanine dye labeling is often used for protein separation and differential selection prior to mass spectrometry (8, 16, 17, 24). Shortcomings of gel-based approaches can include limited resolution, mass range, and reproducibility (3, 25). For example, in a previous TBI study, we utilized 1D difference gel electrophoresis (DIGE) protein separation in series with reversed-phase liquid chromatography tandem mass spectrometry peptide analysis as a means to discover putative TBI biomarkers (3). However, the limited protein separation

confounded the results. Subsequently, we developed a novel multidimensional protein separation and differential analysis platform, comprising the steps depicted in Figure 1, to improve differential protein identification and overcome some of the limitation observed in 1D- and 2D-DIGE (25). Importantly, the platform involves correlating semi-quantitative peptide data with gel-densitometry data to reduce false-positives during differential analysis. Our hypothesis is that the CAX-PAGE/RPLC-MSMS platform will improve discovery of differential protein changes post-TBI and facilitate discovery of biochemical markers and possible therapeutic interventions.

Experimental Procedures

Brain Tissue Collection and Protein Extraction

All procedures involving animal handling and processing were done in compliance with guidelines set forth by the University of Florida Institutional Animal Care and Use Committee and the National Institutes of Health guidelines. A controlled cortical impact (CCI) device was used to model TBI in male Sprague-Dawley rats as described elsewhere (26). TBI injury was performed on seven animals, each mounted in a stereotactic frame and impacted in the right cortex (ipsilateral) with a 5-mm diameter aluminum impactor tip at a velocity of 3.5 m/sec to a depth of 1.6-mm. Simultaneously, seven naïve control animals were kept under the same environmental conditions, but did not receive an impact injury. At 48 hours post-injury, naïve and injured animals were sacrificed by decapitation. TBI and control cortex samples were rapidly dissected, washed with saline solution, snap-frozen in liquid nitrogen, and stored at -80°C for further processing. Naive and TBI cortex tissues were homogenized using a small mortar and pestle set over dry ice. The homogenized cortical tissue powder was then lysed for 90 minutes at 4ºC with a 0.1% SDS lysis buffer containing 150 mM sodium chloride, 1% ethoxylated

octylphenol, 1 mM sodium vanadate, 3 mM ethylenediaminetetraacetic acid, 2 mM ethylene glycol bis (2-aminoethyl ether)-tetraacetic acid, 1 mM dithiothreitol (all from Sigma-Aldrich, St. Louis, MO), with a Complete Mini protease inhibitor cocktail tablet containing EDTA along with a mixture of broad spectrum of serine, cysteine, metalloprotease and calpain inhibitors suited for animal tissues (Roche Biochemicals, Indianapolis, IN). Brain cortex lysates were then centrifuged at 16,000 g for 10 minutes at 4ºC. The supernatant was retained and collected at 4ºC to prevent proteolysis. The protein content was determined using DC Protein Assay (Bio-Rad Laboratories, Inc., Hercules, CA, USA), after which the protein concentration was standardized to 1 µg/µL for immunoblotting analysis.

Combined Cation/Anion-Exchange Chromatography – Polyacrylamide gel electrophoresis (CAX-PAGE)

The CAX chromatography was performed on a Bio-Rad Biologic DuoFlow system with sulfoproyl (S1) and quaternary ammonium (Q1) modified sepharose pre-packed ion-exchange columns (Bio-Rad) connected in tandem along with a QuadTec UV detector and BioFrac fraction collector. A detailed description of the CAX chromatography setup was described recently (25). For the purpose of this study, proteins from the sacrificed rats (n=7) were pooled to amass the required amount of protein and average inconsistent protein levels due to biological variability. Protein concentration of the seven TBI cortical samples was determined, and 0.143 mg of protein from each tissue sample was pooled to constitute 1 mg of protein which was loaded on the liquid chromatography system. A pooled naïve sample (1 mg protein, n=7) was similarly produced. A total of 32 1-mL fractions were collected during CAX chromatography, each concentrated using Millipore YM-10 ultrafiltration units (Millipore Corporation, Bedford, MA) according to the manufacturer instructions. Leammli sample buffer (25 µL) was then added

to the YM-10 collection filters and incubated for 10 minutes prior to collection by centrifugation at 1000 g for three minutes. Protein fractions were run side-by-side (*i.e.*, naïve fraction 1 next to TBI fraction 1, etc.) using 18-well, 10-20% gradient Tris-HCl Bio-Rad Criterion gels for differential comparison of TBI and naïve samples. ImageJ software was used for quantitative densitometric analysis of select gel band intensities. Differential bands were boxed and labeled according to their 2D-position (*e.g.*, the top band excised from the lane of fraction 6 was labeled 6A).

Western Blot Analysis and Antibodies

Four naïve and four TBI samples were processed with 2x Laemmli sample buffer (Bio-Rad with 5% beta mercaptoethanol). 20 µg of protein from each sample was subjected to gel electrophoresis on 10-20% or 6% tris-glycine gels, and then transferred onto PVDF membranes. Following the transfer, the membranes were blocked in 5% nonfat dry milk for an hour and then incubated overnight with the primary antibody at 4^{o}C. On the following day, the membranes were washed three times with 1x tris-buffered saline Tween-20, and probed with the secondary antibody for an hour. Immunoreactivity was detected by using a streptavidin alkaline phosphatase conjugate tertiary antibody. Monoclonal anti-mouse αII-spectrin (Affiniti Research Products, Ltd., UK) and anti-β actin (Sigma Chemical Co., St. Louis, MO), were used at a dilution of 1:4000 in 5% milk. Antibodies for profilin (BD Transduction Labs, San Jose, CA), hexokinase (Chemicon International, Temecula, CA), anti-MAP2A/2B (BD Pharmingen San Jose, CA), anti-synaptotagmin (Abcam Ltd, Cambridge, UK), anti-GAPDH (EnCor Biotechnology, Alachua, Gainesville), anti-cofilin (Cell Signaling Technology, Beverly, MA), anti-C-reactive protein (R&D Systems, Minneapolis, Minn), anti-chicken polyclonal transferrin (Abcam ltd, Cambridge, UK), and anti-CRMP-2 (IBL, Japan) were used at a dilution of 1:1000

in 5% milk. Secondary biotinylated antibody (Amersham Biosciences, United Kingdom) and streptavidin alkaline phosphatase conjugated tertiary antibody (Amersham Biosciences, United Kingdom) were used at a dilution of 1:3000 in 5% milk.

Gel Band Visualization and Quantification

ImageJ densitometry software (version 1.6, NIH, Bethesda, MD) was used for gel band quantitative densitometric analysis. Selected bands were quantified based on their relative intensities. Fold increase or decrease between naïve and TBI samples was calculated by dividing the greater value by the lesser value with a negative sign to indicate a decrease after TBI.

Statistical Analysis of Western Blotting Data

Densitometric quantification of the immunoblot bands was performed using an Epson Expression 8836XL high-resolution flatbed scanner (Long Beach, CA) and ImageJ densitometry software (version 1.6, NIH, Bethesda, MD). Densitometry values of four replicates of naïve and TBI samples were evaluated for statistical significance with SigmaStat software (version 2.03, Systat Software Inc., Ca, USA) and a student's t-test. A p-value of < 0.05 was considered to be significant for data acquired in arbitrary density units.

In Gel Digestion and Reversed-Phase Liquid Chromatography Tandem Mass Spectrometry

A detailed description of the reversed-phase liquid chromatography tandem mass spectrometry (RPLC-MSMS) platform was described elsewhere (25). In brief, differential bands were excised, cut into pieces and washed with HPLC water (Burdick & Jackson, Muskegon, MI) followed by 50:50 100 mM ammonium bicarbonate - acetonitrile (Burdick-Jackson, HPLC grade). Bands were dehydrated with 100% acetonitrile, then re-hydrated with 10 mM dithiothreitol (DTT) for 30 minutes at 56 °C, then alkylated with 55 mM iodoacetamide in 50 mM ammonium bicarbonate for 30 minutes in the dark at room temperature, followed by

acetonitrile dehydration. For protein digestion, 15 µL of a 12.5 ng/µL trypsin solution was added and incubated for 30 minutes at 4°C. An additional 20 µL of 50 mM ammonium bicarbonate was then added and that mixture was incubated overnight at 37°C. The resulting peptide solution was separated, with hydrophobic peptide extraction performed with 50:50 water-acetonitrile. The peptide solution was dried by speed vacuum and the residue was suspended in mobile phase solution for RPLC-MSMS analysis. Capillary reversed-phase liquid chromatography tandem mass spectrometry protein identification was performed by loading 2 µL of sample digest via autosampler onto a 100-µm x 5-cm c-18 reversed-phase capillary column at 1.5 µL/min. Peptides were eluted via a linear gradient: 5% to 60% methanol in 0.4% acetic acid over 30 minutes at 500 nL/min. Tandem mass spectra were collected using a data-dependent method (3 most intense peaks) on a Thermo Electron LCQ Deca XP Plus ion trap mass spectrometer (San Jose, CA). Protein database searching of tandem mass spectra was performed against an NCBI rat indexed RefSeq protein database using Bioworks Browser (version 3.1, Thermo Electron). Subtractive filtering and sorting was performed with DTAselect software (Version 1.9, Scripps CA) on singly, doubly, and triply charged tryptic peptides with a cross-correlation *(Xcorr)* value greater than 1.8, 2.5, and 3.5, respectively. Naïve and TBI data were then compared with the Contrast module of the DTAselect software (27).

Semi-quantitative Differential Correlation of Protein and Peptide Data

The number of identified peptides per protein is tabulated from the filtered Bioworks data for naïve and TBI gel band pairs. Naïve and TBI peptide numbers were compared – those identified proteins with a two or more difference in the number of peptides were retained. The greater peptide number must then correlate with the sample (naïve or TBI) demonstrating the

greater gel band density to be considered a putative differential protein (Tables 1 and 2). We previously reported a correlation rate of 89% utilizing these parameters (25).

Results

[INSERT FIGURE 1]

CAX-PAGE Neuroproteomic Experimental Design

This study utilized a novel neuroproteomics approach as outlined in the systemic seven-step process illustrated in **Figure 1** comprising the multidimensional neuroproteomics platform. Our experimental design called for two pooled rat samples: injured ipsilateral cortical lysate from 48-hours post-TBI animals, and control naïve ipsilateral cortical lysate from uninjured animals. The protein components from each sample were differentially resolved by a two-dimensional protein separation technique termed cationic/anionic-exchange chromatography – polyacrylamide gel electrophoresis, CAX-PAGE. Naïve and TBI lysates were sequentially separated by CAX chromatography based on protein charge; the two chromatograms are shown overlayed in **Figure 2.** The initial impression after the first-dimension separation is that there is a marked difference between the two proteomes, reminiscent of the difference between cortex and cerebellum tissues observed in our first report on CAX separation (25). In this first study, the coefficient of variation (CV) value for repeated CAX separation was determined to be 11%, with no discernable variation in the chromatographic trace. Thus the disparate chromatograms in Figure 2 are attributed to the alteration of the cortical proteome associated with the TBI insult.

[INSERT FIGURE 2]

Thirty-two fractions collected from each CAX experiment were paired (i.e., fraction one of control with fraction one of TBI) and loaded side-by-side onto 1D-PAGE for the second

dimension protein separation. The gels were visualized with Coomassie blue stain for differential band analysis. Thirty-one bands with an observed difference in densitometry were selected and excised for proteomic analysis as boxed and labeled in **Figure 3**. The densitometric values for the targeted differential bands are reported in **Tables 1 & 2**. Relative fold-change was calculated for gel band pairs based on the relative intensities between naïve and TBI. Thirteen gel-bands showed a two-fold decrease compared with 16 having a two-fold increase (**Figure 4**). Fold-changes correlated with peptide data obtained for identified proteins indicated in **Tables 1 & 2**.

[INSERT FIGURE 3]

[INSERT FIGURE 4]

Identification of Differential Proteins by RPLC-MSMS

Following CAX-PAGE separation, the differential bands were processed for peptide separation and analysis by reversed-phase liquid chromatography online with tandem mass spectrometry (RPLC-MSMS). Tandem mass spectra were searched using Bioworks Browser against a rat-indexed protein database revealing between zero and four proteins per gel band, each having two or more peptides. For those bands with multiple identified proteins we utilized the number of matched peptides per protein as a semi-quantitative measure of protein abundance to confirm which protein represents the observed differential gel pattern as illustrated by Peng et al.(28). Using the peptide data we were able in most cases to isolate a single protein that matched the gel data. In a few cases, two or more proteins produced differential peptide numbers as reported in **Tables 1 & 2**. In all, 59 proteins were confirmed by this process to have a different abundance between naïve and TBI samples. The identified proteins were grouped as having decreased (21 proteins) or increased (38 proteins) abundance post-TBI. The proteins that decreased post-TBI included: the cytosolic glycolytic proteins glycerdehyde-3-phosphate

dehydrogenase, enolase, aldehyde dehydrogenase, glutamate dehydrogenase and hexokinase; the cytoskeletal associated proteins profilin and cofilin; and the neuronal specific proteins CRMP-2 and neuronal protein-22 (**Table 1**) (29, 30). Among the TBI increased proteins are: the glycolytic proteins lactate dehydrogenase, brain creatine kinase, and malate dehydrogenase; the ubiquitin associated proteins UCHL1 and proteasome subunit alpha type 7; the cytosolic cell signaling proteins 14-3-3 family members; and the serum derived proteins transferrin, C-RP, ferroxidase, albumin, fetuin, hemoglobin, and serine protease inhibitors (**Table 2**). The functional relevance of the identified proteins is discussed later.

[INSERT TABLE 1]

[INSERT TABLE 2]

Validation of Proteins with Decreased Abundance after TBI

Five of the proteins decreased in abundance after TBI were subjected to biochemical validation by Western blotting – cofilin, profilin, GAPDH, hexokinase, MAP2A/2B and intact CRMP-2 protein (**Figure 5**). Protein selection was based on several factors including antibody availability, literature relevance, and levels of peptide abundance. Based on these criteria several other proteins remain to be validated. Validation by this means is presently the bottleneck in biomarker development where the discovery rate exceeds the rate of preliminary validation by several fold (31). Densitometric analysis showed a statistically significant decrease of cofilin, profilin, hexokinase, GAPDH, MAP2A/2B and intact CRMP-2 proteins ($p<0.05$; Student's t-test) in TBI samples relative to naïve. Beta-actin blotting was used as a control to confirm equal loading of protein for all samples as shown in **figure 6**.

[INSERT FIGURE 5]

Validation of Proteins with Increased Abundance after TBI

Similar to the decreased protein validation, a targeted approach was applied in selecting and validating a number of the proteins that increased after TBI including C-reactive protein and transferrin (31). Densitometric analysis showed a statistically significant increase of C-RP and transferrin proteins ($p<0.05$; Student's t-test) in TBI relative to naïve samples **(Figure 6)**. The biological significance of these 2 proteins is discussed later**.** Beta-actin blotting was used as a control to confirm equal loading of protein for all samples.

[INSERT FIGURE 6]

Validation of Potential Proteolytic Substrates after TBI

Within the group of increased abundance proteins, a specific set reflects proteolytic processing after TBI. These proteins are characterized by a mismatch in their observed (migration) molecular mass and that of their nominal intact molecular mass. Three proteins appeared to shift in molecular mass: αII-spectrin, synaptotagmin, and CRMP-2 (**Table 2**). All were characterized via Western blot, which showed the same molecular mass shift observed in the proteomics data (**Figure 7**). Confidence for our data came from the co-migration of the suspected αII-spectrin breakdown product (intact mass 280 kDa) along with the 120 kDa proteins ferroxidase and ceruloplasmin in gel band 20A that aligned with an observed molecular mass of 120 kDa. The immunoblotting data confirmed the increase in the 120 kDa SBDP (**Table 2 and Band 20A**). Similarly, CRMP-2 (intact mass 62 kDa) co-migrated with GDP dissociation inhibitor-1 (intact mass 51 kDa) and group-specific component protein (intact mass 53 kDa) in gel band 18B that aligned with an observed molecular mass of 54 kDa (**Table 1 and Band 18B**). The immunoblotting data confirmed the increase in a 54 kDa CRMP-2 BDP. Densitometric data indicated that the increase in αII-spectrin, synaptotagmin, and CRMP-2 breakdown products was statistically significant after TBI ($p<0.05$; Student's t-test) relative to naïve samples.

[INSERT FIGURE 7]

Discussion

The CAX-PAGE/RPLC-MSMS neuroproteomics platform, a multidimensional separation technique comprised of tandem column chromatography coupled to 1D-gel electrophoresis (**Figure 1**) was applied to identify proteome changes in rat cortex 48 hours post-TBI, providing more definitive results through better proteome separation and quantitative validation than from our earlier study. To do this, the altered TBI proteome is contrasted against a naïve cortical proteome. In total, 59 proteins showed an altered abundance post-TBI (**Tables 1 & 2**), which were divided into three groups: decreased, increased, or putatively degraded by proteolysis (**Figures 5-7**).

The proteins with decreased abundance post-TBI (**Table1**) were the result of changes in expression, cellular metabolism, and/or proteolytic degradation. Included in this group are the cytoskeletal associated proteins, cofilin (Band 6B), profilin (Band 8A), MAP2A/2B (Band 23A) and hexokinase (a cytoplasmic phosphotransferase, Band 10A), all of which were validated to decrease after TBI by immunoblotting (**Figure 5**). As well, the data revealed a decrease in GAPDH after TBI (Band 9E), denoting the loss of metabolic function. Importantly, GAPDH is widely regarded as an unchanging housekeeping protein used as a loading control in Western blots; however, this would be inappropriate in neurotrauma studies given the data in **Figure 5**. Post-TBI GAPDH dynamics should also be considered in light of its emerging role as a pro-apoptotic enzyme that induces nuclear translocation in a number of neurodegenerative diseases (30, 32). Among other interesting proteins is NP-22, a neuronal protein that mediates interactions

between cytoskeletal proteins (33). Unfortunately, NP-22 was one of the proteins that we could not confirm by immunoblotting due to the lack of an available antibody.

Proteins with increased abundance following TBI (**Table** 2) were either upregulated or accumulated in response to injury (**Figure 6**) (2). The rapid and long-term accumulation of proteins in reaction to axonal injury within different neuronal compartments has already been reported post-TBI and is evident in our study (2). Increased proteins included members of the acute phase protein (APP) family, which are indicative of an inflammatory response (34, 35). The observed APP proteins were C-reactive protein, transferrin, ceruloplasmin, which were all validated by immunoblotting to increase in individual animals. Additional proteins validated by immunoblotting to increase 48 hours after TBI included α1-inhibitors and kininogen proteins. The increased high-molecular mass proteins α1-inhibitors and ceruloplasmin, not observed with alternative 2D-DIGE separation, indicated blood-brain barrier leakage (36). Increased abundance of kininogen, like C-RP a member of the thiostatin family, is also indicative of inflammatory processes, shown previously to be of clinical importance following TBI and ischemic stroke (34, 37). The results correspond well with known post-TBI pathology, which involves inflammation coupled with a breakdown in the blood brain barrier (BBB), leading to the extravasations of plasma proteins (38). Other non-inflammatory proteins that increased after TBI include UCH-L1 (Band 13E), lactate dehydrogenase (Band 9E) (**Table 2**), and members of the 14-3-3 chaperon protein family (Band 20B), which were previously identified by our 1D-PAGE/RPLC-MSMS TBI study (3).

The third group contains protein fragments of decreased mass relative to the intact protein molecular mass, indicating a potential breakdown product. Members of this group were observed exclusively in TBI samples, including apparent breakdown products of αII-spectrin,

CRMP-2, and synaptotagmin. Immunoblots validated the presence of a putative breakdown product with the same mass as the proteomic data (**Figure 7**). The αII-spectrin (nominally 280 kDa, Band 20A) appeared as a 120 kDa SBDP (**Table 2**). αII-spectrin is known to be degraded to a 120 kDa fragment following caspase-3 proteolysis during apoptosis (5, 10). These data correlate with our previously findings of αII-spectrin breakdown products post-TBI (4, 26, 39).

The abundance of intact collapsin response mediator protein 2 (CRMP-2, 62 kDa) was shown to decrease (Bands 17A) while its breakdown product increased at a MW of 54 kDa (Band 18B**)** post-TBI (**Table 2**). Immunoblotting analysis validated the post-TBI proteolytic pattern of CRMP-2 (**Figure 7**). CRMP-2, a cytosolic neuronal protein involved in microtubule assembly, is required for neuronal process elongation and growth cone motility. The presence of a breakdown product after TBI suggests that CRMP-2 is proteolyzed after neurotrauma, differing from CRMP-2 dynamics in mesial temporal lobe epilepsy, indicated by Czech et al. to occur by alternative splicing or other post-translational modifications (40), or in Alzheimer's disease due to down regulation (41).

A third proteolyzed protein was synaptotagmin, an integral membrane protein present on the surface of synaptic vesicles, which is involved in the calcium-mediated release of neurotransmitters. The proteomic data identified synaptotagmin (nominally MW 65 kDa) (**Table 2**) at 37 kDa (Band 29A) suggesting proteolytic degradation as confirmed by immunoblotting data (**Figure 7**). The presence of a synaptotagmin BDP after TBI was independently identified recently in our laboratory using a high throughput immunoblotting analysis (42).

The overactivation of cysteine proteases is an important biochemical process occurring after TBI. Proteolysis leads to the degradation of structural associated proteins in association with necrotic and apoptotic cell death. The observed TBI breakdown products are members of a

TBI degradome, a term first introduced by McQibban et al. to collectively describe the substrate candidates of a protease (43). This was further refined by Lopez-Otal et al. to include the repertoire of protease substrates related to a specific condition such as TBI (44). The results of this study demonstrate that the CAX-PAGE/RPLC-MSMS proteomic platform can systematically detect potential breakdown products by distinguishing them from intact proteins by observation of a molecular mass shift as confirmed by subsequent immunoblotting validation. The greater mass range of CAX-PAGE and side-by-side fraction comparison allows for direct visualization of differential proteome changes providing complementary data to the PI shifts observed by 2D-DIGE (25).

Of interest is the specificity of the different proteins identified which contained a number of brain specific proteins including synaptotagmin, CRMP-2, NP22, MAP-2 and brain creatine kinase. However due to the complexity of the nervous system and the dynamic nature of the proteome expression in general and its dependence on various signals (insults, development, etc..), these proteins can reflect signal-dependent neuroanatomical specificity. One example is the NP-22 protein which shows normal expression in various brain regions. However, upon alcoholism signal, NP22 would show an increased expression in the frontal cortex but not in other brain region (33). Similarly, our current work identified a number of brain specific proteins however it wasn't feasible to validate that these proteins are actually cortex specific especially that relevant literature does not specify brain specific anatomical expression of such proteins but rather are considered to be ubiquitous in expression (NP22, Synaptotagmin and CRMP-2). Interestingly, in a previously published work from our group we compared different protein expression between rat cerebellar and cortex regions (25). In this study, the proteomic map reflected cortical specific proteins (MAP-2, and ά enolase), cerebellar specific proteins (14-3-3

protein family) while brain creatine kinase was comparable in both regions. One major aspect of this study is that it was done under basal condition with no brain injury signal. In our current study TBI reflected the dynamic nature of protein expression rendering the expression of the 14-3-3 and brain creatine kinase to be elevated in TBI shifting the basal cortical map proteomic pattern. Thus, among the current identified proteins, the brain specific ones can be considered cortex specific under TBI insult. Nevertheless, further studies are needed to evaluate the expression of these proteins in different neuroanatomical areas under the same condition.

The initial goal for differential TBI neuroproteomics analysis using the CAX-PAGE/RPLC-MSMS platform is to identify likely biomarker candidate proteins, which will subsequently be validated by immunological studies in biological fluids of animals and eventually humans. Inherent to biomarker development is that putative protein markers may be inadequately detected in biological fluids, and are thus suboptimal as clinical diagnostics (19, 45). Due to the time-consuming nature of devising and optimizing enzyme-linked immunoassay for each putative biomarker protein, it was of critical importance to reduce the number of false-positives identified by proteomics as differentially altered after TBI. To this end, we employed a secondary quantitative evaluation step, utilizing peptide data to correlate protein abundance with densitometry data. Reported (Tables 1 and 2) are those proteins having a two or more difference in the number of identifying peptides when contrasting the naïve and TBI gel-band data, with the greater number in the band with the larger optical density. Thereby, those identified proteins that reportedly do not demonstrate a measurable difference between naïve and TBI samples, likely not differential in nature, or those that do not correlate with the densitometry data are not reported. In our previous report of the differential platform, 89% of selected differential gel bands had correlating differential peptide data. The described quantitative correlation process

effectively reduced the number of false-positive differential proteins reported (and subsequently developed into assays), as evident from our immunological validation work where six of seven putative markers tested were confirmed as differential in multiple naïve and TBI samples. The importance of this process cannot be overstressed, as all multidimensional protein separation techniques lack the necessary resolving capability to only produce fractions, spots or bands that routinely contain only a single protein. The approach however may increase the number of false-negatives, as the acquired peptide data is semi-quantitative in nature. As well, it is anticipated that other differential proteins are not targeted for mass spectrometry analysis as they do not produce a differential band density of two-fold or greater, further confounded by the presence of multiple proteins in a single band; hence, the reported list is not exhaustive in nature. Rather our intention for this study is to identify those differential proteins that are dramatic in nature to be developed into biochemical markers of TBI, whereby an exhaustive differential study is not time-efficient. Beyond biomarker discovery, the identified differential protein changes reflect injury mechanisms that with further study may be relevant to therapeutic intervention, such as the systematic inhibition of proteolytic activity at discrete time-points post-TBI. For this purpose, other differential analysis techniques, such as ICAT or 2D-PAGE methods, can be used in combination with CAX-PAGE/RPLC-MSMS to provide greater coverage of the altered TBI proteome for more detail on mechanisms of cellular injury and death, baring in mind that no one technique can effectively capture an entire proteome (see our recent review, 16, for more on this topic).

Acknowledgments and Disclaimer

We thank Dr. Stephen F. Larner for the insightful discussion and editing of this manuscript. This paper has been reviewed by the Walter Reed Army Institute of Research and there is no objection to its presentation and/or publication. The opinions or assertions contained herein are the private views of the authors, and are not to be construed as official, or as reflecting true views of the Department of the Army or the Department of Defense. This work was supported by the Department of Defense (DOD) grant # DAMD17-03-1-0066, and the National Institutes of Health (NIH) grants R01 NS39091 and R01 NS40182. Drs. Kevin K.W. Wang, Nancy D. Denslow, and Ronald L. Hayes hold equity in Banyan Biomarkers, Inc, a company commercializing technology of detecting brain injury biomarkers

Figure Legends

Figure 1. A schematic illustration of the differential CAX-PAGE/RPLC-MSMS proteomic platform for TBI study. The depicted schematic diagram illustrates the sequential steps following CCI TBI model which is followed by sample pooling and preparation for CAX-1D PAGE considered as the 1st and 2nd dimension of separation. After the CAX chromatography /1D-PAGE, gel bands are excised followed by RPLC/MSMS analysis which is considered as our 3rd separation dimension generating a differential protein list which is subjected for validation via Immuno blot analysis to create a potential TBI markers list.

Figure 2. CAX Liquid Chromatography Overlay of TBI and Naïve CAX-PAGE chromatograms. CAX liquid chromatography separations of naïve and TBI pooled rat cortical lysates (n=7) is overlayed with the same 280nm absorbance scale showing CAX chromatograms of each lysate: naïve in black, TBI in grey. Thirty two fractions were collected from each separate run.

Figure 3. Comparison of Rat Naive and TBI Proteomes via Sequential CAX SDS-PAGE Side-By-Side Separation. One milligram of cortical pooled rat TBI and naïve lysates were sequentially separated on CAX-PAGE liquid chromatography into 32 fractions. **Figure 3** shows the side-by-side (naïve on left; TBI on right) pairing of 29 of the 32 fractions run on 1D-PAGE. Selected bands are boxed and letter labeled for correlation with **Table 1**. Differential bands were number-letter labeled according to their position in each specific gel lane *i.e.* a band with a 6A label represents the first top band excised from lane 6. These bands are then excised for subsequent RPLC-MSMS identification.

Figure 4. Differential Gel Band analysis. Using ImageJ densitometry software differential gel bands intensities of the naïve and TBI were quantified to derive the relative fold increase and decrease. Quantitative densitometric analysis was performed on the selected bands based on their

relative intensities. Sixteen gel bands were found to be with more than 2 fold increase compared 13 gel bands were found with more than 2 fold decrease.

Figure 5. Western Blot Validation of TBI Decreased Proteins Identified by Mass Spectroscopy In Individual Naïve and TBI Cortex Samples (N=4). Western Blot analysis of intact 15 kDa profilin, 120 kDa hexokinase, 19 kDa cofilin, 36 kDa GAPDH and 200 kDa MAP2A/2B proteins comparing 4 individual naïve samples with 4 individual TBI samples. These blots show lower protein expression in the 4 naïve samples compared to the TBI samples. Western blots data are suggestive of either down regulation or degradation post TBI insult. Graphical representation of the densitometric analysis using ImageJ software from the Western Blot data of the 4 individual naïve and TBI showing decreased TBI protein (Profilin, hexokinase, cofilin, GAPDH, and MAP2A/2B). Naïve samples (open bars) and TBI samples (dotted bars) are shown in **Figures 5, 6** and **7**. Student's t-test was performed to evaluate statistical significance, *$p<0.05$; mean ± S.E.M; n=4). Data were expressed in Arbitrary Units.

Figure 6. Western Blot Validation of TBI Increased Proteins Identified by Mass Spectroscopy Post-TBI in Individual Naïve and TBI animals (n=4). Western Blot analysis of intact 75 kDa transferrin and intact 25 kDa C-reactive protein (C-RP) comparing 4 individual TBI samples with 4 individual naïve samples. These blots show higher protein expression in the 4 TBI samples compared to the 4 naïve samples. Western blots data are indicative of blood brain barrier disruption along with inflammatory process occurring within injured brain tissues. Graphical representation of the densitometric analysis using ImageJ software which shows elevated TBI protein (transferrin and C-RP). Student's t-test was performed to evaluate statistical significance, *$p<0.05$; mean ± S.E.M; n=4). Data were expressed in Arbitrary Units. Western Blot of β actin serving as a loading control showing equal loading in both conditions. Naïve samples (open bars)

and TBI samples (dotted bars) are shown in **Figures 5, 6** and **7**. Graphical representation of densitometric data from shows no statistical significance difference (*p<0.05; mean ± S.E.M; n=4).

Figure 7. Western Blot Validation of Potential Protein Breakdown Products (BDPs) Identified by Mass Spectroscopy in Individual Naïve and TBI Cortex Samples (N=4). Western Blot analysis of intact 280 kDa αII-spectrin and the 120 kDa αII-spectrin breakdown product that show to have altered expression by CAX-PAGE/RPLC-MSMS data. Intact 280 kDa αII-spectrin showed higher expression in the 4 naïve samples while the 120 kDa αII-spectrin BDP was identified in all four individual TBI rats. Western Blots analysis of intact 62 kDa CRMP-2 and the 55 kDa CRMP-2 potential breakdown product, which were shown to have altered expression by CAX-PAGE-mass spectroscopy. Intact CRMP-2 showed higher expression in the 4 naïve samples while the 55 kDa CRMP-2 BDP was identified in all four individual TBI rats. Western Blot analysis of intact 65 kDa synaptotagmin and the 37 kDa synaptotagmin potential breakdown product, which was shown to have altered expression by CAX-PAGE/RPLC-MSMS and is confirmed here to be decreased, degraded/or downregulated in all four individual TBI rat sample. . Graphical representation of the densitometric analysis using ImageJ software of the 4 individual naïve and TBI Western Blot data showing potential TBI breakdown products of αII-spectrin, CRMP-2 and synaptotagmin identified by mass spectroscopy post TBI. Student's t-test was performed to evaluate statistical significance, *p<0.05; mean ± S.E.M; n=4). Data were expressed in Arbitrary Units. Naïve samples (open bars) and TBI samples (dotted bars) are shown in **Figures 5, 6** and **7**

Table 1. Proteins with decreased abundance post-TBI

Band	Gel Mr kDa	Intact Mr kDa	Protein Accession #	Protein Name	# pep in Naïve	# pep in TBI	% Cov.
6A	56	72.1	XP_237959	Annexin A11	6	0	11.0%
		57.2	XP_214535	Aldehyde Dehydrogenase Family 7	3	1	7.4%
6B	20	18.5	AAH86533	Cofilin 1	5	3	28.3%
8A	15	14.9	NP_071956	Profilin 1	2	0	22.2%
9B	56	57.8	AAB93667	M2 pyruvate kinase	15	12	29.8%
9C	55	50.9	XP_227366	Alpha enolase (non-neural enolase)	2	0	7.05%
		57.8	AAB93667	M2 pyruvate kinase	7	2	15.40%
9D	50	47.1	AAH78896	Enolse1 protein	5	3	19.30%
9E	34	35.8	XP_573896	Glyceraldehyde-3-phosphate dehydrogenase	5	1	23.0%
10A	105	102.4	NP_036866	Hexokinase 1	4	0	5.5%
10B	85	85.4	NP_077374	Aconitase 2. mitochondrial	7	1	11.2%
10C	72	74.8	XP_215897	Acetyl-CoA synthetase 2	3	0	10.4%
10D	21	22.4	AAL66341	Neuronal protein 22	3	0	18.6%
12A	45	44.8	AAH83568	Phosphoglycerate kinase 2	4	0	10.8%
		44.5	NP445743	Phosphoglycerate kinase 1	5	0	13.2%
13A	70	70.4	CAA49670	Hsc70-ps1	11	5	22.6%
13B	58	61.3	NP_036702	Glutamate dehydrogenase 1	4	0	8.6%
13C	37	39.3	NP_036627	Aldolase A	3	0	9.3%
		39.2	NP_036629	Aldolase C. fructose-biphosphate	4	0	16.5%
13D	34	31.1	NP_071633	Dimethylarginine dimethylaminohydrolase 1	3	1	10.5%
17A	64	62.2	NP_071633	Collapsin response mediator protein 2	7	4	15.9%
23A	200	182.2	NP_037198	Microtubule-associated protein 2	5	1	3.4%

Mr = molecular mass; # pep = number of peptides; % Cov. = % of sequence coverage

Table 2. Proteins with increased abundance post-TBI

Band	Gel Mr kDa	Intact Mr kDa	Protein Accession #	Protein Name	# pep in Naïve	# pep in TBI	% Cov.
1A	31	29.6	XP_226922	Carbonic anhydrase	3	6	30.0%
6B	20	20.6	NP_543180	ADP-Ribosylation Factor 3	1	3	17.7%
7A	75	75.8	NP_058751	Transferrin	0	8	13.2%
		76.7	AAP97736	Liver regeneration-related protein	0	4	5.5%
8A	15	15.2	XP_340780	Hemoglobin alpha chain	0	5	33.8%
		15.9	NP_150237	Hemoglobin beta chain	0	2	15.0%
9A	77	76.7	AAP97736	Liver regeneration-related protein	0	2	2.6%
9B	56	41.5	NP_445800	Fetuin beta	0	4	11.6%
		55.9	XP_227088	3-Oxoacid CoaTransferase	1	4	10.4%
9E	34	36.4	NP_150238	Malate dehydrogenase 1. NAD (soluble)	0	2	5.7%
		36.6	NP_036727	Lactate dehydrogenase B	1	4	13.8%
		35.6	AAH63165	Malate dehydrogenase. mitochondrial	0	2	7.6%
10C	72	75.8	NP_058751	Transferrin	0	3	13.2%
13A		60.1	JX0054	Carboxylesterase E1 precursor	0	5	13.6%
13B	58	46.1	NP_071964	Serine protease inhibitor alpha 1	0	8	15.8%
13D	34	38.5	NP_036714	Haptoglobin	0	4	11.8%
13E	22	24.8	JX0222	Ubiquitin carboxy-terminal hydrolase L1	1	3	13.9%
14A	50	46.1	NP_071964	Serine protease inhibitor alpha 1	0	8	14.8%
17A	64	68.2	NP_872280	Serine protease inhibitor 2a	0	7	10.0%
		47.7	AAA41489	T-kininogen.alpha-1 major acute phase protein	0	4	9.5%
		68.7	AAH85359	Albumin	8	11	23.0%
		47.7	NP_001009628	Alpha-1 major acute phase protein prepeptide	0	2	5.8%
18A	160	165.2	NP_075591	Murinoglobulin 1 homolog	0	5	4.5%
18B	54	53.5	NP_036696	Group specific component protein	0	7	11.6%
		50.5	P50398	Guanosine diphosphate dissociation inhibitor 1	1	4	17.6%
		62.2	NP_071633	Collapsin response mediator protein 2 *(BDP)	0	3	5.9%
19A	160	165.2	NP_075591	Murinoglobulin 1 homolog	4	9	7.9%
		163.7	XP_216246	Similar to alpha-1-inhibitor III precursor	3	7	5.5%
20A	120	120.6	A35210	Ferroxidase	0	15	14.5%
		122.2	AAA40917	Ceruloplasmin	0	9	6.6%
		271.6	P16086	Spectrin alpha chain. brain *(BDP)	0	4	1.9%
20B	25	25.5	NP_058792	C-reactive protein	0	2	8.7%
		42.6	AAH87656	Brain creatine kinase *(BDP)	1	3	13.6%
		27.8	NP_001008218	Proteasome subunit. alpha type 7	0	4	19.7%
		27.7	BAA04534	14-3-3 protein zeta-subtype	2	5	22.4%
		27.7	BAA04533	14-3-3 protein theta-subtype	1	3	13.9%
		28.2	BAA04259	14-3-3 protein eta-subtype	0	3	13.8%
		28.3	BAA04261	14-3-3 protein gamma-subtype	0	2	8.1%
29A	37	47.4	XP_343206	Synaptotagmin *(BDP)	0	4	10.7%

Mr = molecular mass; # pep = number of peptides; % Cov. = % of sequence coverage
* (BDP) denotes a suspected breakdown product

Figure 1

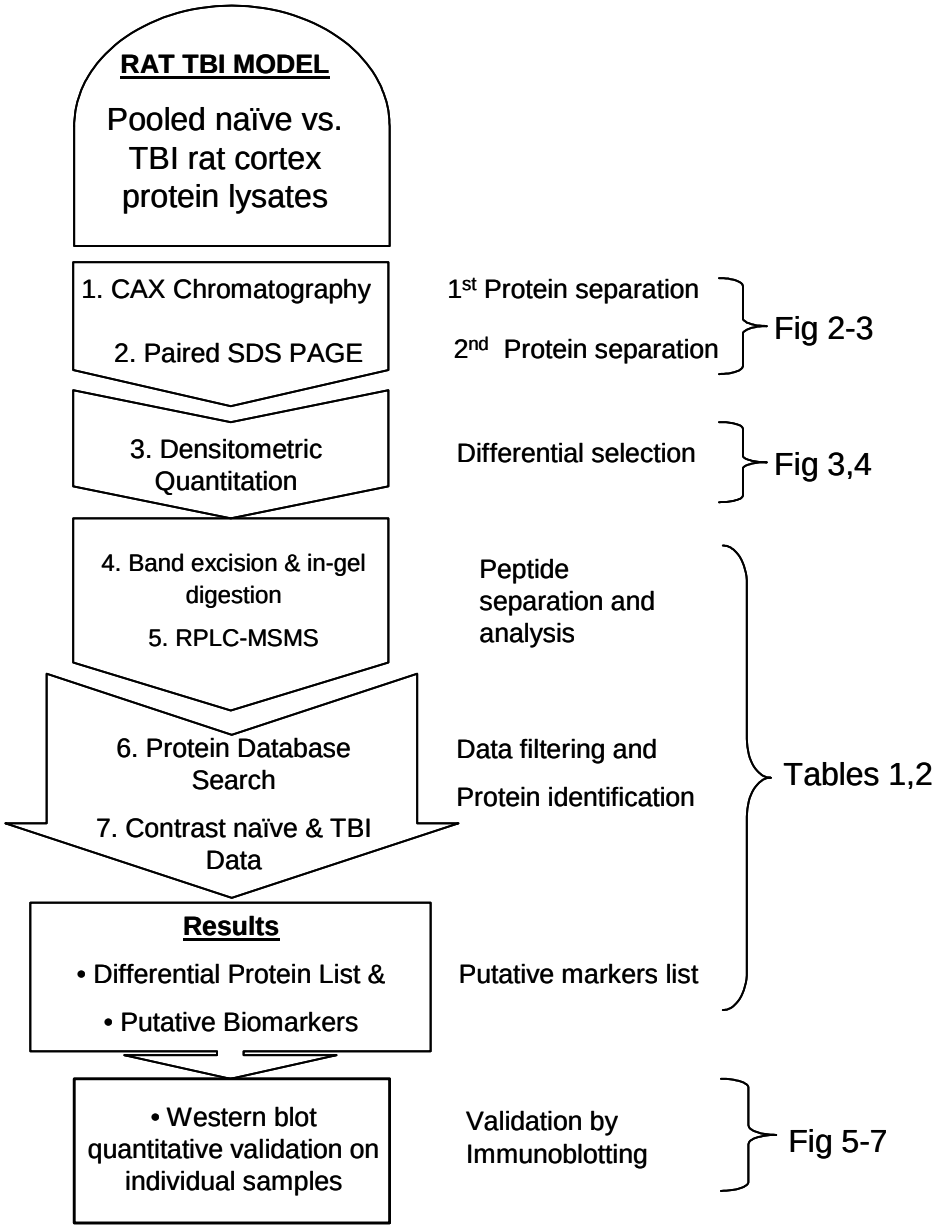

Figure 2

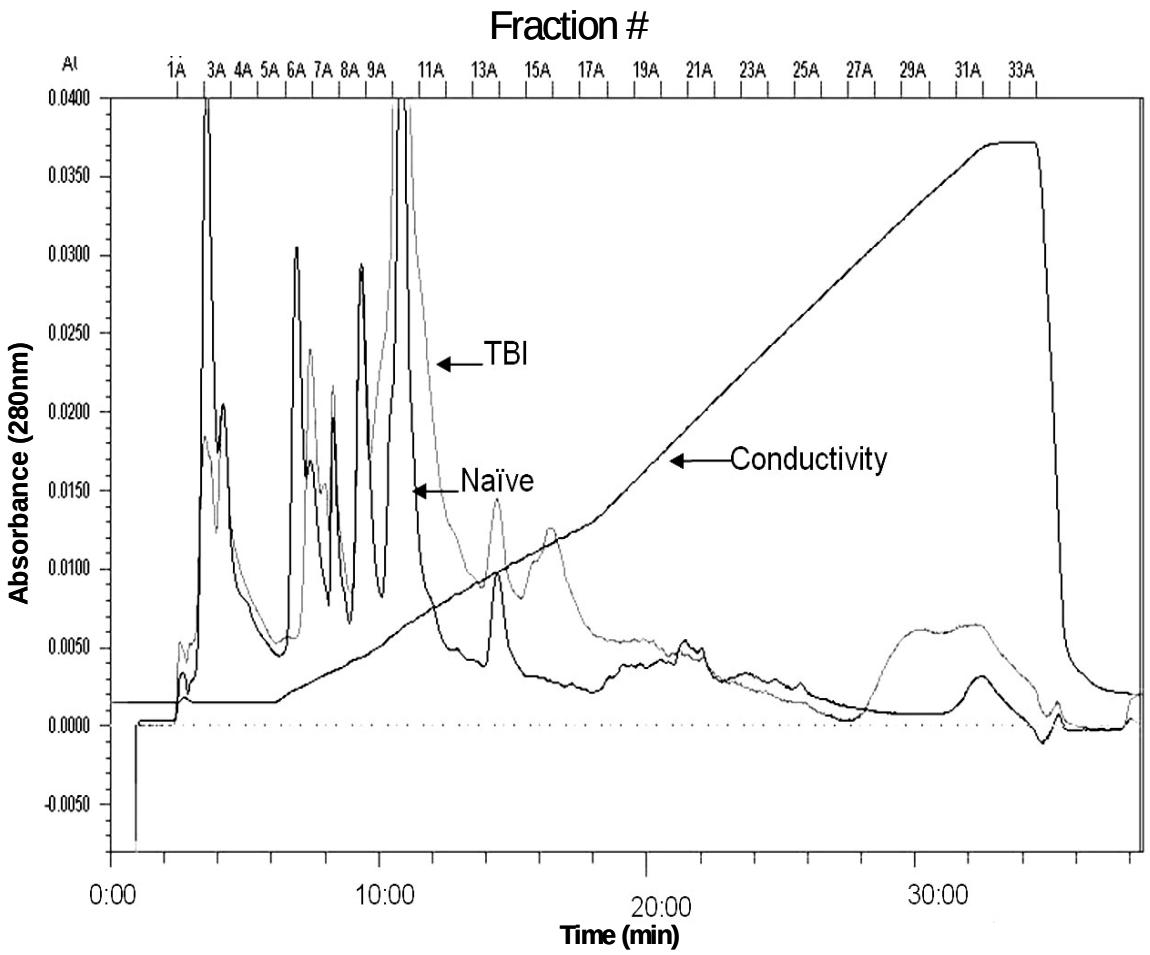

Figure 3

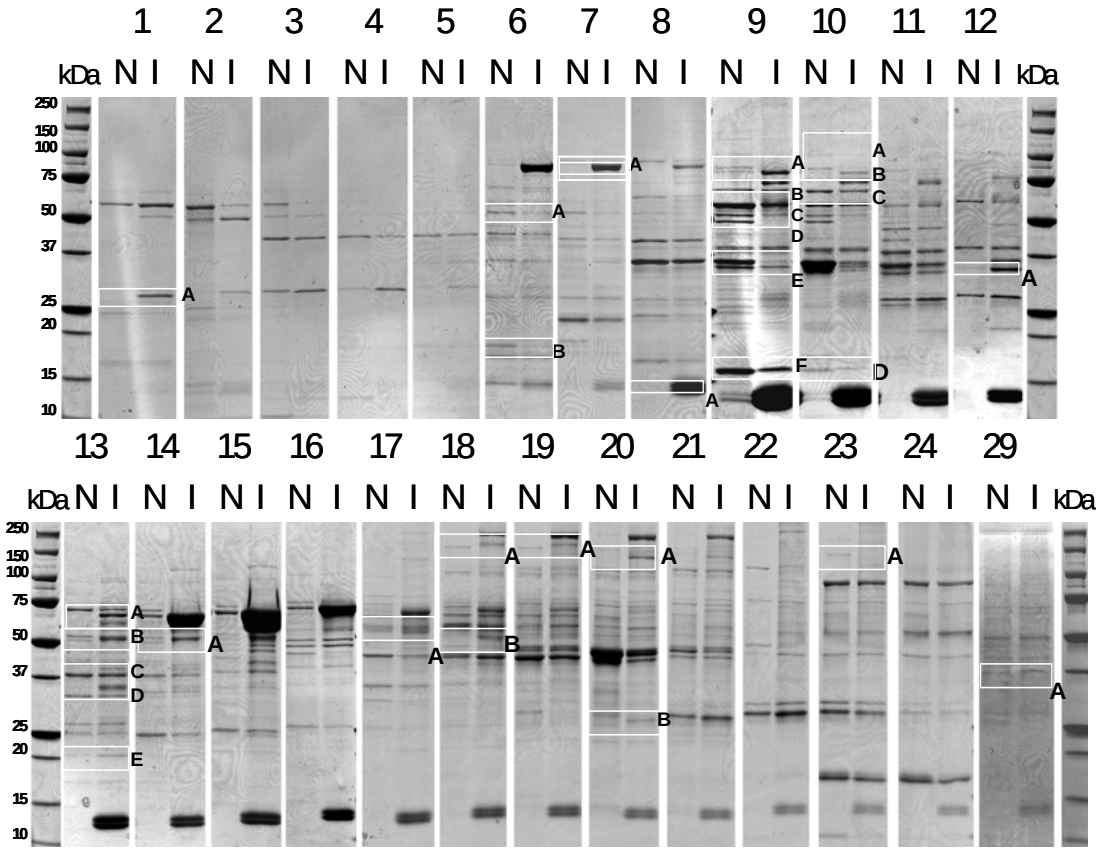

Figure 4

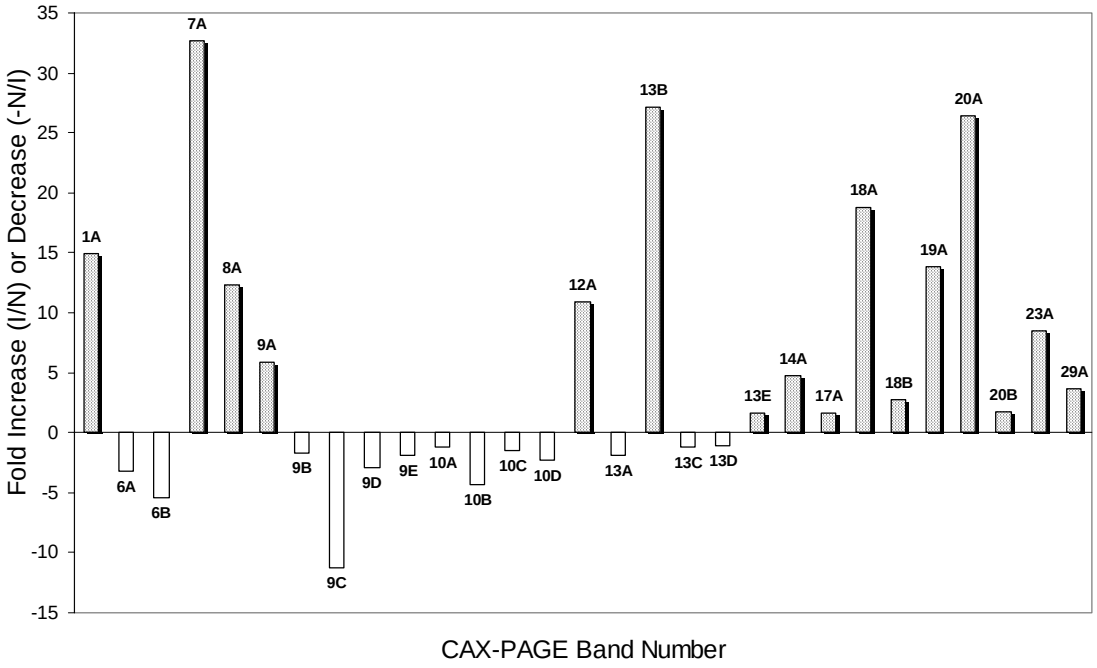

Figure 5

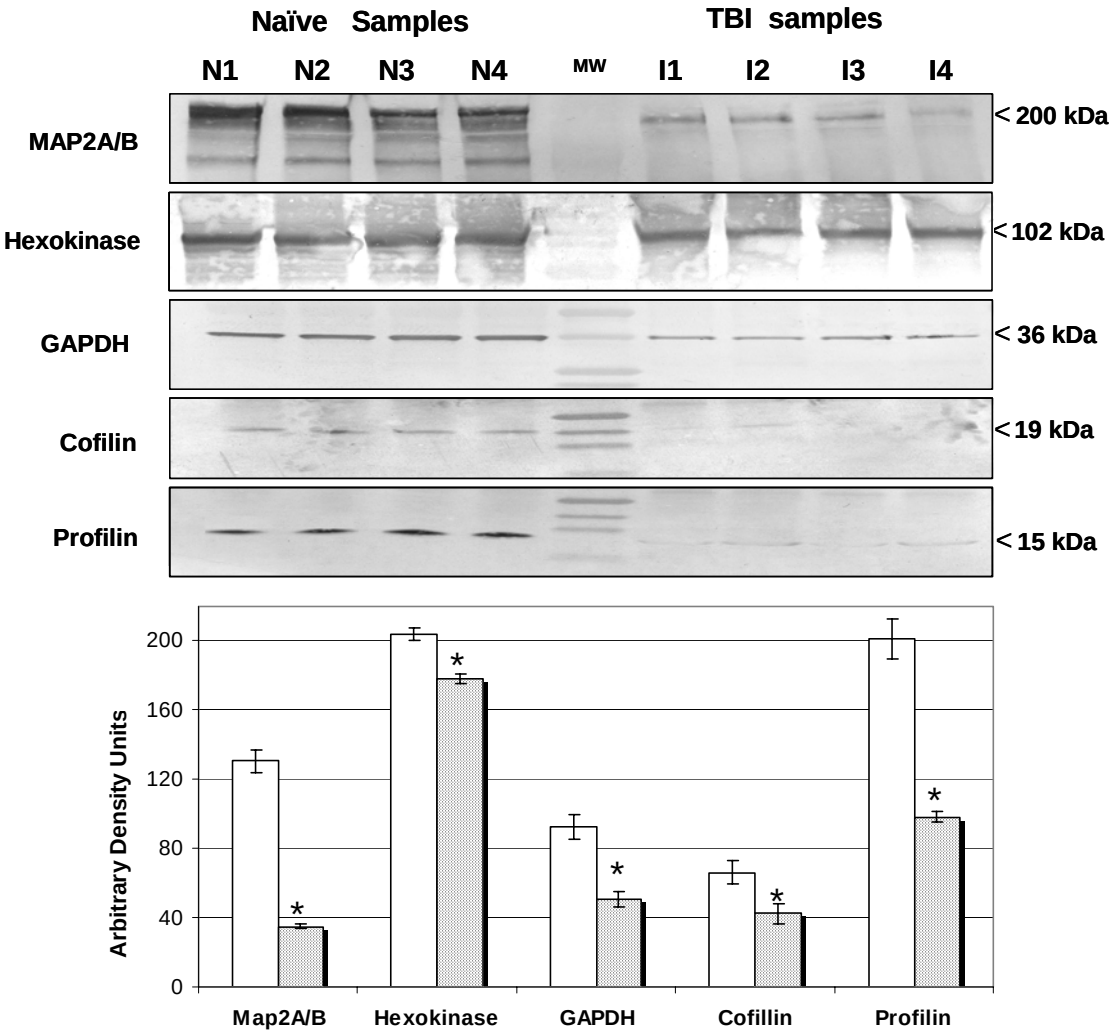

Figure 6

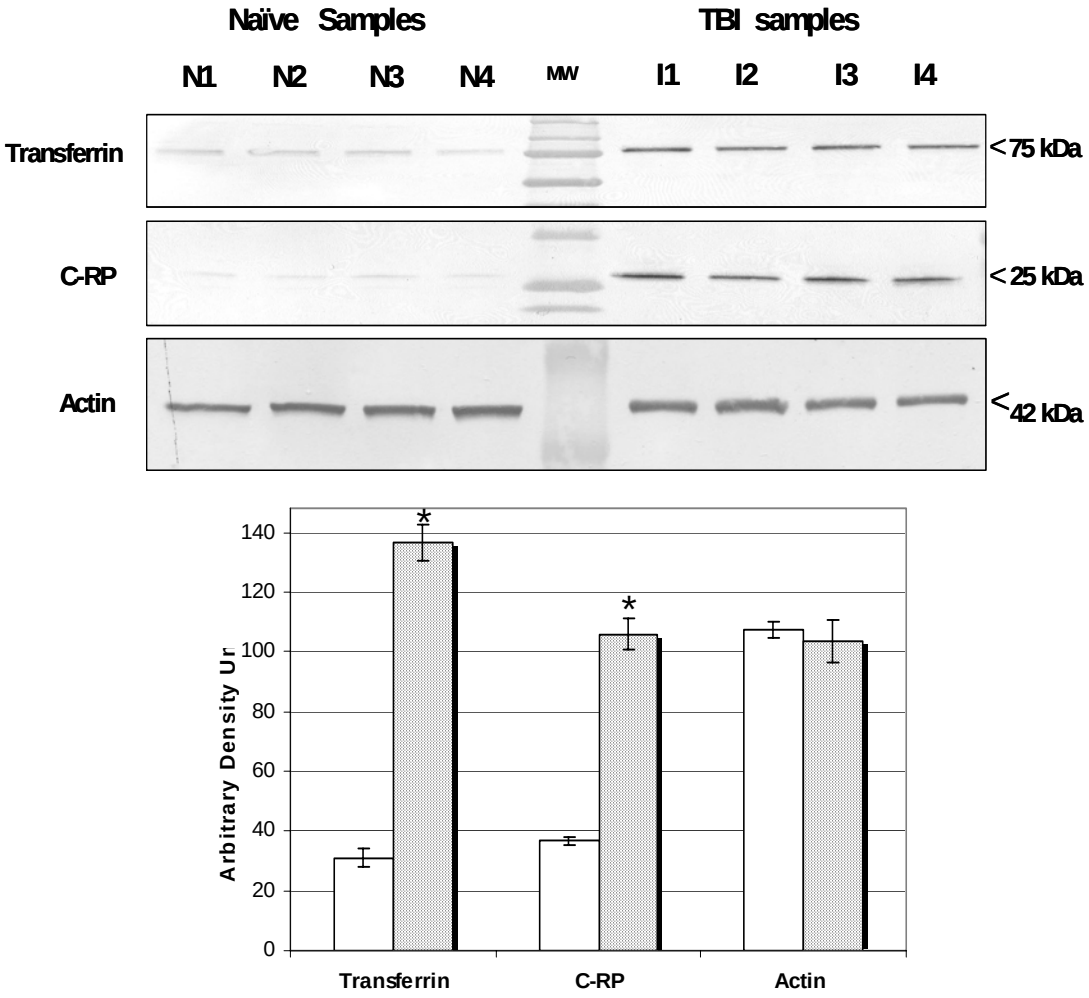

Figure 7

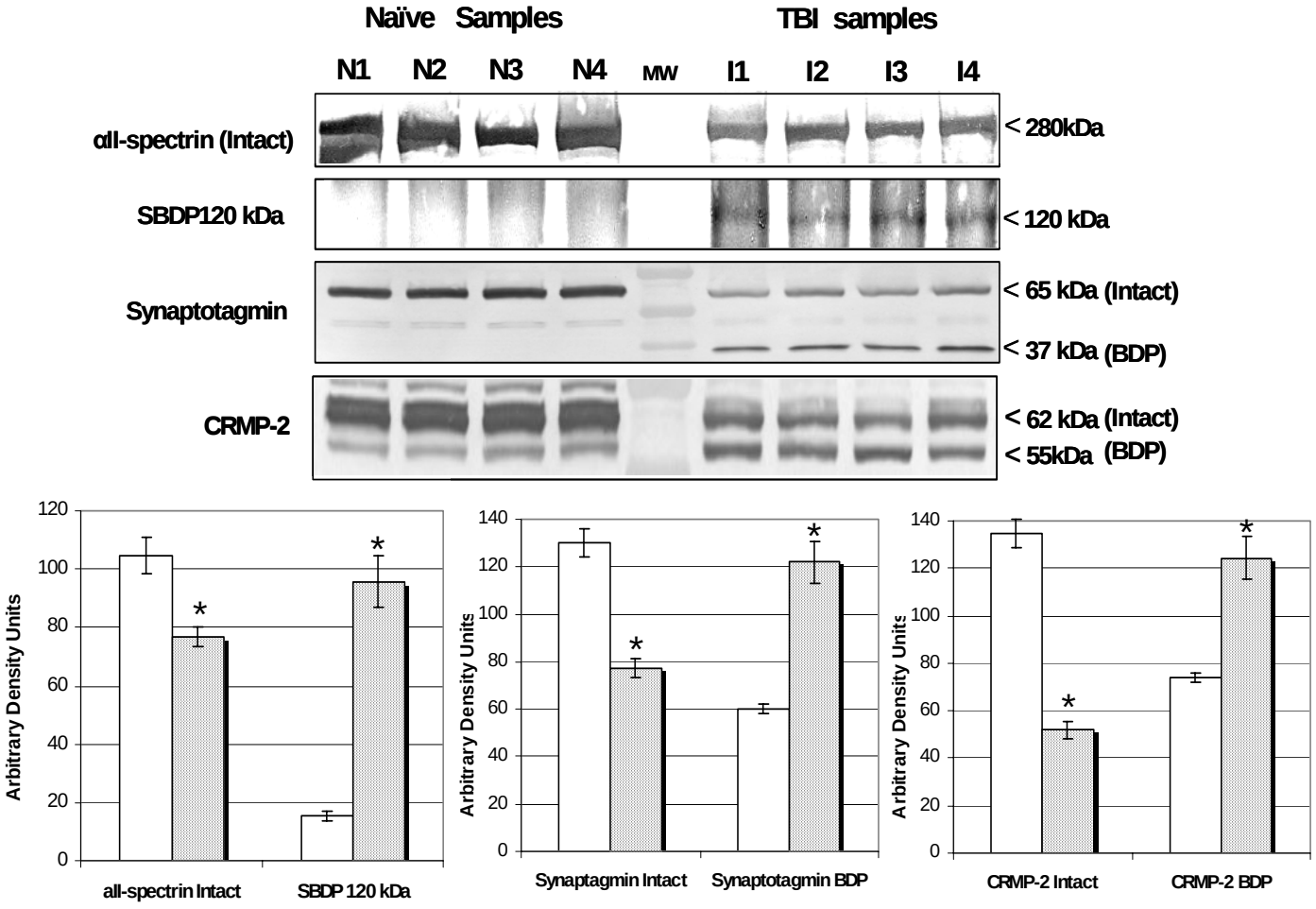

References

1. http://www.ninds.nih.gov/disorders/tbi/detail_tbi.htm (2006).

2. Smith, D. H., Uryu, K., Saatman, K. E., Trojanowski, J. Q., and McIntosh, T. K. (2003) Protein accumulation in traumatic brain injury. *Neuromolecular Med* 4, 59-72.

3. Haskins, W. E., Kobeissy, F. H., Wolper, R. A., Ottens, A. K., Kitlen, J. W., McClung, S. H., O'Steen, B. E., Chow, M. M., Pineda, J. A., Denslow, N. D., Hayes, R. L., and Wang, K. K. (2005) Rapid discovery of putative protein biomarkers of traumatic brain injury by SDS-PAGE-capillary liquid chromatography-tandem mass spectrometry. *J Neurotrauma* 22, 629-44.

4. O, F., B, P., Szekeres-Bartho, J., Doczi, T., Povlishock, J. T., and Buki, A. (2005) Spectrin breakdown products in the cerebrospinal fluid in severe head injury - preliminary observations. *Acta Neurochir (Wien)* 147, 855-61.

5. Pineda, J. A., Wang, K. K., and Hayes, R. L. (2004) Biomarkers of proteolytic damage following traumatic brain injury. *Brain Pathol* 14, 202-9.

6. Ingebrigtsen, T., and Romner, B. (2003) Biochemical serum markers for brain damage: a short review with emphasis on clinical utility in mild head injury. *Restor Neurol Neurosci* 21, 171-6.

7. Pelsers, M. M., Hermens, W. T., and Glatz, J. F. (2005) Fatty acid-binding proteins as plasma markers of tissue injury. *Clin Chim Acta* 352, 15-35.

8. Denslow, N., Michel, M. E., Temple, M. D., Hsu, C. Y., Saatman, K., and Hayes, R. L. (2003) Application of proteomics technology to the field of neurotrauma. *J Neurotrauma* 20, 401-7.

9. Bandyopadhyay, S., Hennes, H., Gorelick, M. H., Wells, R. G., and Walsh-Kelly, C. M. (2005) Serum neuron-specific enolase as a predictor of short-term outcome in children with closed traumatic brain injury. *Acad Emerg Med* 12, 732-8.

10. Siman, R., McIntosh, T. K., Soltesz, K. M., Chen, Z., Neumar, R. W., and Roberts, V. L. (2004) Proteins released from degenerating neurons are surrogate markers for acute brain damage. *Neurobiol Dis* 16, 311-20.

11. Lotocki, G., Alonso, O. F., Frydel, B., Dietrich, W. D., and Keane, R. W. (2003) Monoubiquitination and cellular distribution of XIAP in neurons after traumatic brain injury. *J Cereb Blood Flow Metab* 23, 1129-36.

12. Shimamura, M., Garcia, J. M., Prough, D. S., Dewitt, D. S., Uchida, T., Shah, S. A., Avila, M. A., and Hellmich, H. L. (2005) Analysis of long-term gene expression in neurons of the hippocampal subfields following traumatic brain injury in rats. *Neuroscience* 131, 87-97.

13. Sullivan, P. G., Rabchevsky, A. G., Waldmeier, P. C., and Springer, J. E. (2005) Mitochondrial permeability transition in CNS trauma: cause or effect of neuronal cell death? *J Neurosci Res* 79, 231-9.

14. Czogalla, A., and Sikorski, A. F. (2005) Spectrin and calpain: a 'target' and a 'sniper' in the pathology of neuronal cells. *Cell Mol Life Sci* 62, 1913-24.

15. Wennersten, A., Holmin, S., and Mathiesen, T. (2003) Characterization of Bax and Bcl-2 in apoptosis after experimental traumatic brain injury in the rat. *Acta Neuropathol (Berl)* 105, 281-8.

16. Ottens, A. K., Kobeissy, F. H., Golden, E. C., Zhang, Z., Haskins, W. E., Chen, S. S., Hayes, R. L., Wang, K. K., and Denslow, N. D. (2006) Neuroproteomics in neurotrauma. *Mass Spectrom Rev*.

17. Wang, K. K., Ottens, A., Haskins, W., Liu, M. C., Kobeissy, F., Denslow, N., Chen, S., and Hayes, R. L. (2004) Proteomics studies of traumatic brain injury. *Int Rev Neurobiol* 61, 215-40.

18. Wang, K. K., Ottens, A. K., Liu, M. C., Lewis, S. B., Meegan, C., Oli, M. W., Tortella, F. C., and Hayes, R. L. (2005) Proteomic identification of biomarkers of traumatic brain injury. *Expert Rev Proteomics* 2, 603-14.

19. Davidsson, P., and Sjogren, M. (2005) The use of proteomics in biomarker discovery in neurodegenerative diseases. *Dis Markers* 21, 81-92.

20. Celis, J. E., Gromov, P., Cabezon, T., Moreira, J. M., Ambartsumian, N., Sandelin, K., Rank, F., and Gromova, I. (2004) Proteomic characterization of the interstitial fluid perfusing the breast tumor microenvironment: a novel resource for biomarker and therapeutic target discovery. *Mol Cell Proteomics* 3, 327-44.

21. Gao, J., Garulacan, L. A., Storm, S. M., Opiteck, G. J., Dubaquie, Y., Hefta, S. A., Dambach, D. M., and Dongre, A. R. (2005) Biomarker discovery in biological fluids. *Methods* 35, 291-302.

22. Shin, B. K., Wang, H., and Hanash, S. (2002) Proteomics approaches to uncover the repertoire of circulating biomarkers for breast cancer. *J Mammary Gland Biol Neoplasia* 7, 407-13.

23. McDonald, W. H., and Yates, J. R., 3rd (2002) Shotgun proteomics and biomarker discovery. *Dis Markers* 18, 99-105.

24. Van den Bergh, G., and Arckens, L. (2004) Fluorescent two-dimensional difference gel electrophoresis unveils the potential of gel-based proteomics. *Curr Opin Biotechnol* 15, 38-43.

25. Ottens, A. K., Kobeissy, F. H., Wolper, R. A., Haskins, W. E., Hayes, R. L., Denslow, N. D., and Wang, K. K. (2005) A multidimensional differential proteomic platform using dual-phase ion-exchange chromatography-polyacrylamide gel electrophoresis/reversed-phase liquid chromatography tandem mass spectrometry. *Anal Chem* 77, 4836-45.

26. Pike, B. R., Zhao, X., Newcomb, J. K., Posmantur, R. M., Wang, K. K., and Hayes, R. L. (1998) Regional calpain and caspase-3 proteolysis of alpha-spectrin after traumatic brain injury. *Neuroreport* 9, 2437-42.

27. Tabb, D. L., McDonald, W. H., and Yates, J. R., 3rd (2002) DTASelect and Contrast: tools for assembling and comparing protein identifications from shotgun proteomics. *J Proteome Res* 1, 21-6.

28. Peng, J., Kim, M. J., Cheng, D., Duong, D. M., Gygi, S. P., and Sheng, M. (2004) Semiquantitative proteomic analysis of rat forebrain postsynaptic density fractions by mass spectrometry. *J Biol Chem* 279, 21003-11.

29. Lubec, G., Krapfenbauer, K., and Fountoulakis, M. (2003) Proteomics in brain research: potentials and limitations. *Prog Neurobiol* 69, 193-211.

30. Jenkins, L. W., Peters, G. W., Dixon, C. E., Zhang, X., Clark, R. S., Skinner, J. C., Marion, D. W., Adelson, P. D., and Kochanek, P. M. (2002) Conventional and functional proteomics using large format two-dimensional gel electrophoresis 24 hours after controlled cortical impact in postnatal day 17 rats. *J Neurotrauma* 19, 715-40.

31. Bodovitz, S., and Joos, T. (2004) The proteomics bottleneck: strategies for preliminary validation of potential biomarkers and drug targets. *Trends Biotechnol* 22, 4-7.

32. Hara, M. R., Agrawal, N., Kim, S. F., Cascio, M. B., Fujimuro, M., Ozeki, Y., Takahashi, M., Cheah, J. H., Tankou, S. K., Hester, L. D., Ferris, C. D., Hayward, S. D.,

Snyder, S. H., and Sawa, A. (2005) S-nitrosylated GAPDH initiates apoptotic cell death by nuclear translocation following Siah1 binding. *Nat Cell Biol* 7, 665-74.

33. Fan, L., Jaquet, V., Dodd, P. R., Chen, W., and Wilce, P. A. (2001) Molecular cloning and characterization of hNP22: a gene up-regulated in human alcoholic brain. *J Neurochem* 76, 1275-81.

34. Kosinska, K. (1992) [Serum C-reactive protein monitoring in children after injuries of closed body cavities]. *Ann Acad Med Stetin* 38, 67-78.

35. Sironi, L., Tremoli, E., Miller, I., Guerrini, U., Calvio, A. M., Eberini, I., Gemeiner, M., Asdente, M., Paoletti, R., and Gianazza, E. (2001) Acute-phase proteins before cerebral ischemia in stroke-prone rats: identification by proteomics. *Stroke* 32, 753-60.

36. Sironi, L., Guerrini, U., Tremoli, E., Miller, I., Gelosa, P., Lascialfari, A., Zucca, I., Eberini, I., Gemeiner, M., Paoletti, R., and Gianazza, E. (2004) Analysis of pathological events at the onset of brain damage in stroke-prone rats: a proteomics and magnetic resonance imaging approach. *J Neurosci Res* 78, 115-22.

37. Di Napoli, M., Papa, F., and Bocola, V. (2001) C-reactive protein in ischemic stroke: an independent prognostic factor. *Stroke* 32, 917-24.

38. Liu, H. M., and Sturner, W. Q. (1988) Extravasation of plasma proteins in brain trauma. *Forensic Sci Int* 38, 285-95.

39. Pike, B. R., Flint, J., Dutta, S., Johnson, E., Wang, K. K., and Hayes, R. L. (2001) Accumulation of non-erythroid alpha II-spectrin and calpain-cleaved alpha II-spectrin breakdown products in cerebrospinal fluid after traumatic brain injury in rats. *J Neurochem* 78, 1297-306.

40. Czech, T., Yang, J. W., Csaszar, E., Kappler, J., Baumgartner, C., and Lubec, G. (2004) Reduction of hippocampal collapsin response mediated protein-2 in patients with mesial temporal lobe epilepsy. *Neurochem Res* 29, 2189-96.

41. Castegna, A., Aksenov, M., Thongboonkerd, V., Klein, J. B., Pierce, W. M., Booze, R., Markesbery, W. R., and Butterfield, D. A. (2002) Proteomic identification of oxidatively modified proteins in Alzheimer's disease brain. Part II: dihydropyrimidinase-related protein 2, alpha-enolase and heat shock cognate 71. *J Neurochem* 82, 1524-32.

42. Liu, M. C., Akle, V., Zheng, W., Dave, J. R., Tortella, F. C., Hayes, R. L., and Wang, K. K. (2006) Comparing calpain- and caspase-3-mediated degradation patterns in traumatic brain injury by differential proteome analysis. *Biochem J* 394, 715-25.

43. McQuibban, G. A., Gong, J. H., Tam, E. M., McCulloch, C. A., Clark-Lewis, I., and Overall, C. M. (2000) Inflammation dampened by gelatinase A cleavage of monocyte chemoattractant protein-3. *Science* 289, 1202-6.

44. Lopez-Otin, C., and Overall, C. M. (2002) Protease degradomics: a new challenge for proteomics. *Nat Rev Mol Cell Biol* 3, 509-19.

45. Dunckley, T., Coon, K. D., and Stephan, D. A. (2005) Discovery and development of biomarkers of neurological disease. *Drug Discov Today* 10, 326-34.